Studies of Cationic Amphiphilic Drug Catalysed Membrane Degradation

Sarra C. Sebai

Department of Chemistry

Imperial College London

A Thesis submitted for the degree of Doctor of Philosophy

May 28, 2007

Abstract

Although drug molecules are designed to bind specifically to targets such as receptors that are embedded within biological membranes, it is becoming increasingly evident that a large fraction of these compounds interact non-specifically with the membrane and / or other proteins. In particular, the non-specific binding of positron emission tomography (PET) radioligands to tissue, both *in-vivo* and *in-vitro*, is poorly understood. This phenomenon is a major confounding factor in the development of new radioligands for receptor imaging *in-vivo*.

To address this issue, studies on the interaction of central nervous system (CNS) drugs, belonging to the cationic amphiphilic drug (CAD) family, with model membrane assemblies were conducted.

Experiments were performed using three CADs: Haloperidol (HPD), Spiperone (SPIP) and WAY, on condensed fluid lamellar phases and membrane vesicles. CAD-membranes interactions were studied by small angle X-ray scattering (SAXS), solid-state nuclear magnetic resonance (SS-NMR), fluorescence assays, and fluorescence microscopy.

CADs were found to partition rapidly to the polar / apolar region of the membrane; this was demonstrated by SAXS where CADs affected the bilayer spacing. At physiological pH, the protonated groups on the CAD catalyze the acid-hydrolysis of the ester linkage present in the phospholipid chains, producing a fatty acid and single-chain lipid. The single-chain lipids destabilize the membrane, causing membranous fragments and small vesicles to separate and diffuse away from the host. These membrane fragments carry the drug molecules with them. The entire process, from

drug adsorption to drug release within micellar fragments, occurs on a timescale of seconds / minutes. Given the rate at which this occurs it is probable that this process is a significant mechanism for drug transport.

Kinetic studies were conducted to determine the rate of the lipid hydrolysis in the condensed fluid lamellar phase, by varying CAD's counterions, the lipid composition and the stored curvature elastic stress in the bilayer. The lipid hydrolysis kinetics was fitted to a pseudo-first order exponential decay, and hydrolysis rates were determined. Hydrolysis rates are specific to the CAD molecules, with WAY hydrolysing the bilayer as twice as fast as SPIP. In addition, evidence is presented that the stored curvature elastic stress in the membrane modulates the hydrolysis kinetics.

Interestingly, the rate of membrane hydrolysis appears to correlate with *in-vivo* non-specific binding of the PET radioligands. The measured rate of membrane hydrolysis may provide useful insight into the mechanism of non-specific binding on a molecular level and possibly in the design of new radiotracers.

Acknowledgments

Over the last four years, I have had the opportunity to work with a group of very talented, enthusiastic and wonderful people. I would like to take the opportunity to thank the people who believed in me and allowed me to take part in this fantastic project.

I would like to thank my supervisors, Prof. Richard Templer, Dr. Rob Law and Prof. Tony Gee, who have guided me during my thesis and provided excellent support. I would also like to thank GlaxoSmithKline plc for funding this project.

Special thanks to Dr Oscar Ces, for his invaluable experience and advice, time and patience, sense of humour, friendship, and support; to Xavier Mulet, for the remarkable microscopy data, collected on a late friday night, and also for friendship and support throughout these years (Merci!); to Dr Gemma Shearman, for her involvement in the project, discussions, advice and for friendship; to Dr James Clarke, for his great help with the Solid-State NMR data, friendship and inspiring discussions; to Duncan Casey for synthesising the CADs counterions, and his contribution to the project; and also to Dr. Andrew Heron for the excellent software for the X-ray diffraction analysis.

I am also grateful to the GSK team involved in the "Non-Specific Binding Initiative", in particular Dr Vincent Cunningham, Prof Roger Gunn, Dr Christine Parker and Dr. Christophe Plisson for the data on non-specific binding.

Among the other people who helped me in various way are all the past and present members of the liquid crystals, membrane biophysics and solid-state NMR group,

including Steven Alley, Christina Turner, Charlotte Conn, Beatrice Gauthe, Arach Goldar, Nick Brooks, Rebecca Ling, Jessica Knott, Chandrashekhar Kulkarni, Emma Clay, Dora Tang, Natalia Goehring, Claire Stanley, Annela Seddon, Magdalen Baciu Deborah Gater, Karen Shaw, Alex Trevenen, Arwen Tyler and also Nuria Roque-Rosell

Finally, I would like to thank all my friends who have been there for me throughout the project for their patience during this time. Thanks to my family, particularly my mum and dad, for their love and support.

A tous ceux qui me sont chers...

Contents

Abstract 1

Acknowledgements 3

Abbreviations 11

Chapter 1 Introduction 14

I.1 Non-specific binding and physicochemical properties of drugs. Relevance to Positron Emission Tomography (PET) 15

I.1.1 Definition and characterisation of Non-Specific Binding (NSB) 15

1.1.2 Non-Specific Binding as measured by PET 17

I.1.2.1 Description of PET 17

I.1.2.2 Description of PET 18

I.1.2.3 The degree of NSB as determined by PET 19

I.1.3 Molecular basis of NSB 24

1.1.3.1 Lipophilicity measurements 25

I.1.3.2 Prediction of NSB for central nervous system drugs 26

I.1.4 Application to Cationic Amphiphilic Drugs (CADs) 27

1.2 Biological membranes and membrane biophysics 30

1.2.1 Cell membranes 30

I.2.2 Transport models across membranes 31

I.2.2.1 Passive transport 32

1.2.2.2 Facilitated transport 33

1.2.2.3 Active transport 33

I.2.3 Model membranes, bilayers properties and structure 34

I.2.3.1 Lipid description 34

I.2.3.2 Forces in the bilayer 35

I.2.3.3 Interfacial curvature 37

I.2.3.4 Stored curvature elastic energy 40

I.2.3.5 Bilayer mesophases 41

I.2.3.6 Electrostatic properties of membranes 44

I.3 Cationic amphiphilic drug (CAD) interactions with membranes 46

I.3.1 CNS drugs interactions with membranes 46

I.3.1.1 Chlorpromazine (CPZ) 47

I.3.1.2 Haloperidol (HPD) 47

I.3.2 Biological relevance: CADs induced phospholipidosis 48

I.4 Aims and approaches 49

Chapter 2 Theory and Methods **51**

II.1 X-ray diffraction 51

II.1.1 X-ray generation 51

II.1.2 X-ray diffraction theory 52

II.1.3 Identification of bilayer mesophases by SAXS and WAXS 53

II.1.4 Instrumentation 55

II.1.4.1 The "kinetics" beamline 56

II.1.4.2 The "osmotic" beamline 56

II.1.4.3 The nanoSTAR 57

II.1.4.4 Image analysis 57

II.2 Solid-State Nuclear Magnetic Resonance (SS-NMR) 59

II.2.1 NMR principles 59

II.2.2 SS-NMR of liquid crystals 63

II.2.2.1 Principles 63

II.2.2.2 Application to liquid crystals 65

II.3 Fluorescence binding studies 69

II.3.1 Theory 69

II.3.2 Experimental 72

II.4 Methods 74

II.4.1 Lipids 74

II.4.2 Drugs 75

II.4.3 Buffers 75

II.4.4 Sample preparation for SAXS, SS-NMR and HPLC 75

II.4.5 SAXS 75

II.4.6 NMR 76

II.4.7 Normal Phase High Performance Liquid Chromatography 76

II.4.8 Vesicles preparation 77

II.4.9 Binding studies using fluoresceinphosphatidylethanolamine 77

II.4.10 Dynamic Light Scattering (DLS) 78

II.4.11 Fluorescence microscopy 78

II.4.12 Polarising microscopy 79

Chapter 3 Degradative Transport of Haloperidol and Spiperone Across Bilayers **80**

III.1 Background 80

III.1.1 DOPC systems 81

III.1.2 Drug systems 82

III.2 Biophysical measurments 82

III.2.1 SAXS 83

III.2.2 SS-NMR 86

III.2.2.1 ^{31}P static SS-NMR 87

III.2.2.2 ^{13}C MAS SS-NMR 90

III.2.3 CADs induce the acid hydrolysis of the bilayer 93

III.3 Detection of the hydrolysis products by normal phase HPLC 96

III.3.1 HPLC system 96

III.3.2 Standards 96

III.3.3 Detection of the hydrolysis products in DOPC: CAD systems 99

III.4 Direct visualisation of the degradation 101

III.4.1 Use of GUVs as model membranes 101

III.4.2 Electroformation of GUVs with HPD. The co-lyophilised method 102

III.4.3 Addition of fluorescently labelled SPIP to GUVs 104

III.5 Importance of the phospholipid ester linkage 106

III.5.1 Evidence from static ^{31}P SS-NMR 107

III.5.2 Fluorescence microscopy 106

III.6 Binding and partitioning of CADs into vesicles 109

III.6.1 Background 109

III.6.2 Binding kinetics of HPD and SPIP to vesicles made of DOPC 110

III.6.2.1 DOPC vesicles labelling 110

III.6.2.2 Addition of HPD and SPIP to FPE lablled DOPC vesicles 113

III.6.3 Detection of the bilayer hydrolysis 115

III.6.4 Addition of HPD to FPE labelled ether-linked PC vesicles 119

III.7 Model proposed 123

III.8 Biological relevance 125

Chapter 4 Effects of CAD's formulation on the kinetics of the membrane hydrolysis: towards an understanding of the molecular basis of non-specific binding **128**

IV.1 Crystallisation of the CADs and counterion recondensation 129

IV.1.1 Background 129

IV.1.2 Crystallisation of the CADs in the presence of the bilayer and counterion recondensation 131

IV.1.3 Optimisation of sample preparation 136

IV.2 Kinetics of the membrane degradation 137

IV.2.1 Kinetic model of the degradation 137

IV.2.2 Effect of different CADs on membrane degradation 139

IV.2.3 Effect of chloride, formate, trifluoroacetate and maleate counterions on the hydrolysis 151

IV.2.4 Influence of salt on the membrane hydrolysis 157

IV.3 Correlation between the membrane degradation and NSB 161

IV.3.1 Background 161

IV.3.2 Hydrolysis rates as parameters revealing the degree of NSB 162

Chapter 5 Modulation of the hydrolysis kinetics by membrane curvature elastic stress **166**

V.1 Background 166

V.2 Effect of systems with reduced curvature elastic stress on hydrolysis kinetics; DLPC systems 168

V.2.1 DOPC vs. DLPC bilayers 168

V.2.2 Determination of the hydrolysis kinetics in DLPC: WAY and DLPC: HPD systems 169

V.3 Effects of systems with increased curvature elastic stress; DOPC: DOPE systems 173

V.3.1 DOPC: DOPE systems 173

V.3.2 Effect of DOPE on the hydrolysis kinetics 174

V.3.3 DOPC and DOPE relative degradation rates 179

V.4 Summary 182

Chapter 6 Conclusion and future work **183**

List of figures **186**

List of tables **192**

Bibliography **193**

Abbreviations

Å	Angstrom
AC	Alternative Current
B	Bound Ligand Concentration
BBB	Blood Brain Barrier
B_{max}	Total Number of Binding Sites
BMP	Bis-monoglycerolphosphate
BP	Binding Potential
°C	Celsius Degree
CAD	Cationic Amphiphilic Drug
CCT	CTP-Citidylyltransferase
C_i	Radioligand Concentration in the *i* Compartment
CNS	Central Nervous System
CSA	Chemical Shift Anisotropy
CTP	Citdyltriphosphate
CPZ	Chlorpromazine
D	Diffusion Coefficient
DLPC	Dilauroylphosphatidylcholine
DLS	Dynamic Light Scattering
DMPC	Dimiristoylphosphatidylcholine
DMPE	Dimiristoylphosphatidylethanolamine
DMSO	Dimethylsulfoxyde
DOPC	Dioleoylphosphatidylcholine
DOPE	Dioleoylphosphatidylethannoamine
$\Delta\psi$	Transmembrane Potential
e.g.	Exempli Gratia
ELS	Evaporative Light Scattering
E / M	Excimer / Monomer ratio

ESR	Electron Spin Resonance
F	Free ligand Concentration
FA	Fatty Acid
FID	Fee Induction Decay
FPE	Fluoresceinphosphatidylcholine
FT	Fourier Transform
FT-IR	Fourier Transform Infra Red spectroscopy
GTP	Guanosintriphosphate
GUV	Giant Unilamellar Vesicle
HPD	Haloperidol
HPLC	High Performance Liquid Chromatography
H_I	Normal Hexagonal Phase
H_{II}	Inverse Hexagonal Phase
I	Spin Angular Momentum
i.e.	Id Est
IUPAC	International Union of Pure and Applied Chemistry
k	Boltzmann constant
K_d	Dissociation constant
LC	Liquid Chromatography
LPC	Lyso-phosphatidylcholine
LPE	Lyso-phosphatidylethanolamine
Log P	Partition coefficient between a highly non-polar and polar solvent
L_α	Fluid Lamellar Phase
L_β	Gel Lamellar Phase
L_C	Crystal Lamellar Phase
L_o	Liquid Ordered Phase
λ_d	Debye Length
MAS	Magic Angle Spining
Mm	millimetre
mM	millimolar
mg	milligram
µg	microgram
µl	microlitre
µmol	micromol
µM	micromolar
NBD-tagged-SPIP	Nitrobenzoxadiazol-Aminohexanolylaminophenetylspiperone

nm	Nanometre
NMR	Nuclear Magnetic Resonance
NSB	Non-Specific Binding
OA	Oleic Acid
PA	Phosphatidic Acid
PC	Phosphatidylcholine
PE	Phosphatidylethanolamine
PG	Phosphatidylglycerol
PI	Phosphatidylinositol
pk_a	Acidity Constant
PLA	Phospholipase A
ppm	Part Per million
PS	Phosphatidylserine
Pt	Platinum
Φd	Dipole Potential
Φs	Surface Potential
R	Gas Constant
RF	Radiofrequency
SAR	Structure Activity Relationship
SAXS	Small Angle X-ray Scattering
SB	Specific Binding
SM	Sphingomyeline
SPIP	Spiperone
SS-NMR	Solid-State Nuclear Magnetic Resonance
T	Temperature
TFA	Trifluoroacetate
T_m	Melting Temperature
TMS	Tetramethylsilane
V_i	Distribution volume
WAXS	Wide Angle X-ray Scattering
Z	Number of Charges

CHAPTER 1

Introduction

Each year thousands of chemical compounds designated to be potential central nervous system (CNS) drugs are synthesized and tested in an effort to find one that can achieve a desirable result. From this large number of drug candidates, more than 70% fail when entering clinical drug development [1]. Numerous causes can be responsible for this, one of them being the poor correlation between *in-vitro* and *in-vivo* measurements, which mainly arises from the non-specific binding signal of the tested drug compounds *in-vivo*. In this matter, the tested drug is trapped at any location other than its specific target, one of them being the plasma membrane. This phenomenon highlights the lack of data on drug interactions with membranes since drug discovery research mainly focuses on drug / ligand interactions with specific targets in the form of ligand / membrane receptor complexes; it is generally assumed that the lipid environment only plays a passive role. The non-specific binding of drugs *in-vivo* implies that the interactions between ligands and membrane embedded receptors may be more complex than those described by the traditional ligand / receptor model, and that the plasma membrane characteristics are to be considered in a higher extent. To overcome this issue, screening methods that encompass pharmacological and physicochemical properties of the tested drug and its binding environment need to be developed to predict and map the non-specific binding *in-*

vivo. In this respect, the focus of this thesis is on the effect of CNS drugs upon phospholipids present in membranes.

This section will first give an introduction to non-specific binding in relation to the physicochemical properties of CNS drugs, in particular the cationic amphiphilic drugs (CAD), followed by a description of the biophysical characteristics of phopholipid membranes. Then, an overview of CAD-membrane interactions and their relevance *in-vivo* will be presented.

I.1 Non-specific binding and physicochemical properties of drugs: Relevance to Positron Emission Tomography

I.1.1 Definition and characterization of Non-Specific Binding (NSB)

Drug molecules are designed to bind specifically to their target which typically consists of membrane embedded receptors or enzymes. When the drug molecule reaches its target it may also bind to sites other than its specific site. Other binding sites (which can include binding to cell membranes [2], and other receptors or sites distinct from the active site) will be referred to as non-specific sites.

Specific binding is characterized by a saturation profile, i.e. the specific sites are all filled by the substrate, whereas the NSB is non-saturable. NSB can be determined experimentally by radioactivity measurements, using a saturating concentration of a drug, which is chemically different from the radioligand to be tested but is specific for the same receptor [3]. To determine the non-specific binding component for a particular compound, radioligand binding studies need to be performed in order to record two measurements.

(a) The amount of bound radioactivity for a specific displacer for a specific protein (in a protein-rich tissue). This measurement will record the total amount of bound radioactivity which will be due to specific labelling of the protein of interest, plus the labeling of non-specific sites (as defined above).

(b) The second set of measurements will be recorded in exactly the same manner as in (a) except they will be recorded in the presence of a saturating concentration of a chemically dissimilar unlabelled compound highly selective for the specific binding site on the protein. Therefore this measurement will only record the amount of bound radioactivity associated with the non-specific sites. The specific binding (SB) component is the difference between the total amount of bound radioactivity (T) and the non-specific amount of bound radioactivity (NSB). (Figure I.1) [3].

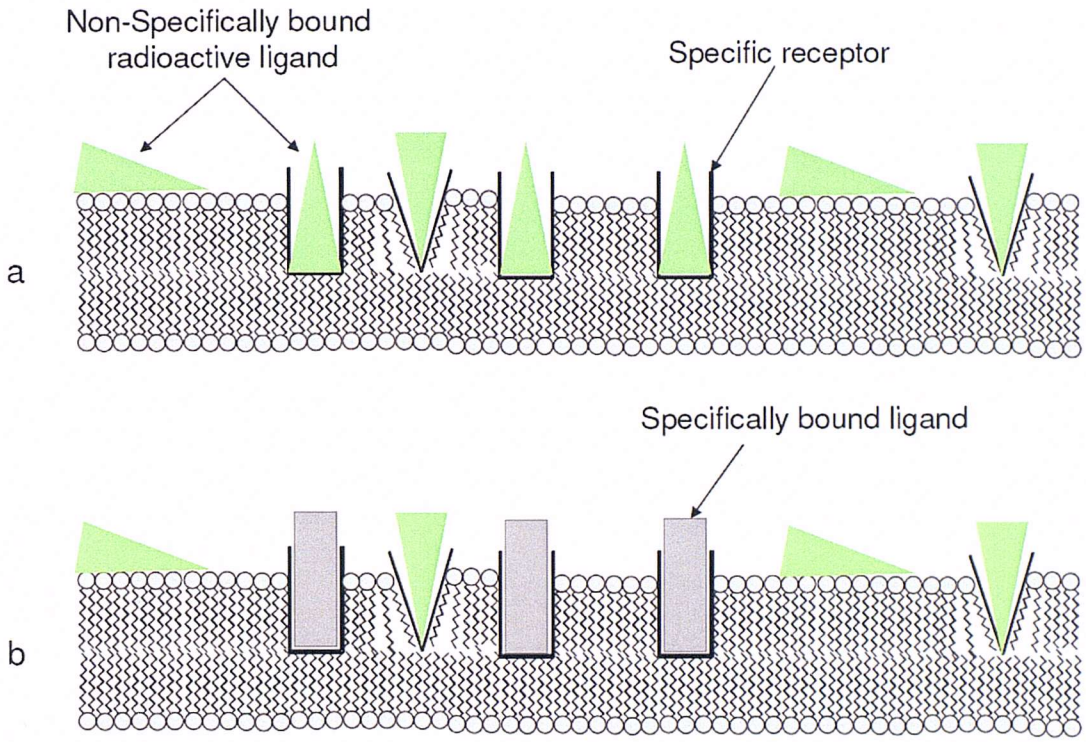


Figure I. 1: Cartoon representing the determination of specific binding of a given compound. (a) A radioactive ligand is added to the tissue and bind to specific and non-specific sites. The radioactivity corresponds to the total binding (T). (b) The radioactive ligand is added to the tissue in the presence of a more selective compound that is not radioactive. The radioactivity measured corresponds to the non-specific binding (NSB) sites only. The specific binding is calculated by substracting the NSB to the total binding.

Figure I.2 represents the signal obtained for a saturation analysis with the linear NSB trace and the resulting hyperbolic specific binding curve. The saturation curve allows the determination of the drug's dissociation constant K_d, that is the concentration of drug which, at equilibrium, occupies 50% of the receptors.

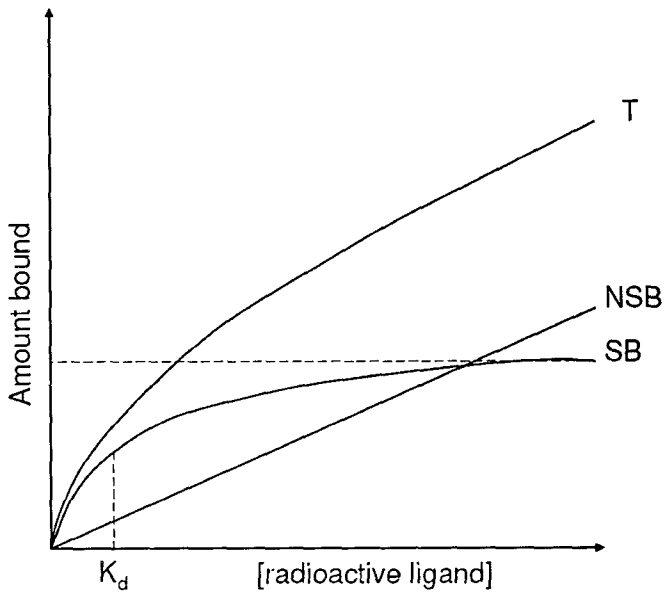


Figure I. 2: A saturation diagram for the binding of a radioligand. The graph is constructed from the total binding values (T), and the non-specific binding values are calculated from the presence of the unlabelled compound. The specific binding (SB) signal is obtained from subtracting the NSB values to the T values.

The non-specific binding phenomenon applies to many systems, from DNA binding to nuclear receptors [4], to protein-protein interactions, protein binding to cell cytoplasm, drug-protein interactions [5, 6] and ligand-membrane interactions [7]. NSB is a major confounding factor in the development of new molecules, and its molecular origin is poorly understood. However, a huge effort and a wide variety of experimental techniques are undertaken to unravel its origins and minimize its effect.

I.1.2 NSB as measured by Positron Emission Tomography (PET)

I.1.2.1 Description of PET

Positron Emission Tomography (PET) is an analytical molecular medical imaging technique that has the ability to localize the distribution of specific proteins in target organs / tissues *in-vivo* [8-10]. PET is used to examine the molecular basis of biological functions of receptors and cells [11] and is a distinctive technology in the comparison to that of traditional imaging techniques such as bone X-rays and molecular resonance imaging (MRI) which primarily assesses morphology and function of general structures [12]. In PET, proteins are labeled with specific

radiotracers over time; this implies the development of PET radioligands designated to bind specifically to their targets.

I.1.2.2 Physics of PET

The binding of the radiotracer to the proteins is detected using a PET camera with the target organ / tissue placed in the field of view. This technique requires the utilization of radiolabeled agents emitting positrons as a molecular probe. PET can measure the concentration and movement of a positron emitting isotope in living tissue. ^{18}F and ^{11}C are common radioisotopes used in PET studies. These radioisotopes have very short-half lives (20 minutes for ^{11}C and 109 minutes for ^{18}F) and subsequently more than one scan may be performed in a subject per day. A dose of radiolabeled compound is injected into a subject, followed by scanning the individual using a tomographic system. During the radiotracer decay process, the radionuclide emits a positron which, travels a distance of 2-3 mm before it encounters an electron from the surrounding environment. The two particles combine and annihilate each other resulting in the emission in opposite directions of two gamma rays of 511 keV each. These two gamma rays are then detected by an array of detectors surrounding the subject in the PET camera. Quantification of the regional concentration and the distribution of the injected radiopharmaceutical over time in organs such as the brain can subsequently be determined from the acquired datasets. Data are reconstructed as slices of few a millimeters in thickness to allow clinical read out (Figure I.3).

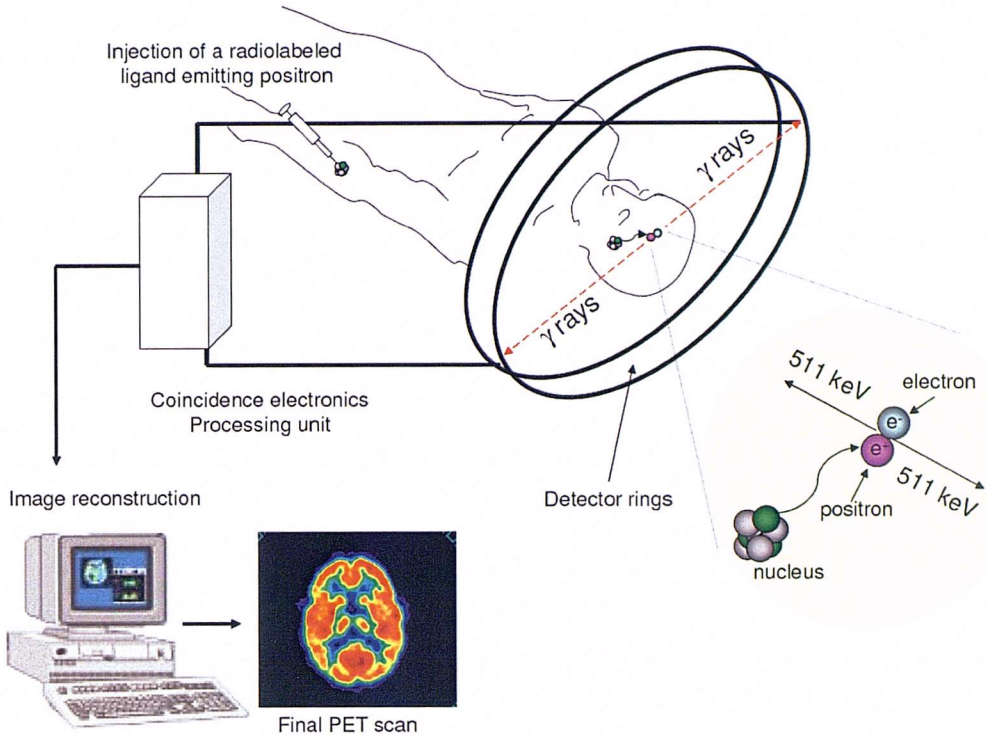


Figure I. 3: Principles of PET. A radiolabeled ligand is injected and spreads throughout the body via the bloodstream. A positron is emitted from the labeled nucleus (^{18}F or ^{11}C) travels a short distance and annihilates with an electron. The collision energy is converted into two γ rays of 511keV traveling at 180° to each other, which are detected by the scanner. The data are then processed and tomographic images reconstructed accordingly.

PET is able to aid in the investigation of molecular mechanisms of human disease and facilitate the development of new drugs [13]. At a molecular level, PET allows the evaluation of binding properties *in-vivo* (see section 1.1.2.3). Several radiotracers have been developed for imaging specific molecular targets such as the brain dopamine system. The neurotransmitter systems, which have been the most extensively studied, are the serotoninergic and the dopaminergic systems [14, 15]. However, there are few appropriate selective radiotracers available for use in humans with a known ability to cross the blood brain barrier (BBB) and gain entry into the brain.

I.1.2.3 The degree of NSB as determined by PET

Accurate determination of neuroreceptor binding properties in the brain requires fitting to a mathematical model. A widely used approach is the three compartment models, in which the ligand concentration is assumed to be homogeneous [16]. The ligand concentration exchanges between compartments (each represents a

physiological space). This model takes into account the free ligand concentration in the plasma and the ligand concentration that is specifically and non-specifically bound in the tissue (Figure I.4).

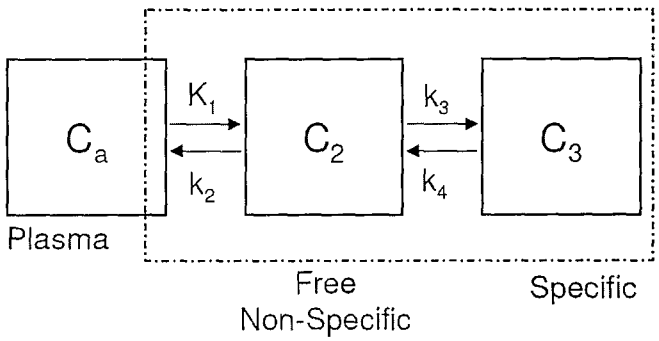


Figure I. 4: Configuration of the three compartment model for neuroreceptor analysis used in PET studies. C_a is the concentration of the ligand in the plasma (arterial compartment), C_2 is the concentration of the free and non-specifically bound ligand, and C_3 is the concentration of the specifically bound ligand. K_1, k_2,k_3 and k_4 are the rate constants for the transfer between each compartments [15].

PET allows the quantification of the binding potential (BP) which is the ratio of the bound radiotracer / radioligand concentration (B) over the free ligand concentration (F). According to the law of mass action, BP is generally given by dividing the total number of binding sites B_{max} by the equilibrium dissociation constant (K_d) of the radiolabelled compound (Equation I.1)

$$BP = \frac{B_{max}}{K_d} = \frac{B}{F}$$

Equation I. 1

Compartments are characterized by distribution volumes *Vi*, which is defined as the ratio of the ligand concentration in the compartment *i* to the free arterial concentration at equilibrium C_a (equation I.2)

$$Vi = \frac{C_i}{f_1 C_a}$$

Equation I. 2

where f_1 is the plasma free fraction of the compound. Hence this equation is applicable to C_2 and C_3 (equation I.3) where:

$$V_2 = \frac{C_2}{f_1 C_a} \text{ and } V_3 = \frac{C_3}{f_1 C_a}$$

Equation I. 3

and the total volume V_T is defined as (equation I.4):

$$V_T = V_2 + V_3$$

Equation I. 4

Equation I.1 states that BP is equal to the ratio of bound concentration to free concentration of ligand. As the bound concentration is C_3, the free concentration is not C_2 but f_2C_2, with f_2 being the free fraction in the non-specific compartment. This leads to equation I.5, where

$$BP = \frac{B_{\max}}{K_d} = \frac{B}{F} = \frac{C_3}{f_2 C_2}$$

Equation I. 5

At equilibrium the concentration of the free ligand in the plasma equals to the concentration of the free ligand in the tissue, i.e. the brain (equation 1.6):

$$F = f_1 C_a = f_2 C_2$$

Equation I. 6

Therefore, a new expression for BP can be written (equation 1.7):

$$BP = \frac{B_{\max}}{K_d} = \frac{B}{F} = \frac{C_3}{f_1 C_a} = \frac{C_3}{f_2 C_2} = V_3$$

Equation I. 7

f_1 is considered as being constant across experiments [17], hence BP is defined as BP' (equation I.8) :

$$BP' = \frac{f_1 B_{\max}}{K_d} = \frac{f_1 B}{F} = \frac{C_3}{C_a} = V'_3$$

Equation I. 8

Similarly, V_2 can be rearranged to (equation I.9):

$$V_2 = \frac{C_2}{f_1 C_a} = \frac{C_2}{f_2 C_2} = \frac{1}{f_2}$$

Equation I. 9

This leads to a third expression of BP (equation I.10):

$$BP'' = \frac{f_2 B_{max}}{K_d} = \frac{B_{max}}{V_2 K_d} = \frac{f_2 B_{max}}{F} = \frac{C_3}{C_2} = V''_3$$

Equation I. 10

This quantity obtained from equation I.10 is used to quantify the degree of non-specific binding.

C_2 is assumed to be constant in all brain regions [17]; therefore C_2 can be determined from reference regions devoid of specific receptors. Thus BP'' can be obtained from the difference between the total concentration $C_T = C_2 + C_3$ from the region of interest containing the receptor and the reference region.
Therefore BP'' can also be represented by the specific (SB) to non-specific coefficient (NSB) (equation I.11):

$$BP'' = \frac{SB}{NSB}$$

Equation I. 11

A high BP'' value is expected for compounds with low non-specific binding.

An ideal brain penetrant radiotracer can be chosen according to many criteria. The radiotracer should be easy to label and pass toxicological profiling. Its metabolism should not produce radiolabelled metabolites or pharmacologically active unlabelled metabolites, which are centrally penetrant. The selectivity and the affinity for the target protein should be high, along with a high target protein density in order to detect a useful quantifiable signal using PET. Additionally, it should cross the blood brain barrier (BBB), thus implying an appropriate lipophilicity (log P 1.5-4.0), and exhibit a high BP'' value i.e. a low degree of non-specific binding [18].
Figure I.5 illustrates PET images for two radiotracers specific for the D_2-dopamine receptor, raclopride and remoxipride. A baseline is made by injecting ^{11}C remoxipride (figure I.5a) and ^{11}C raclopride (figure I.5b). This step shows the binding of the molecule to the proteins of interest, here the D_2-dopamine receptor in the striatum, plus the labeling of non-specific sites. Then a pretreatment is made by injecting remoxipride, which has a lower affinity to the receptor (K_i=200nM). Remoxipride exhibits little specificity to the D_2-dopamine receptor, and also binds to different regions of the brain.

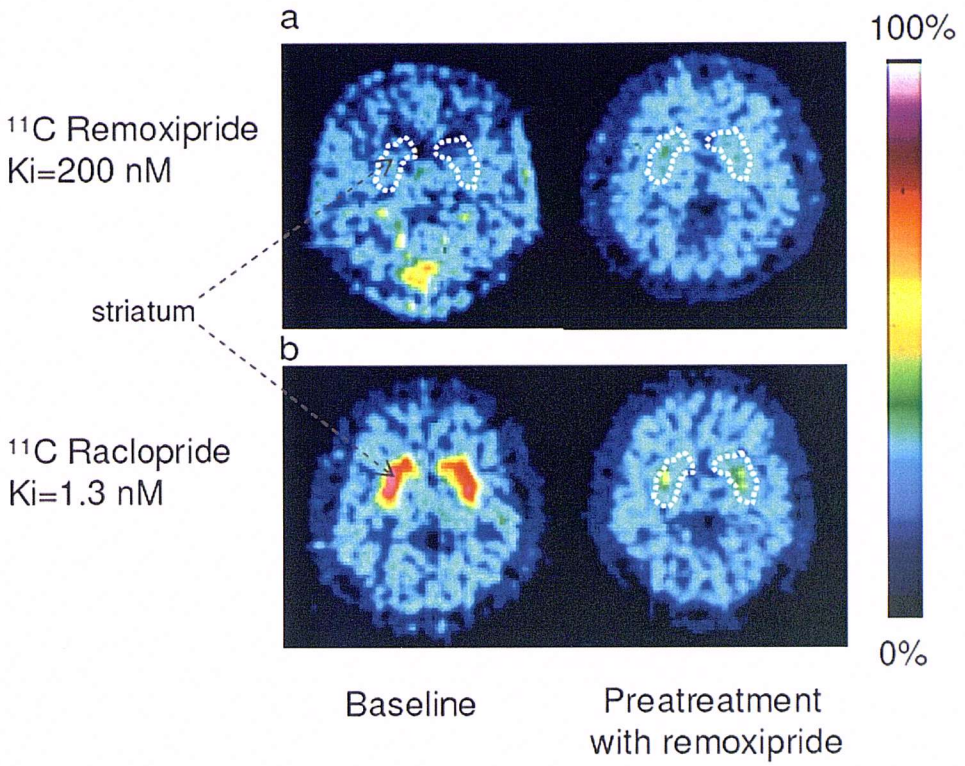


Figure I. 5: PET images for radiotracers exhibiting high specific binding (raclopride system) and high non-specific binding (remoxipride system). Both molecules are specific to the D_2-dopamine receptor, but raclopride exhibits higher specific binding (Courtesy of Pr.A.D.Gee).

PET is a very useful tool for the investigation of the NSB *in-vivo*; however it gives no information of the origin and the molecular basis of the NSB of drugs.

I.1.3 Molecular basis of NSB and lipophilicity

Lipophilicity is a critical parameter for the permeation of the BBB by central nervous system (CNS) drugs [19]. Crossing the BBB is complex as it is formed by brain capillary endothelial cells that form tight junctions which separate the brain from the blood periphery (Figure I.6).

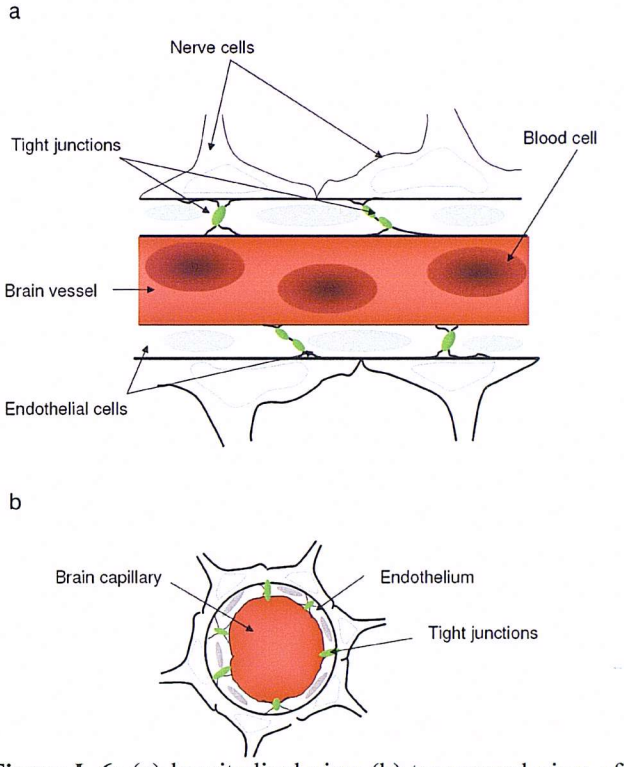


Figure I. 6: (a) longitudinal view (b) transversal view of the BBB. Brain endothelial cells are joined by tight junctions that form a highly impermeable barrier.

The BBB exists within 400 miles of capillaries that course through the brain [20] and limits to a certain extent the delivery of drugs to the CNS by it high impermeability. In addition, the presence of specific metabolizing enzymes and efflux pumps located within the endothelial cells rejects exogenous molecules out of the brain. Drug molecules can traverse the BBB by passive diffusion; this requires an appropriate lipophilicity (See section below). Molecules can also undergo active transport across the BBB [21]. At a molecular level, the BBB consists of a lipid bilayer [22]. Investigation of lipid composition from *in-vitro* BBB systems involving endothelial cell lines has been undertaken. The BBB lipid composition consists of glycosphingolipids, glysosylceramides, sphingomyelins, and phosphatidylcholine lipids [23-25]. The lipid composition in these cells lines is inhomogeneous from one

cell line to the other, nevertheless, it has also been established that phosphatidylcholine (PC) and phosphatidylethanolamine (PE) lipids are present in varying ratios, and that a relatively high fraction of long polyunsaturated fatty acids is present [26, 27].

I.1.3.1 Lipophilicity measurements

Lipophilicity as defined by the International Union of Pure and Applied Chemistry (IUPAC) is the affinity of a compound towards a lipophilic environment. Parameters such as the molecular weight, size, and hydrogen bonding capacity are involved in its characterization. Several methods such as experimental and computational methods exist to measure a drug's lipophilicity. Reviews on computational methods can be found in references [28-30]

One of the most popular experimental methods is the liquid-liquid partitioning between two solutions, referred to the shake-flask method. Lipophilicity is measured as the partition coefficient of the compound between a highly polar solvent such as water and buffer and a highly non-polar solvent such as octanol, heptane, or hexane [31]. Once the partitioning has occurred, the unbound fraction is measured by analytical or / and spectroscopic techniques. The log of the compound concentration in octanol and water / buffer (log $P_{oct\ /\ water}$) is given as the measure of lipophilicity. Highly lipophilic molecules exhibit a log $P_{oct\ /\ water}$ value higher than 6 [32]. This method was first used in 1900 to establish a linear relationship between narcotic activity and an oil-water partition coefficient [33], it has been concluded that some biological activities were observed within a certain range of lipophilicity.

Log $P_{oct\ /\ water}$ is the most frequently exploited property in structure activity relationship (SAR). Its use has led to a huge log $P_{oct\ /\ water}$ data base available for pharmaceutical compounds [32]. The use of log $P_{oct\ /\ water}$ is also assumed to mimic the partition coefficient of compounds within biological membranes, in particular it is thought to be a model for crossing the BBB [34]. Nevertheless, log $P_{oct\ /\ water}$ refers to the partitioning of only neutral species and does not take into account any charged groups on the drug molecule nor its hydrogen bonding capacity which leads to an enormous discrepancy between the partitioning of drugs between octanol and water,

and partitioning in biological membranes. Octanol fails to mimic biological membrane features [35] (see section I.2), such as their ionic interactions. Membranes are proton acceptors as a result of the polar and negative charged surface of the phospholipids with varying headgroups. These features are of importance in characterizing the membrane environment. However correlation measurements between log $P_{oct / water}$ and partition coefficients using lipid membranes in the forms of vesicles showed contradictory results ranging from poor correlations [36, 37] to more accurate correlations [38].

I.1.3.2 Prediction of the NSB for CNS drugs

Drug lipophilicity has been extensively studied and analyzed to probe the NSB phenomenon related to crossing the BBB. As said above, relationships have been established between drug's physicochemical properties and SAR, i.e. CNS chemical properties and the BBB crossing. In this regard, the Lipinski rule of five has been developed [39] to probe successful ligands. This rule of thumb describes successful brain penetration by taking into account various parameters such as the molecular weight, log $P_{oct / water,}$ and the hydrogen bonding capacitiy of the CNS drug. Successful CNS drugs are characterized by: a molecular weight smaller than 500 $g.mol^{-1}$, a log $P_{oct / water}$ smaller than 5, and less than 5 H-bond donors (expressed as the sum of OHs and NHs). Diffusion across the BBB is dependent on these factors.

Although a linear correlation exists between passive diffusion across the BBB and lipophilicity of CNS compounds *in-vitro* [40]; a highly lipophilic compound can also increase the non-specific binding *in-vivo*. This is observed by a parabolic feature (Figure I.7) [41]. Figure I.7 represents the correlation between Log P for spiperone (SPIP), a successful ligand used in many PET studies, and SPIP based molecules. A significant increase of the brain uptake is seen in N-methyl-SPIP, whereas increasing the alkylation considerably reduces the brain uptake. This is not unexpected since increasing SPIP molecular weight by alkylation increases the lipophilicity, and therefore the NSB [41].

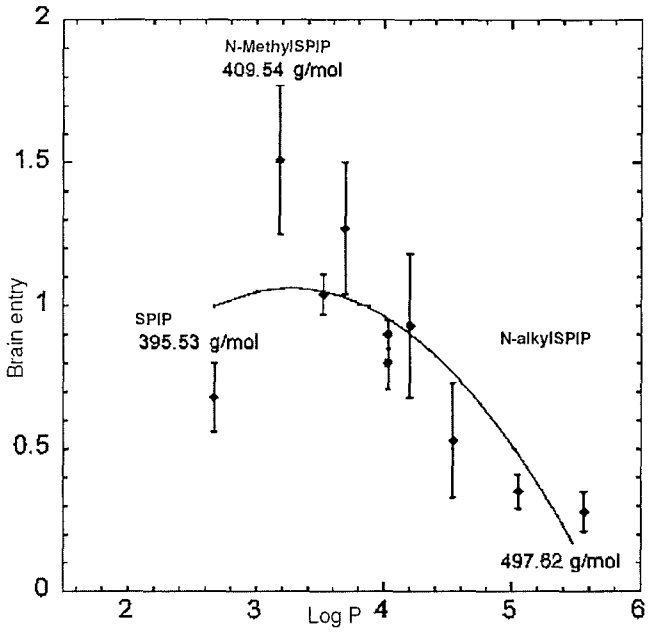


Figure I. 7: correlation of Log P values and rate brain uptake for spiperone and N-alkyl spiperone derivatives. Figure adapted from reference [41].

The lipophilicity has a major impact on the CNS PET radioligands. This quantity is constantly measured when a new compound is designed and synthesized and usually lies in the range of 1.5–3 for useful radioligands. However, lipophilicity alone is not a sufficient parameter to guarantee brain entry with a high degree of specific binding. A more systematic study of small molecule physicochemical properties and their interaction with biological membranes may provide a valuable insight into the poorly understood phenomenon of non-specific binding.

I.1.4 Application to Cationic Amphiphilic Drugs (CAD)

CNS drugs represent the fastest growing therapeutic field in pharmaceutical research. It appears that these molecules share common structural features as they contain a hydrophilic moiety consisting of one or more primary substituted nitrogen, and a hydrophobic moiety that consists of an aromatic or aliphatic ring, potentially substituted by a halide moiety. These molecules are also protonated at physiological pH on the nitrogen (pk_a~7-9) [42-44]. Therefore, CNS drugs belong to the Cationic Amphiphilic Drug (CAD) family. Examples of CADs acting as successful CNS drugs are given in figure I.8.

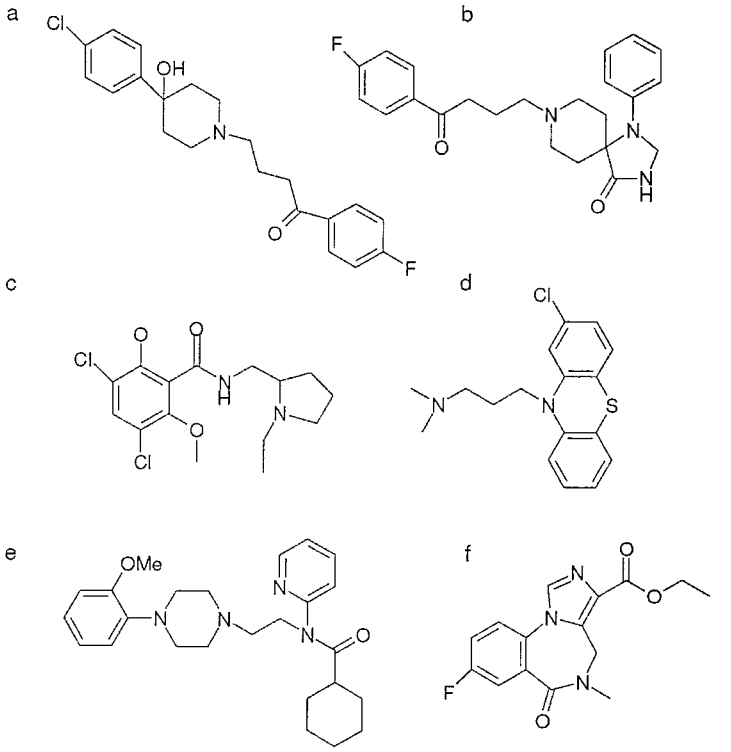


Figure I. 8: Examples of CADs of the CNS drug family. (a) Haloperidol (b) Spiperone (c) Raclorpide (d) Chlorpormazine (e) WAY (f) Flumazenil

All drugs listed in figure I.8 are specific to neurorecptors such as D_2-dopamine receptors, benzodiazepine receptors, and 5-HT_2 serotonin receptors and all exhibit different good specific binding ratios *in-vivo*, implying that they have crossed the BBB readily, with log P values being within the right range to give a specific signal. Physicochemical characteristics of these molecules are given in table I.1.

CAD	Log $P_{oct/water}$	pK_a	MW ($g.mol^{-1}$)
WAY	3.1	8.6	422.64
Flumazenil	1.1	7.9	303.29
Spiperone	1.7	8.3	395.47
Raclopride	1.2		347.32
Haloperidol	2.2	8.7	375.86
Chlorpromazine	5.8	8.6	355.33

Table I. 1: CNS CADs physicoproperties (from ref [42-45].

CADs exhibit different lipophilicities and remain poorly water soluble. When they interact with membranes, they tend to migrate to the bilayer interface due to the hydrophobic effect, and are able to form lipid / CAD conjugates [38, 46]. This has

been specifically studied with WAY, haloperidol and spiperone (please refer to chapter 3 for more details).

CADs bind to membranes, readily cross the BBB and exhibit a relatively high lipophilicity associated to a high specific to non specific binding ratio. Hence, it is getting increasingly evident that the interactions of CADs with membranes are very complex and have to be considered in order to answer the following questions: What are the effects that govern CADs interactions with membranes? How does the membrane contribute to non-specific binding?

I.2 Biological membranes and membrane biophysics

I.2.1 Cell membrane

Cell membranes are structures that compartmentalize cells and their intracellular components such as nuclei, endoplasmic reticulum and mitochondria [47]. They are essential structures that maintain a difference between the cytosol and the extracellular environment and regulate the concentration of ions and metabolites. Cell membranes all have a common feature: they are all formed by the non-covalent assembly of various amphiphilic phospholipids, in different proportions organized in bilayers and associated to peripheral or embedded proteins [48, 49]. The lipid bilayer provides the basic structure of the membrane and acts as an impermeable barrier to the passage of most solutes such as ions, sugars and peptides, though specific transport processes exist to allow them to cross the cell membrane [50]. Transportation processes will be defined in section I.2.2. Biological membranes contain hundreds of lipid components [51] with the exact lipid composition varying between membranes and being asymmetric in the outer and the inner leaflet. Species such as sphingomyelins (SM) and phosphatidylcholine (PC) lipids are predominant in the outer layer, and phosphatidylserine (PS) and phosphatidylethanolamine (PE) are localized mainly in the inner layer [52].

Biological membranes were described in 1972 by Singer and Nicholson as forming a "fluid mosaic" system [53] where the lipids arrange themselves to form a two dimensional fluid system where lipids and proteins are able to diffuse freely in the plane of the bilayer and exhibit rapid lateral diffusion (Figure I.9).

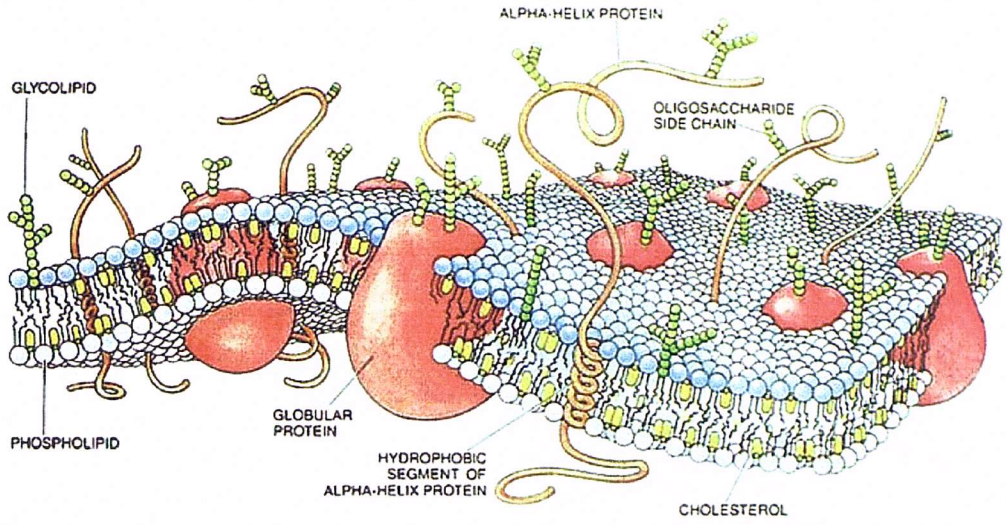


Figure I. 9: A cartoon representing the plasma bilayer as a fluid mosaic system where lipids and proteins can diffuse freely in the plane of the bilayer. (fromwww.ncnr.nist.gov)

In such structures, lipids are also able to undergo free rotation around their vertical axes (~10^{-7}s) and diffuse within the plane of the bilayer (~10^{8}cm^{2}.s^{-1}) [54]. Lipids can exchange between the outer and the inner layer via "flip-flop", this process is facilitated by lipid flippases, as the movement of lipids across the bilayer is energetically unfavorable [55].

Limitation of this model comes from the ability of specific phospholipid types to segregate into domains and recruit specific receptors [56]. It is believed that these domains are important in signalizing processes where the receptors are activated, but a big controversy still exists about the nature of these domains and their physiological implication [57], even if they were detected soon after the development of the fluid mosaic model of lipid membranes [58, 59].

I.2.2 Transport models across membranes

It is of great importance to the cell to be able to transport molecules for its own survival [47]. Given the importance of membrane transport, cells utilize a wide range of transport mechanisms which fall into three categories: simple diffusion, facilitated diffusion, and active transport. Although there are numerous features that do not allow the free diffusion of molecules across the lipid bilayer, under certain circumstances free diffusion is mainly seen for drug molecules.

I.2.2.1 Passive transport

Simple diffusion means that molecules can pass directly through a membrane. Diffusion is always down a concentration gradient without the expenditure of energy. This limits the maximum possible concentration of the molecule inside the cell, or outside the cell if it is a waste product. The effectiveness of diffusion is also limited by the diffusion rate that is slowed down due to the complexity of biological membranes.

The rate of diffusion of a molecule from two compartments separated by a homogeneous lipid bilayer follows Fick's law [60]:

$$dQ/dt = (DAK_p/d)(C_1 - C_2)$$

Equation I. 12

where D is the diffusion coefficient, C_1 and C_2 the species concentration in the outer and inner compartment respectively, A the surface area of the membrane, K_p the partition coefficient and d the membrane thickness.
Since D, K_p and d are constant for a given drug-membrane system and $C_1 >> C_2$, the diffusion rate can be simplified to:

$$dQ/dt = PC_1$$

Equation I. 13

where P is the permeability constant. Greater P leads to faster equilibrium.
Many CNS drugs are believed to transverse the BBB by passive diffusion as a result of their favorable lipophilicity [61].
Although diffusion is an effective enough transport mechanism for lipophilic substances, the cell must utilize other mechanisms for the transport of polar compounds.

I.2.2.2 Facilitated transport

As some molecules are too big or too polar to diffuse freely through the bilayer, their diffusion is facilitated by transport intermediates [62]. Facilitated diffusion is a process of diffusion where molecules cross membranes with the aid of integral membrane proteins such as ion transporter or glucose transporters [63]. After the binding of the molecule, the protein changes its shape and allows the molecule to reach the other side of the membrane. Facilitated transport is driven by a gradient of concentration and does not require the expenditure of energy.
Penicillin [64], biotin [65], dopamine and morphine are examples of drug molecules that are transported via facilitated transport.

I.2.2.3 Active transport

Active transport is a process that requires energy as it goes against a gradient of concentration. It requires the presence of a transmembrane protein such as the P-glycoprotein, which avoids toxic compounds from entering the brain [66].

The three types of transport described above are represented on figure I.10.

.

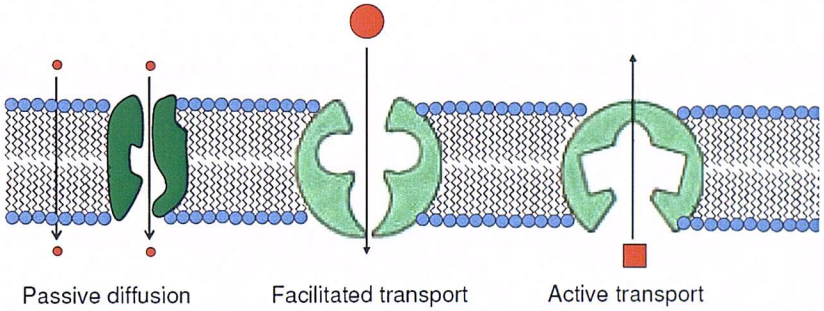


Figure I. 10: Transport mechanisms across membrane bilayers. Passive diffusion follows a gradient of concentration and facilitated transport is mediated by a carrier protein. Active transport goes against a gradient of concentration and requires expenditure of energy.

Substances such as hormones can diffuse through the hydrophobic core of the bilayer whereas molecules like neurotransmitters bind preferentially to their specific receptors.

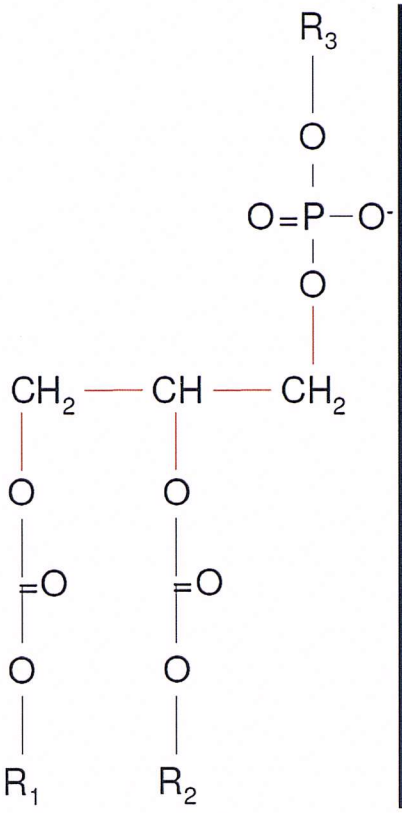
I.2.3 Model membranes, bilayer properties and structure

The complexity of the plasma membrane has led to the development and use of model membranes, simplified to one or two lipid species. Analysis of the component in the model membrane leads to a better understanding of the plasma cell membrane. The most common model membranes can be classified into categories such as monolayers, bilayers, giant vesicles and inverted structures [67-69]. Structural data can be obtained from model membranes by using complementary techniques such as Small Angle X-ray Scattering [67], Electron Spin Resonance (ESR) [70], Solid-State Nuclear Magnetic Resonance (SS-NMR) [71, 72], Fourier Transform Infrared Spectroscopy (FT-IR)[73], and fluorescence; these can also be used to study biological events such as binding of molecules to membranes.

I.2.3.1 Lipid description

Lipids are surfactant molecules that consist of a polar entity, which is a headgroup and a non-polar entity corresponding to the hydrocarbon tail. Three main classes of lipids exists in cell membranes, the glycerophospholipids, sphingolipids and sterols [47].

The lipids investigated in this work belong to the glycerophospholipid family. They are glycerol-based phospholipids with saturated or unsaturated fatty acids esterified to the glycerol backbone. The phosphate headgroup can vary with the diacyl-phosphatidyl base; this produces a variety of lipid headgroup species (Figure I.11).



R_3	Headgroup
—H	Phosphatidic Acid (PA)
NH_3+	Phosphatidylethanolamine (PE)
N^+	Phosphatidylcholine (PC)
NH_3+ $COO-$	Phosphatidylserine (PS)
OH OH	Phosphatidylglycerol (PG)
OH OH HO HO OH	Phosphatidylinositol (PI)

Figure I. 11: Glycerolipid structure that are present in biological membranes. The glycerol backbone is represented in red. R_1 and R_2 represent the saturated / unsaturated fatty acid chains and R_3 the headgroup.

Lipids can adopt various structures varying with the type of fatty acid and headgroup. PE and PC lipids are zwiterrionic lipids with no net charges, whereas PG, PS and PI are anionic lipids with a net negative charge.

I.2.3.2 Forces in the bilayer

When dissolved in water the lipids arrange themselves so that the polar heads are in contact with the water and the hydrocarbon tails are associated together due to the hydrophobic effect [74]. As described above; lipids have different structures and shapes so when associated they will form different mesophases that are characteristic [75, 76] (see section I.2.3.4). The formation of a mesophase is controlled by numerous forces that are present in the bilayer at the headgroup and hydrocarbon chain region.

A bilayer is formed by two monolayers that sit back to back, and its formation is driven by attractive forces such as the hydrophobic effect which is stabilized by

hydrogen bonding around the headgroups and van der Waals interactions. At the interface, the hydrophobic effect acts to reduce the contact between the hydrocarbon chains and the water. Repulsive forces are also found both in the headgroup and chain regions such as the pressure in the chain region that is mainly due to the trans / gauche rotation in the C-C bonds, and the hydrational forces, steric and repulsive interactions around the headgroup [68, 75]. Lateral forces in a bilayer and a lateral stress profile across a lipid are represented on figure I.12, where *t(x)* is the distribution of the lateral stress, and *x* the depth in the membrane.

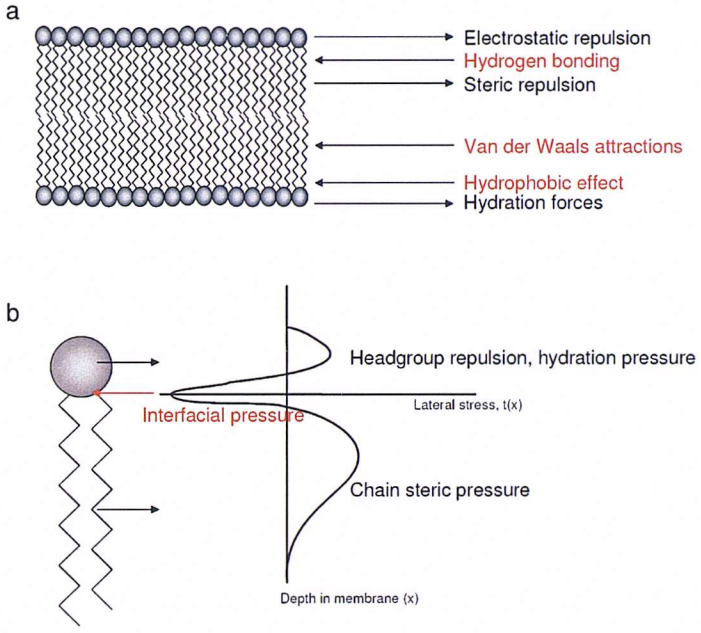


Figure I. 12: (a) The lateral forces within a bilayer. (b) The lateral stress profile across a lipid monomer. The headgroup and chain pressure are repulsive lateral forces.

The lateral pressure resulting from the forces mentioned above is zero at equilibrium (equation I.14).

$$\int t(x)dx = 0$$

Equation I. 14

However, the first moment of the lateral pressure profile is not equal to zero. This is indicative of a torque being stored in a monolayer (equation I.15).

$$\int t(x)xdx \neq 0$$

Equation I. 15

The torque that is stored within the bilayer is referred as the stored curvature elastic energy.

I.2.3.3 Interfacial curvature

Amphiphiles impart a desire for interfacial curvature. As the distribution of lateral pressure is non-uniform in the bilayer, they bend toward the chain region if the headgroup pressure is dominant; or toward the water if the repulsive forces due to the chains are dominant. However, because bilayers are composed of two superimposed monolayers, they will want to bend in the same direction, leading to a frustration state, until they reach a phase which is the most favourable energetically.

To describe interfacial curvature, we first have to define the geometrical concepts of membrane curvature. Biological membranes are described as a two-dimensional surface that spans three dimensional space. The interfacial curvature c at a point p in the monolayer is defined by a normal to the surface, as shown in figure I.13. R_1 and R_2 are the principle radii of curvatures and the principle curvatures c_1 and c_2 are their inverse values (equation I.16). c_1 and c_2 can be obtained as the maximum and minimum values of curvatures respectively [67, 68].

$$c = \frac{1}{R}$$

Equation I. 16

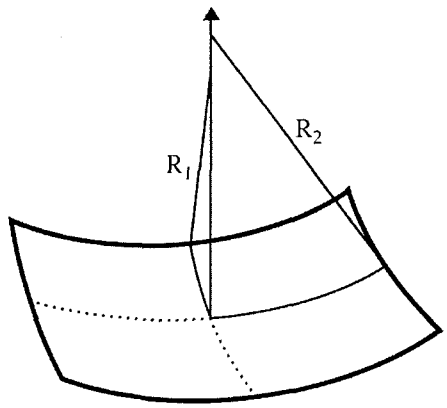


Figure I. 13: The curvature of a surface is characterized by a maximum and minimum value of curvature such as $c_1=1/R_1$ *and* $c_2=1/R_2$. (Figure adapted from ref [68]).

The total curvature J and the mean curvature H are then defined by equation I.17 and equation I.18 respectively:

$$J = (c_1 + c_2)$$

Equation I. 17

$$H = \frac{1}{2}(c_1 + c_2)$$

Equation I. 18

and the Gaussian curvature is defined by

$$K = c_1 c_2$$

Equation I. 19

The shape of the surface can be determined from the mean and Gaussian curvatures. For example, a flat surface has a zero mean curvature; therefore the Gaussian curvature is zero too. The mean curvature changes in a cylinder, but its Gaussian curvature remains zero [68, 77].

To define the sign of the membrane curvature we need to distinguish between the two sides of the surface i.e. the monolayer. Any lipid monolayers have curvature that will depend on the shape and size of the polar headgroups and tails. By convention monolayers that bend towards the polar headgroup have a negative curvature and inversely monolayers that bend towards the tails have a positive curvature (figure I.14).

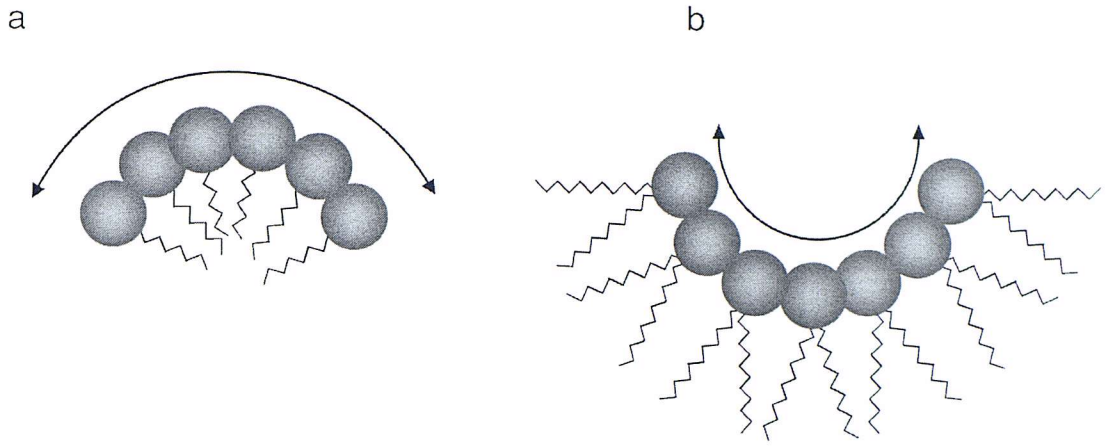


Figure I. 14: Examples of (a) positive and (b) negative curvatures.

It is reasonable to classify lipids into shapes according to their spontaneous curvature [78]. The shape of lipids or "packing parameters" S is defined by equation I.20:

$$S = \frac{v}{a_0 l_c}.$$

Equation I. 20

a_0 is the headgroup surface area, l_c the lipid chain length, and v the molecular volume of the chains. The shape of lipid aggregates in water is directly related to packing parameter S. Thus if the monolayer has a negative spontaneous curvature the lipid molecular shape is conical (Type II). The positive curvature is associated with molecules with the shape of an inverted cone (type I) and finally molecules with a cylinder shape will be considered as type 0 molecules that remain flat in a bilayer (Figure I.16) [67, 68, 77] . An estimation of lipids spontaneous curvature J_s can be found in reference [77]

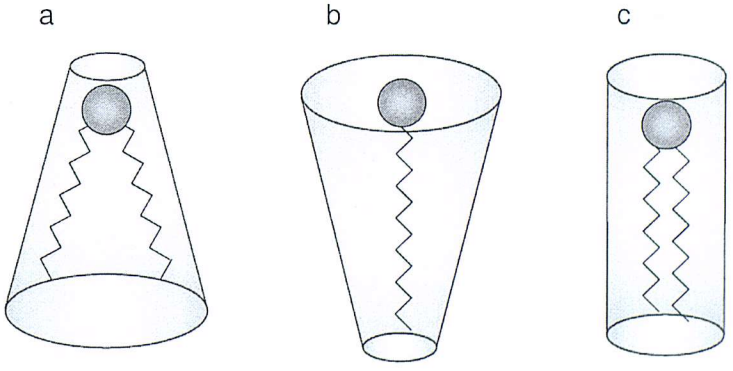


Figure I. 15: Shape of lipid. (a) type II lipids are represented as an inverted cone, (b) type I lipids as a cone and (c) type 0 lipids as cylinders,

The estimation of the membrane curvature is based on the bilayer thickness d. The curvature *c* is said to be large when the radius of curvature R is much larger than d and inversely.

I.2.3.4 Stored curvature elastic energy

In a bilayer, the two monolayers are forced to sit back to back. When type I and type II lipids are, they both tend to curve away or towards the water according to their spontaneous curvature. Deformations from the spontaneous state lead to a deviation from the spontaneous state to the frustrated state. These deformations have an associated energy cost (g_C) dependent on the mean and Gaussian curvatures *H* and *K*. The energy cost per unit area is given by the bending modulus κ and the Gaussian modulus κ_G. These parameters were combined by Helfrich [79] to give the curvature elastic energy per unit area g_C for a membrane (Equation I.21):

$$g_C = 2\kappa(H - H_o)^2 + \kappa_G K$$

Equation I. 21

where H_0 is the spontaneous mean curvature.

The first term of the equation describes the energy that is required to deform a monolayer from its spontaneous shape. The second term is characterized by the Gaussian elastic moduli κ_G that describes the energy accumulated in the monolayer in response to the creation of the Gaussian curvature [77].

Instinctively if the spontaneous curvature of the outer lipid monolayer is larger than the inner one, the bilayer tends to have a positive curvature with the direction of the bilayer curvature controlled by the outer monolayer and vice versa. If the tendencies of the monolayers to bend are balanced, than the bilayer membrane curvature will equal zero.

I.2.3.5 Bilayer mesophases

The four main lyotropic mesophases are the micellar phase, the lamellar phase, the hexagonal phase and the bicontinuous cubic phase; which are described below [67, 76].

- *Micellar phase:*

Micelles are spherically shaped entities formed by amphiphiles. A positive spontaneous curvature facilitates the formation of micelles in a polar solvent such as water or buffer. According to the amphiphiles shape, there are two micelle types: Type I and Type II. Type I micelles (also called normal micelles) occur when the hydrocarbon chains are associated together and the polar headgroups are pointing towards the water. Type I micelles are formed by conical amphiphiles (e.g. monoacyl-chained lipids lyso-PC (LPC)) [80]. Type II micelles are structured so that the water is enclosed within the polar headgroup. Type II micelles occur with some double-chained amphiphiles such as DOPE (figure I.16). Micelles are all of the same size for a given hydrocarbon chain length. The more concentrated the micelle the greater their ability to dissolve non-polar compounds.

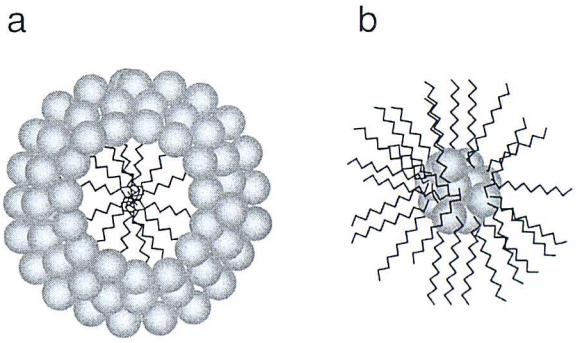


Figure I. 16: Representation of a (a) normal type I micelle, and (b) inverted type II micelle.

- *Lamellar phase*

At higher concentrations the amphiphiles aggregate to form built mesophases of bilayer systems separated by water layers. The lamellar phase is organised so that the hydrophobic tails are facing each other and the polar head groups are facing the water.

There are three main types of lamellar phases: the L_α (fluid), L_β (gel) and L_c (crystal). All three are temperature dependant [75]. The L_α fluid lamellar phase occurs at high temperatures, when the hydrocarbon chains are melted leading to a high degree of disorder with a large proportion in the gauche / trans state. This low viscosity phase allows the free lateral diffusion of molecules. The molecules have typically lateral diffusion constants of 10^{-12}-10^{-11} $m^2.s^{-1}$, and have long–axis rotational correlation times of 10^{-9}-10^{-8} s [81]. The L_α fluid lamellar phase is used to mimic biological plasma membranes properties, as cells keep their membrane bilayers in the L_α fluid lamellar phase until a certain point [75]. When cooling, the L_β gel phase arises. The hydrocarbon chains are all in a trans conformation. Finally the L_c crystal phase occurs when the chains are all frozen into the trans position. The L_β and L_C phases are also characterised by a higher viscosity relative to the L_α phase that reduces the motion of molecules. The L_o liquid ordered phase is another type of lamellar phase, which appears when cholesterol is added to the bilayer [82]. The acyl chains are constrained and ordered but the lateral diffusion is still comparable to the L_α phase (Figure I.17).

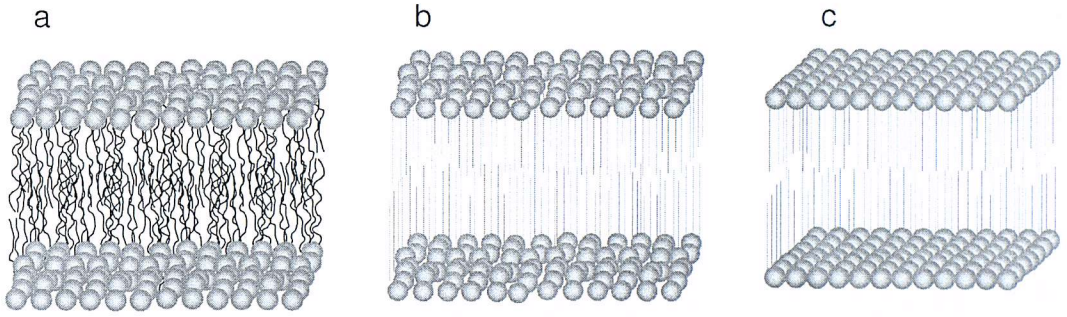


Figure I. 17: Cartoon representing (a) the L_α fluid lamellar phase, (b) the L_β gel phase, (c) the L_C lamellar crystal phase.

- *Hexagonal phase*

The hexagonal phase is a phase that is involved in several biological processes including cell division and membrane fusion [83]. This phase is formed by cylindrical aggregates packed in a two-dimentional lattice where the chains remain fluid [76]. Lipids can produce hexagonal shapes when the spontaneous curvature has a value J_s = 1/2R. There are two types of hexagonal phases: the H_I (normal) hexagonal phase and the H_{II} (inverted) hexagonal phase. Lipids having small weakly hydrated headgroups

and attractive headgroup-headgroup interactions such as PE, form preferentially H_{II} phases. (Figure I.18)

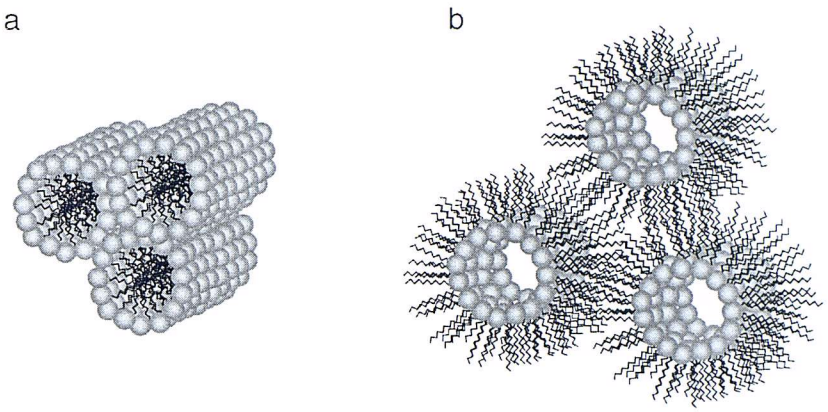


Figure I. 18: Cartoon representing the (a) normal hexagonal H_I and (b) the inverse hexagonal H_{II} phase.

- *Bicontinuous cubic phases*

Bicontinuous cubic phases are complex systems, where the bilayer is draped over a periodic minimal zero surface with mean curvature at all points, and where the amphiphiles and solvent can diffuse in three dimensions. Cubic phases are extensively investigated for elucidating the mechanism of cell membrane fusion [84] and for gene and drug delivery applications [85, 86] (Fig I.20).

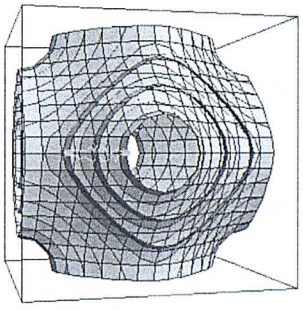


Figure I. 19: Representation of the Im3m bicountinuous cubic phase (from ref [87]).

I.2.3.6 Electrostatic properties of membranes

Charged lipids are found in biological membranes. Lipids such as PS, PG and PI are present give a net negative charge on biological membranes [88]. Electrostatic interactions are very important as they are involved in several biological processes such as cell adhesion [88]. These interactions are also important in membrane biology, as they affect conductance of channels in membranes [89], ion transport processes [90], and the catalytic properties of certain enzymes [91], although these interactions can be screened because of the high salt concentration in biological systems.

Charges associated with the membrane surface give rise to electric potentials, which participate to biological processes and interactions. Membrane potentials are described in chapter 2 (section II.3.1).

Charges on membranes create electric fields which act on and depend upon the distribution of ions near the membrane surface. Electric charges also regulate the adsorption of charged species [88], and consequently the binding of cationic amphiphilic drugs as they are protonated at physiological conditions (pH=7.4).

Many membrane structural properties depend on electrostatic interactions. A bilayer that is immersed in an ionic environment such as a buffer has the property of attracting a cloud of opposite charges that will form "the diffuse electric double layer" with a thickness equal to the Debye length [92, 93]. This is controlled by the coulombic surface-ion interaction. In other words, the double layer is appearing when an ion with a distinctive charge is in a bulk aqueous phase containing an electrolyte; it will then attract counterions, and repel co-ions, and produce an ionic atmosphere in its vicinity. The Debye length λ_D equals 1nm for a 100 mM salt solution, (Equation I.22)

$$\lambda_D = \sqrt{\frac{\varepsilon_0 \varepsilon_r RT}{4\pi F^2 \sum C_i Z_i^2}}$$

Equation I. 22

where ε_0 is the permittivity of the free space, ε_r the dielectric constant of the solution, F the faraday constant, R the gas constant, T the temperature, and C_i the ions concentration with a valence of Z_i.

The diffuse double layer is composed of one layer where the counterion is strongly bound: the Stern layer and a layer where it diffuses away of the surface, the diffuse layer (Figure I.20). Gouy and Chapman [92] have extensively described these electrostatic interactions and predicted the statistical tendency of the counterions to diffuse away from a region of high concentration, with the membrane potential varying with distance from the surface.

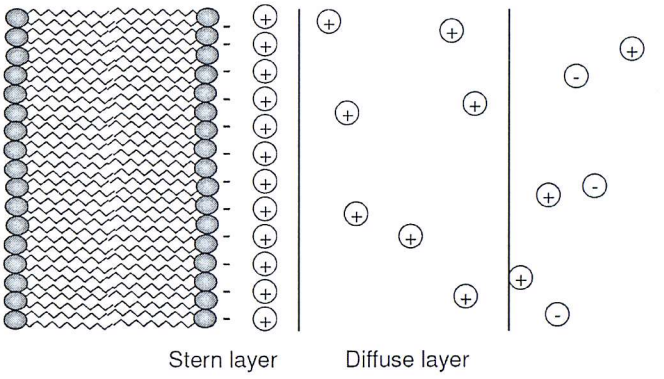


Figure I. 20: Representation of the Stern layer and the diffuse layer (Adapted from ref [87]).

As part of transverse interactions, electrostatic forces act between adjacent bilayers and tend to stabilize bilayer mesophases that were described in section I.2.3.4 [94].

1.3 Cationic Amphiphilic Drug (CAD) interactions with membranes.

Most cellular activities involve membrane based ligand interactions and it is assumed that most ligand binding occurs with membrane-embedded proteins. However, a large portion of these ligands also interact with the plasma membrane in particular in the non-specific binding issue. Consequently plasma membranes are potentially targets for drugs of different therapeutic classes.

1.3.1 CNS drugs interaction with membranes

Amphiphilic molecules affect membrane bilayer properties and induce membrane disorders in the lipid packing, which may lead to the expansion, fluidization, and permeabilisation of the membrane [95, 96]. Binding of the drugs is affected by the membrane heterogeneity, phospholipid headgroups, chain types, and also temperature [97].

Drugs can reach the phospholipid hydrocarbon chain, this is the case for anesthetics such as lidocaine [98], and reorganize the headgroup orientation, as seen by ^{31}P solid state NMR of antidepressants such as imipramine [99]. Amphiphilic drugs also bind to the water-membrane interface, and alter membrane's physicochemical properties and the lateral stress profile [100]. For example, anti-arrhythmic drugs bind to the bilayer interface, inducing a hexagonal packing of the hydrocarbon chains and disruption of DMPC bilayers as detected by X-ray scattering [101].

Interestingly, it appears that binding at the interface and changing the lateral organization of the bilayer also modulates the activity of membrane proteins such as the opiate receptor which is a target of neuroleptic amphiphilic drugs [102]. Amphiphilic drugs bind to phospholipid bilayers specifically, as the observed change in the lateral stress profile is dependant on the structure of the drug [97]. The

following sections describe how popular CNS drugs such as CPZ and HPD interact with membranes, *in-vitro* and *in-vivo*.

1.3.1.1 Chlorpromazine (CPZ)

The interaction of CPZ with membranes has been extensively reported in the literature. CPZ is an antipsychotropic drug of the phenothiazine group which is believed to antagonize neuronal D_2-dopamine receptors. CPZ is a CAD which partitions effectively in both biological and model membranes, with a hydrophobic tricycling ring partitioning into the bulk hydrocarbon phase of the bilayer system, and a hydrophilic propylamine tail interacting with the phospholipid head group [103]. CPZ is known for perturbing the shape of human erythrocytes by creating an "intrabilayer non-bilayer phase" [104]. At concentrations above 40 μM, CPZ makes the cells permeable for low molecular weight molecules and at 100 μM CPZ makes a 14 Å hole in red cell membranes [105].

In model membranes, CPZ perturbs the bilayer properties in the headgroup and the chain regions [106-108] and also affects electrostatic properties [109]. This CAD increases the lipid headgroup mobility and strongly binds to charged lipids such as PS [110] and forms a 1:1 complex with the headgroup [111]. It has also been shown that CPZ increases the molecular area of phospholipids like PS, PA and PI, but had no effect with neutral phospholipids like PC and PE. Other studies revealed that CPZ also penetrates the acyl chain region of phospholipids [106]. Studies showed that at a 1:1 molar ratio of CPZ: DMPC, CPZ disrupted the bilayer structure whereas at a 1:1 molar ratio of CPZ:DMPE, the drug had no effect on the bilayer structure [112]. Therefore, the membrane perturbation depends strongly on the lipid composition and the headgroup type.

1.3.1.2 Haloperidol (HPD) and Spiperone (SPIP)

Unfortunately, not many studies have been undertaken on HPD and SPIP binding to membranes. HPD and SPIP are neuroleptic drugs belonging to the butyrophenone drug family that binds specifically to the D_2-dopamine and 5-HT_2-serotonin receptors

respectively [42, 113]. Haloperidol was reported to increase the lipid peroxidation in brains [114], which could affect the functionality of the D_2-dopamine receptor [115]. Contradictory effects of HPD interacting with membranes were reported *in-vivo*. HPD tends to decrease the permeability of a variety of biological membranes for various molecules; this effect is generally exerted at low concentrations [116]. However, recent fluorescence polarization studies showed that HPD increased the fluidity and permeability of rat brain; which could be responsible for neurotoxic effects [117, 118].

At the membrane bilayer level, HPD and SPIP binding is controlled by electrostatic interactions as these drugs are protonated, but also by hydrophobic forces [119]. Similarly to CPZ, their incorporation in the bilayer depends on the lipid composition and the temperature [37]. HPD and SPIP induce disorders in the lipid chains, at different depths in membrane lipid brain extracts [120]. HPD increases the disorder to a greater degree in the interfacial region than in the hydrophobic core [97]. It also incorporates better to short aliphatic chains than to longer chains, reducing then the voids for the drug molecule.

1.3.2 Biological relevance: CADs induced phospholipidosis

CADs have been reported to induce phospholipid disorders and cytotxic effects upon cells. This effect, better known as phospholipidosis is characterised by the development of excessive membrane growth and accumulation of concentric lamellar bodies within the cells [121]. The lamellar bodies (Figure I.22) appear as storage vesicles [122], where the membranous structures are tightly packed. The mechanism by which this phenomenon occurs is poorly understood, and it is believed that CADs inhibit phospholipases (PLA) activity, by forming a complex with the lipid or the protein [123]. Phospholipidosis is CAD dose dependant, and its effect is suppressed once the CAD is removed [121].

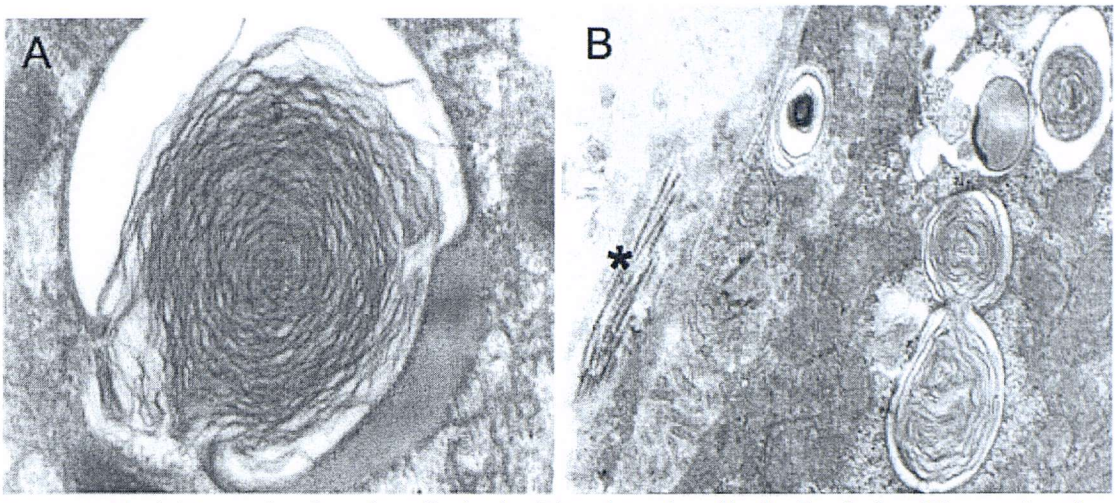


Figure I. 21: (A)Example of one lamellar body, (B) and two lamellar bodies fusion (Figure taken from ref [122]).

Efforts have been undertaken towards understanding the molecular basis of phospholipidosis. NMR experiments reported that strong interactions occur between lipids and CADs which cause the formation of complexes driven by hydrophobic and electrostatic forces [124]. Other studies showed that CADs interact specifically with PC anc PE lipids [125]. Also some phospholipidosis biomarkers were identified such as bis-monoglycerolphosphate (BMP) which is also referred to as lyso-bis-phosphatidic acid [123, 126]; phenylacetyglycine [127] and an increase in the level of polyunsaturated fatty acids. In addition, changes in the phospholipid profile have been reported where the level of PC, PE and PI lipids has increased [126, 128].

1.4 Aims and approaches

Although drug molecules are designed to bind specifically to targets such as receptors that are embedded within biological membranes it is becoming increasingly evident that a large fraction of these compounds interact non-specifically with the membrane.

The aim of this thesis is to understand and elucidate the molecular interaction between a phospholipid bilayer and CADs. Many studies have shown that CADs bind to membranes in the interfacial region, and hence affect bilayer properties and change the membrane lateral organisation. However, in the literature there is a paucity of consistent data regarding CADs or CNS drugs molecular interactions with

membranes. A second aspect is to correlate CADs membrane binding properties to the NSB *in-vivo*.

These investigations have been undertaken by using a variety of biophysical techniques including Small Angle X-ray Scattering, Solid-State Nuclear Magnetic Resonance and Fluorescence on ternary lipid:CAD:buffer samples, where the lipid type and the CAD have been varied.

CHAPTER 2

Theory and methods

CAD interactions with membranes were monitored using biophysical and biochemical techniques that give complementary information on this topic. This chapter will focus on the theory of the techniques employed such as small angle X-ray scattering (SAXS), solid-state nuclear magnetic resonance (SS-NMR), both describing the microsopic and macroscopic state of the bilayer when the drug is added to it, and fluorescence binding studies that inform on the binding constant and kinetics.

II.1 X-ray diffraction

X-rays are primarily used for medical diagnostics and crystallography. SAXS is a reliable and non destructive technique for the analysis of structured materials on the macroscopic scale.

II.1.1 X-ray generation

X-rays are electromagnetic waves whose wavelengths are of the same order of magnitude as the separation of atoms, i.e. 1-2 Å. They are generated when accelerated electrons bombard a piece a metal such as copper, tungsten or molybdenum. After the

collision the electrons are decelerated and eject an electron from the inner shell of the metal atom. As a result electrons from higher energy levels then fill up the vacancy and X-rays are emitted. Not all the electrons are decelerated at the same rate; consequently a continuous spectrum of differing wavelength is obtained for a given accelerating voltage. K_α and K_β are produced when the vacancy is filled by an electron from the L or M shell respectively. For X-ray diffraction experiments K_β will be removed by a monochromator.

II.1.2 X-ray diffraction theory

What happens when X-rays interact with a crystal? X-rays have a wavelength of the order of 1-2 Å; they will be diffracted when they interact with a structured matter such as lyotropic liquid crystals. William Bragg showed that X-ray diffraction patterns are the result of X-rays reflected from different planes interfering constructively or destructively. The geometry of X-ray diffraction is illustrated on figure II.1 and Bragg's law derived accordingly (Equation II.1):

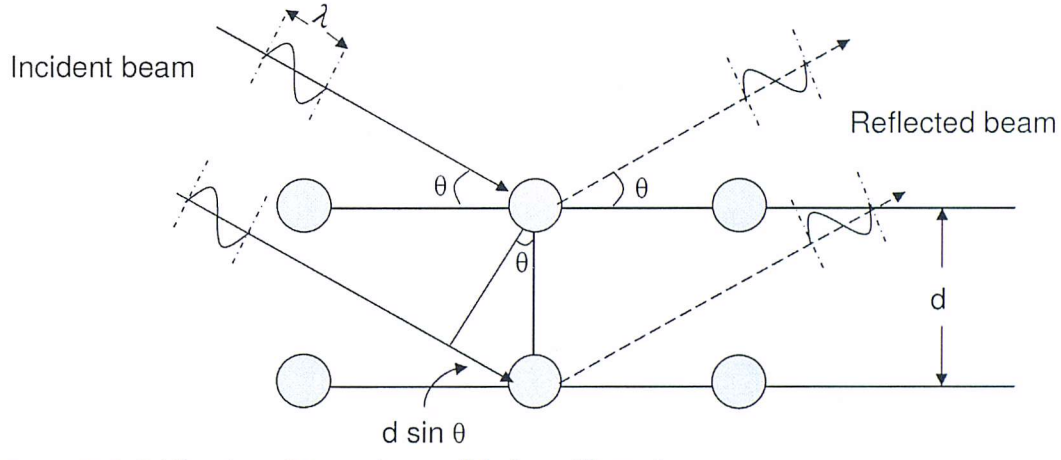


Figure II. 1: Diffraction of X-rays by parallel planes illustration.

$$n\lambda = 2d\sin\theta$$

Equation II. 1

where:

λ is the wavelength of the incident X-ray

d is the distance between the planes of atoms

θ is the incidence angle

and n is an integer multiple of the wavelength.

The angle between the incident beam vector s_0 and the vector of the diffracted beams s is defined as 2 θ. The magnitude of the two vectors is equal and defined as the reciprocal wavelength (Equation II.2):

$$s = s_0 = \frac{1}{\lambda}$$

Equation II. 2

and the scattering vector as S (equation II.3):

$$S = 2s\sin\theta = \frac{2\sin\theta}{\lambda}$$

Equation II. 3

Diffraction techniques allow the determination of various lipid mesophases based on the symmetry of the phase. The long range organization of the lipid mesophase appears in the low angle regime, with the diffraction very close to the direct beam (SAXS), whereas the structural information on the headgroup and chain packing can be deduced from the wide angle regions (WAXS).

II.1.3 Identification of bilayer mesophases by SAXS and WAXS

Lipid mesophases are ordered structures that can produce characteristic X-ray diffraction patterns satisfying the Bragg's law conditions, whose reciprocal spacing ($s_{h,k,l}$) occurs at characteristic ratios [75] (equation II.4)

$$s_{(h,k,l)} = \frac{1}{d_{(h,k,l)}}$$

Equation II. 4

where $d_{(h,k,l)}$ is the spacing between successive lattice planes, characterized by the Miller indices h,k,l.

The lamellar phase consists of a one dimensional stack of bilayers, therefore two of the Miller indices are set to zero (Equation II.5) [67].

$$s_l = \frac{l}{d}$$

Equation II. 5

For lamellar phases, the diffraction pattern will consist of equally spaced concentric rings that will index as 1, 2, 3, 4 etc..... Parameters such as the d-spacing can be determined from the diffraction pattern. Most of the time, diffraction from the lamellar phase is well defined and easily recognised. Swollen diffuse lamellar phases can also be detected when the lipid system hasn't reached equilibrium, and when small molecules such as CADs are added to the system.

The hexagonal phase consists of a two dimensional regular lattice of lattice parameter a, hence:

$$s_{(h,k)} = 2((h^2 + k^2 + hk)^{\frac{1}{2}} / \sqrt{3}a)$$

Equation II. 6

and the peaks index as 1, $\sqrt{3}$, 2, $\sqrt{7}$, 3 etc...

As already described in chapter I, two types of hexagonal phases exist: the normal (H_I) and inverted (H_{II}) hexagonal phases, however they lead to the same diffraction pattern. Figure II.2 illustrates the typical diffraction patterns obtained for a lamellar and hexagonal phase.

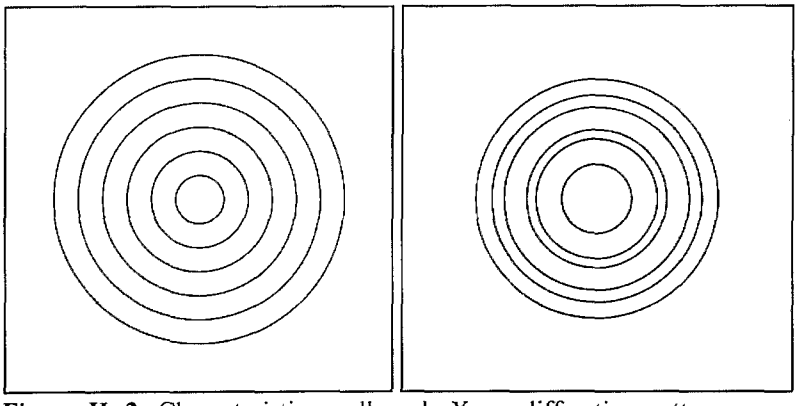


Figure II. 2: Characteristic small angle X-ray diffraction patterns for a lamellar (left) and hexagonal phase (right).

WAXS uses the same diffraction principles, but gives information on the short order of the bilayer sample, such as the headgoup and chain packing. WAXS is a very useful technique for distinguishing between the L_α, L_β and L_c phases as they give distinctive diffraction patterns.

II.1.4 Instrumentation

Three X-ray beamlines were used over the course of this study. The next section will give an overview of the used instrumentation.

The principle features of an X-ray beamline are shown in Figure II.3. It consists of an X-ray generator, followed by a focusing optics chamber equipped with collimators and pinholes which enable the intensification of the X-ray beam. The X-ray beam passes through the sample and is diffracted. The main beam is terminated by a beam-stop while the diffracted beam is collected on the detector.

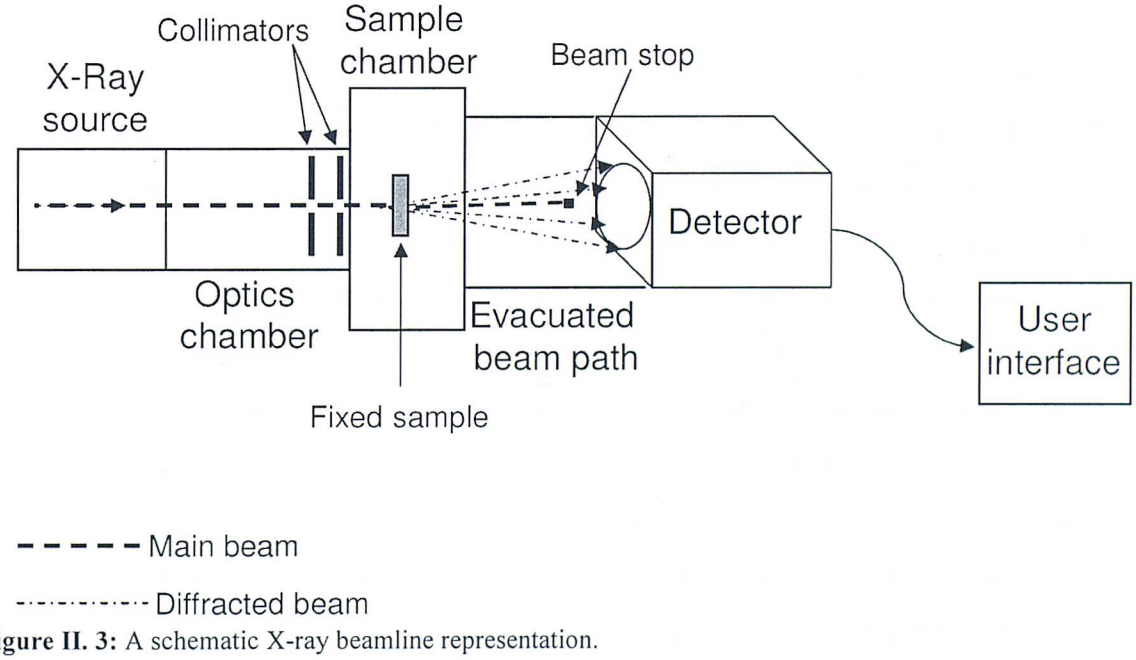


Figure II. 3: A schematic X-ray beamline representation.

The X-ray beamlines used in the project mainly differ with respect to their optics apparatus.

II.1.4.1 The "kinetics" beamline

The kinetics beamline used in this project was based around a FR591 rotating anode X-ray generator (Nonius-Netherland). A Ni filter is used so as to monochromate and isolate the CuK_α radiation (λ=1.54Å). The Ni-filtered CuK_α was focused using toroidal optics, which gives a high level of X-ray flux and focuses the beam into a focal point in the range of 400 μm-700μm. The sample was inserted in glass capillaries (*GLAS*-1.5 mm diameter- Germany) and then in a sample holder that is electronically linked to and controlled by a Scorpion Micro-Controller unit. Typical exposure times were 90 seconds and samples were allowed to equilibrate for 60 seconds. Once the beam passes through the sample, the scattered X-rays were detected by a camera (XIDIS Photonic Science), with the main beam blocked by a lead stop. The image was read out and transferred to a local PC and analysed using the IDL-based Axcess software package, developed by Dr A.Heron at Imperial College (see section 2.1.4.4 below).

II.1.4.2 The "osmotic" beamline

The osmotic beamline is based around a Bede (Durham, UK), copper Microsource X-ray generator with integrated monolithic polycapillary optics which can achieve high collimation and focusing of the main beam. The X-ray beam passes through the sample in the sample chamber, and is evacuated through the evacuated beam path, and terminates against the beam stop. Diffracted X-ray beams are collected via a Gemstar intensified CCD X-ray detector, which is connected to the beamline PC for image acquisition and analysis. The beamline is mounted on an Ealing linear transition stage for the orientation of the mounted beamline components parallel to the main beam. Cumulative diffraction plots were obtained after 5 x 60s X-ray exposures at room temperature. The osmotic beamline can be used to analyze samples with a d-spacing range from 2.5 Å to 150 Å. The resulting diffraction patterns were analyzed with the IDL based AXcess software package.

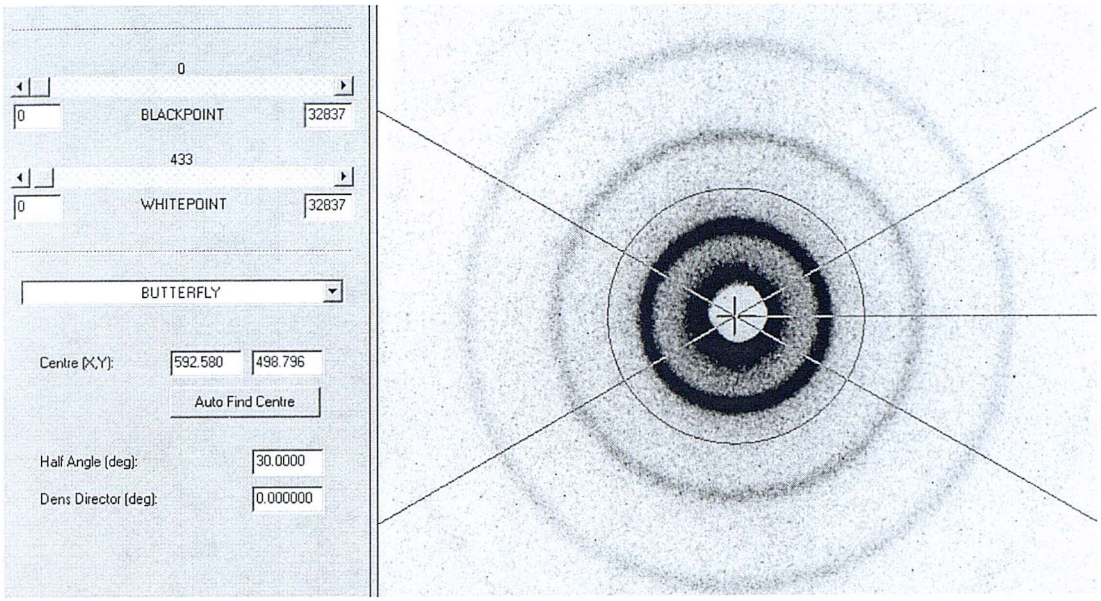
II.1.4.3 The nanoSTAR

The nanoSTAR beamline is coupled to a kristalloflex 760 X-ray generator with a copper source and cross-coupled Göebel mirror optics. The monochromated X-ray beam is passed through a 100 μm diameter pinhole and to a 300 μm anti scatter pinhole that forms a focus beam. The temperature was controlled by a eurotherm 847 series controller. This beamline was used to analyze samples with large d-spacings as this system can be used to obtain diffraction pattern from systems exhibiting spacings up to 300Å. Samples were also inserted in glass capillaries. The whole system was linked to a computer terminal and the nanoSTAR operation was controlled using the bruker AXS program. The images were transferred and analysed using AXcess software.

II.1.4.4 Image analysis

Images are collected and analysed using Axcess software package developed at Imperial College by Dr A.Heron. The program automatically locates the centre of the image. The diffraction pattern is integrated radially through a user defined section in order to visualise a one-dimensional linear intensity plot of intensity vs pixel number. Each peak can be indexed individually and the mesophase and lattice parameter (d-spacing) determined accordingly. Each experiment requires a prior calibration with silver behenate (d-spacing = 58.38 Å) (Figure II.4).

a



b

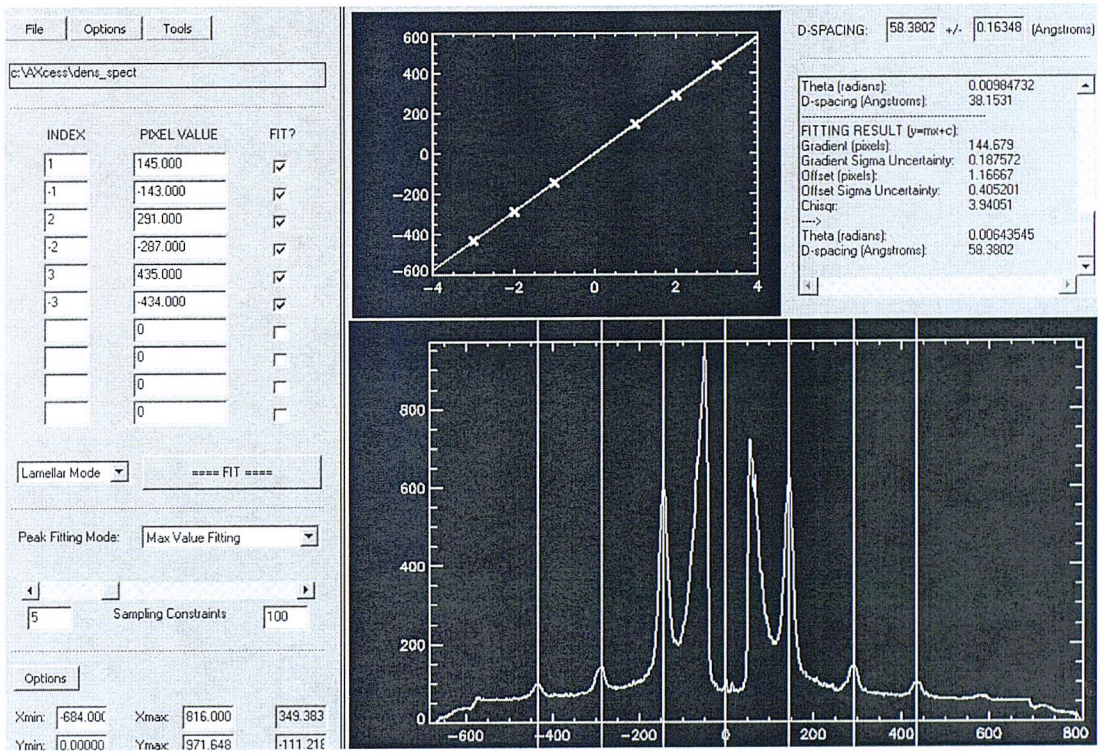


Figure II. 4: The Axcess software package for analysis of X-ray data. (a) Silver Behenate powder diffraction pattern. (b) 1D density plot that allows the determination of the lattice parameter, d-spacing =58.38±0.16Å.

II.2 Solid-state Nuclear Magnetic Resonance

Nuclear magnetic resonance spectroscopy is a powerful and complex technique, which is based on the nuclei of atoms placed in a magnetic field. This section will give a succinct introduction of NMR principles and its application to liquid crystals. A more extensive coverage of NMR theory can be found in references [129-131].

II.2.1 NMR principles

Briefly, the NMR concept can be described as follows: if a sample is placed in a magnetic field, and subjected to radiofrequency (RF) radiations at the appropriate frequency, then nuclei in the sample are able to absorb this energy.

Subatomic particles (electron, proton and neutron) possess a nuclear magnetic moment μ which interacts with an external magnetic field. The magnetic moment μ, is characterized by a property called spin angular momentum, I, which arises from the ratio of protons to neutrons in the nucleus. According to quantum mechanics, the nuclear magnetic moment μ of a nucleus will align with an externally applied magnetic field B_0 in only 2I+1 ways. As a result a nucleus with spin I=1/2 will have two possible orientations. The energetically preferred orientation has the magnetic moment aligned parallel to B_0 (spin m=+1/2), and is given the notation α whereas the higher energy anti-parallel orientation (spin m=-1/2), is referred as β. The transition between the two energy states is determined by equation II.7:

$$E = h\nu$$

Equation II. 7

where h = Plank's constant = 6.626×10^{-34} J s

ν is the resonance frequency (Larmor frequency).

The energy level for a nucleus with a spin I=1/2 placed in a magnetic field is represented by the following diagram (Figure II.5).

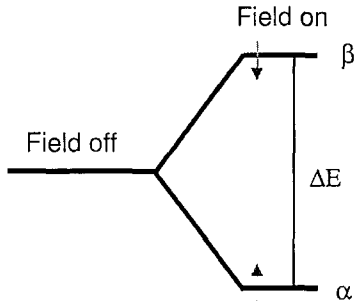


Figure II. 5: Diagram representing the level energy of two spin state in a magnetic field.

Nuclear spins are able to interact with the applied magnetic field; this is called the Zeeman effect.

The populations of energy levels follow Boltzmann statistics, for I = ½ (Equation II.8):

$$\frac{N_\alpha}{N_\beta} = e^{\frac{E}{kT}}$$

Equation II. 8

where N_α is the number of nuclei in the α-state and N_β the number of nuclei in the β-state, T is the temperature in Kelvin and k is the Boltzmann constant. The difference in population between the N_α and N_β state is very small.

The rotational axis of the spinning nucleus is not perfectly parallel or anti-parallel, but must precess at an anglular velocity as defined by equation II.9:

$$\omega_0 = \gamma B_0$$

Equation II. 9

where ω_0 is the Larmor frequency and γ a proportionality constant; the magnetogyric ratio, that relates the magnetic moment μ and the spin I, defined as (equation II.10)

$$\gamma = \frac{2\pi\mu}{I}$$

Equation II. 10

If a RF corresponding to ω_0 is applied to the sample, the nuclear spin absorbs the energy, this causes a transition form higher to lower energy state, as well from lower to higher energy state. This feature is defined as the resonance or exchange of energy at a specific frequency between the spins. The absorption of the energy causes the spin to reach a non equilibrium state. After the excitation the individual spins of the system will decay exponentially with time and return to equilibrium through a relaxation process. This process creates a voltage that can be detected and amplified, and a time domain emission signal is emitted and displayed as a free induction decay (FID). The FID signal is transformed by a Fourier Transform (FT) that allows the detection of the signal as a function of the frequency (Figure II.6).

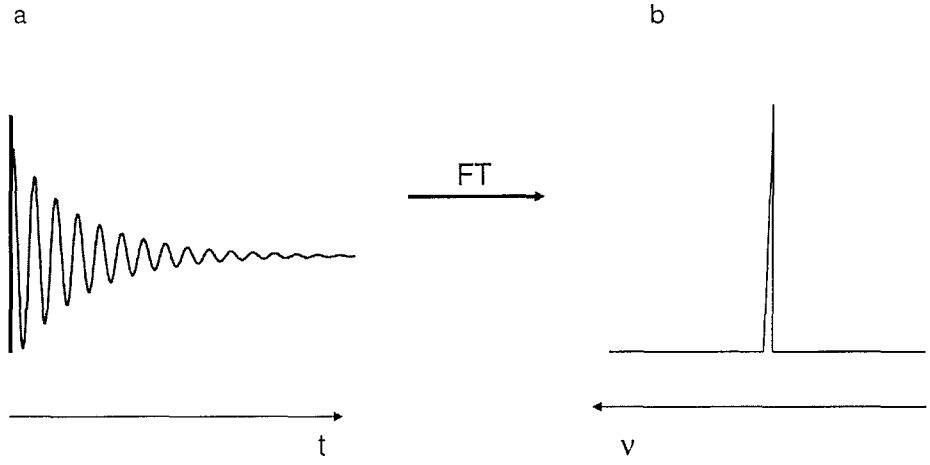


Figure II. 6: An FID signal (a) and FT specrum (b).

NMR is an absorption process and nuclei must relax and return to the ground state. There are two relaxation processes, the longitudinal, or spin-lattice relaxation and the transverse, or spin-spin relaxation. The longitudinal relaxation energy is transferred to the molecular framework or lattice, and is lost as vibrational or translational energy. It is characterized by the spin-lattice relaxation time T_1. T_1 can be in the order of seconds. Transverse relaxation energy is transferred to a neighbor nucleus and is characterized by the spin-spin relaxation time T_2. The peak width on the spectrum is dependent on both T_1 and T_2.

The precise frequency at which each atom comes into resonance is determined by the applied magnetic field and also from differences in the magnetic moment experienced by each nucleus. The movement of electrons creates a local magnetic field which shields the nuclear spin from the external magnetic field. This results in individual chemical groups having distinct resonances in NMR, characterized by the chemical shift. The chemical shift is commonly reported as a value δ, defined by equation II.11:

$$\delta = \frac{\omega_0 - \omega_{0ref}}{\omega_{0ref}}$$

Equation II. 11

where $\omega_{0\ ref}$ is the chemical shift associated to a reference peak, such a tetramethylsilane (TMS) for carbon and hydrogen nuclei , and HPO_4 for phosphorus. δ has no dimension and is expressed as part per million (ppm). The different chemical shift expected for ^{13}C and ^{31}P NMR are represented on Figure II.7 and II.8.

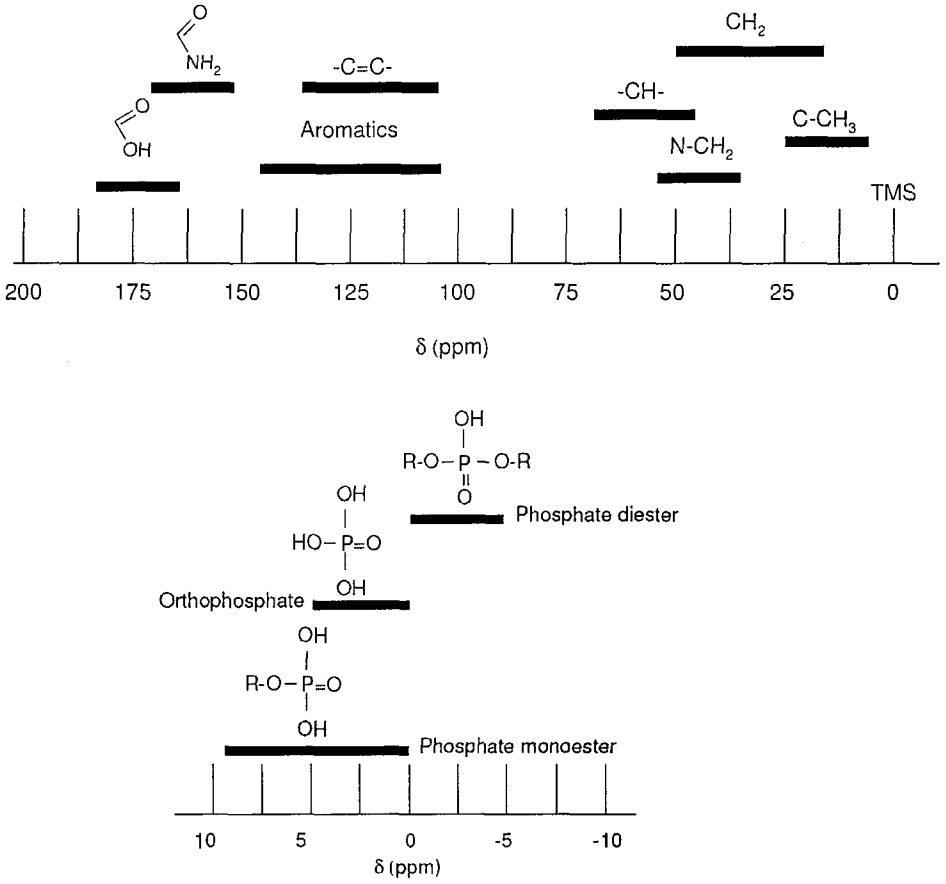


Figure II. 7: *Chemical shifts ranges for common functional groups in* ^{13}C NMR (top) and ^{31}P NMR (bottom) spectroscopy.

II.2.2 SS-NMR of liquid crystals

II.2.2.1 Principles

This section will give a brief introduction of SS-NMR principles and its application to liquid crystals. A more exhaustive coverage of SS-NMR principles can be found in references [132, 133].

SS-NMR applies to solids and also obeys the fundamentals properties mentioned above. SS-NMR spectroscopy is a particularly sensitive technique, allowing the determination of the three-dimensional organization of phospholipids in membranes. However the resolution of NMR in solids suffers from a number of intrinsic problems which will give broad lines while acquiring the data. Spectral manifestations of anisotropic interactions are averaged to zero in solution by fast and isotropic motions; this does not happen in solids as the motion is usually absent, which causes the line broadening of the resonance. The main cause of line broadening in solids comes from the chemical shift anisotropy (CSA) and the dipolar coupling.

- The chemical shift anisotropy (CSA)

The chemical shift is a nuclear-electron interaction, and a very important concept of SS-NMR is that the chemical shift of a given nucleus within a solid depends on the orientation of the solid, therefore, the resonance frequency will vary with the orientation of the molecules. This orientation dependence of the chemical shift is referred to as chemical shift anisotropy (CSA). The CSA which arises from a non uniform electronic environment can be described by a 3x3 tensor which consists of nine independent components (equation II.12). The chemical shift tensor is expressed in a coordinate frame where all off-diagonal elements vanish. This results in the detection of broad peaks on the NMR spectrum. The corresponding signal corresponds to a powder pattern or CSA pattern.

$$\sigma = \begin{pmatrix} \sigma_{11} & 0 & 0 \\ 0 & \sigma_{22} & 0 \\ 0 & 0 & \sigma_{33} \end{pmatrix}$$

Equation II. 12

The components can be read from the NMR spectrum (please refer to section 2.2.2.2).

- The dipolar coupling

The dipolar coupling arises from electron-electron interactions. Each nucleus has a magnetic moment μ, which interacts with a neighboring magnetic moment. This effect depends on the distance and the geometry of the molecule. Dipolar coupling generates line broadening in solids because of the presence of multitude of spins, but is averaged to zero in solution due to molecular tumbling.

- Magic Angle Spinning (MAS)

The CSA and the dipolar interaction give rise to broad spectral lines in the NMR spectra of solid samples. The restoration of high-resolution spectra is realized using the magical angle spinning method (MAS). The orientational dependence of the magnetic interaction varies according to equation II.13:

$$3\cos^2\theta_m - 1 = 0$$

Equation II. 13

and averages to zero when $\theta_m = 54.7$.

Experimentally, the sample is rotated at the magic angle $\theta = 54.7°$ relative to the magnetic field, and spun to remove the line broadening, with the frequency of spinning exceeding the magnitude of the dipolar coupling in order to completely remove the line broadening (Figure II.8).

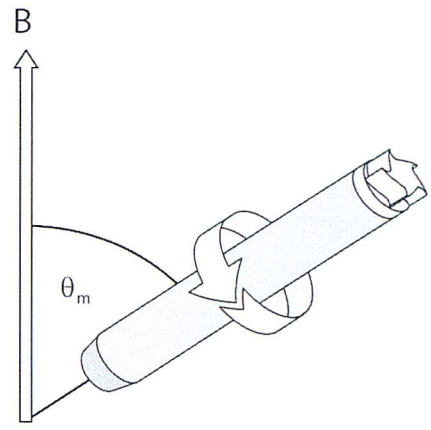


Figure II. 8: Magic Angle Spinning. The sample is rotated at θ_m=54.74° and spun so the line broadening is removed (Figure taken from ref [134].

MAS also removes the CSA by averaging the chemical shift tensor. This generates a spectrum where each chemical shift is represented by a single isotropic value, and is equivalent to the solution state.

II.2.2.2 Application to liquid crystals

Liquid crystals are not real solids. Lipids in membranes are able to undergo fast rotational motions around the normal of the bilayer in a limited angular domain. NMR of membrane samples can provide information on local molecular motions in lipid assemblies. This gives rise to characteristic signals for lipid mesophases. Two main nuclei were investigated in this thesis: ^{31}P and ^{13}C.

- ^{31}P SS-NMR of phospholipids

As ^{31}P is present in biological membranes and has a spin I=1/2, it is therefore a useful probe to determine structure and motion. Phospholipids contain ^{31}P nuclei in the headgroup region, which have a natural abundance of 100%. This feature allowed for the studies of natural membranes using ^{31}P NMR. The NMR signal is dominated by the CSA, and the shape of the CSA powder pattern gives an insight in the structure of the phase as well as information on the motional degree around the lipid headgroup [71]. The dipolar coupling may be removed from long axis rotation and molecular diffusion through the bilayer.

For membranes in the liquid crystalline state, fast rotation of the lipid molecules around an axis perpendicular to the bilayer surface can occur. This generates effective tensors which are axially symmetric to the director axis (rotation axis). The effective tensor σ_{eff} can be treated mathematically by a 3x3 matrix (equation II.14):

$$\sigma_{eff} = \begin{pmatrix} \sigma_{\perp} & 0 & 0 \\ 0 & \sigma_{\perp} & 0 \\ 0 & 0 & \sigma_{\parallel} \end{pmatrix}$$

Equation II. 14

and $$\Delta\sigma = \sigma_{\parallel} - \sigma_{\perp}$$

Equation II. 15

where $\sigma_{\perp}$ and $\sigma_{\parallel}$ are the chemical shift tensors perpendicular and parallel to the director axis. The CSA can be derived from NMR spectra.

Static ^{31}P patterns can show line broadening that occurs in the lipid mesophases such as the lamellar phase, the inverse hexagonal phase and the isotropic phase.
The NMR signal obtained for lamellar phases is characteristic and is the result of an averaged powder pattern where $\Delta\sigma$ corresponds to the shoulder of the powder pattern, as exemplified on figure II.9a with $\sigma_{\perp}$ corresponding to the lower intensity region and $\sigma_{\parallel}$ corresponding to the higher intensity region. $\Delta\sigma$ =50 ppm in the case of DOPC fluid lamellar phase. It is not possible however to distinguish between L_{α}, L_{β}, L_c and L_o phase. In order to distinguish between a fluid and gel lamellar phase, other NMR experiments such as ^{13}C MAS NMR can be done (see section below).
Phospholipids arranged in a hexagonal lattice possess an additional averaging mechanism which corresponds to the diffusion of the lipid around the cylinder (D= $\sim 10^{-8}$ cm^2s^{-1}) [75]. The lipids rapidly diffuse around the cylinders, while the cylinders are organized around a main axial symmetry. Then the chemical shift tensor can be defined as follows: $\sigma_{\parallel}$ corresponds to the case where the cylinder has a collinear axis to the magnetic field, and $\sigma_{\perp}$ corresponds to the case where the axis cylinder is normal to the magnetic field. The phosphorus pattern corresponds to the reversed lamellar pattern with a width corresponding to the half of the magnitude of the

lamellar phase (Figure II.9b). Details on the calculation of CSA tensor can be found in reference [71].

Isotropic phases such as micellar phases lead to a complete averaging of the chemical shift tensor, due to fast tumbling comparable to solution state. The recorded signal corresponds to a single sharp peak (Figure II.9c).

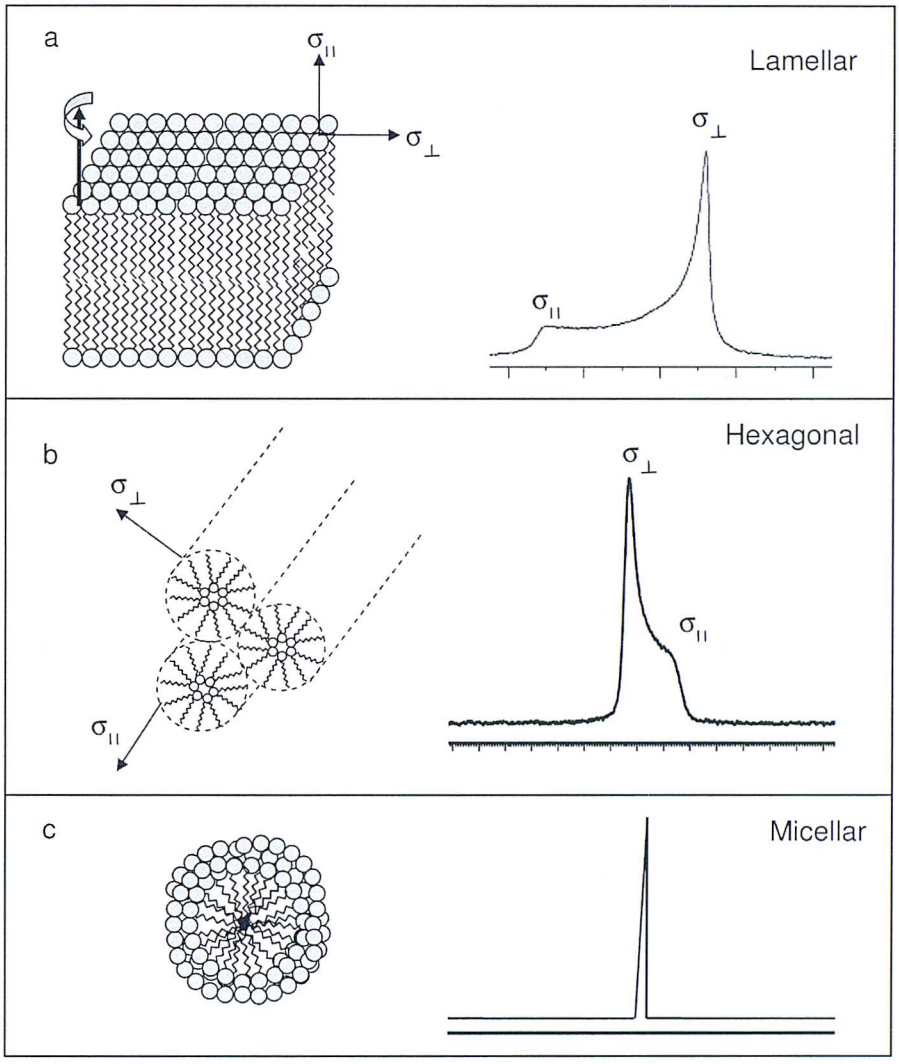


Figure II. 9: Typical ^{31}P CSA pattern of (a) lamellar, (b) hexagonal, and (c) micellar phase.

- ^{13}C MAS SS-NMR of phospholipids

^{13}C NMR provides a useful tool to probe the state of the lipid polar headgroup and the hydrocarbon chain, thanks to the natural abundance of ^{13}C (~1%). As discussed

above, MAS removes all anisotropic interactions, so NMR signals are only dictated by chemical shift interactions.

The distribution of the chemical shifts corresponds to lipid segments such as the methyl end group, the hydrocarbon chain, the interface and the headgroup. ^{13}C MAS SS-NMR experiments can be undertaken to determine if the lipid system is in a fluid or gel phase. The rate of exchange between lipid chain conformations i.e. the trans / gauche effect is slow in a gel phase, which is detected by a broad peak whereas the exchange between the allowed conformations occurs faster in a fluid phase. This is characterized by sharp well resolved peaks on the NMR spectrum which corresponds to an average of all conformations. In the gel phase, the peaks appear broader because of the packing of the chains that does not allow the trans / gauche isomerisation, and the lower motion of the lipid in the bilayer.

Combination of static ^{31}P and ^{13}C MAS SS-NMR measurements will inform about the membrane state, i.e. the conformation of the lipid headgroup and the state of the hydrocarbon chain, in particular when CADs are added to bilayers (see chapter 4).

II.3 Fluorescent binding studies

Binding of charged CADs at physiological pH can be evaluated and measured using an original method developed by O'Shea and coworkers [135] which involves the electrical properties of the bilayer. This section will describe the theory underlying this method.

II.3.1 Theory

Molecular interactions in nature are essentially electrical, and some of the physical properties of membranes contribute to these interactions. Membrane electrical properties are believed to participate to biological events [88, 135, 136]; therefore, these properties can be used to investigate them. Membrane electrostatics and the underlying physical properties have been extensively reviewed by McLaughlin [92] and Cevc [88].

Membranes can be characterized by three electrical potentials, which are: the transmembrane potential $\Delta\psi$ which is associated to a gradient of electric charges across the lipid bilayer, the membrane surface potential Φ_s which arises when net excess electric charges are bound to the membrane interface, and finally the membrane dipole potential Φ_d which arises from electrical dipoles associated to the carboxylic group and the oxygen-bonded phosphate components of the membrane [137]. The $\Delta\psi$ and Φ_d will not be discussed any further, a more exhaustive coverage of these potentials are found in references [136, 138-140].

The membrane surface potential's feature can be investigated in binding studies, in particular in the detection of the physical parameters that underlie the molecular interactions between charged CADs and phospholipid membranes. The membrane surface potential can be described by the Gouy-Chapman theory (equation II.16):

$$\Phi_s = \frac{\sigma}{\varepsilon_a \varepsilon_0 \lambda}$$

Equation II. 16

where σ is the surface charge density, λ the Debye length, ε_a the dielectric constant of the aqueous phase, and ε_0 the permittivity of the free space.

The membrane surface potential can also vary with distance from the surface *x* according to equation II.17:

$$\Phi(x) = \Phi_s e^{(-\lambda x)}$$

Equation II. 17

This potential can be described as adjacent to a phospholipid bilayer membrane.

The membrane surface potential depends on the presence of ions and charges, and acts upon them. This potential causes an irregular distribution of charges at the membrane surface, as counterions are attracted to the surface, whereas ions of the same charges are repelled. Therefore, the concentration of ions at the membrane surface is dependent on the membrane surface potential Φ_s and is described by the Boltzman equation (equation I.18):

$$C_{i,s} = C_{i,b} \exp(\frac{-Z_i F \Phi_s}{RT})$$

Equation II. 18

where C_s is the concentration of ions at the surface, C_b the concentration of ions in the bulk phase, Z the number of charges, F the Faraday's constant, R the gas constant and T the temperature (K). Therefore, any change in the ionic concentration will result in a change of the surface potential.

Characterization of electric features of membrane potentials can be achieved by using fluorescent lipids which have the advantage of being non invasive as they don't alter the integrity of the membrane. These lipid probes can also be utilized at low concentration in the lipid bilayer. Fluoresceinphosphatidylethanolamine (FPE) whose structure is represented on figure II.10 has proven to be remarkably indicative of

membrane electrostatic features, in particular the membrane surface potential in both model and cell membranes.

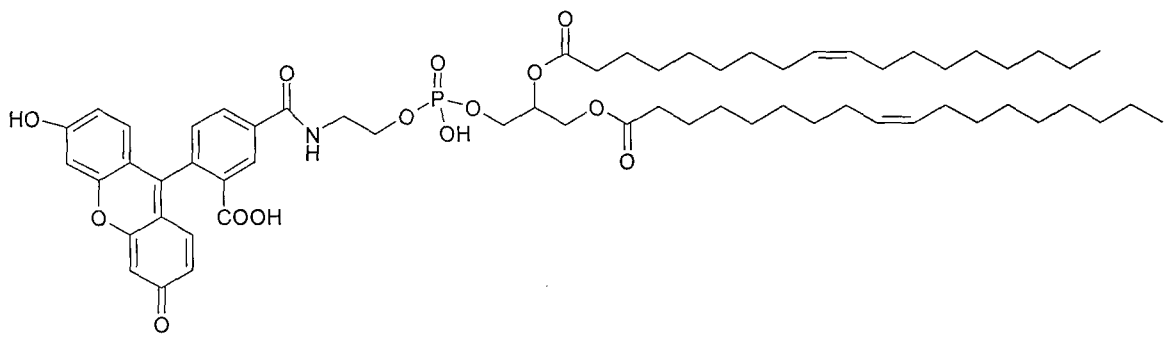


Figure II. 10: Structure of fluoresceinphosphatidylethanolamine FPE.

This fluorescent lipid was initially used to assay the proton pumping function of reconstituted cytochrome c oxidase in liposomes by measuring the intra liposomal pH [141].

FPE has the ability to incorporate into lipid bilayers via its phosphatidylethanolamine segment, while the fluorescein moiety is exposed to the aqueous phase. Fluorescein is a widely used fluorescent probe in biology, biochemistry and chemistry research. It is well characterized and its spectral properties have been widely studied. Fluorescein can exist in several ionization states [142]. As a result, FPE is also sensitive to a change in the surface potential induced by addition of charges.

The Hendersson-Hasselbach equation, describes the derivation of the pH with acidity (equation II.19):

$$pH = pk_a + \log\frac{C_B}{C_{HB}}$$

Equation II. 19

where pk_a is the acidity constant, C_B and C_{HB} the concentration of the dissociated and protonated species of the acid-base pair of the fluorescein moiety.

Rearranging equation II.14 and II.15 yields equation II.20:

$$\log\frac{C_B}{C_{HB}} = pH - \left[pka - \frac{F\Phi_s}{RT\ln 10}\right]$$

Equation II. 20

The quantity $pka - \frac{F\Phi_s}{RT\ln 10}$ is considered as the pk_{app} for proton binding of the acid-base pair on the membrane surface.

Equation II.16 shows that FPE is sensitive to a change in the surface potential Φ_s, thus a change in the fluorescence corresponds to a change of the surface potential.

Therefore, FPE can be used to study charged molecules, i.e. CADs binding to membranes by following the change in the fluorescence, as addition of charged molecules alters the value of the surface potential and consequently the fluorescence.

II.3.2 Experimental

FPE fluorescence signals can be used to monitor the interactions of charged molecules with membranes in real time with great sensitivity. Additions of charged molecules cause an alteration in the surface potential, which leads to the protonation or deprotonation of the fluorescein ring, which results in an enhancement or decrease in the fluorescence intensity.

Extruded unilamellar vesicles were labeled with the fluorescent probe in the outer layer. The labeling is stable as no flip-flop was observed over a week [143]. Subsequent additions of positively charged molecules of known concentration are reflected by a sharp increase in the fluorescence signal; the increase is proportional to the added quantity (Figure II.11). Additions are made until no further fluorescence change is observed. At this point the binding is considered to be saturated. Binding events occur within the mixing procedure and can be resolved by using stopped-flow rapid mixing techniques [144].

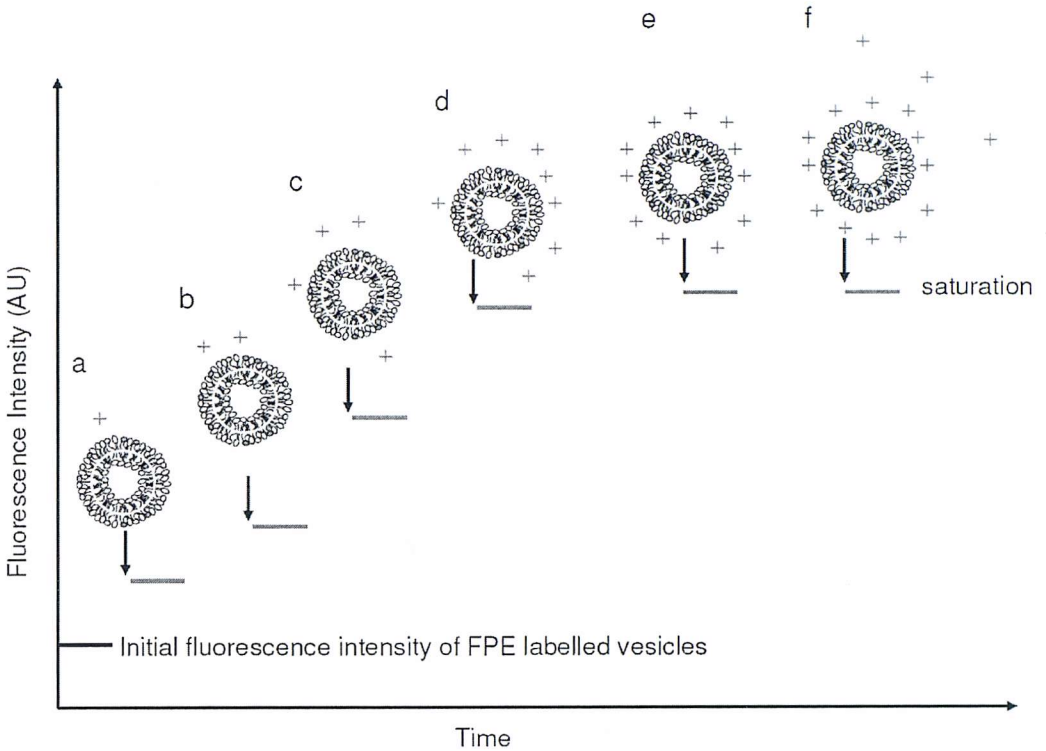


Figure II. 11: Schematic representing the FPE fluorescence assays. Vesicles are fluorescently labeled in the outer layer, which yields an initial fluorescence intensity value. Positively charged molecules added to the labeled vesicles cause an increase in the fluorescence intensity. The increase is relative to the added quantity of molecules, (a,b,c), until saturation is reached (d,e,f). Subsequent additions are represented by black arrows.

The overall fluorescence change due to subsequent additions of charged molecules can be utilized to construct binding profiles (Figure II.12). The obtained data points are fitted to a hyperbolic function, which yields binding constants such as K_d values (Equation II.21).

$$F = \frac{F_{max}[M]}{K_d + [M]}$$

Equation II. 21

where F is the fluorescence change, F_{max} the maximum fluorescence change, [M] the concentration of the charged added molecule and K_d the affinity of the molecule for the membrane.

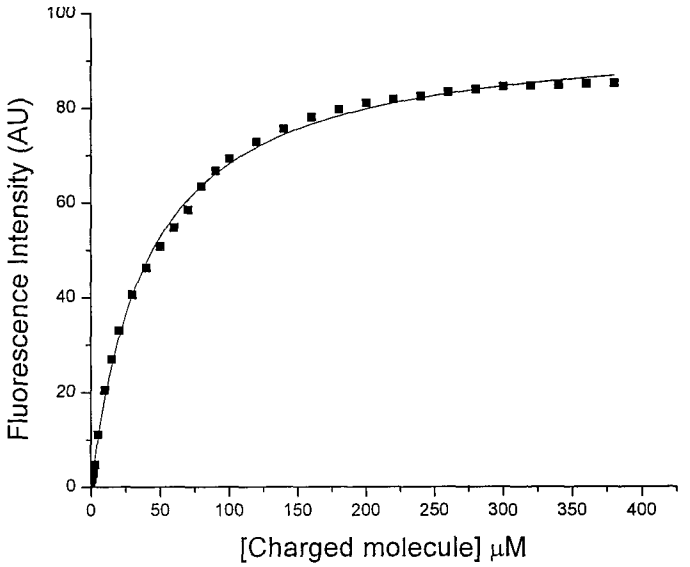


Figure II. 12: Typical binding profiles obtained from FPE fluorescence assays. Data points are fitted to a hyperbolic function from which a K_d value is calculated.

The use of PFE fluorescent assay is highly revealing as it allows real time measurements of charged molecules to membranes. Therefore, this technique will be applicable to CADs since they are charged at physiological pH and binding properties will be investigated (Chapter 3).

II.4 Methods:

II.4.1 Lipids

1,2-Dioleoyl-*sn*-Glycero-3-Phosphocholine (DOPC), 1,2-Dilauroyl-*sn*-Glycero-3-Phosphocholine (DLPC), 1,2-dioleoyl-*sn*-glycero-3-phosphoethanolamine (DOPE), 1-Oleoyl-2-Hydroxy-*sn*-Glycero-3-Phosphocholine (MOPC) and 1,2-Di-O-Octadecenyl-*sn*-Glycero-3-Phosphocholine (Ether linked-PC) were purchased from Avanti Polar Lipids Inc., (Alabaster USA, 99.0%) in lyophilized powder form and used with no further purification. Fluoresceinphosphatidylethanolamine (FPE) was purchased from Sigma Aldrich (Gillingham UK).

II.4.2 Drugs

Haloperidol HCl and Spiperone HCl were purchased from Tocris-Cookson. Fluorescent-tagged spiperone (NBDAminohexanoylaminophenetylspiperone) and WAY 100635 were obtained from Sigma Aldrich (Gillingham UK). Haloperidol salts (Formate, TFA and Maleate) salt, were synthesized in house as described in reference [145].

II.4.3 Buffers

Experiments were performed in using the following buffers:
Buffer A: 50 mM Bis Tris (Fluka 99%), 100 mM NaCl (Fluka 99%) pH 7.4
Buffer B: 10 mM Tris HCl (Sigma 99%) pH 7.4
Buffer C: 10 mM Tris HCl, 100 mM NaCl pH 7.4

II.4.4 Sample preparation for SAXS, Solid State NMR and HPLC

Dry lipids and drugs were dissolved in chloroform methanol (1:1) to obtain a 4:1, 9:1 or 20:1 lipid to drug molar ratio. The solvent was then removed gently with a nitrogen stream and the samples were left to dry in a vacuum oven at 40°C at 1000 mBars for 36 hours. The obtained dried lipid-drug mixture was hydrated with the desired buffer at a 1:3 lipid: buffer mass ratio, vortexed until homogenized and left to equilibrate for 15 min. At that point the samples are labeled t=0.

II.4.5 Small Angle X-ray diffraction

Three beamlines were mainly used in this project, namely the "kinetics beamline", "the Bede" and the "nanoSTAR". Samples for x-ray measurements were prepared by transferring the required amounts of co-lyophilised lipid / CAD / buffer to glass x-ray capillary tubes with a diameter of 1.5 mm (Gulmay Medical, TBD). The capillaries were flame sealed and then a silicon sealant plug (Dow Corning Corp) was applied to

ensure airtight sealing required to maintain the excess water hydration level. SAXS patterns were obtained by using a high intensity laboratory point source. The X-ray experiments were computer controlled using software originally developed by E.F. Eikenberry (Paul Scherrer Institute, Switzerland) and S.M. Gruner (Cornell University, New York) and now customized for use at Imperial College. Image analysis was performed using the Axcess software package developed by Andrew Heron (Imperial College, London). (Please refer to chapter 2 for more details on the beamlines, the X-ray generators used and the image analysis procedure).

II.4.6 Nuclear Magnetic Resonance

The homogenised sample was placed in a 4mm zirconium rotor in a 4 ml probe. NMR spectra were acquired on a Bruker 600 MHz FT-NMR spectrometer (14.09T) with the following frequencies: ^{31}P = 242 MHz, ^{1}H = 600 MHz, and a ^{13}C =150 MHz. The magic angle spinning experiments were done at speeds of 3 kHz with θ=54.74. Single pulse and proton-decoupled experiments were acquired using standard Bruker pulse programs

II.4.7 Normal Phase High Performance liquid chromatography

Normal phase liquid chromatography was carried out using a HPLC system consisting of an autosampler (Waters 717 plus autosampler), dual pump (Waters 626) operated by a 600S controller (Waters) with a 100 µl loop connected to a Kromasil Diol column (25 cm long, 60 Å pore size, 5 µm particle size, HiChromLtd, Berkshire, UK). Eluate from the column was sent to the evaporative light scattering (ELS) detector (ESA 301- ESA Analytical Ltd, Buckinghamshire, UK). The ELS detector nebulisation and evaporation temperatures were set at 31°C and 55 °C respectively and the N_2 flow pressure was set to 1.5 bars. The data were collected with the millenium LC system software (Waters).

Two solvents at a constant flow rate of 1 ml / min were used to elute the lipids. The solvent gradient involved an increase in hydrophylicity: Solvent A: 101:21:2:0.1 Hexane, Isopropanol, Acetic Acid, Triethylamine (v/v/v/v), Solvent B: 105:17.5:2:0.1 Isopropanol, Water, Acetic Acid, Triethylamine (v/v/v/v). All solvents used were

HPLC grade. The gradient was set to 0%B to 30%B from 2min to 7 min, 30%B to 50%B from 8 min to 37 min, 50%B to 0%B from 37min to 40min, and the system was held in 100%A for 5 min to regenerate the column. Blanks were run every 10 samples to avoid any contamination.

II.4.8 Vesicle preparation

The desired lipids were dissolved in chloroform (2mg/ml) and dried under a nitrogen stream in a round bottom flask to form a homogeneous film [146]. The film was then left under vacuum for 8 hours and hydrated with the desired buffer to the desired concentration and left to interact overnight. The resulting multilamellar solution was freeze-thawed 10 times and extruded 20 times trough a 100 nm diameter polycarbonate filters (Nucleopore). The resulting vesicles were found to be homogeneous in size. Monodispersity of the vesicles was checked with dynamic light scattering.

II.4.9 Binding studies using Fluorescein Phosphatidylethanolamine (FPE)

The formed vesicles were labeled on the outer layer with FPE added in ethanol (5 μl of a $1mg.ml^{-1}$ stock solution in chloroform) in a 0.05 mol% lipid: probe ratio and left to incubate for an hour at 37 degrees in the dark. Fluorescence measurements were performed by adding the desired amount of drug solution in DMSO (3 mM) to 3 ml of a 300μM vesicle solution. Kinetics measurements were recorded on a Perkin –Elmer LS 50B Luminescence Spectrometer. The excitation and emission wavelength were 490 and 530 nm respectively with the slits 5 nm wide. All experiments were done under controlled light conditions.

The fluorescence amplitude of FPE was averaged and standarised so the initial intensity was equal to zero. The change in fluorescence was plotted against the drug concentration and fitted according to equation II.21 [147].

II.4.10 Dynamic light scattering

The mean diameter, size-distribution, and polydispersity index of the DOPC vesicle preparations were monitored by dynamic light scattering (DLS) (HPPS 5001 Malvern Instruments). The instrument was equipped with a He–Ne laser operating at a wavelength of 633 nm. The size analysis was made at a lipid concentration of 400 μM, at 25 °C. In each measurement the buffer was filtered through a 0.22 μm filter (Sartorius).

II.4.11 Fluorescence microscopy

Giant Unilamellar Vesicles (GUV) were electroformed as described previously [148] at room temperature, with an custom built in-house designed device (Figure II.13).

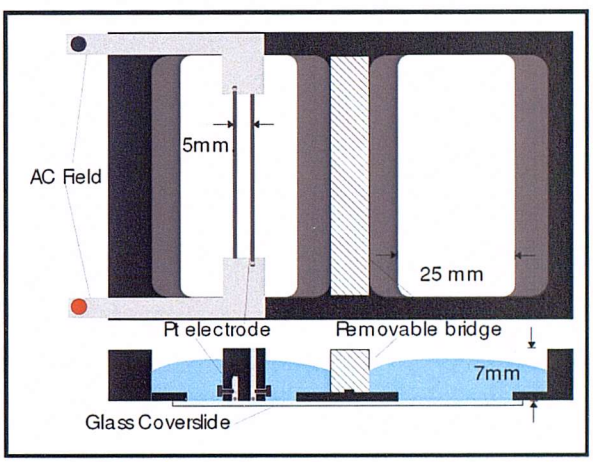


Figure II. 13: Electroformation set-up (Courtesy of X.Mulet)

Lipids were dissolved in 9:1 chloroform: methanol mixtures and deposited on Pt electrodes 5mm apart. Once the solvent had been removed in vacuo, the electrodes were hydrated in 100mM sucrose, 10 mM bis-tris pH 7.4 at 25°C solution. The A.C field applied was slowly varied from 0.2V to 1.0V at 10 Hz over 10 mins. The vesicles were allowed to grow for one hour before the field was slowly reduced and finally stopped. The vesicles grown by this method were stable for 6 hours. The GUVs were imaged on an inverted Nikon TE2000 microscope fitted with DIC set up (Nikon UK Limited, Surrey) equipped with a 100W Xenon burner and a CFI Plan

Fluor 20X optic. For fluorescence imaging a cube fitted with a 465 nm excitation filter and 505nm emission filters (Chroma Technology, Rockingham USA) was used. An ND4 filter was used to minimise the effects of photo bleaching. The images were acquired on a Hamamatzu Orca ER camera set to maximum gain for the fluorescence data acquisition. The exposure lengths were 150 ms, with a 5 s delay between each frame. The total time period for the video was 500 frames (2500 s).
The fluorescent Spiperone (NBDAminohexanoylaminophenetylspiperone) was added in ethanol in the presence of non-fluorescent spiperone HCl in a 1:100 molar ratio.

II.4.12 Polarising microscopy

Observation of lipid CAD samples was performed at room temperature with direct light and polarizing microscopy using a Nikon E600 polarizing microscope, equipped with a Nikon DXM1200F digital camera at a magnification of 40 x. Images were analyzed with the NikonACT-1 software.

CHAPTER 3

Degradative transport of Haloperidol and Spiperone across bilayers

The results presented in this section have been published in the "Philosophical Transactions of The Royal Society" Oct 2006, 364(1847):2597-614 [149].

III.1 Background

Studies of drug interactions with membranes have been widely investigated in the literature from the early eighties to the present [32] [150] [100]. Advances in the understanding of effects of drugs on membranes were achieved using a wide array of techniques [151] [152] [153] [105]. These studies are of importance as biological bilayers act as a barrier to the passage of many molecules including drugs. As already described earlier, the elucidation of the mechanisms associated with drugs binding to membranes is relevant to numerous problems occurring in membrane biology such as drug transport through membranes and the non-specific and specific binding of drugs to receptors and membranes. As the non-specific binding is related to diffusion of central nervous system (CNS) drugs through the BBB [17], it is of main importance to investigate the CNS drugs interactions with bilayers in general.

This section will describe the preliminary results concerning the interaction of two CNS cationic amphiphilic drugs, haloperidol (HPD) and spiperone (SPIP), on bilayers made of dioleoylphosphatidylcholine (DOPC) (Figure III.1). A description of the lipid:drug systems will be followed by a investigation of the drug catalysed membrane degradation by spectroscopic and biophysical techniques.

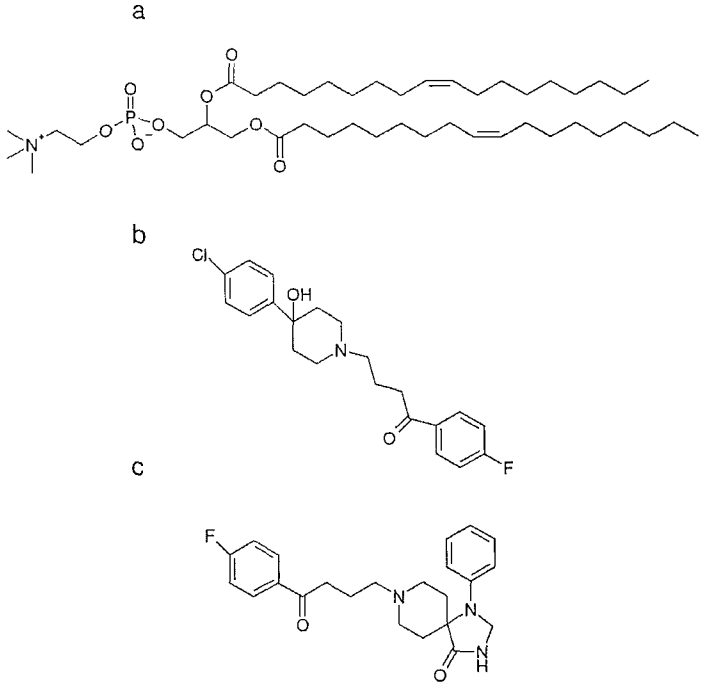


Figure III.1: Structures of DOPC (1,2-Dioleoyl-*sn*-Glycero-3-Phosphatidylcholine, (a), HPD, (b) and SPIP (c).

III.1.1 DOPC systems

The investigation of the lipid drug system was carried out using phosphatidylcholine (PC) lipids. These lipids are extensively used in model systems as they are one of the major constituents in mammalian cells [154] [49]. PC lipids have a common headgroup which is phosphatidylcholine, but differ according to their hydrocarbon chains in terms of the number of carbons as well as degree of unsaturations. For example, DOPC lipids have 18 carbons and one double bond (C18:1) at carbon 9 [75].

When DOPC lipids are mixed together in excess buffer (buffer A: 50mM Bis-Tris, 100mM NaCl, pH 7.4), they will tend to form the L_α fluid lamellar phase at room temperature (T_m=-22°C) as described in chapter one. As stated, this phase has the

ability to mimic the plasma membrane bilayer as it is fully hydrated and the lateral diffusion coefficients are in the same order of magnitude (~ 10^{-8} cm^2) [54]. Therefore the self-assembled bilayer stacks can also be compared to a hydrophobic barrier i.e. the BBB as the latter consists of a number of a highly anisotropic lipid bilayers [21].

III.1.2 Drug systems

The drugs that will be investigated in this section belong to the CNS family and are extensively used to treat neuro-psychiatric diseases such as Parkinson's disease, Alzheimer's disease, psychosis, and schizophrenia [113] [155]. These drugs have features common to the cationic amphiphilic drugs (CAD) family, as they consist of a hydrophobic and a hydrophilic moiety. One of the major features of CADs that is relevant to this work is the protonation of the nitrogen at physiological pH.

From their amphiphilic character, it is expected that CADs partition effectively into both biological [156] and artificial bilayers [150] [103] and bind preferentially to the bilayer interface causing bilayer perturbation [107] [110] [157] as was described for HPD and SPIP causing disorder in the interfacial region [120]. Partitioning of CADs changes the degree of membrane lateral organization and is dependent on the membrane composition as well as the drug's structure, showing that these changes are caused by specific interactions between the compounds and the lipids [158].

III.2 Biophysical measurements

Small Angle X-ray Scattering (SAXS) and Solid State-Nuclear Magnetic Resonance experiments were undertaken on condensed fluid lamellar phases made of DOPC in the presence of HPD and SPIP at various lipid:drug molar ratio in excess buffer (25 wt % lipid 75 wt % buffer A).

III.2.1 Small Angle X-ray Scattering (SAXS)

SAXS studies have the advantage of giving macroscopic details including identifying the membrane mesophase and determining the spacing between the bilayers (d-spacing). DOPC: CAD samples at different molar ratios were investigated over the course of one month.

Figure III.2a depicts a typical diffraction pattern corresponding to a DOPC lamellar phase that consists of spaced rings with a repeat spacing of 61.76 Å. In the presence of HPD at a molar ratio of 4:1 (Figure III.2b), 9:1 (Figure III.2c) and 20:1 (Figure III.2d) a marked swelling is noted. The 4:1 sample gives a very broad, diffuse diffraction pattern, where it is difficult to distinguish between the first and the second order rings as the first is probably obscured by the beam stop and the second is very broad (Figure III.2.d). This could be a result of a high drug to lipid ratio disrupting the bilayer. For these reasons, it was not possible to determine a d-spacing for this system. The 9:1 and 20:1 samples also gave broad diffuse diffraction patterns but with the two first order rings distinguishable and typical of a lamellar phase with d-spacing values at 35Å higher that of pure DOPC (Figure III.2b,c).

The diffraction patterns obtained are markedly different to that of pure DOPC. The presence of the drug is characterized by a marked swelling of the phospholipid bilayer. The broad diffuse diffraction pattern is a result of a wide distribution of d-spacing in between the bilayer stacks. This may be a result of sample metastability. This has been observed previously with chlorpromazine, another CAD molecule with dimyristoylphosphatidylcholine (DMPC) [112].

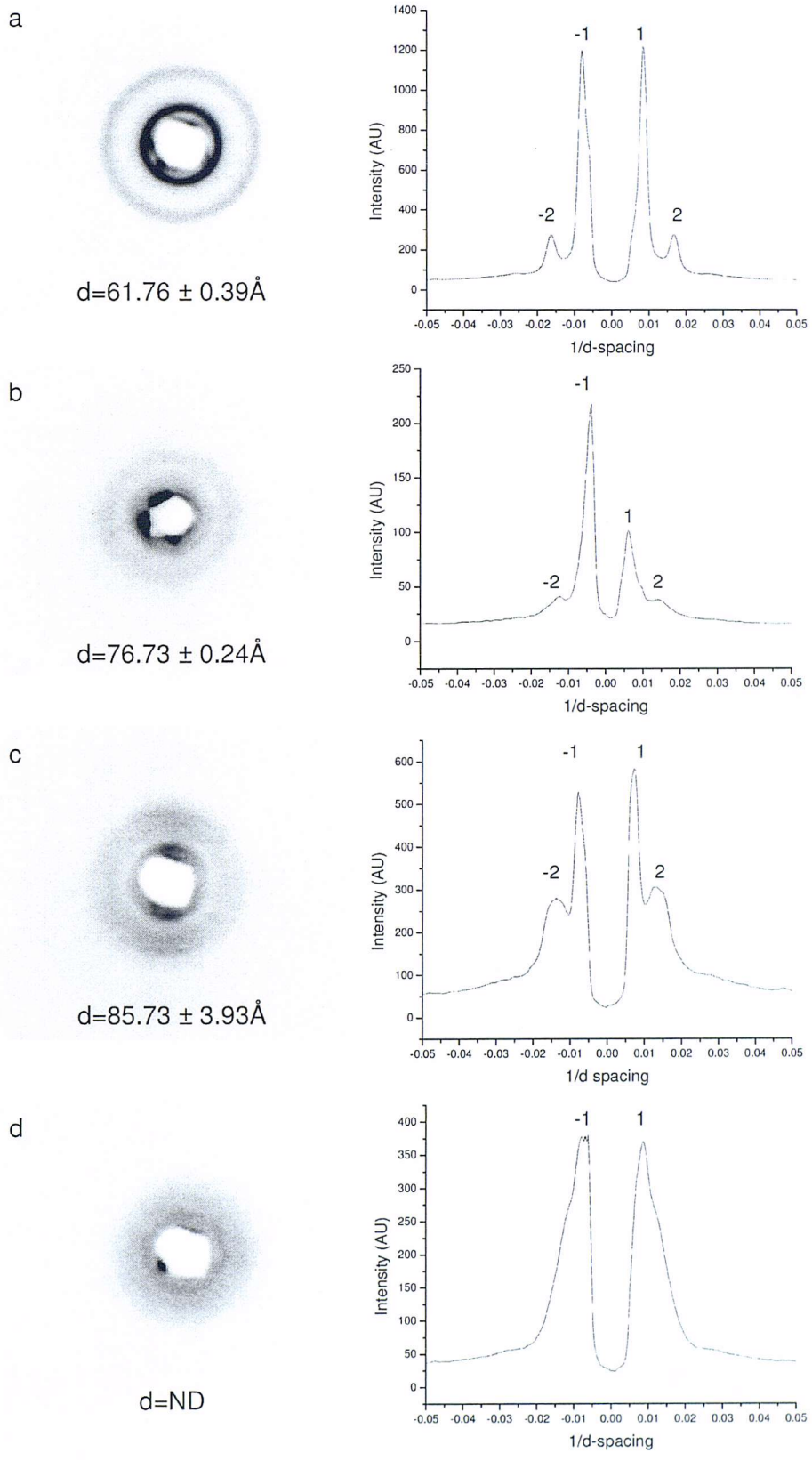


Figure III.2: SAXS diffraction pattern of (a) pure DOPC in physiological buffer A, and (b) DOPC: HPD 20:1, (c) DOPC:HPD 9:1, and (c) DOPC:HPD 4:1 systems in physiological buffer A. The presence of the HPD is represented by a marked swelling of the DOPC bilayers that is a result of a low degree of ordering of the system.

This swelling of all of the DOPC: HPD samples was also found to be time dependent. The d-spacing was seen to increase over a period of a week reaching a plateau at 82.72 Å in DOPC: HPD 20:1 samples at 35°C. This is contrary to pure DOPC systems that are known to equilibrate after 20 minutes. The DOPC lattice parameter is stable at 62 Å over the course of the experiment (Figure III.3).

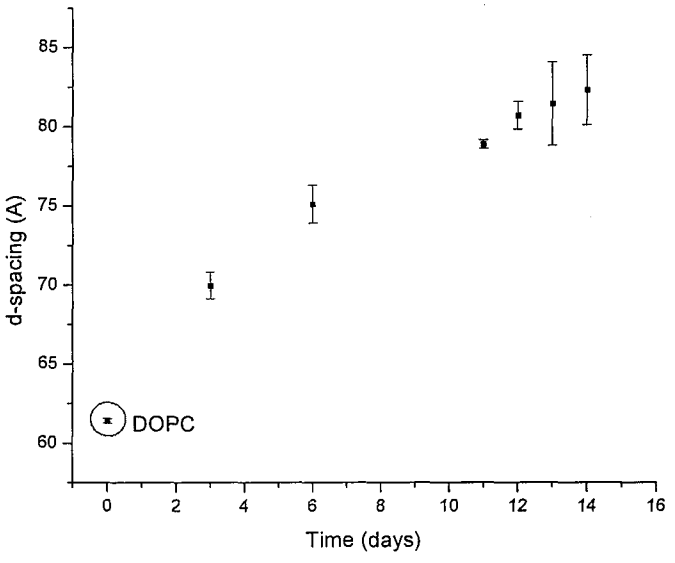


Figure III.3: Evolution of the d-spacing in DOPC: HPD 20:1 samples with time in physiological buffer A. The sample equilibrates after one week at 82.72 A. The d-spacing value for DOPC is shown in a red circle.

The broad diffraction pattern with high d-spacing associated values is what might be expected from a charged membrane interface which causes the bilayers to repel each other, leading to an increase of the lattice parameter [159]. Here, DOPC: HPD systems are made in buffer; therefore HPD is protonated at pH 7.4 (pKa=8.7) [42], consequently the protonation of the drug at the interface triggers the repulsion between the bilayers. This result suggests that HPD resides at the membrane interface.

The swelling behavior was also noticed for SPIP which is the other protonated CAD (pKa=8.3) [42] investigated in this section. Broad and diffuse diffraction patterns characterized by high d-spacing values are observed in DOPC: SPIP 20:1 systems, with the lattice parameter reaching 76.0 Å after 17 days. However the system is seen to evolve into another liquid crystalline mesophase after 3 weeks, with the formation of an H_{II} inverse hexagonal phase at 35°C. The H_{II} inverse hexagonal phase does not

occur in the control as bilayers made of DOPC lipids over this timescale form preferentially the L_α phase at room temperature (Figure III.4).

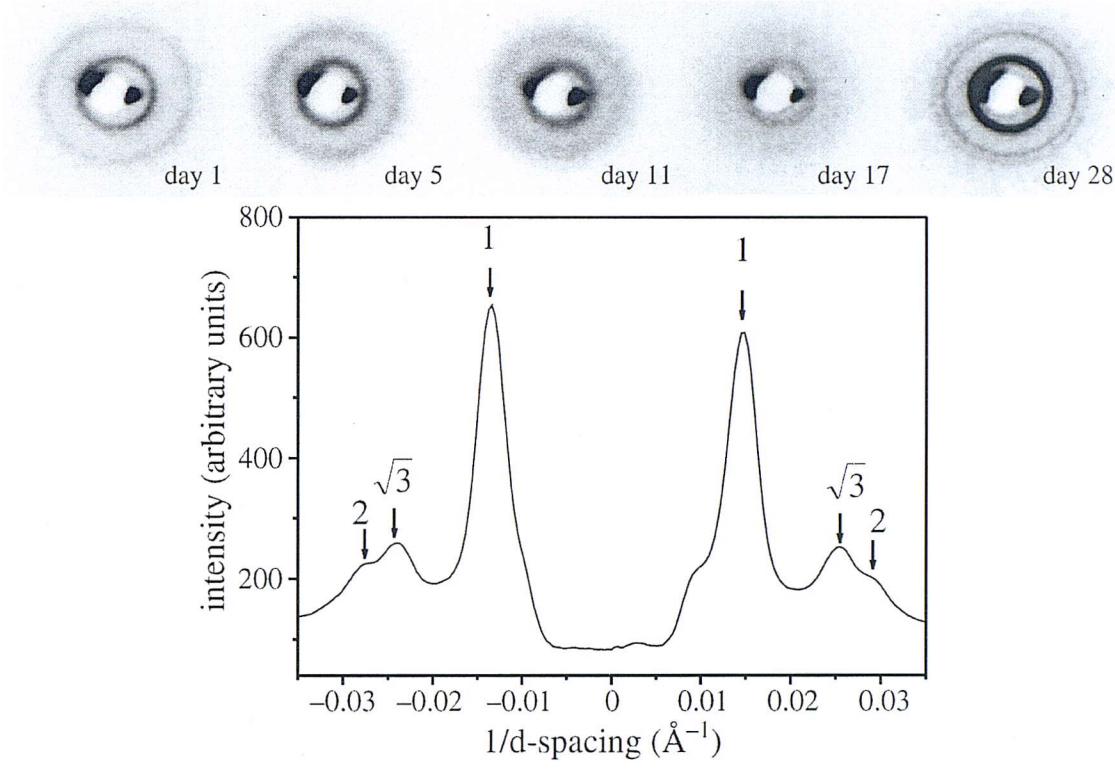


Figure III.4: SAXS pattern obtained for DOPC:SPIP 20:1 in physiological buffer A (50mM Bis Tris, 100 mM NaCl, pH 7.4). The presence of the SPIP is characterized by a distinct swelling of the phospholipid bilayers until breaking up into the inverse hexagonal phase after 28 days (Figure taken from ref [149]).

III.2.2 Solid State NMR (SS-NMR)

SS-NMR spectroscopy is a particularly sensitive technique for the determination of the three-dimensional structure of membranes with atomic resolution [71]. Static ^{31}P SS-NMR allows the distinction of the three main lipid mesophases: lamellar, hexagonal and isotropic phases i.e. cubic or micellar phases. Specific powder patterns are obtained from the chemical shift anisotropy (CSA) that is related to the average orientation of the phospholipid headgroup and the molecular motion of the lipid. Removing anisotropic interactions using ^{13}C SS-NMR magic angle spinning (MAS) gives high resolution information about the framework and structure of the phospholipid bilayer such as the state of the chains (see chapter II for more details). Therefore ^{31}P and ^{13}C SS-NMR MAS give complementary information on the structure and the phase of bilayer systems.

III.2.2.1 Static ^{31}P solid state NMR

Figure III.5a illustrates a characteristic lamellar powder pattern of DOPC bilayers that arises from the broadening of the CSA. This pattern also shows that the sample is in a single phosphorous environment with a CSA of 50 ppm.

In the presence of HPD at 20:1 and 4:1 lipid to drug molar ratios, the static ^{31}P pattern is drastically altered (Figure III.5b,c). The static ^{31}P powder pattern of DOPC: HPD 4:1 consists of a single large peak centered at ~3ppm, showing that the sample has evolved into an isotropic environment (Figure III.5c). In DOPC: HPD 20:1 samples an additional narrow lamellar powder pattern is superimposed upon the original one with a CSA of 30ppm, as well as a sharp peak that appears at ~3 ppm (Figure III.6b). These features show that the samples are in different mesophases at different CAD concentration.

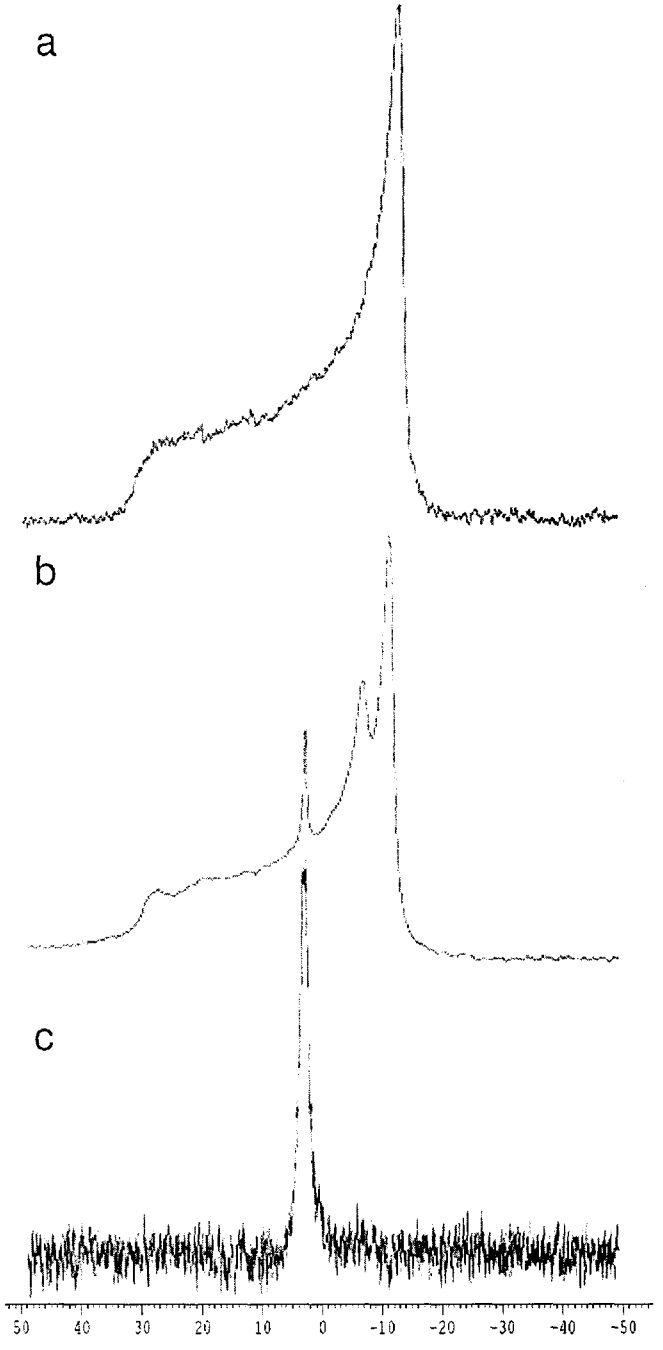


Figure III.5: Static ^{31}P Solid-State powder pattern for (a) pure DOPC, (b) DOPC:HPD 20:1, (c) DOPC:HPD 4:1. The appearance of an isotropic peak at 3ppm is revealing of the formation of an additional mesophase.

The sharp isotropic peak observed at 3 ppm in DOPC: HPD 20:1 and 4:1 is what could be expected from an isotropic phase such as a cubic or micellar phase as sharp isotropic lines arise from the rapid averaging on the NMR timescale. This result can be correlated to SAXS data where assumptions of the presence of micellar phases were made.

The second superimposed narrower lamellar powder pattern is characteristic of interactions of single chained lipids with phospholipids [160]. The narrower CSA arises from the increase of conformational freedom of the glycerol region of lipid in the bilayer. Single chained lipids can also form micellar phases when aggregated together, with the hydrocarbon chains sequestered from the polar aqueous medium by a spherical shell formed by the polar headgroups. The single chained lipid formed in this sample is a lysoPC lipid or LPC (1-oleoyl-2-hydroxy-*sn*-glycero-3-phosphocholine). The LPC signal evolves with time. The static ^{31}P SS-NMR powder pattern of DOPC: HPD 20:1 starts from a lamellar mesophase with one CSA environment to two lamellar mesophases with two CSAs due to the presence of LPC in the bilayer within one day (figure III.6b). After three days, the sample reaches an isotropic / micellar phase (figure III.6c); this pattern is similar to the static ^{31}P NMR DOPC: HPD 4:1 described above. Similar patterns were obtained with DOPC: SPIP 20:1.

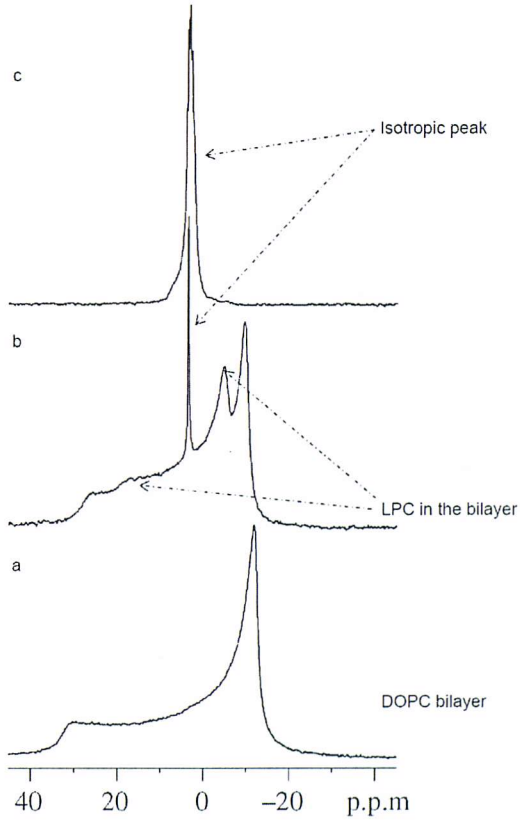


Figure III.6: Evolution of the static ^{31}P powder pattern with time for DOPC:HPD 20:1 in physiological buffer A. (a) Pure DOPC, (b) 1day: The presence of LPC in the bilayer leads to a change of the ^{31}P pattern with a narrower CSA. (c) 3 days: the LPC is predominant and leads to the formation of the isotropic phase. The sample has evolved from a lamellar phase to an isotropic phase that is predominant after 3 days.

Figure III.7 gives a schematic representation of the evolution of the bilayer as seen by ^{31}P SS-NMR. From SAXS and ^{31}P SS-NMR data it is reasonable to assume that the CAD resides at the bilayer interface and also that the DOPC: CAD systems evolve from a lamellar phase to an isotropic micellar phase that causes the disruption of the lamellar state.

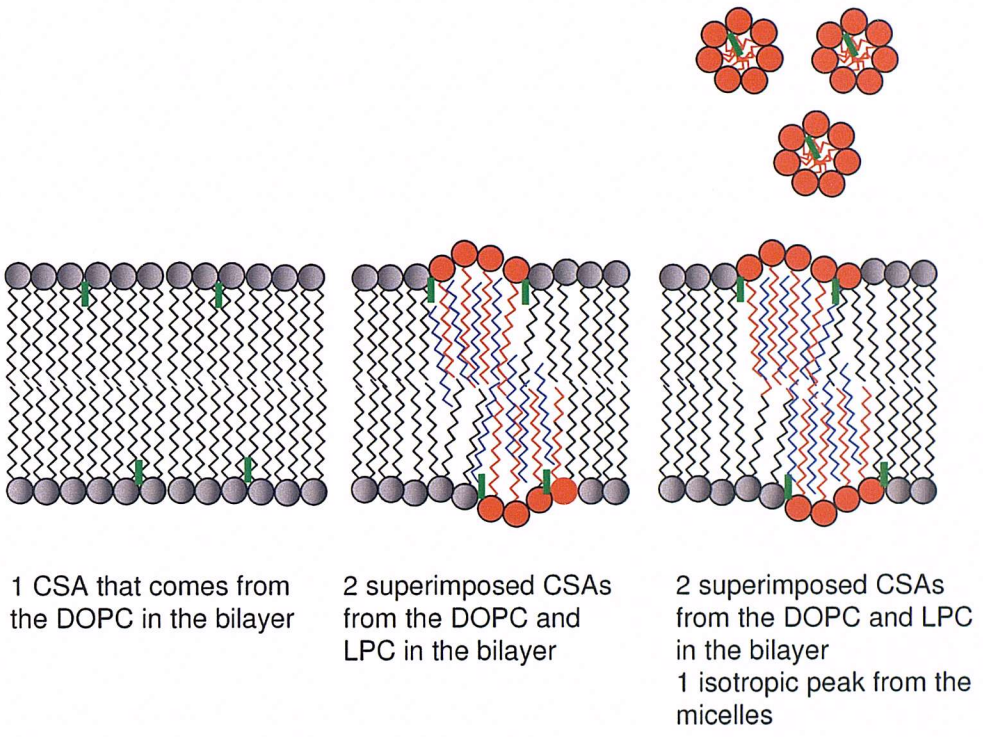


Figure III.7: Evolution of the DOPC bilayer in the presence of the CAD. The CAD resides at the polar / apolar interface and triggers the formation of LPC (red) that gives a narrower CSA in the bilayer superimposed to the DOPC CSA. The LPC phase separates into micelles / fragments that give the isotropic signal on the ^{31}P powder pattern.

III.2.2.2 MAS ^{13}C solid-state NMR

MAS ^{13}C solid-state NMR is a highly revealing technique as it shows clear signals from the ^{13}C nuclei in the structure of the phospholipids. Rapid trans / gauche isomerisation conformation leads to sharp and well resolved peaks for the fluid lamellar phase.

Figure III.8a shows the characteristic spectrum obtained from DOPC L_α phase samples as the peaks are sharp and well resolved. The fluid phase is correlated to

sharp peaks as a result of an averaging of the lipid trans / gauche isomerisation. The spectrum can be divided into four regions that correspond to the hydorophobic core (10-50 ppm), the glycerol backbone (50-80 ppm), the C=C bond at 133 ppm and the esterified carbonyl at 177.1 ppm. The peak assignments are given in Table III.1.

Chemical shift δ (ppm)	Assignement
177.1	DOPC carbonyl
133.0	DOPC double bond C8-C9
74.2	Cg2
69.4	Cβ
67.2	Cg3
66.8	Cg1
63.1	Cα
57.8	Cγ
26.1-37.6	DOPC chain
17.4	Chain methyl end group

Table III.1: ^{13}C NMR DOPC peak assignments.

In the presence of the HPD, the system remains in the fluid lamellar state with the peaks being sharp and well defined. The spectrum shows a large number of peaks, which correspond to the DOPC and HPD signals confirming the binding of the HPD to the membrane. The state of the chains is not altered in DOPC: HPD samples but is in the carbonyl region (~175-185 ppm) where an extra peak is appearing at 181 ppm and also a minor peak at 178 ppm in addition to the ester carbonyl group of DOPC at 177 ppm (figure III.8b). The chemical shifts of these two additional peaks are indicative of the presence of the carbonyl group of a fatty acid i.e. oleic acid (OA) (181 ppm). The minor peak can be attributed to the ester carbonyl group from LPC [161].

The appearance of the oleic acid in a DOPC: CAD sample has a critical effect on DOPC lamellar mesophases. OA has been reported to promote the formation of the H_{II} phase in PC bilayers [162].

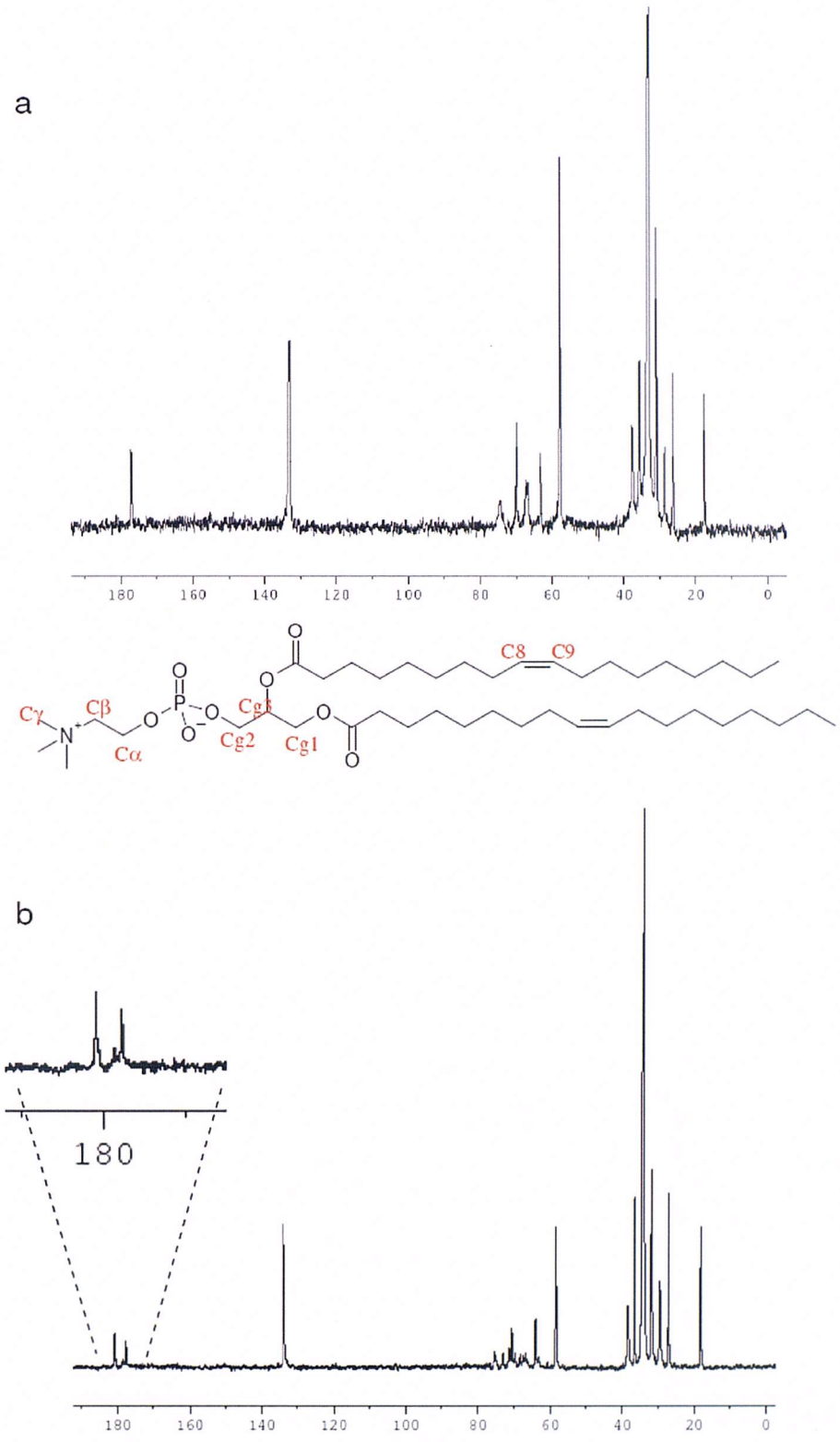


Figure III.8: (a) ^{13}C MAS spectrum of pure DOPC in the fluid state. (b) ^{13}C MAS spectrum of DOPC: HPD in physiological buffer A showing the evidence for the formation of oleic acid at 181.0 ppm and LPC at 178 ppm (expanded region) 3 days after the sample was made.

III.2.3 CADs induce the acid hydrolysis of the bilayer

From both the SAXS and NMR studies it is evident that in the presence of the CADs, the fluid L_α lamellar phase coexists with a micellar phase before ultimately forming a new phase, the H_{II} phase. From the results discussed above, it appears that CADs have a considerable effect on DOPC bilayers in a buffered system.

First, it was shown by SAXS that HPD and SPIP have an effect on the d-spacing at every ratio. It was found that the DOPC bilayer was completely disrupted showing only one broad ring reflecting the presence of a micellar phase in DOPC: HPD systems at a molar ratio of 4:1. There is still some residual integrity of the lamellar bilayer at a ratio of 9:1 and 20:1, however the d-spacing is seen to increase considerably with time reaching equilibrium at a value of 81 Å after one week. At this time the diffraction pattern is similar to the 4:1 ratio, showing very broad and diffuse rings. This swelling behaviour is due to the charged DOPC: CAD interface with the protonation of the drug repelling the membranes. The CAD is seen to bind to the water-bilayer interface as described elsewhere [97] [37] [107] [110] [157]. SAXS diffraction patterns also showed that the CAD promoted the formation of another mesophase: the inverse hexagonal phase H_{II}.

Secondly, from the SS-NMR results it appears that HPD and SPIP had a critical effect on the membrane shape and integrity as it was established from the ^{31}P static spectra where the isotropic peak appeared at ~3ppm which corresponds to the appearance of LPC. In addition, this isotropic peak can also be the result of the formation of fragments and small vesicles [163]. ^{31}C MAS spectra showed the formation of oleic acid at 181 ppm and confirmed the presence of LPC in DOPC: HPD samples. The same effects were observed for DOPC: SPIP.

Membrane fragments formation has been observed previously in CAD-lipid systems, and has been attributed to the formation of CAD-lipid conjugates [46] [164]. However, this cannot explain the time-dependent formation of the inverse hexagonal phase as well as the isotropic micellar phase. The simplest hypothesis to explain the appearance of both these phases is that an acyl chain is being formed via the

hydrolysis of DOPC, resulting in the creation of a single chained lipid i.e. LPC and the associated fatty acid, OA. It is known that LPC will phase separate from the parent membrane at high concentration and form micelles [165] [166] [163].

CADs potentially act as an acid catalyst until the whole membrane is degraded into LPC and the associated fatty acid, oleic acid. Protonated CADs reside at the water-lipid interface of the bilayer, which enable them to activate the lipid ester function and therefore catalyse the hydrolysis of the ester bond. The mechanism by which the lipid is degraded by the CAD follows the classical pathway of an ester acidic hydrolysis by water, is shown on Figure III.9.

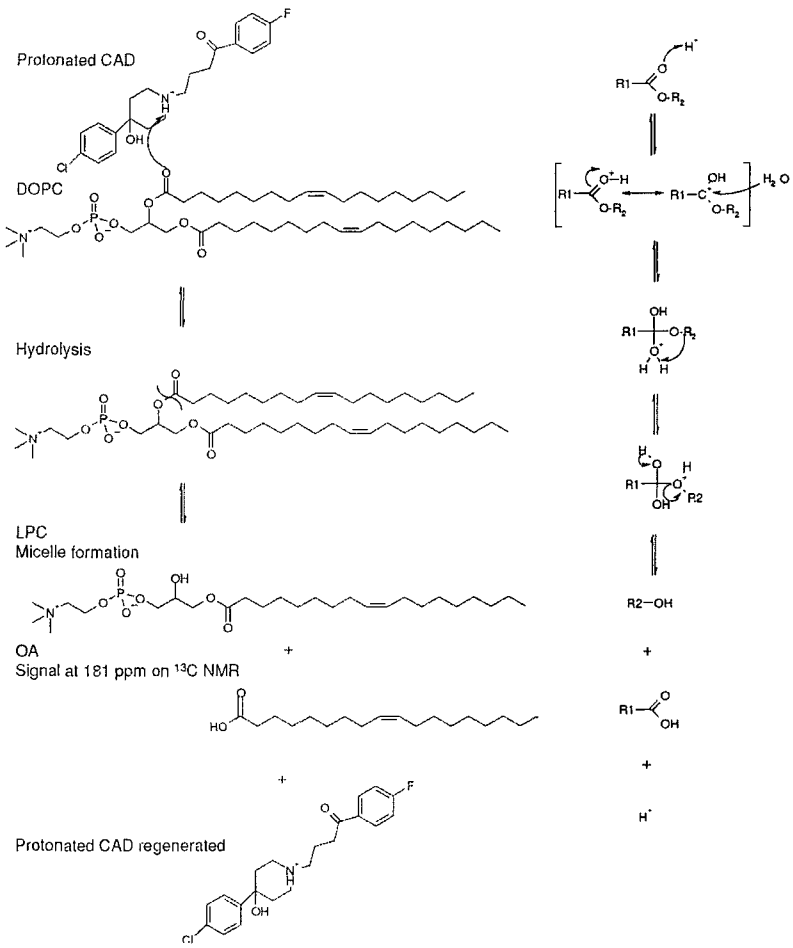


Figure III.9: Representation of DOPC: CAD catalyzed digestion. The hydrolysis of the DOPC in LPC and OA is represented on the left hand side: The protonated CAD resides at the lipid interface, and activates the lipid ester carbonyl bond to make it more electrophilic. The mechanism of the ester acid hydrolysis is given on the right hand side: The electrophilic carbon is attacked by water, which leads to the formation of a tetrahedral intermediate. The oxygen is deprotonated by water to neutralize the charge, and the R2-O group is protonated to be a good leaving group. The electrons of the adjacent oxygen push out the neutral R2-OH (LPC) and reveal the C=O of the carboxylic acid (fatty acid). The acid catalyst is regenerated.

It is expected that CADs dissolve into OA / LPC fragments once LPC molecules are able to form micelles i.e when there are about 30 % of LPC molecules in the membrane [163], although lysolipids and fatty acids form bilayers and are stable in the membrane [167]. Finally it is likely that the LPC ester bond is degraded into OA molecules as the reaction progresses.

III.3 Detection of the degradation products by normal phase high pressure liquid chromatography.

III.3.1 HPLC system

Detection of DOPC and CADs as well as degradation products LPC and OA was investigated by normal phase HPLC equipped with an evaporative light scattering detector (ELSD). Normal phase HPLC consists on separating the lipid: drug mixture according to their polarity. They are separated using a polar stationary phase made of silanol and a nonpolar mobile phase made of hexane, isopropanol, water and acetic acid. After dissolution into the mobile phase, the lipid:drug mixture is injected and run by the mobile phase through the column. The products associate with the matrix and are retained on the column. Adsorption strengths increase with an increase in the compound's polarity. Elution of lipid: drug species is possible when a more polar mobile phase is run through the column. Detection was possible with the ELSD detector that converts the effluent off the column into lipid nebulized lipid droplets that scatter a beam of light. The detector response is a function of the quantity of lipids within the droplets. Therefore, attribution of retention times for each lipid species as well as its quantification is possible. Normal phase HPLC was a system of choice as it allowed the separation of the DOPC, LPC, CAD and OA on the same chromatogram with a gradient from an apolar mobile phase, mobile phase A to a more polar mobile phase, mobile phase B (details on the mobile phase composition and gradient as well as detector descriptions are given in chapter II).

III.3.2 Standards

Standards were dissolved in mobile phase B and injected separately to determine retention times and resolution of peaks. Figure III.10 shows chromatograms of DOPC, HPD, SPIP, LPC and OA. Each peak looks sharp and well resolved. Attribution of retention time is therefore possible apart from the OA that is eluted at 3 min, which overlaps with the injection peak. The minor peaks present in figure III.10 b,c,d at 2

and 11 min correspond to the injection peak and the mobile phase respectively. Table III.2 shows retention times attributed to each species.

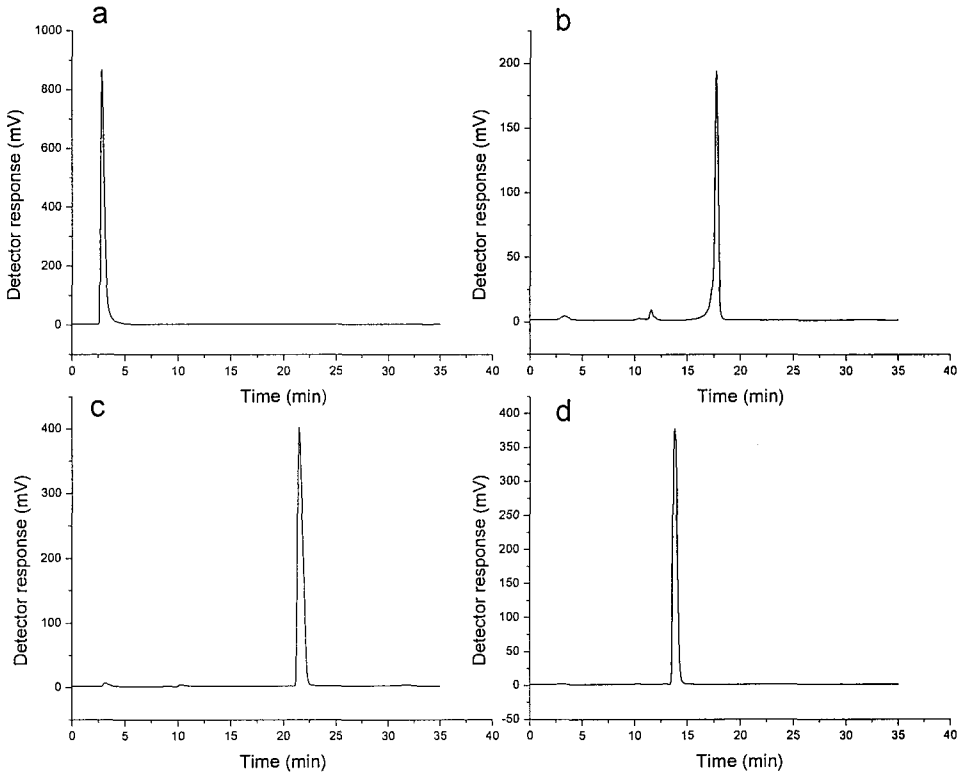


Figure III.10: Normal phase HPLC elution profile for (a) OA, (b) DOPC, (c) LPC, (d) HPD.

Injected molecules	Retention time (min)
OA	2.80
DOPC	17.75
LPC	21.48
HPD	13.85

Table III.2: Standard elution times

Injection of the four compounds together showed a clear separation of peaks on the chromatograms. These sets of results are encouraging as they allow the separation of the 4 main compounds, namely DOPC, LPC, CAD and OA. All chromatograms obtained have a clear baseline and peaks are well resolved, showing the accuracy and efficiency of the ELSD detector (Figure III.11).

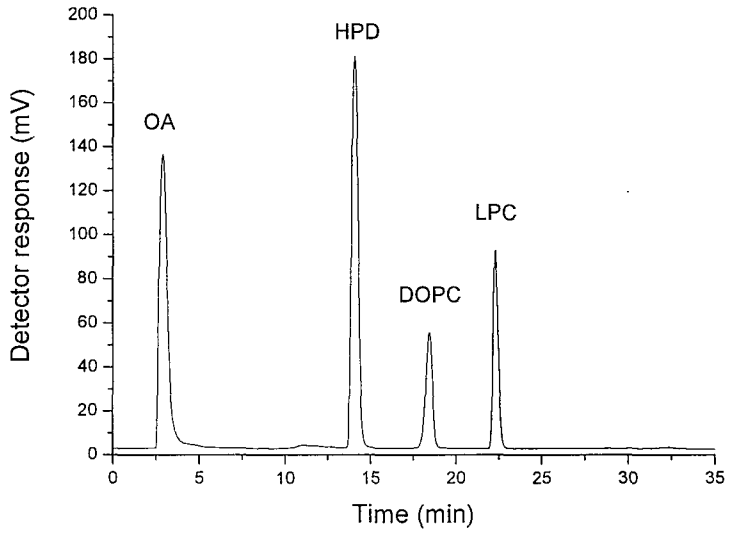


Figure III.11: Normal phase HPLC elution profile for a mixture of the 4 standards.

The fatty acid is eluted first at 2.80 min, followed by HPD at 13.84 min, DOPC at 17.75 min and finally LPC at 21.48 min. This elution profile was already observed in the literature [168].

Calibration curves were obtained for individual lipid or fatty acid molecules by injecting a range of concentrations from 0.002 μg to 1 μg of compound in the HPLC system. The results showed a linear response of the detector, with a range of linearity being around 0.99, the base line was stable and the retention times reproducible. Therefore it is possible to quantify precisely the amount of lipid species and drug that are present in the system except for the fatty acid, where an error coming from the injection peak is added to the fatty acid signal, is not possible to quantify. The calibration curves for DOPC, LPC and OA are represented on figure III.12.

The normal phase HPLC system investigated in this section is very accurate and reliable, with reproducible DOPC, LPC and HPD retention times, and a linear calibration curve.

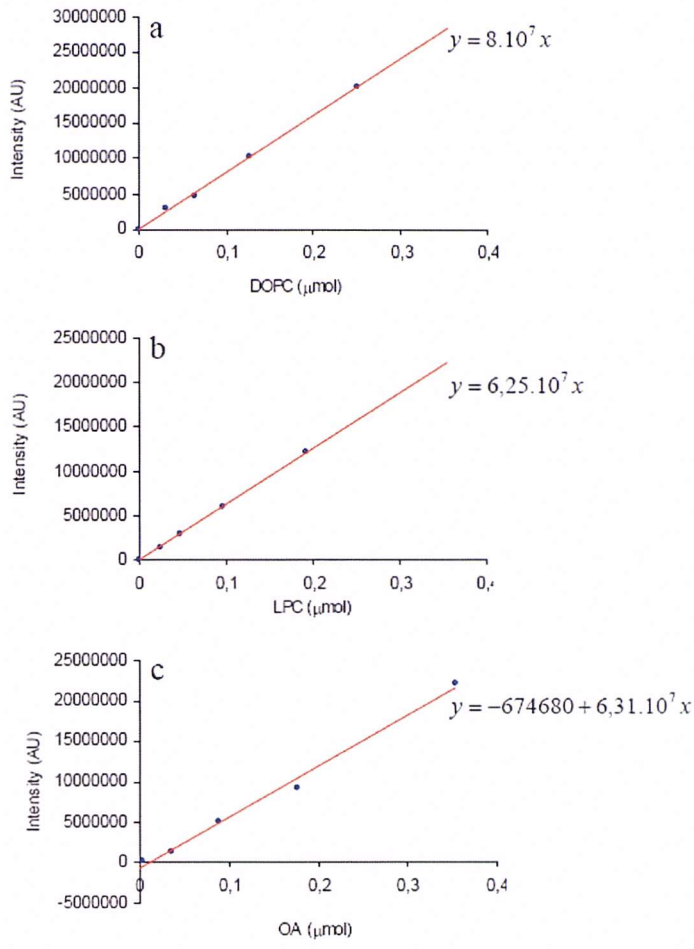


Figure III.12: Calibration curves for DOPC (a), LPC (b) and OA (c). These calibrations were used to calculate the quantity of DOPC remaining and LPC formed in the samples at different times.

III.3.3 Detection of the degradation products in DOPC: CAD systems

Detection of degradation products was undertaken in DOPC: HPD systems with the system described above. Figure III.13 depicts the chromatograms obtained after dissolving a DOPC: HPD 20:1 sample four days old in the mobile phase B. The chromatogram shows four sharp and well resolved peaks, of which the retention times all correlate with the standards i.e. 3 min for OA, 13.84 min for HPD, 18 min for DOPC and 21.48 min for LPC. The DOPC: HPD and DOPC: SPIP have effectively degraded into OA and LPC. The peak emerging at 12.73 min is attributed to the mobile phase signal; this peak is present in all samples as well as blanks.

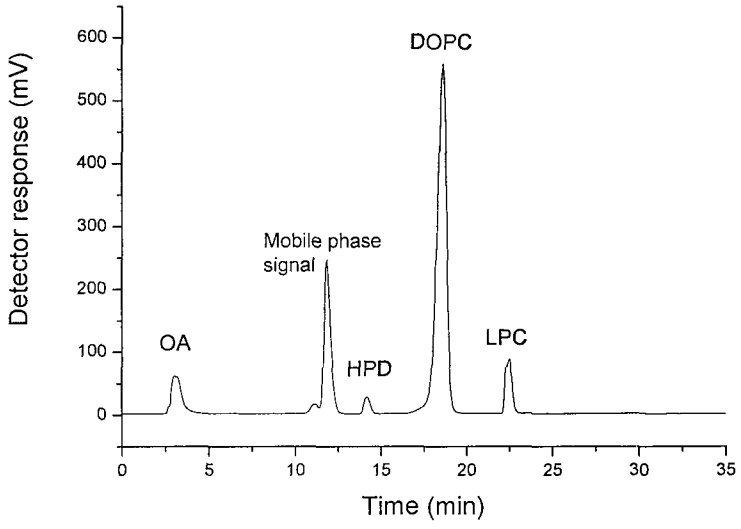


Figure III.13: Detection of the degradation products in DOPC:HPD samples after 3 days at room temperature.

Normal phase HPLC allows the detection of the degradation products as well as their quantification. However care must be taken when measuring the OA peak, as this also correlates with the injection peak. Different gradient systems were tried but none could shift the OA peak away from the injection peak. This might suggest that the OA is not retained on the column at all.

III.4 Direct visualization of the degradation

III.4.1 Use of giant unilamellar vesicles (GUVs) as model membranes.

Giant unilamellar vesicles (GUVs) are model systems with a diameter range of 1 μm to100 μm. Correlation between GUVs and biological cells is possible thanks to numerous features such as size, lipid composition and osmotic balance inside and outside the vesicle. GUVs are attractive systems to examine biological functions ranging from membrane fusion to membrane fission [169]. They can be used for physical and biological investigations and are convenient models that can be observed directly under a light microscope. Observation of shape changes of GUVs induced by interactions of small molecules have been extensively investigated in the literature [170] [171]. Shape changes are directly correlated to elastic properties of the phospholipids that form the vesicles, this feature allows the detection of the change in the area of the membrane with high sensitivity [172] [173]. Several methods exist to form GUVs, the most used ones being the spontaneous swelling [174] and the electroformation [148]. Electroformation was the method employed in this section. It consists of drying the lipids on a platinium electrode followed by hydration under alternative current. The GUVs formed are mostly unilamellar with a size greater than 1 μm.

The use of electroformed GUVs allowed the direct visualization of the CAD interacting with the phospholipid bilayer. Two main experiments were performed: the electroformation of GUVs where DOPC and HPD were dried and electroformed together, this method will be referenced as "the co-lyophilised method"; and the addition of fluorescent SPIP to electroformed DOPC vesicles "the addition method". The co-lyophilisation method enables the drug to sit at the water-bilayer interface during the electroformation, whereas the addition method consists of injecting the fluorescent drug to preformed vesicles.

III.4.2 Electroformation of Giant Unilamellar Vesicles with HPD. The co-lyophylised method.

Giant DOPC:HPD co-lyophilised vesicles grown in a buffered system at a 4:1 molar ratio were observed with transmission microscopy over an hour. Figure III.14a shows a micrograph of GUVs made of pure DOPC. The vesicles adopt a perfect spherical shape under minor tension, are symmetrical with a large internal core, and reach a size of 10 μm. These vesicles are stable for more than 6 hours.

Electroformation of GUVs made of DOPC and HPD appears to be complex. The formed vesicles encounter difficulties to grow, and they do not reach the expected size nor the shape of a pure DOPC GUV vesicle. The DOPC: HPD vesicles appear small, elongated, distorted and disproportionate (Figure III.14b). In addition, membranous fragments are being formed as well as an appearance of vesicles inside other vesicles that are not present in the pure DOPC vesicles. Figure III.14c shows how the vesicles are destabilized in the presence of HPD, until they lose their shape and shrink to a uniform size, over 30 minutes.

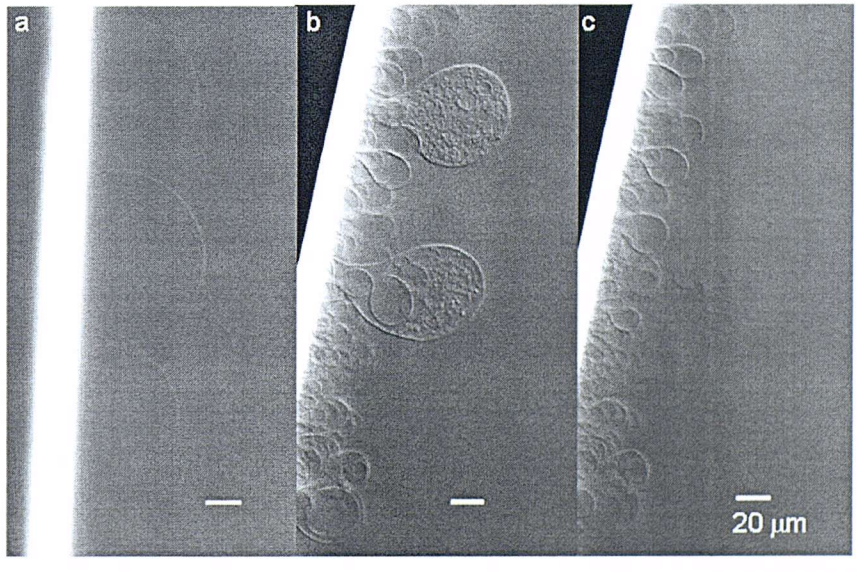


Figure III.14: Electroformation of DOPC: HPD GUVs in physiological buffer. (a) Electroformation of pure DOPC GUVs. The vesicles are symmetrical and spherically shaped. (b) The electroformed DOPC: HPD GUVs are irregularly shaped and distorted. Membranous fragments are also observed inside the vesicles. (c) The DOPC:HPD GUVs are short lived and shrink to a multi-layered vesicles of drug / lipid mixture that is monodisperse.

Electroformed DOPC: HPD GUVs are unstable and short lived, and typically mutate into severely distorted vesicles, in which there are a myriad of different smaller vesicles evident. From these results combined with SAXS and NMR it is reasonable to assume that the shrinkage of the vesicles is due to the degradation of the DOPC bilayer by the CAD, that takes place during the electroformation of the GUVs. The DOPC: HPD GUVs cannot grow and are elongated because of the appearance of LPC and oleic acid as the degradation goes on. The effects of LPC and oleic acid on vesicles made of DOPC were described to significantly decrease the size of the vesicles as well as promoting the formation of disc-like structures and threadlike cylindrical micelles. The small membranous fragments seen to appear inside the vesicles can be attributed to the formation of CAD / lipid / fatty acid / micelle mixture as a result of the catalytic reaction. As the reaction proceeds the vesicles shrink and result in small monodisperse vesicles that aggregate together. It has been already observed that equimolar mixture of PC:LPC:OA would form monodispersed closed structures, whereas the presence of more fatty acid considerably alters the shape of the vesicles (Figure III.15b,c) [165].

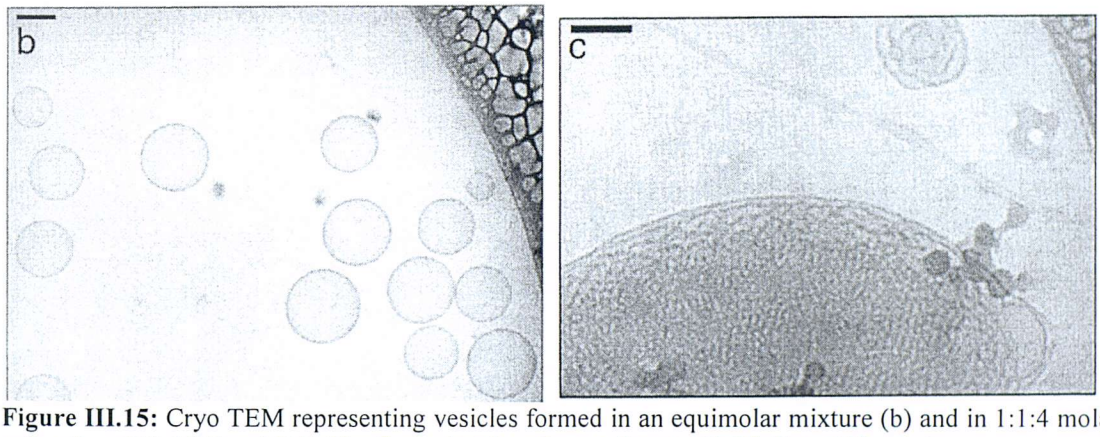


Figure III.15: Cryo TEM representing vesicles formed in an equimolar mixture (b) and in 1:1:4 molar ratio of eggPC, LPC and OA. The figure is taken from reference [165]. Bar=100nm.

III.4.3 Addition of Fluorescently labeled SPIP to GUV

Visualization of the degradation was also carried out using fluorescence microscopy by injecting fluorescent NBD-tagged-SPIP which is a SPIP analogue, to electroformed GUVs made of DOPC residing on the electrode in buffer. The structure of NBD-tagged-SPIP is shown on figure III.16.

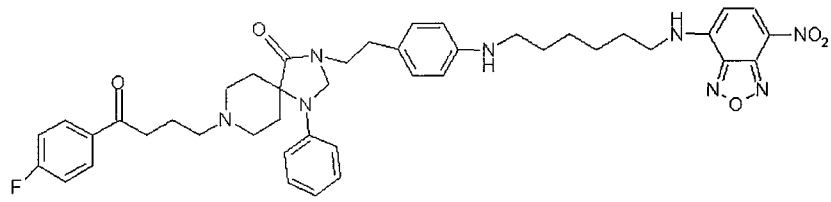


Figure III.16: Chemical structure of the NBD-tagged-SPIP (NBD-Aminohexanoylaminophenetylspiperone)

In this method, the fluorescent CAD is injected to the vesicles whereas in the colyophilised method, the drug was already sitting at the interface. GUVs made of DOPC were grown and stabilised as desribed in chapter II. NBD-tagged-SPIP and SPIP were solubilised together in a 1:1000 molar ratio in pure ethanol prior to injection. The CADs were then injected outside the DOPC vesicles and left to interact with the lipids. A movie showing the degradation of DOPC vesicles was recorded over 40 min (Please see DVD attached).

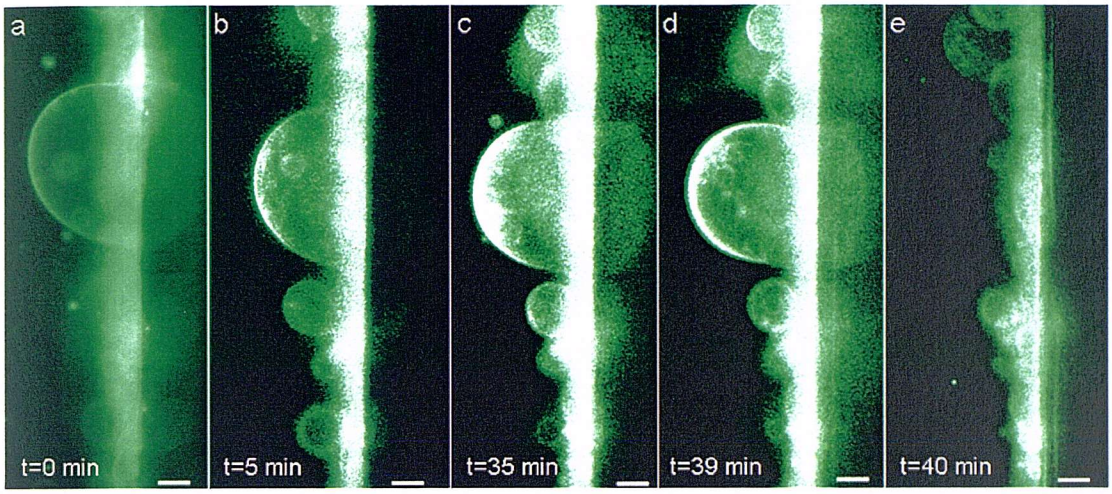


Figure III.17: Injection of NBD-tagged-SPIP to GUVs made of DOPC. (a) Binding of the fluorescent drug occurs within 150 ms and is uniform on the bilayer (GUVs and the platiniu wire). (b) The vesicles are being distorted and membranous fragments are present. (c) The fluorescence intensity increases on the surface of the vesicle due to more membranous fragments formed. (d) The vesicle acquires an irregular shape caused by the lipid hydrolysis until it is destabilized (e) and leaves the electrode after 40 min.

Uniform distribution of NBD-tagged-SPIP is initially evident on the vesicles as well as on the platinum wire. Binding of NBD-tagged-SPIP to DOPC vesicles occurs within 150ms, confirming the preference of the CAD at the membrane interface (figure III.17a) despite the NBD tag that makes it more soluble. The degradation takes place in the first minute, where membranous fragments and small vesicles are visualized. After 5 min, the vesicles are visibly distorted and elongated, confirming the results obtained with the colyophilised method (Figure III.17b). Fluorescent membranous fragments containing SPIP and NBD-tagged-SPIP are also being formed inside and outside the vesicles and float away from the host GUV (figure III.17c) as a result of the action of the drug. There is evidence of vesiculation and detachment of lipids from the vesicle as a result of the hydrolysis of the ester carbonyl bond of DOPC. The intensity of fluorescence increases on the surface of the vesicle due to newly formed micelle / membrane fragments and small vesicles [175] (Figure III.17d). The hydrolysis goes on with enrichment of membrane fragments and fatty acid both on vesicles and the platinium wire, until the vesicle becomes unstable at 39 min, which subsequently triggers the detachment of the vesicle from the wire at 40 min (Figure III.17e).

Here evidence of the hydrolysis of the lipids comes from the shape shrinkage distortion of the vesicles and formation of fluorescent membranous / micelle

fragments. Morphological modifications of GUVs due to lipid hydrolysis by phospholipases showing significant shrinkage of the vesicles inducing vectorial budding of smaller vesicles from the surface of the GUVs was already described in the literature [176] [177]. Fluorescence microscopy was found to be highly revealing showing the GUVs being chemically degraded by the CAD when it is added to the bilayer, this occurring on time scales consistent with observed pharmacokinetics [178].

Direct visualization of the degradation of the phospholipid fabric of GUVs was observed with transmission and fluorescence microscopy. The formation of membrane fragments is a result of drug-induced ester-hydrolysis at the membrane level. The results described above confirmed the initial assumption made from SAXS and NMR data.

III.5 Importance of the phospholipid ester linkage

The above sections demonstrated how CADs catalyse the acid-hydrolysis of the ester linkage present in the phospholipid chains, producing a fatty acid and single-chain lipid. To test the hypothesis of the membrane hydrolysis through acid catalysed ester cleavage, interactions of CADs with ether-linked PC lipids (dioctadecenylphosphatidylcholine) were investigated by SS-NMR and fluorescence microscopy. Ether-linked PC lipids are species that are present in nature; in particular they can be found in tissues such as heart muscles and in the nervous system [179]. Ether-linked PC lipids are characterized by an ether bond in the glycerol vicinity resulting in the absence of hydrogen that prevents them from taking part in hydrogen bonding (Figure III.18).

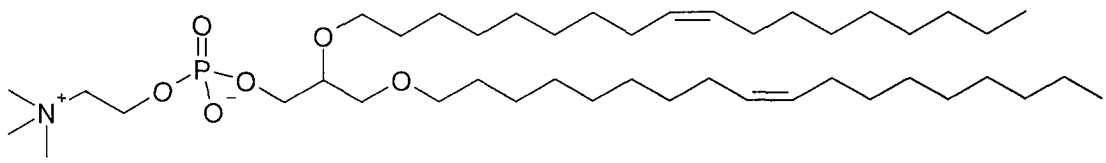


Figure III.18: Structure of the ether-linked PC lipid used (1,2-Di-O-Octadecenyl-*sn*-Glycero-3-Phosphocholine)

These lipids are stable with the ether bond remaining intact under the conditions of the experiments and therefore are not subject to acidic hydrolysis. Therefore in the presence of an ether linkage the proposed reaction mechanism should be incapable of causing chain hydrolysis.

III.5.1 Evidence from static ^{31}P solid-state NMR

Figure III.19a illustrates a characteristic lamellar powder pattern obtained by ^{31}P static NMR, similar to that of DOPC bilayers that comes from the broadening of the CSA. This pattern shows that ether linked PC bilayers are in a single phosphorous environment with a CSA of 50 ppm. Ether-linked PC bilayers are in the fluid lamellar phase L_α at room temperature (T_m= -22°C) [75].

In the presence of DOPC: HPD 4:1 lipid to drug molar ratio, the static ^{31}P pattern is unaltered over two weeks (Figure III.19b,c), this is contrary to DOPC systems where an isotropic peak is evident after one day at that lipid: drug ratio. The ether-linked PC: HPD system is very stable over two weeks, showing no signs of micellar isotropic phases.

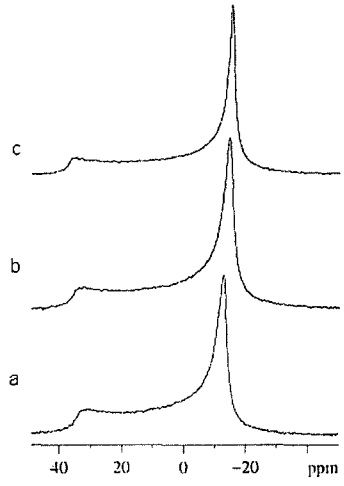


Figure III.19: ^{31}P solid-state NMR time evolution of Ether-linked PC: HPD 4:1 in physiological buffer A. (a) Ether-linked PC powder pattern appears characteristic of a lamellar phase with a CSA of 50 ppm. (b) Ether-linked PC:HPD 4:1 powder pattern after two days and (c) two weeks. The system is stable and remains in the lamellar phase.

III.5.2 Fluorescence microscopy

Similarly to DOPC experiments, injection of fluorescent NBD-tagged-SPIP to electroformed GUVs made of ether-linked PC was undertaken in a buffered environment. It is shown on figure III.20a that the drug binds homogeneously to the ether-linked lipids confirming the ability of the drug to reside at the water-bilayer interface. The vesicles are spherically shaped and symmetrical upon the addition of the drug and stay stable for more than 40 min. There is no evidence of distortion of the vesicles as described for DOPC or presence of membranous fragments at any point over the course of the experiment (Figure III.20b,c).

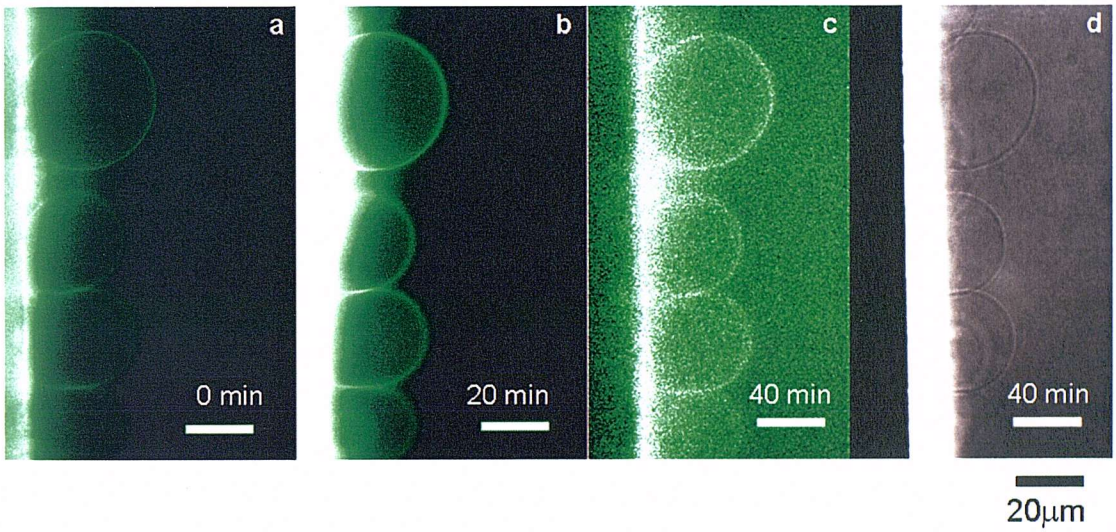


Figure III.20: Injection of NBD-tagged-SPIP to GUVs made of ether-linked PC. (a) The fluorescent drug binds homogeneously to the vesicles. (b) After 20 min the GUVs are perfectly stable and spherically shaped. (c) There is no evidence of formation membranous fragments after 40 min due to the absence of ester linkage. (d) Transmission micrograph confirms the integrity of the vesicles.

The major difference between this set of experiments and the former ones is the lack of ester bonds in the phospholipids. The lipid bilayer is not degraded by the drug when an ether bond replaces the ester bond; therefore the presence of the ester linkage of the phospholipids is compulsory for the reaction to occur.

III.6 Binding and partitioning of the CADs into vesicles

This section will focus on the investigation of HPD and SPIP binding properties to bilayers made of DOPC followed by an examination of its hydrolysis using an original fluorescence technique [143]. Binding constants of these drugs to DOPC bilayers will be also determined.

III.6.1 Background

The basis of the detection method for measuring CAD binding phenomena to lipid bilayers is linked to variations in membrane electrostatic potentials. It is well known that when molecules such as ions, peptides, drugs bind to membranes, they induce a change in the bilayer electrostatic potentials in both biological and model systems [92, 135, 180].

Three electrostatic potentials are associated with membranes: the transmembrane potential $\Delta\psi$, the dipole potential Φ_d and the surface potential Φ_s. The transmembrane potential arises from a gradient of electric charges across the membrane, the dipole potential originates from the molecular dipoles of the lipids that form the bilayer and the surface potential arises from a net electric charge at the membrane surface.

The surface potential represents the potential difference between the membrane surface and the bulk aqueous phase [137]. In that respect, Φ_s properties can be utilized to characterize binding events by monitoring changes and variation of Φ_s upon addition of CADs to lipid bilayers. It has been reported that electrostatic details can be obtained by using spectrospcopic probes that change their spectral properties according to their electrostatic potentials [181]. Characterization of the variations of Φ_s upon addition of various types of molecules to cell membranes and model membranes has been studied extensively using the fluorescent lipid fluoresceinephosphatidylethanolamine (FPE) [143, 147, 182]. FPE, which contains

the phosphatidylethanolamine motif, has the ability to incorporate into lipid bilayers, leaving the fluorescein moiety exposed to the aqueous phase. This enables the probe to be sensitive to changes in the surface potential Φ_s. FPE is a real time probe for the study of molecules binding to lipid bilayers.

Adding positive charges to a bilayer system containing FPE will reduce the size of the membrane electronegative potential that deprotonates the fluorescein xanthene group. This is reflected by an increase in the fluorescence signal. The theory of the fluorescence binding assay involving the use of FPE is fully described in chapter II.

III.6.2 Binding kinetics of HPD and SPIP to vesicles made of DOPC.

As described in chapter I, HPD and SPIP exhibit common structural features that allow their classification into the cationic amphiphilic drug family. It has been noted that these type of drugs have the ability to partition into lipid bilayers according to their amphiphilic properties [123, 149]. Moreover, these molecules are protonated at pH 7.4, as HPD pKa= 8.7 and SPIP pka= 8.3 [42, 44]. Therefore binding properties of the mentioned drugs can be investigated using the FPE and are expected to alter the surface potential Φ_s.

III.6.2.1 DOPC vesicle labeling

Figure III.21 shows the absorption and emission spectrum of 100 nm extruded FPE labelled DOPC vesicles. The obtained spectrum shows the excitation and emission of the fluorescein at the bilayer surface, with an excitation wavelength λ_{exc}=495 nm and an emission wavelength λ_{em}=530 nm.

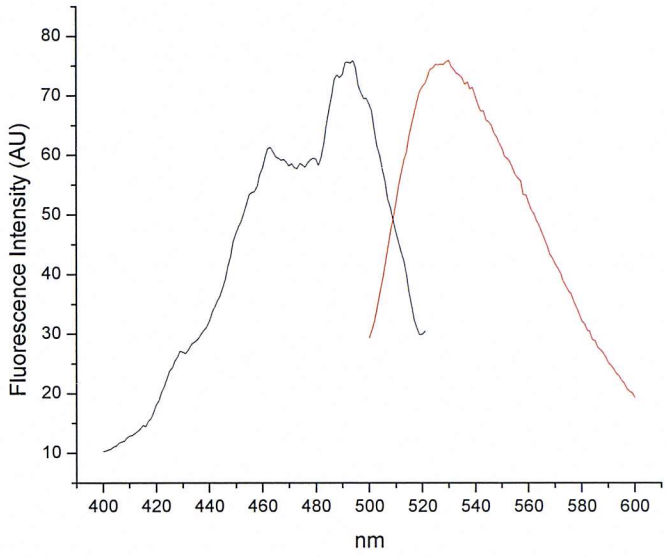
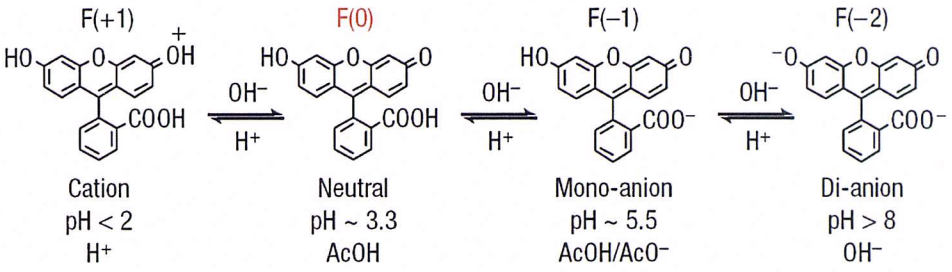


Figure III.21: Absortpion (black) and emission (red) spectra obtained for FPE labelled DOPC vesicles.

The shoulder observed at 463 nm on the excitation spectra is due to the presence of the mono-anionic form of the fluorescein at pH 7.4 (figure III.22).

a



b

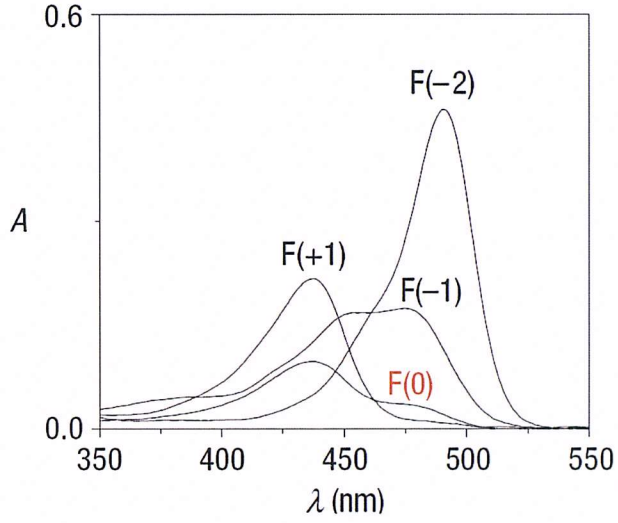


Figure III.22: The four ionization states of fluorescein (a). Each state has a distinctive excitation spectrum (b). As FPE is inserted in phospholipids vesicles at pH 7.4, it is expected that its excitation spectrum correspond to a mixture of the monoanionic and dianionic form. (figure taken from reference [142]).

The absorption emission spectra obtained are in accordance with the literature [142, 184]. The absorption as well as the emission fluorescence of FPE is responsive to the surface potential. As emission fluorescence is more sensitive than absorption [143], only the change in the fluorescence emission will be considered and correlated to a change of the surface potential. The maximum emission intensity corresponds to labelled vesicles before the addition of drug molecules.

III.6.2.2 Addition of HPD and SPIP to FPE labelled DOPC vesicles.

The change in fluorescence was monitored upon injection of the protonated drug. Addition of protonated HPD and SPIP to FPE labelled DOPC vesicles triggered an increase in fluorescence intensity reflecting a decrease in the surface electronegativity and deprotonation of the fluorescein xanthene ring. Figure III.23 represents the change of fluorescence intensity after subsequent additions of 1μmol of HPD to FPE labelled vesicles.

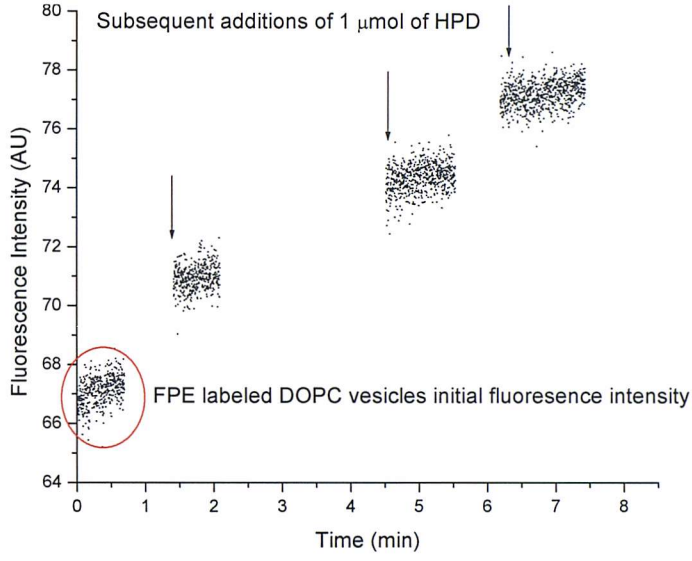


Figure III.23: Additions of protonated HPD induces a change in the fluorescence intensity, indicating a decrease in the electronegative potential. The initial fluorescence is circled in red. The arrows represent subsequent additions of HPD.

The rapid increase of fluorescence indicated that the binding of the protonated drug occurs within the timescale of mixing. Binding of protonated HPD to the vesicles is observed in real time with great sensitivity. The interruption of the fluorescence is caused by the closure of the fluometer shutter during the addition of HPD. Interestingly, the change in fluorescence intensity is relative to the amount of protonated CAD added at a constant lipid concentration. Figure III.24 shows an increase in fluorescence as a function of the amount of HPD added before reaching a saturation value. A similar profile is also obtained in the presence of SPIP.

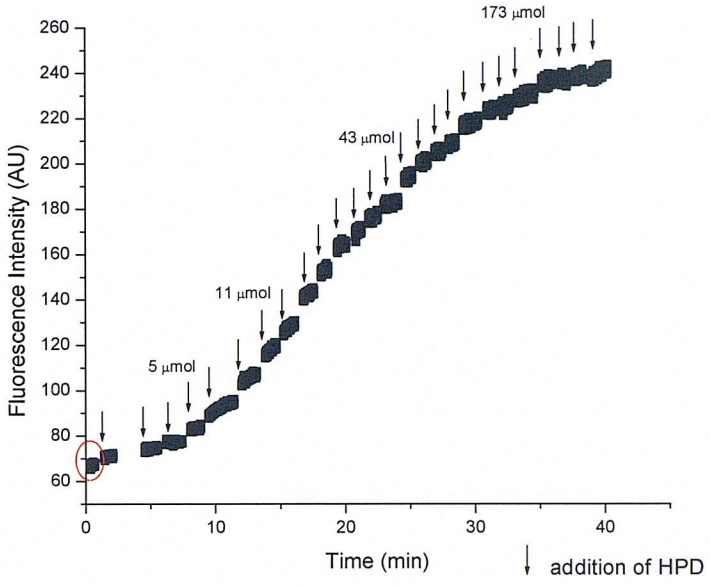


Figure III.24: Subsequent additions of protonated HPD to FPE labelled DOPC vesicles cause an increase in fluorescence until saturation is reached. The initial fluorescence is circled in red.

The fluorescence traces are also seen to evolve with time when more than 5 µmol of HPD are added. This feature is explained in section III.6.3.

The change in fluorescence intensity F associated with the CAD titration was calculated from the initial fluorescence value corresponding to the fluorescent labelled vesicles before the addition of CADs. To disregard the increase of fluorescence with time, only the early points were taken into account for the absolute fluorescence calculation.

From these values binding curves were extracted and data were fitted to a single site binding model, (equation III.1) [143]

$$F = \frac{F_{\max}[CAD]}{K_d + [CAD]}$$

Equation III.1

where F is the fluorescence change, F_{max} the maximum fluorescence change, [CAD] the concentration of the added drug and K_d the affinity of the drug for the membrane. Fitting the single site binding model leads to HPD K_d = 40.38 ± 1.09 µM and SPIP K_d = 102.60 ± 4.64 µM (Figure III.25).

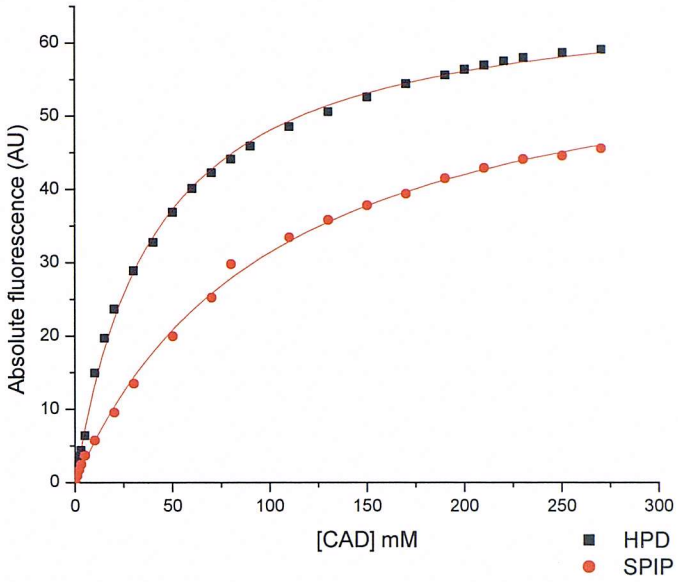


Figure III.25: Absolute fluorescence correlation with HPD and SPIP titration. The data were fitted by a single binding site model and yielded a HPD K_d=40.38±1.09μM and SPIP K_d=102.60±4.64 μM.

III.6.3 Detection of the bilayer hydrolysis

Protonated HPD and SPIP bind rapidly to FPE labelled vesicles; this is observed from the rapid increase of the fluorescence intensity. The fluorescence traces resulting from the HPD binding are flat when the concentration is less than 5 μM; which confirm that the system is at equilibrium. However, further additions of HPD led to different fluorescence traces; these are seen to constantly increase with time. Therefore the surface potential is constantly altered when more HPD binds to the vesicles (Figure III.26).

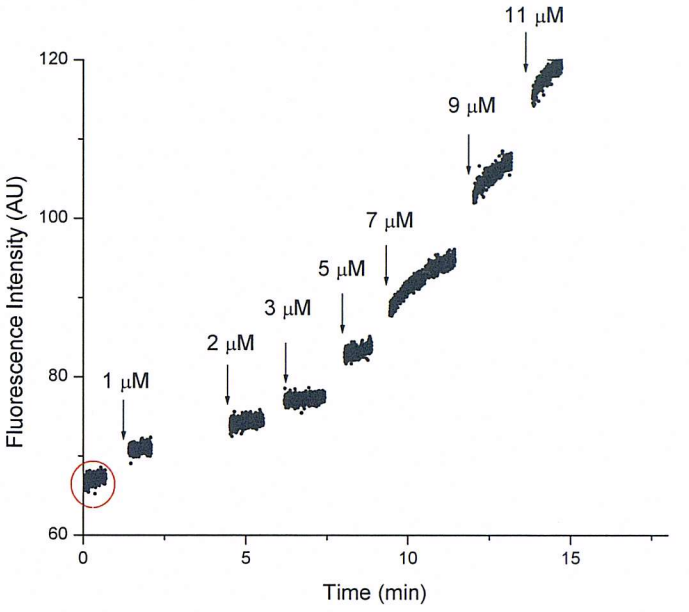


Figure III.26: Addition of protonated HPD to FPE labelled vesicles. The initial fluorescence is circled in red. The system is at equilibrium up to 5 μM of added HPD. When more HPD is added, the fluorescence traces are seen to increase with time.

This unusual fluorescence profile can be attributed to several reasons; the most obvious one being that the system is not at equilibrium when more HPD is added and it can be argued that protonated HPD binds more slowly to the vesicles. This would be true if there was no change in fluorescence at all when more HPD is added, which is not the case. Addition of HPD triggers a change in the fluorescence until saturation at 200 μM as reported on figures III.24 and III.25.

The action on HPD upon FPE labelled vesicles was followed by a real time experiment by recording the fluorescence evolution with time after subsequent additions of HPD. The system was left to equilibrate after addition of 57 μM of HPD (Figure III.27).

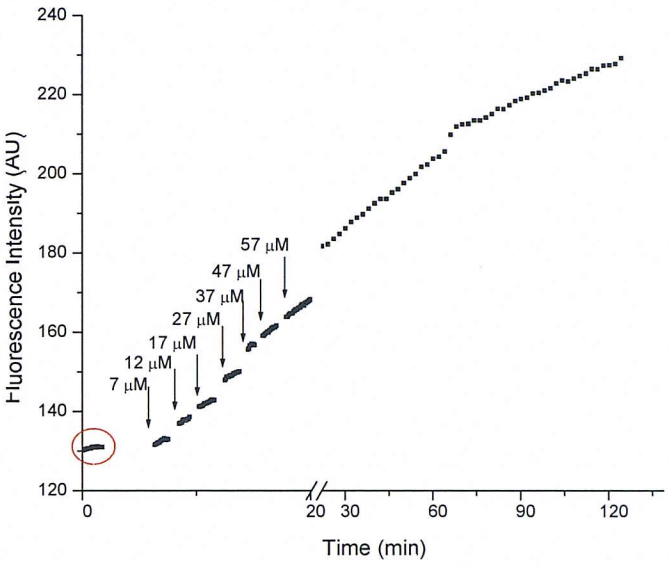


Figure III.27: Time dependence of the addition of 57 μM of HPD on the fluorescence of FPE labelled vesicles. The initial fluorescence is circled in red. The arrows represent subsequent additions of HPD.

The fluorescence is seen to increase with the amount of added HPD, which is consistent with previous results, but also with time after addition of 7 μM of HPD. The same pattern is observed with other concentrations tested. The DOPC: HPD system is left to equilibrate after addition of 57 μM of HPD, which results in the increase of the fluorescence linearly with time. The system cannot reach equilibrium after 90min. This time dependent fluorescence behavior is not dependent on the CAD concentration. This observed profile is expected for a surface potential becoming more positive with time. Comparable traces were observed with SPIP binding to FPE labelled DOPC vesicles.

Wall and coworkers have observed similar fluorescence traces for the action of neuraminidase upon FPE labeled erythrocytes ghosts membranes [135]. The neuraminidase is an enzyme that removes sialic acid from the cell surface. Fluorescence traces are explained as sialic acid being removed from the membrane, causing a loss of negative charge from the cell surface that leads to an increase in the surface potential (Figure III.28).

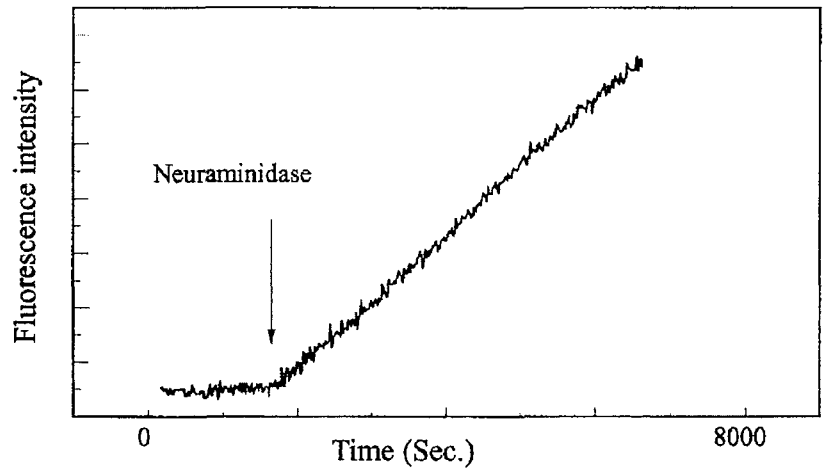


Figure III.28: Time dependence of the effect of neuraminidase on FPE labeled erythrocytes ghosts membranes. The fluorescence is linearly increasing with time, due to the removal of sialic acid from the membrane surface (Figure taken from reference [135]).

Fluorescence traces of HPD binding to FPE labeled vesicles are similar to that of neuraminidase binding to erythrocyte ghosts; a linear relationship between the fluorescence intensity and the surface potential is observed for both neuraminidase action on cell membranes and HPD action on DOPC bilayers. The fluorescence trace is due to removal of negatively charged molecules from the membrane surface; consequently the surface potential becomes more positive with time.

The use of FPE labeled vesicles can be used to demonstrate that kinetic events such as the bilayer hydrolysis occur at the membrane surface upon addition of protonated drugs which strongly correlates with the previous results on the membrane digestion by CADs. It is indeed expected that half of membranous fragments composed of LPC and OA will be negatively charged at pH 7.4, as it was determined that fatty acids pk_a in a bilayer is approximately 7.5 [160]. This will cause an alteration of the membrane surface potential, which can be followed by an increase of the FPE fluorescence intensity with time, as it was described for neuraminidase action on membranes [135].

This brings the conclusion that membrane hydrolysis can also be detected using FPE labeled vesicles. The removal of charges from the membrane surface due to membrane hydrolysis can easily be followed by an increase of FPE fluorescence with time. To confirm this hypothesis, studies involving the use FPE labeled vesicles made of ether-linked PC were undertaken.

III.6.4 Addition of HPD to FPE labeled ether-linked PC vesicles.

As it was described previously, the presence of the carbonyl ester function is compulsory for the membrane degradation to occur. Therefore, vesicles made of ether-linked PC were made and FPE labeled. Addition of protonated HPD should not cause any linear increase of fluorescence with time.

III.6.4.1 Ether-linked PC vesicles labeling

Figure III.29 represents the excitation and emission of FPE labeled ether-linked PC vesicles. The maximum excitation wavelength is 494 nm, and emission is 524 nm. The shoulder due to the mono-anionic form of the fluorescein is also seen at 460 nm. These values are similar to that of FPE labeled DOPC vesicles (Figure III.21).

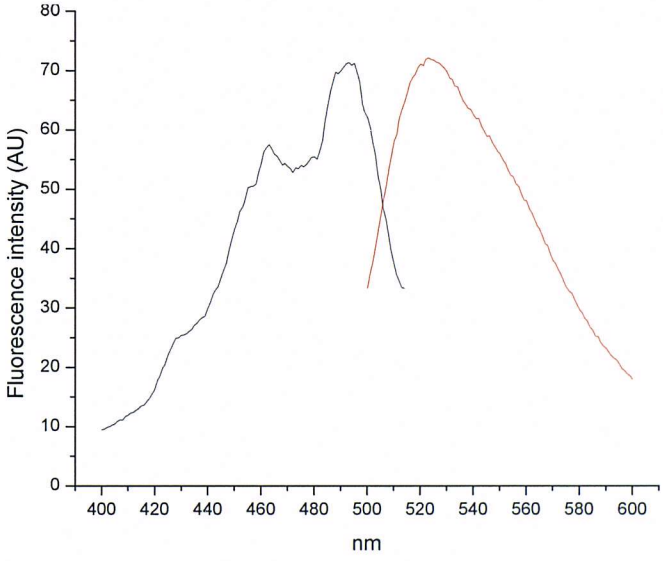


Figure III.29: Excitation (black) and emission (red) spectra of FPE labeled ether-linked PC vesicles. $\lambda_{max\ exc}$=494 nm, $\lambda_{max\ em}$=524 nm.

III.6.4.2 Addition of HPD to FPE labeled ether-linked PC vesicles.

Addition of protonated HPD to FPE labeled ether-linked PC vesicles triggered an increase in fluorescence due to an increase of the membrane surface potential electropositivity. HPD binds rapidly to ether-linked PC bilayers, as it was observed for FPE labeled DOPC vesicles. Similarly to DOPC systems, the change in the fluorescence intensity is dependent on the quantity of added HPD, leading to a saturation effect with 220 μM of added HPD leading to a K_d = 32.99 ± 1.51 μM (Figure III.30).

Fluorescence traces resulting from the binding of HPD to the vesicles are relatively flat and stable with time, even after the addition of 220 μM of drug in contrast to the results with DOPC vesicles. Additions of protonated HPD affect the membrane surface potential; however there is no evidence of a linear relationship between the surface potential and the fluorescence intensity evolution with time. Therefore there is no sign of membrane hydrolysis in vesicles made of ether-linked PC lipids.

It has already been shown that the membrane digestion does not occur in ether-linked PC membranes, this is due to the stability of the ether bond in these experimental conditions [149].

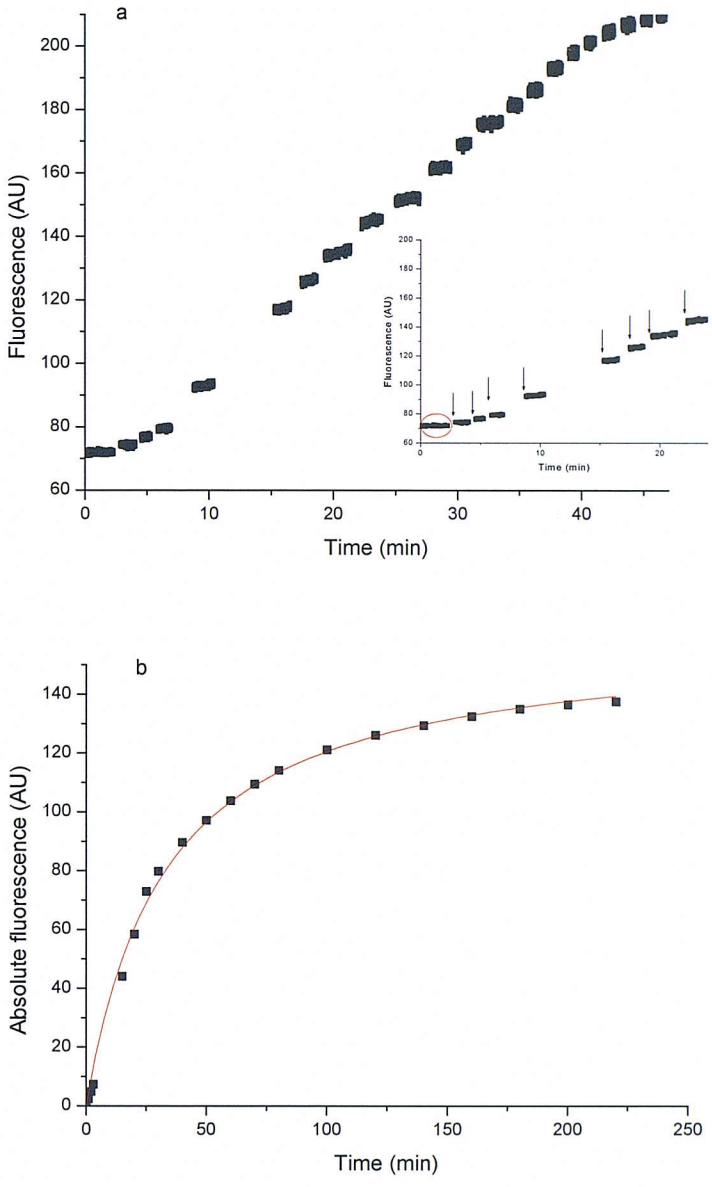


Figure III.30: (a) Addition of protonated HPD to FPE labeled ether-linked PC vesicles. The arrows represent subsequent additions of HPD (1,2,3,5,20,30,40μmol). The initial fluorescence is circled in red. The fluorescence increases with the amount of drug added. The fluorescence signal remains flat with time, this shows that no hydrolysis occurs in the ether-linked PC bilayer. (b) Absolute change of fluorescence association to HPD titration. The data were analysed according to a single site binding model that yielded a K_d=32.99±1.51 μM.

It is interesting to observe that the HPD binding constant is in the same order of magnitude in DOPC and ether-linked PC systems. This implies that the binding of HPD at the interface is independent of the type of linkage. This was also observed for Raclopride, another CAD, which had the same binding affinity for DOPC and ether-linked PC vesicles [185].

The fluorescent probe FPE can be used to estimate the binding kinetics of CADs to membrane bilayers. This technique is innovative, and allows real time measurements of binding in a non invasive manner. HPD and SPIP interact with the membrane bilayer in a saturation binding manner. Both drugs have an affinity for the membrane interface and partition thanks to driving forces such as the hydrophobic effect. HPD exhibits a higher affinity for the membrane interface than SPIP according to the K_d values. Therefore, only HPD was tested on ether-linked PC vesicles. Moreover FPE measurements can also be used to detect the membrane acidic hydrolysis triggered by the protonated drug as a function of removal of charges from the parent bilayer. This hypothesis was confirmed by using FPE labeled ether-linked PC vesicles where no hydrolysis was detected.

III.7 Model proposed

HPD and SPIP are CADs that were shown to bind rapidly and avidly to bilayers made of DOPC. It was shown by SAXS, fluorescence microscopy and FPE fluorescence assays that they partition at the water-bilayer interface close to the ester carbonyl vicinity; this is in good agreement with the literature [46, 97, 107]. CADs are protonated at physiological pH and when bound to the lipids, they were shown to destabilize the physical structure of the bilayer over time by i) altering the membrane surface potential, ii) repelling the bilayers apart, iii) disrupting the lamellar stacks, and iv) promoting the formation of two other mesophases i.e. the micellar and inverse hexagonal phase H_{II}. These effects were shown by fluorescence assays, SAXS, SS-NMR, and confirmed by microscopy.

The simplest hypothesis to explain the appearance of both these phases and the earlier visual observations is that an acyl chain is being formed from the hydrolysis of the DOPC ester structural group, resulting in the creation of single chained lipid LPC and oleic acid. LPC in the fluid lamellar phase shows a narrower CSA pattern due to the increased conformational freedom of the interfacial region. When LPC monomers aggregate together, they phase separate [165] leaving behind a membrane enriched in oleic acid and DOPC which will ultimately drive the remaining membrane mixture into an inverse hexagonal phase. When fatty acids interact with phosphatidylcholine bilayers, they are solubilised in the mesophase and alter the hydrophilic / hydrophobic balance, thus reducing the headgroup area relative to its volume [186]. Fatty acids bind to the carbonyl group of DOPC molecules resulting in a larger chain pressure, promoting the formation of the H_{II} phase. However, formation of the inverse bicontinuous cubic phase using lipid systems other than DOPC has been described in the literature [187].

The presence of LPC in the bilayer induces a desire for positive curvature, whereas the presence of OA induces negative curvature. This change in lipid composition with time has a serious effect on the bilayer topology leading to the formation of membrane fragments and the H_{II} phase. It has been established that lysolipids

detabilise membrane morphology, which makes bilayers more sensitive to fusion and fission processes [188]. In addition, small vesicles can be formed due the presence of the LPC, this was detected by ^{31}P SS-NMR and cryo-microscopy [163], and confirmed by the fluorescence experiment described above (section III.4.3).

The presence of fatty acids in the bilayer induces the formation of non-lamellar structure [187] thus destabilising the membrane which becomes sensitive to fusion processes [94].

Therefore, it is likely that the degradation products induce the formation of membrane fragments, micelles, and vesicles via local rearrangement of the lipid species as described for vesicle budding [189] (Figure III.31). In this process, products of the lipid hydrolysis induce the formation of intermediate structures, which require the deformation and the disruption of the parent membrane [190]. The membrane adopts a neck-like shape and the formation of intermediate structures is observed. By creating a negative curvature, the fatty acid might controle the orientation of lipid fragments and small vesicles towards the inner side of the membrane.

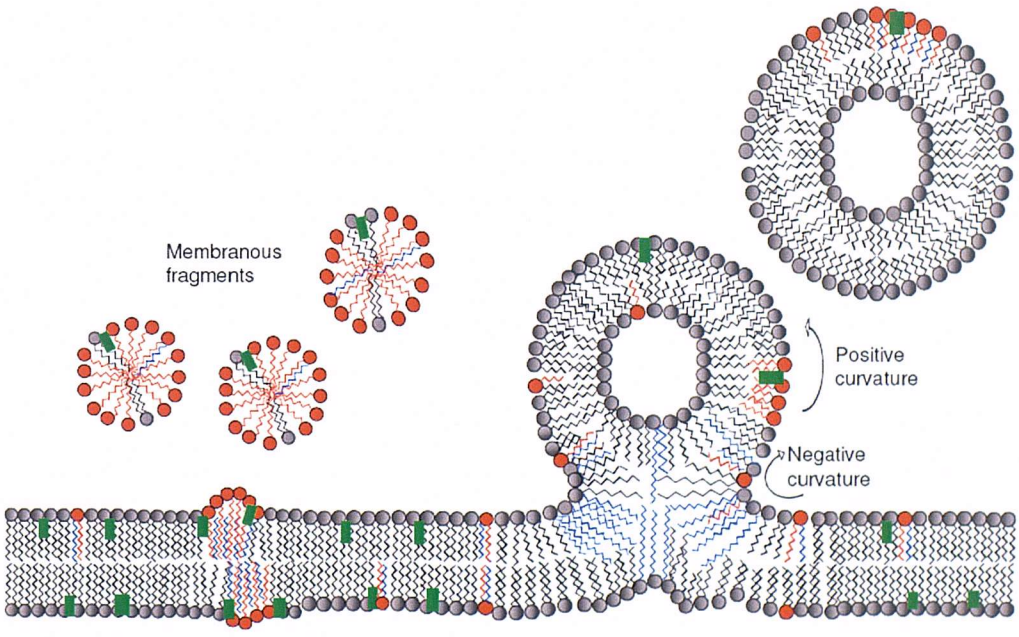


Figure III. 31: DOPC (grey circles) hydrolysis by the CAD (green rectangles) generates two products, the LPC (red circles) and the OA (blue chains). The LPC induces the desire of positive curvature, whereas the OA induces the formation of inverted phases. The lipid rearrangement in the bilayer induces the formation small vesicles. When about 30% of LPC is produced, micelles are formed. The presence of OA creates negative curvature which might orientate the direction of the fragments. However, the orientations of the vesicles and fragments remain unclear.

Requirements for the hydrolysis to occur are the binding of the protonated drug in the close vicinity of the lipid ester bond and protonation of the nitrogen, the latter being an absolute requirement for the hydrolysis to start. Protonation and charge ensure that the CAD will reside in the vicinity of the ester bond that is essential for the hydrolysis to happen. The DOPC: CAD system must be in excess buffer thus providing a big water reservoir available for the hydrolysis. The mechanism by which the lipid is degraded by the CAD follows the classical pathway of an ester acidic hydrolysis by water. Degradation of the lipid bilayer is time dependent, the lipids will be consumed until no or few LPC molecules remain in presence of a high number of oleic acid molecules.

III.8 Biological relevance

This chapter has highlighted a new type of CAD interaction with fluid lamellar bilayers, leading to their disruption as a result of ester acid hydrolysis. The resulting membraneous micellar products are highly dynamic structures that are reflected by the motional properties of the monomers within the micelle, allowing rotation about their long molecular axes, and lateral diffusion along the micellar surface. Therefore CADs bound to micelles are likely to be transported to the next membrane interface to undergo the same process of degradation again (figure III.32). These features would allow CADs to effect a new transport pathway involving the degradation of the phospholipid matrix of the bilayer into membrane fragments.

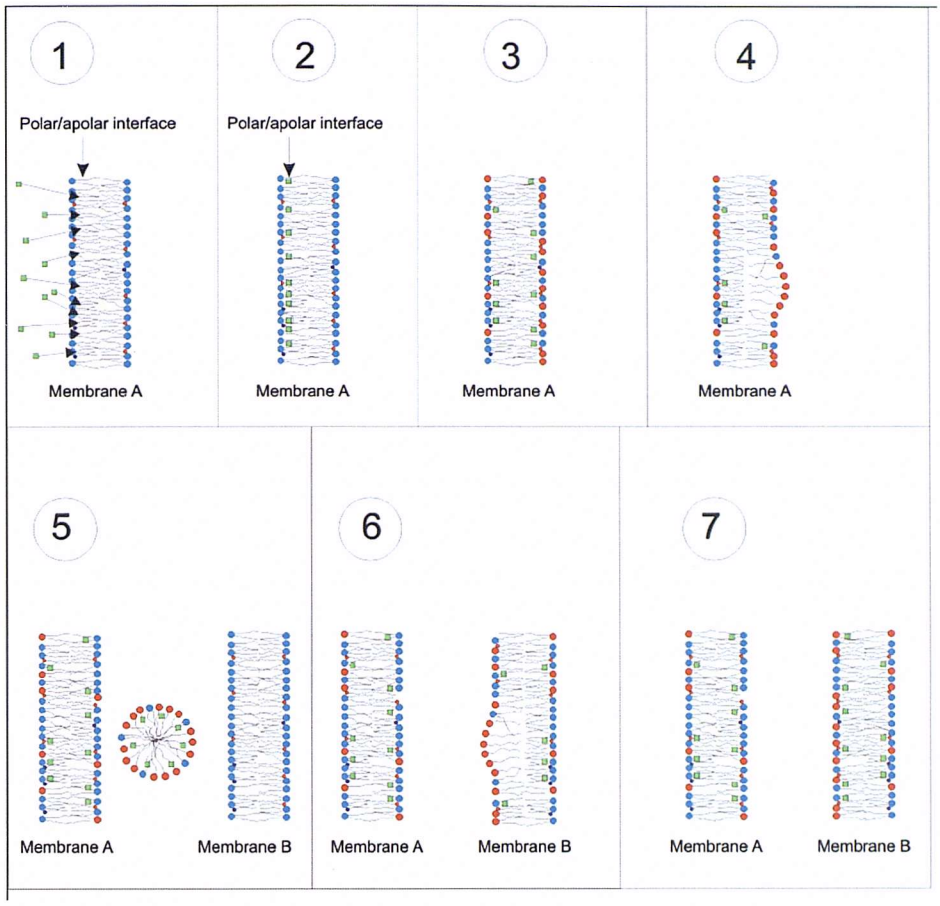


Figure III.32: Cartoon for the proposed mechanism for the membrane translocation of CADs. (1) CADs (green) bind avidly at the polar / apolar interface. (2) Once bound, they initiate the ester acidic hydrolysis of the phospholipid fabric that generates LPC (red) and fatty acid (dark blue) (3). The drug diffuse through the bilayer and (4) generates more LPC. (5) The LPC that is created will form phase separated micelles and other membrane fragments on either side of the parent membrane. (6) CADs bound to these fragments are then carried in the micelle to the next membrane interface to undergo the same process again (7). (Figure taken from ref [149])

The effects of CADs *in-vivo* have been reported as inducing cytotoxic effects in cells. They induce the development of excessive membrane growth and accumulation of abnormal vesicular bodies [123]. This effect known as phospholipidosis is also characerised by a high level of PC fragments [121] which could be due to the hydrolysis process depicted above. In addition, it has been reported that PC production is dependent on the level of stored curvature elastic stress in membranes [191], and this level is altered by the change of lipid composition due to CADs actions.

Moreover, the effect of membrane hydrolysis can also be triggered by other molecules than CADs. For example, it has been shown that dynorphin, a peptide that binds to

opiate receptors, is able to induce the formation of the isotropic micellar phase in bilayers made of DMPC [192]. Therefore, this mechanism can take place for peptides that are protonated at physiological pH and are susceptible to bind to bilayers, such as the arginin rich proteins which sequences are found in HIV.

CHAPTER 4

Effects of CAD's formulation on the kinetics of the membrane hydrolysis: Towards an understanding of the molecular basis of non-specific binding.

This chapter will firstly describe the effect of the CAD's counterion on binding events and hydrolysis of the bilayer. Because of a decrease in the solubility of the bought CADs, crystallization events were observed in DOPC: CAD systems. As this phenomenon was related to counterion recondensation, different experimental conditions were studied. To avoid the crystallization of the drug and increase its solubility, DOPC: CAD systems with different counterion were studied and hydrolysis kinetics measured. Then a kinetic model of the bilayer hydrolysis by three CADs, (HPD, SPIP and WAY) was investigated. Hydrolysis rates were determined from HPLC traces that were shown to detect the reactants and products of the reaction, i.e. DOPC, CAD, LPC and OA. Comparisons of hydrolysis rates in DOPC bilayer systems have been considered for each drug and related to biological processes that occur *in-vivo* such as the non-specific binding (NSB) of CADs. The hydrolysis rates of DOPC bilayers by CADs give the first insight of the molecular basis of the NSB *in-vivo*.

IV.1 Crystallization of the CADs and counterion recondensation

IV1.1 Background

The nature of the counterion has already been described to be of major importance as it affects drug's solubility. Different salts are also critical factors in the development of pharmaceutical formulations as more than half of the drugs used in medicinal therapy are administrated as salt forms [193]. Factors such as the intrinsic solubility of acidic or basic drugs, solubility of salt forms, and concentration of buffering agent contribute to the dissolution of the drug [194]. Specifically, the effect of the Cl^- anion was shown to slow down the dissolution process of HPD whereas the mesylate and the phosphate salt were shown to enhance the dissolution of the drug [195, 196] as these salts have a higher aqueous solubility than that of hydrochloride salts.

Altering the counterion has been shown to affect the solubility of many systems [197, 198]. This a phenomenon was first seen by Hofmeister in the ability of certain salts to precipitate a mixture of hen egg white protein [197].

The Hofmeister series was used to measure the strength of hydration between of the ions. When in the water, ions perturb the natural hydrogen bonding network of water. Ions can be divided into two categories; they are chaotropic, or "structure breakers" when the interactions with water molecules are weaker than the water itself, or kosmotropic "structure makers" when the interactions with water are stronger. Characteristics of anions belonging to the Hofmeister series were studied and classified according to their charge density, size, polarisability and potentiality of loosing their hydration sheath. Therefore, kosmotropic anions are small, usually with a small polarisability and need a great energy to lose their water hydration layer, whereas chaotropic anions are big, and characterized by a significant polarisability, they can also lose their water layer easily [199]. The Hofmeister series is listed below

with the ions on the left of Cl^- being referred to as salting-out (kosmotropic ions) and on the right being referred to salting-in ions (chaotropic ions).

$$SO_4^{2-} \sim HPO_4^- > OH^- > F^- > HCOO^- > CH_3COO^- > Cl^- > Br^- > I^- > SCN^-$$

Salting-out ions were shown to reside preferentially in the water, as they do not bind to micelles [200], they were also found to stabilize proteins solubility [201]. Small ions are strongly hydrated and create local order. Oppositely to salting-out ions, salting-in ions such as Cl^- and Br^- can loose their water easily, this leads them to bind and interact preferentially with bilayer surfaces and perturb the lipid headgroup [202]. These anions were also shown to denature proteins. The less hydrated large singly charged ions act like hydrophobic molecules that bind to surfaces; this is dependent on the charges and the van der Waals interactions.

Table IV.1 recapitulates the properties of anions belonging to the Hofmeister series.

	Anion	**Radius (Å)**	**Δ_G Hydr. kcal/mol**	**Polarisability α (Å^3)**
Stabilizing	SO_4^{2-}	2.30	-258	6.33
	HPO_4^-			
Salting-out	OH^-	1.33	-102.8	2.25
	F^-	1.33	-111.1	1.30
Kosmotropic	$HCOO^-$			4.2
	CH_3COO^-			
Destabilizing	Cl^-	1.81	-81.3	3.76
Salting-in	Br^-	1.96	-75.3	5.07
Chaotropic	I^-	2.20	-65.7	7.41

Table IV.1: Physical properties of anions belonging to the Hofmeister series (adapted from references [201], [199] and [203]). The size of the multicentred anions formate and acetate have not been measured.

Moreover, studies undertaken by Shearman [87] showed that chaotropic ions such as Cl^- caused membranes in the lamellar gel phase to collapse due to the ion's condensation into the bilayer; the direct result of such a process being the water expelled from the system and the membrane to shrink considerably. The collapsed

lamellar phase is more likely to occur in the presence of chaotropic ions than kosmotropic ions.

As counterions have an effect on a CAD's solubility as well as on the bilayer organization, it is therefore likely that they have an effect on DOPC: CAD systems.

IV.1.2 Crystallization of the CADs in the presence of the bilayer and counterion recondensation

While determining the kinetic rates of bilayer degradation, the solubility profile of the CADs provided by the manufacturer had substantially reduced. HPD was initially soluble in 5mM water, 50 mM ethanol and 25 mM DMSO, but its solubility decreased to 10mM in ethanol and 25 mM in DMSO over the course of this study. As a result HPD was found to be less soluble in our experimental conditions which affected the binding kinetics and as a consequence the hydrolysis reaction. HPD was no longer residing at the bilayer interface, which mitigated against the bilayer hydrolysis as observed by using SAXS.

Figure IV.1 represents the evolution of a DOPC: HPD 20:1 sample over 8 days. The obtained diffraction patterns are typical of a diffuse swollen lamellar phase in the presence of the CAD as already observed in chapter 4. At day one and five, the lattice parameter increases from 94.71±0.54 Å to 107.70±3.20 Å. This effect is associated with the protonated HPD partitioning at the bilayer interface which causes bilayer-bilayer repulsion (Figure IV.1a,b). However, after 5 days, the DOPC: HPD system is seen to reorganize to a distinct lamellar phase, with less diffuse rings and a d-spacing collapsing to 89.46±1.07 Å (Figure IV.1c). Although this value is still higher than a pure DOPC L_α phase (61.36±0.57 Å), the system exhibited no degradation, with no OA and LPC detected by HPLC. Therefore, we hypothesized that the HPD was not residing long enough at the bilayer interface having been expelled to form crystals. This mechanism would prevent the hydrolysis of the bilayer, as was observed.

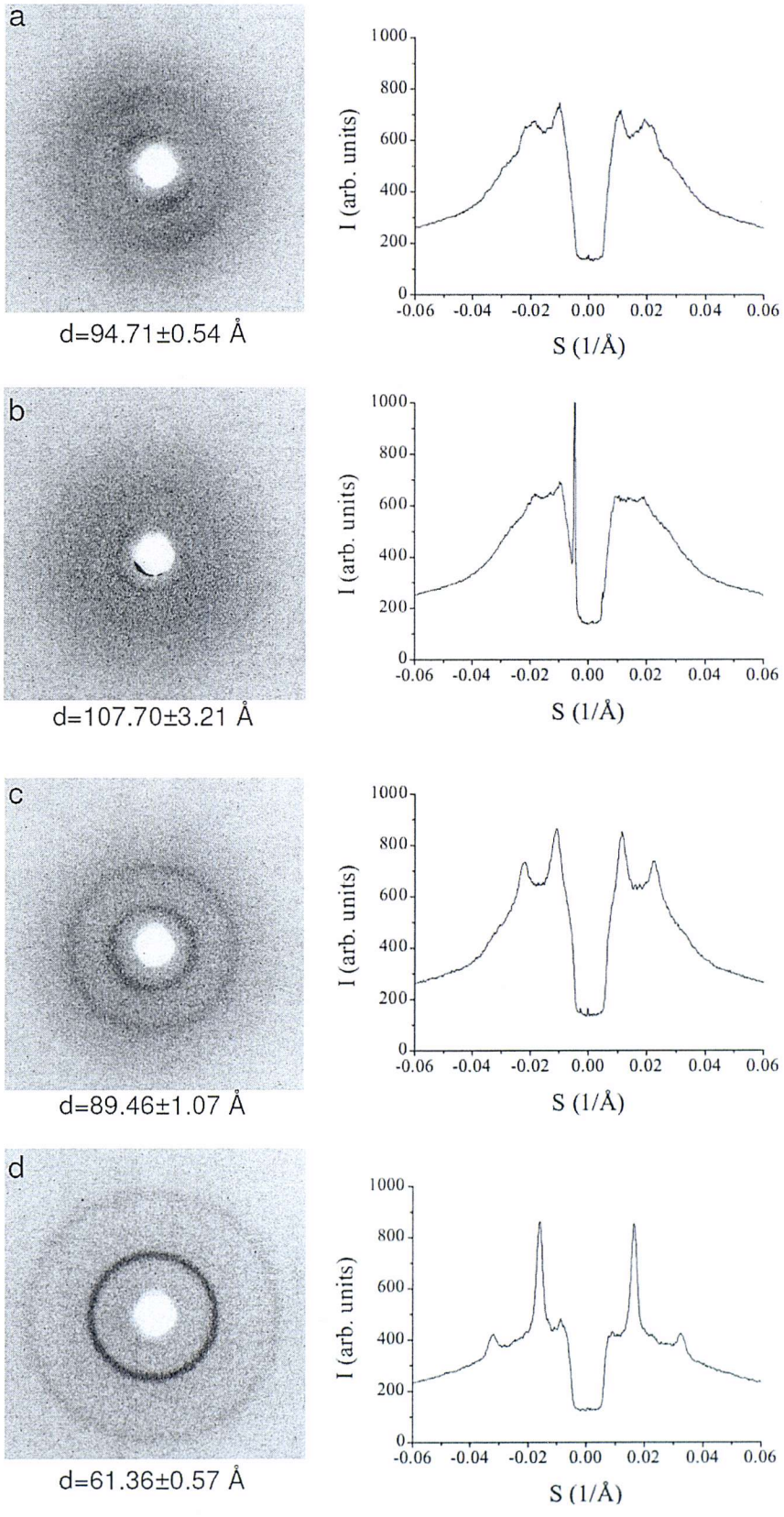


Figure IV.1: DOPC: HPD 20:1 SAXS diffraction patterns evolution with time. The obtained diffraction pattern (a) corresponds to a swollen lamellar phase with the lattice parameter d-spacing= 94.71±0.54 Å one day after the sample was made; (b) d-spacing=107.70±3.20 Å five days after the sample was made. (c) After eight days, the DOPC:HPD 20:1 system is reorganizing to a less swollen lamellar phase with d-spacing=89.46±1.07 Å. (d) d-spacing=61.32±0.57 Å for DOPC.

Crystallization of the CAD was also detected from other SAXS studies on DOPC: HPD 20:1 systems, where no swelling was observed at all, and where the bilayer repeat spacing was found to be smaller than expected for pure DOPC systems (Figure IV.2).

The obtained diffraction patterns depict a DOPC: HPD system in the lamellar state with equally spaced well defined rings with a repeat spacing of 56 Å. The lack of swelling on these diffraction patterns are indicating that the CAD is not bound at the bilayer interface. In addition, the calculated d-spacing is constant over a week which is again contrary to what has been observed previously. The repeat spacing value is 5Å smaller than pure DOPC implying a significant loss of water / buffer between bilayers. As a result, the loss of water would also enhance crystal formation. This might explain the CAD's crystallization.

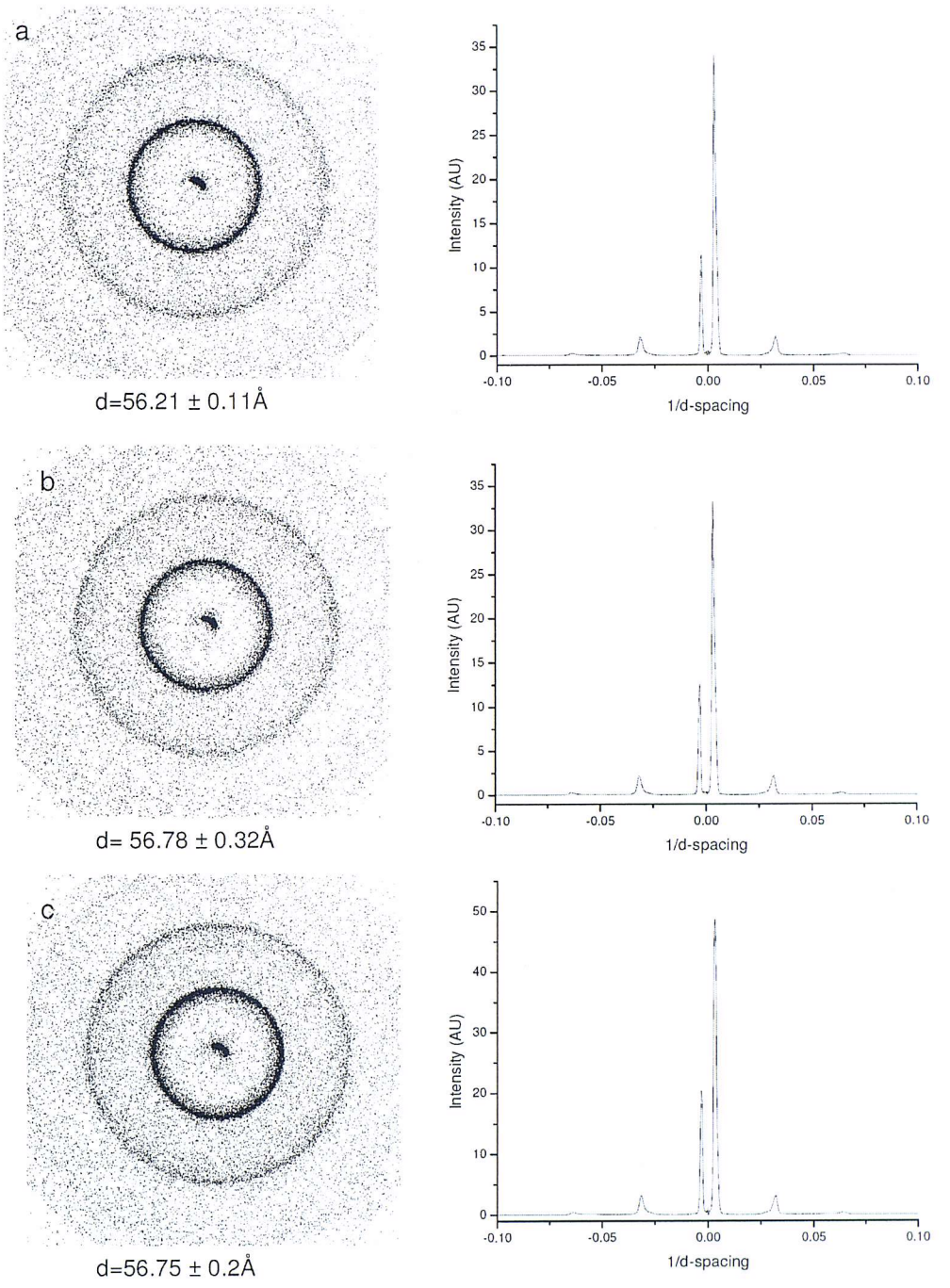


Figure IV.2: SAXS diffraction pattern evolution with time of DOPC: HPD 20:1 systems. No swelling is observed over the course of one week. The d-spacing value is 5Å smaller than for a pure DOPC system, and is constant 1 day (a), 4 days (b) and 7 days (c) after the sample was made.

HPD crystallization was confirmed by microscopy which showed the formation of HPD crystals in DOPC: HPD 20:1 samples as exemplified on figure IV.3. HPD was excluded from the bilayer interface which was detected by SAXS and crystallized out of the bilayer. Crystals of HPD are also seen to grow with time.

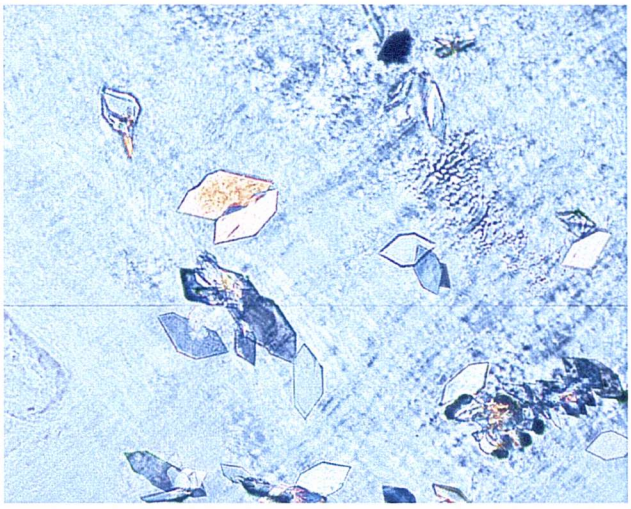


Figure IV.3: Bright field micrograph (x40) representing DOPC: HPD 20:1 sample. The HPD has been expelled from the bilayer interface which led to crystal formation.

These results correlate strongly to the Hofmeister effect, where chaotropic ions are able to bind to bilayer surfaces [202] and precipitate proteins [204]. The HPD counterion in this sample is Cl^- which belongs to chaotropic counterions; as a result, it is likely that this anion condenses onto the bilayer. Hence, a simple assumption can be made for the reason of HPD crystallisation: if the Cl^- counterion is likely to bind at the membrane surface, therefore it is also likely to be attracted back by the protonated drug, leading to recondensation and precipitation of the drug away from the bilayer interface. This would mitigate the hydrolysis reaction.

Counter ion recondensation on bilayer surfaces affects the lamellar organization. It has been reported that chaotropic solutes have an effect on altering phase transitions of bilayers [205], but also these anions can cause the collapse of the L_β phase resulting in the water / buffer expelled off the water channels, and drive the formation the L_c phase [87]. These results lead to the conclusion that the CADs catalysed bilayer hydrolysis is strongly dependent on the solubility and formulation i.e. the nature (chaotropic / kosmotropic) of the counterions of the CADs. For the hydrolysis to occur, at least two conditions have to be fulfilled: 1) the CAD must reside at the bilayer interface; 2) CAD's counterion must not recondense onto the bilayer as it will cause the crystallization of the CAD and the collapse of the bilayer. These features explain the absence of hydrolysis in these samples. This shows that CADs counterions have an important effect on its ability to bind at the bilayer interface and thus on the

bilayer hydrolysis. Therefore, the lipid: CAD preparation protocol was optimized to increase the CAD's solubility and minimize the crystallization effects.

IV.1.3 Optimization of sample preparation

The initial sample preparation consisted of dissolving the lipid and the CAD together in organic solvent to assure complete homogenization. The solvent was removed and the lipid: CAD mixture dried under vacuum until complete dryness. Then the dried mixture was hydrated by the required amount of buffer and the sample left to equilibrate for 15 minutes before any measurements were made. This procedure as well as the sample storage was undertaken at room temperature. One of the major changes in the sample preparation was the drying procedure that involved the use of a vacuum oven at 40°C for 24hours. Then the sample was hydrated by the appropriate buffer, left to equilibrate and stored at 37°C.

The increase of the temperature during the sample preparation and storage had a profound effect as the crystallization of the CADs was stopped. This was confirmed by polarizing microscopy on DOPC: HPD 20:1 samples (Figure IV.4) and HPLC, where LPC and OA were detected (see next section).

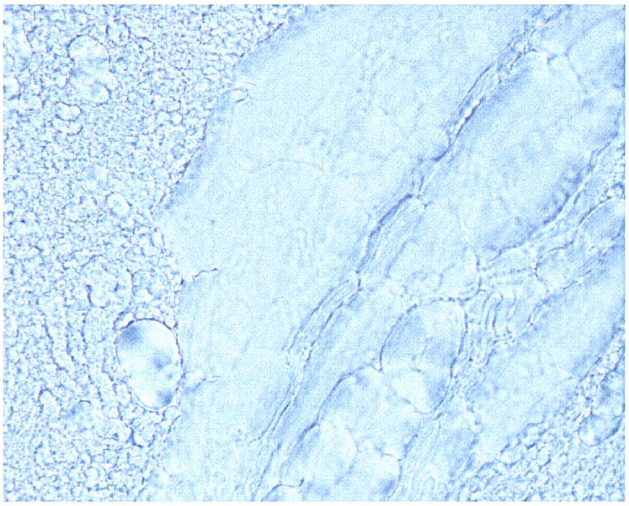


Figure IV.4: Bright filed micrograph (x40) representing DOPC: HPD 20:1 sample after optimization of the sample preparation protocol. No crystals of drug are detected.

Crystallization processes are controlled by numerous factors depending on experimental conditions (concentration, temperature, presence of salt). As reported elsewhere, the effect of temperature strongly influences the rate of crystal growth in crystallization processes, in particular in the nucleation sites [206]. Keeping the samples at higher temperature mitigates the formation of nucleation sites and also weakens the crystal's packing forces. In addition, it has been reported that the counterion condensation effect was considerably diminished by increasing the temperature [87]. Elucidation of the kinetics of crystal growth is beyond the scope of this thesis.

Optimization of the sample preparation protocol was a major step in the elucidation of the counterion recondensation issue and the CADs crystallization. Using the new optimized protocol allowed better control of sample handling and thus of the hydrolysis processes. The following sections will describe the kinetics of the membrane hydrolysis using different CADs with different counterions.

IV.2 Kinetics of the membrane degradation

IV.2.1 Kinetic model of the degradation

The bilayer hydrolysis comprises three steps which are 1) proton transfer of the protonated CAD to the lipid ester function, 2) hydrolysis of the lipid chain into LPC and FA, and 3) hydrolysis of the produced LPC into another molecule of FA.
Protons are propagated by water through a random walk that is controlled by the membrane electrostatic potential. The mechanism of proton transfer necessitates a donor and acceptor that are the CAD and the lipid ester function in this case. The proton transfer depends on the distance and orientation of the reactants, which are only a few Å apart. It has been reported that proton transfer between molecules occur in the picosecond - nanosecond time range [207]. Early experiments showed that the rate CADs binding to the bilayer and the bilayer hydrolysis were in the range of minutes - hours. Therefore, the step of proton transfer and the rate at which it occurs will be ignored for the determination of the rate of the bilayer hydrolysis.

The degradation model of the bilayer involves the formation of three mesophases, the lamellar phase where the reaction starts, the inverse hexagonal phase that is a result of the fatty acid curving the membrane towards the water / buffer, and the micellar phase that arises from the aggreagation of LPC molecules. Each of these mesophases exhibits a different degree of stored curvature elastic stress. Therefore it is expected that the rate of hydrolysis is dependant on the bilayers mechanical state, as has already been described for the action amphipathic molecules at the membrane interface [191].

Degradation rates were defined by using the model depicted on figure IV.5.

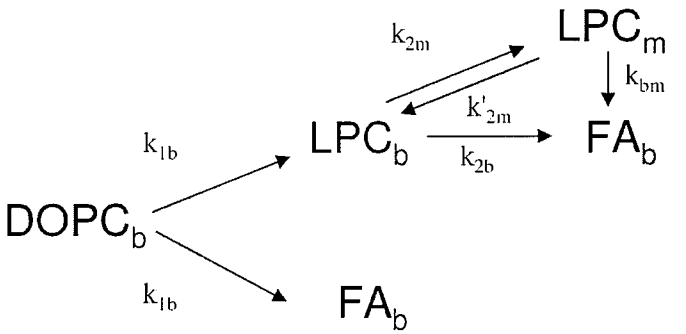


Figure IV.5: Kinetic model describing the degradation kinetics of the DOPC bilayer into LPC and FA. The model comprises the degradation products in the bilayer and micellar state. The kinetic parameters are k_{1b}, the rate of degradation of DOPC into LPC and FA in the bilayer, k_{2b} the rate of degradation of LPC in the bilayer into FA in the bilayer, k_{2m} the rate of formation of LPC micelles from LPC in the bilayer, k'_{2m} the rate of LPC molecules partitioning into bilayers and k_{bm} the rate of degradation of LPC micelles into FA that reintegrates the bilayer.

This model involves numerous kinetic parameters such as k_{1b}, the rate of degradation of DOPC into LPC and FA in the bilayer, k_{2b} the rate of degradation of LPC in the bilayer into FA in the bilayer, k_{2m} the rate of formation of LPC micelles from LPC in the bilayer, k'_{2m} the rate of LPC molecules partitioning into bilayers, k_{bm} the rate of degradation of LPC micelles into FA that reintegrates the bilayer; this could happen through fusion processes. Unfortunately the model does not comprise the choline headgroup as it was not possible to detect it using the normal phase HPLC system due to its high hydrophilicity, which prevents its elution.

The degradation kinetics follows a catalytic hydrolysis process where the disappearance of DOPC, the appearance of LPC or the appearance of FA can be detected. The CAD molecule is regenerated after the hydrolysis is completed and its concentration is constant over the course of the reaction; therefore because of this catalytic process the concentration of the CAD will not be taken into consideration in the model. This also assumes that CADs work independently from each other.

The disappearance of DOPC into LPC is only due to the action of the CAD that remains constant during the whole process; therefore the disappearance of DOPC follows a pseudo first order exponential decay as

$$\frac{dDOPC}{dt} = -k_{1b}[DOPC_b]$$

Equation IV. 1

$$[DOPC] = [DOPC]_o e^{-k_{1b}t}$$

Equation IV. 2

The rate of formation of LPC depends on the disappearance of DOPC but also on the rate of formation of LPC micelles and formation of FA in the bilayer and in the hexagonal phase. Similarly, the rate of appearance of FA depends on the rate of disappearance of DOPC into LPC and FA in the bilayer and on the disappearance of LPC micelles. The determination of k_{2m}, k'_{2m}, k_{bm} and k_{2b} requires an accurate measurement of the FA signals; this is found to be complicated as the FA signals overlap with the injection peak signal on the HPLC (see chapter 3 for more details). Therefore, the only parameter that can be determined accurately is k_{1b} that corresponds to the disappearance of DOPC upon addition of the CAD. k_{1b} will be determined according to equation IV.1.

IV.2.2 Effect of different CADs on the membrane degradation

Kinetics of the membrane hydrolysis were followed by using normal phase HPLC equipped with an ELS detector. Normal phase HPLC was the method of choice in the

detection of the membrane degradation products. The measurement consisted of injecting an aliquot of a DOPC: CAD mixture of known mass into the HPLC system. The amount of each product formed was determined from the area under the peak according to the prior calibration curves obtained for each standard. Errors in the measurements were calculated from three sets of experiments.

A typical degradation diagram obtained from HPLC traces of the membrane hydrolysis is depicted on figure IV.6.

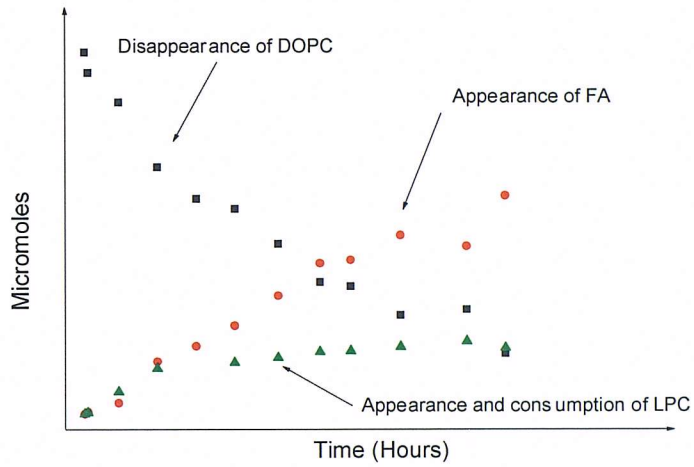


Figure IV.6: Qualitative diagram representing the membrane degradation into LPC and FA. The DOPC in consumed into LPC and FA. LPC is ultimately degraded to FA with time.

The disappearance of DOPC follows an exponential decay model, whilst LPC and OA appear initially at equal rates. The LPC formed is then consumed leading to the production of FA; this is seen with a plateau on the LPC signal. As already described, the LPC formed firstly resides in the bilayer; when enough LPC monomers are formed, they will aggregate into micelles that are able to leave the bilayer. It is unfortunately not possible to measure the LPC micelles formation in this system as only total LPC entities are measured. However, it is assumed that LPC monomers have to form 30% of the bilayer to form micelles [163]. The FA formed comes from the degradation of DOPC and from LPC in the bilayer and in micelles.

IV.1.2.2 Comparison of the hydrolysis kinetics due to three CADs: HPD, SPIP and WAY.

The three different CADs: HPD, SPIP and WAY were tested on condensed fluid lamellar phase bilayers made of DOPC in a 20:1 lipid: drug ratio. The effect of HPD and SPIP has already been described previously [149], but the kinetics of the membrane hydrolysis had not be fully investigated at this stage. Therefore, comparisons between the rate of hydrolysis in the presence of HPD, SPIP and WAY have been undertaken.

These studies were carried out to establish a relationship between the hydrolysis reaction and the type and specificity of CAD investigated. Specific actions of CADs were already described on the membrane lateral organization with clozapine, another CAD, increasing the average area / molecule more than HPD [97]. In addition, and as shown in chapter 4, CADs exhibit different binding affinities for PC bilayers [38] and also different partition coefficients values depending on their structure [119]. Therefore, the hydrolysis rate is expected to be dependent on the CAD itself.

Figure IV.7, IV.8 and IV.9 show the typical chromatograms obtained for DOPC:HPD, DOPC:SPIP and DOPC:WAY at a molar ratio of 20:1 after 1h, 4h, 72h and 152 h respectively. Each chromatogram depicts the DOPC peak (17.7 min), the drug peak (13 min) and the hydrolysis products LPC (21.4 min) and OA (2.8 min). The HPLC traces are seen to evolve with time. Additional peaks are also present at 11min. Mass spectrometry did not reveal any new products that could have been formed from the interaction between the products of the hydrolysis reaction. Therefore these peaks were attributed to the mobile phase signal as they are also present in the blanks.

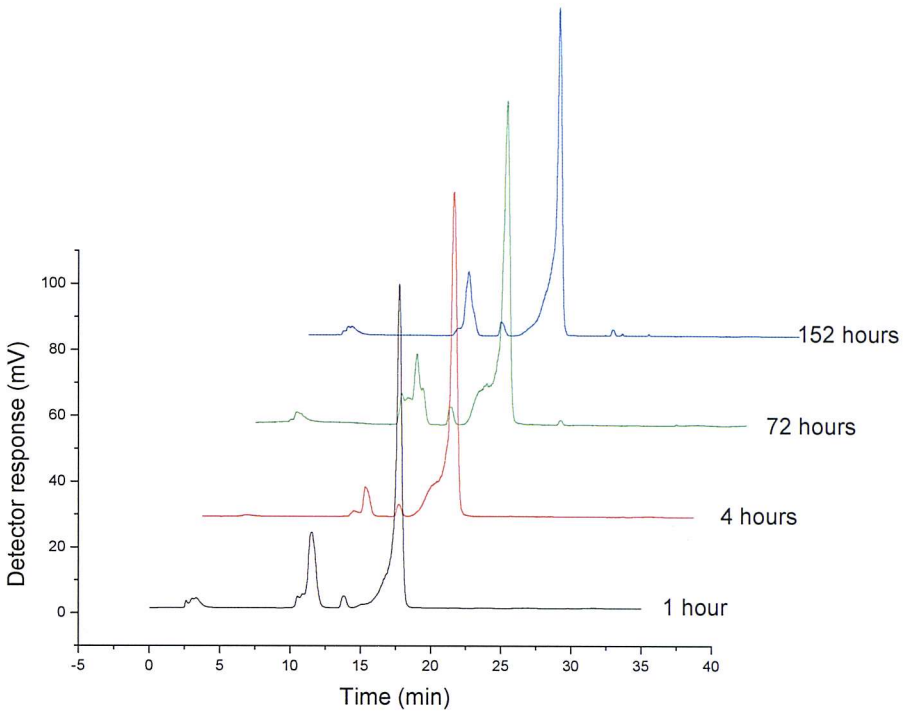


Figure IV.7: Normal phase HPLC chromatograms representing the evolution of DOPC: HPD 20:1 samples with time. There is little formation of LPC in these samples with time. The chromatograms are normalized so the DOPC peak is constant.

Figure IV.7 represents the evolution of DOPC: HPD 20:1 samples with time. Surprisingly there is very little LPC produced, even after 152h. This is contrary to what was observed in chapter 4 where HPD was shown to completely degrade the bilayer after 3 days at this ratio. This could be due to numerous factors such as the sample preparation method that is different from the one used in chapter 4. Also the change in ionic strength of the buffer might have a significant effect on the hydrolysis properties. These sets of samples are made in buffer B (10 mM Tris pH 7.4) whereas the former results were obtained in buffer A (50 mM Bis-Tris, 100 mM NaCl) which has a considerable effect on screening the electrostatic interactions at the membrane surface [88, 158], as well as increasing the drug's solubility [195]. The effects of the ionic strength are discussed in section IV.2.4.

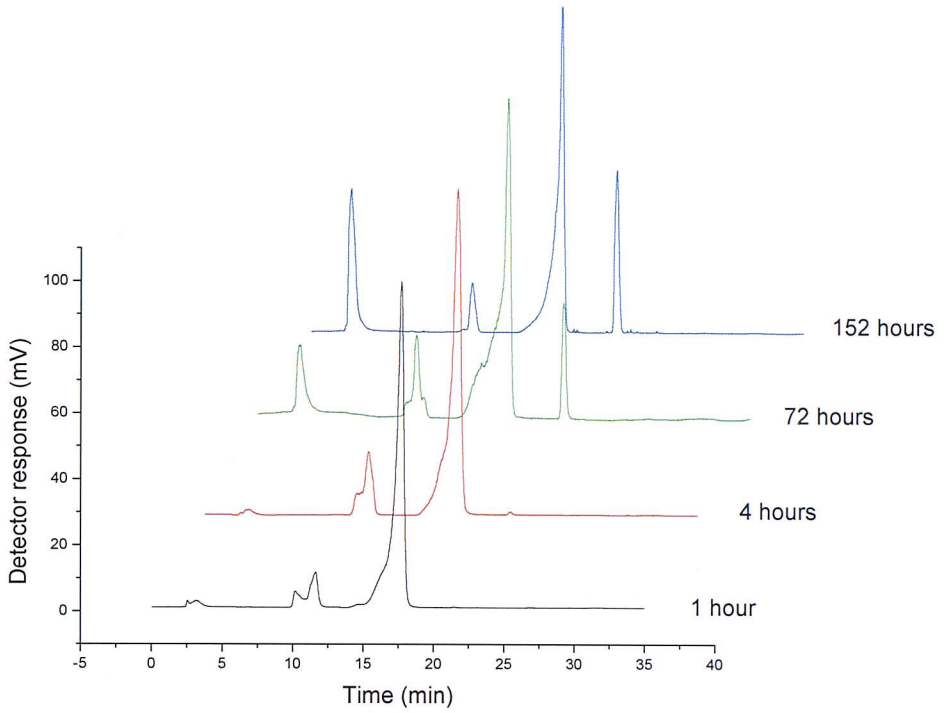


Figure IV.8: Normal phase HPLC chromatograms representing the evolution of DOPC:SPIP 20:1 samples with time. LPC is already present after 4h, and is half of the height size of the DOPC peak after 72h. The OA signal is also see to grow with time. The chromatograms are normalized so the DOPC peak is constant.

Figure IV.8 represents the HPLC traces obtained for DOPC: SPIP 20:1 evolution with time. Here again, the traces of the blank are present at 11min. In addition, the LPC is present 4 hours after the sample was made, and the signal is constantly evolving until the peak reaches half of the size of the DOPC peak in height. The OA signal is barely present after 4 hours, but is growing with time. Although the OA signal cannot be measured accurately, trends are seen in the evolution of the OA with the signal increasing with time. According to the kinetic model, the DOPC is consumed to form the products LPC and OA. This is not shown on these graphs as the DOPC peaks were normalized to 100 to observe the growth of the LPC and OA signal. The disappearance of the DOPC peak will be investigated in the following section.

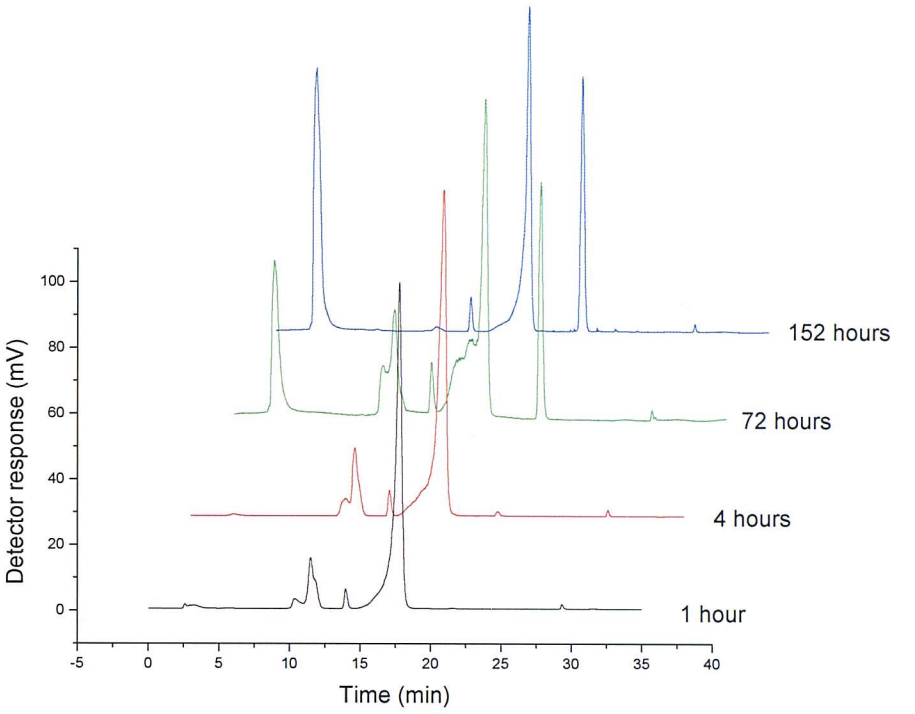


Figure IV.9: Normal phase HPLC chromatograms of DOPC: WAY 20:1 samples evolution with time. The LPC is present 1 hour after the sample was made, and is constantly growing with time. More OA signal is also produced with time. The chromatograms are normalized so the DOPC peak is constant.

Figure IV.9 represents the HPLC traces of DOPC: WAY 20:1 samples. Two additional peaks are present on the chromatogram: the mobile phase signal at 11min and the maleate counterion at 29 min. It is noticeable that the LPC is present 1h after the sample was made; this already indicates that this drug degrades the bilayer quicker than SPIP and HPD. After 4h, the LPC signal is more intense. The LPC and OA signals are significant after 72h and 152h. The DOPC peak is altered at 72h, showing a large shoulder starting at 15min. Assumptions on the formation of DOPC: WAY intermediates were made, but no evidence was shown by mass spectrometry.

The amounts of DOPC, OA and LPC were calculated from the area under the peaks, and correlated to the calibration curves obtained for each standard. From these values degradation profiles were constructed, where the DOPC is seen to disappear, and the LPC and OA to appear (figure IV.10). The degradation profiles obtained correspond to the typical profiles shown on figure IV.6.

The combination of these three sets of chromatograms and degradation profiles lead the following conclusion: the hydrolysis rate is dependent on the type of drug. Early

assumptions can be made on the rate of reactions, with WAY being the fastest drug, followed by SPIP and HPD. These kinetic results differ from those presented in chapter 3; this is due to a change in the solubility of the drug, which led to a change of the sample preparation protocol. (See chapter 2 for more details). In addition, there is no NaCl in the buffer used in these experiments. The effect of NaCl is investigated in section IV.2.4.

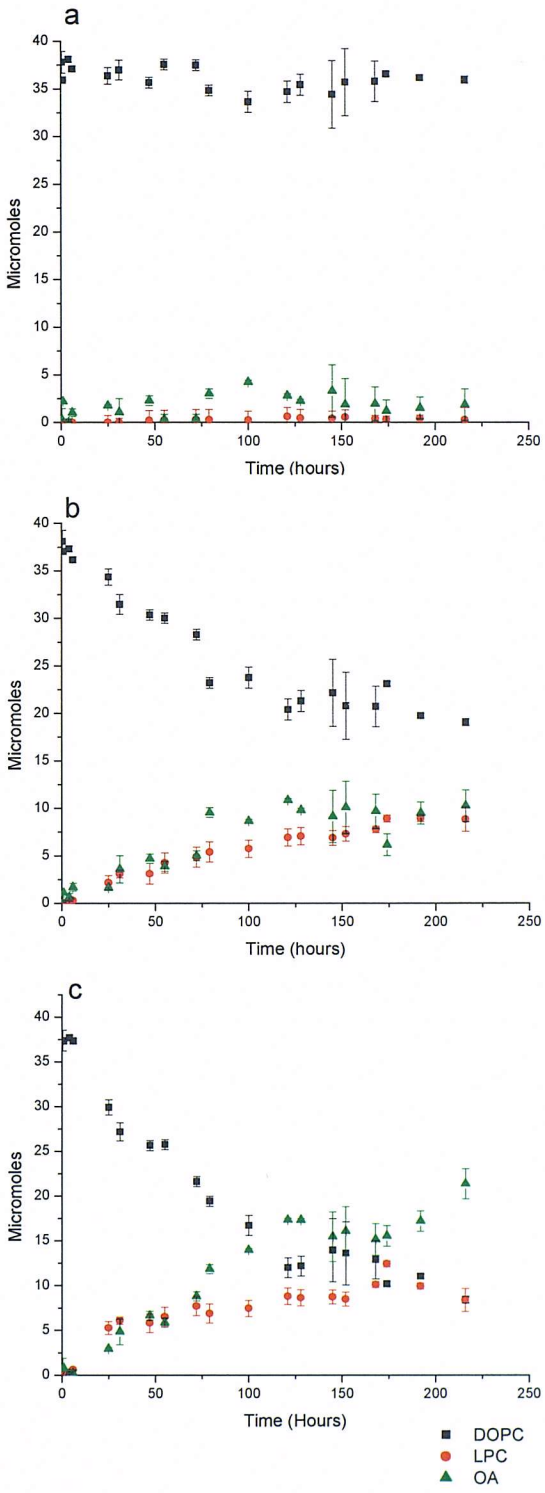


Figure IV.10: Degradation profile obtained for the action of three CADs: (a) HPD, (b) SPIP and (c) WAY on DOPC bilayers in 10 mM Tris, pH 7.4. Error bars represent estimated experimental error on three experiments.

- Disappearance of DOPC

For the sake of consistency, the degradation parameter k_{1b} will be referred to as k_{1DOPC}. k_{1DOPC} was determined according to equation IV.1 from the hydrolysis profile shown on figure IV.11. As previously stated, k_{1DOPC} is the only parameter that can be measured accurately from the experimental data.

The values obtained are $k_{1\ DOPC\ WAY}=7.72x10^{-3} \pm 0.27x10^{-3}$ µmol.h^{-1}, $k_{1\ DOPC\ SPIP}= 3.96\ x10^{-3} \pm 0.20\ x10^{-3}$ µmol.h^{-1} and $k_{1\ DOPC:\ HPD}= 0.33\ x10^{-3} \pm 0.04\ x10^{-3}$ µmol.h^{-1}. From these rates, it is possible to determine that WAY degrades DOPC bilayers twice as fast as SPIP and that HPD exhibit the slowest rate.

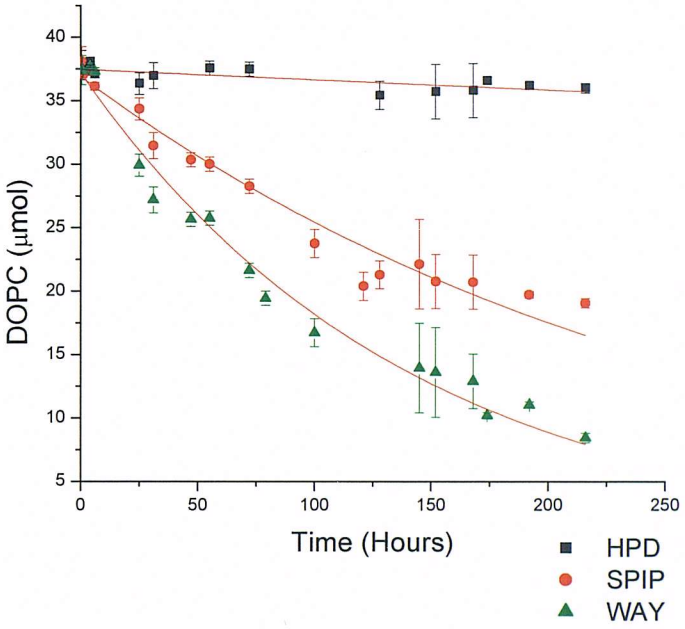


Figure IV.11: DOPC hydrolysis profile by the three CADs, HPD, SPIP and WAY. Curves were fitted using equation IV.1. Error bars represent experimental errors on three experiments.

- Initial rates of appearance of LPC and OA

Determination of the rate of appearance of LPC and OA is complex as it requires an accurate measurement of k_{2b} which depends on the appearance of the OA. This is found to be difficult because the OA elution time also corresponds to the injection peak that is not constant.

For these reasons, the initial rates of formation of LPC and OA $k_{0\ LPC}$ and $k_{0\ OA}$ were determined. This only involves the measurement of the reaction at very short times when the bilayer is still in the fluid lamellar state with no micellar or H_{II} phases present, which would affect the hydrolysis rates. Initial rates can be calculated from the slope of the tangent to the curve at t=0. Initially LPC and OA appear with the same rate as 1 molecule of DOPC is hydrolyzed into 1 molecule of LPC and OA; this can be seen on figure IV.10 where LPC and OA appear with the same slope. This feature will make possible the determination of the initial rate of formation of LPC and consequently the OA (Figure IV.12).

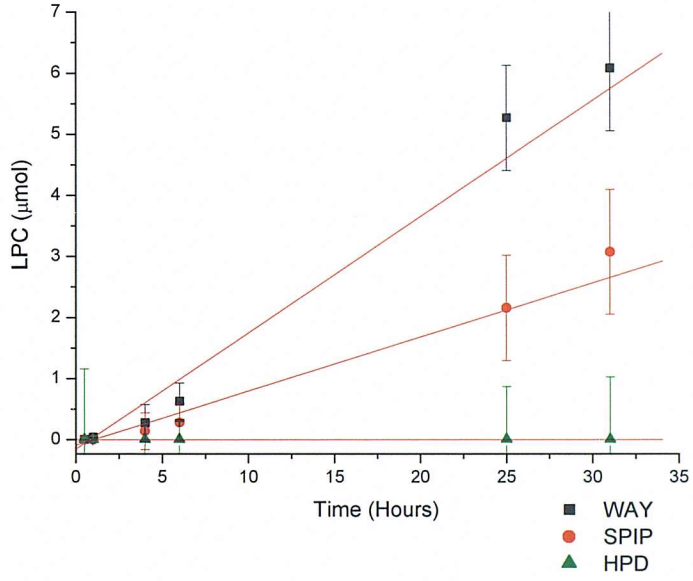


Figure IV.12: Initial rates of the appearance of LPC in DOPC: WAY, DOPC: SPIP and DOPC: HPD 20:1 samples.

Calculations of the slopes yielded the following initial rates: $k_{0\ LPC\ WAY} = 0.1984$ $\mu mol.h^{-1}$, $k_{0\ LPC\ SPIP} = 0.0924$ $\mu mol.h^{-1}$ and $k_{0\ LPC\ HPD}$ was not detectable. These values are in accordance with the k_1 values obtained earlier for the disappearance of DOPC with WAY hydrolyzing the bilayer as twice as fast as SPIP, and HPD exhibiting the slowest rate.

- DOPC initial degradation rate $k_{0\ DOPC}$

Initial rates k_{0DOPC} of the DOPC degradation were calculated from the slope of the tangent at t=0, and led to $k_{0\ DOPC\ WAY} = 0.3317 \mu mol.h^{-1}$, $k_{0\ DOPC\ SPIP} = 0.1877\ \mu mol.h^{-1}$ and $k_{0\ DOPC\ HPD} = 0.00237\ \mu mol.h^{-1}$ (Figure IV.13).

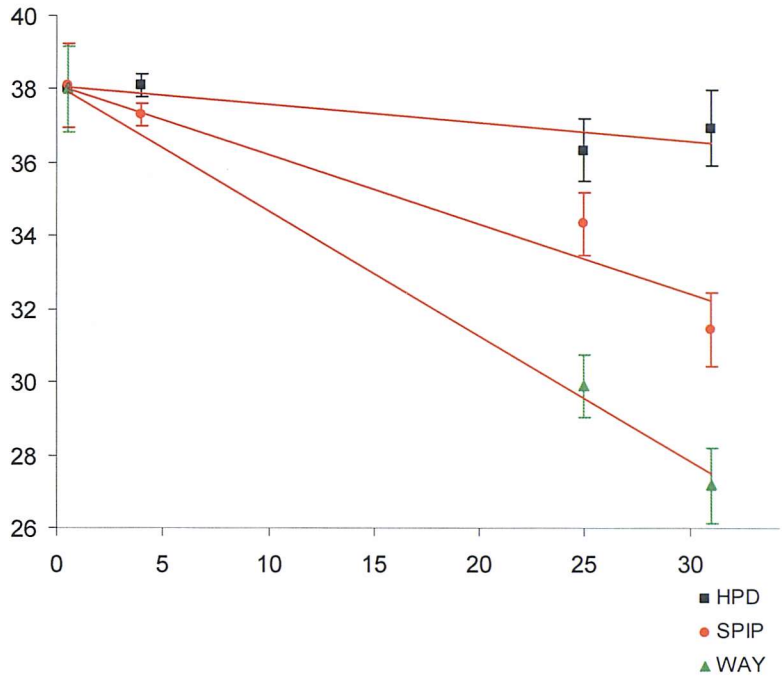


Figure IV.13: Initial rates of the disappearance of DOPC in DOPC: WAY, DOPC: SPIP and DOPC: HPD 20:1 samples.

The initial rates of disappearance of DOPC and appearance of LPC / OA correlate with the stoichiometry of the degradation model of one molecule of DOPC into one molecule of LPC and one molecules of OA. Although the initial rates are greater than the reaction rates, these cannot be compared directly as they both come from different curve fit equations. However, an assumption can be made on the rate being faster initially as the DOPC is in excess. Also the reaction starts when the system is still in the fluid lamellar phase where DOPC is predominant. When more LPC i.e. type I molecules and OA i.e. type II molecules are appearing, the membrane mechanics is altered with a drop in the stored curvature elastic stress. Therefore, the kinetic rates are expected to slow down. This effect is related to the stored curvature elastic energy that evolves in the system; this has already been described as having an impact on the modulation of amphipathic molecules such as the CTP: phosphocholine

citidyltransferase (CCT) or other enzymes such as phospholipases activity [191, 208]. The effects of curvature elastic stress on the membrane hydrolysis will be fully investigated in chapter 5.

The calculated degradation parameters for each drug are summarized in Table IV.2.

	$k_{0\ DOPC}$ ($\mu mol.h^{-1}$)	$k_{0\ LPC/OA}$ ($\mu mol.h^{-1}$)	k_{1DOPC} ($\mu mol.h^{-1}$)
WAY	0.3317	0.1984	0.00772±0.00027
SPIP	0.1877	0.0924	0.00396±0.00020
HPD	0.0024	-	0.00033±0.00004

	$k_{0\ DOPC}$ (molecules.s^{-1}.CAD molecules^{-1})	$k_{0\ LPC/OA}$ (molecules.s^{-1}.CAD molecules^{-1})	k_{1DOPC} (molecules.s^{-1}.CAD molecules^{-1})
WAY	$4.91x10^{-5}$	$2.93x10^{-5}$	$1.14x10^{-6}$
SPIP	$2.68x10^{-5}$	$1.36x10^{-5}$	$5.86x10^{-7}$
HPD	$3.50x10^{-7}$	-	$4.88x10^{-8}$

Table IV.2: Rates obtained for DOPC bilayers hydrolysis by WAY, SPIP and HPD. $k_{0\ DOPC}$ and $k_{0\ LPC/OA}$ are the initial rates obtained by calculating the slope of the tangent at t=0; k_{1DOPC} is the rate obtained from the disappearance of DOPC calculated from equation IV.1. Values were converted in molecules.s^{-1}.CAD molecules^{-1}

These sets of results show that a trend exists between the rate of hydrolysis and the different CADs. Therefore it is reasonable to assume that each drug has a distinctive effect on the bilayer, and that the hydrolysis rates are dependent on the drug itself as shown by WAY exhibiting the fastest degradation rate, and HPD the slowest. These parameters are of main importance, they can allow the classification of the drugs according to their efficiency to hydrolyze the bilayer. However, the rate values obtained after correlation to the number of CAD molecules present in the system yielded an insignificant rate. From these values, it can be calculated that only one molecule of DOPC can be hydrolyzed in ten hours in the presence of WAY. This is not consistent with the experimental data as LPC and OA are detected one hour after the sample was made. Therefore, these degradation rates show that not all CADs reside in the bilayer interface and that some CADs might have precipitated out of the bilayer, as described in section IV.1.2. To get an absolute rather than relative rate, we therefore need to know how many CAD are actually resident in the membrane. In

addition, it is also important to notice that the water availability is restricted between the lamellar stacks in these systems, in comparison to vesicles where water / buffer is largely in excess.

Although the CADs studied are planar molecules, it can be observed that WAY, SPIP and HPD exhibit dissimilar bilayer hydrolysis rates. HPD, WAY and SPIP have similar protonation sites which consist of a piperidine function and is localized in the middle of the molecule. The proton transfer from these functions to the lipid ester function is essential for the hydrolysis to occur; this depends on the proximity and the steric hinderance around the protonation site of the drug at the bilayer interface. One of the main differences between these three CADs is the counterions, with the maleate being WAY's counterion and the hydrochloride being HPD's and SPIP's counterion, this might also play a role in the difference of kinetics observed between the CADs, due to counterion recondensation onto the bilayer. Counterion recondensation and its effect on the bilayer hydrolysis kinetics will be discussed in the following section.

IV.2.3 Effect of chloride (Cl^-), formate ($HCOO^-$), trifluoroacetate (TFA-CF_3COO^-) and maleate ($HO_2CCHCHCO_2H$) counterions on the hydrolysis

This section will describe the effect of different CAD's counterions on the hydrolysis kinetics. As described in the beginning of the chapter, the solubility features of the HPD reduced dramatically during storage and this led to its crystallization. As this process ended the hydrolysis reaction, swapping the Cl^- counterion for more aqueous soluble counterion would increase the CAD solubility and therefore allow a more efficient hydrolysis reaction as the counterion does not condense onto the bilayer surface. This was already verified by the kinetics of the reaction of WAY carrying a maleate counterion and being twice as fast as SPIP and much faster than HPD. Therefore, CADs with four different counterions from the Hofmeister series namely chloride, formate, maleate and TFA were synthesized [145] and tested on bilayers made of DOPC. This was based upon the hypothesis that different counterions with a large hydration shell will reside preferentially in the aqueous medium, leaving the CAD at the interface, making the recondensation impossible.

The formate counterion is a kosmotropic ion that would therefore reside preferentially in the aqueous medium leaving the CAD at the interface enhancing the hydrolysis rate. The position of the TFA is unclear in the series, but as a hydrophobic ion i.e. chaotropic, it is expected to bind to the bilayer. TFA was also reported to behave as a co-surfactant in micellar systems [209] and to have a salting-in effect similar to that of thiocyanate [210]. The use of the maleate counterion was undertaken as this counterion was present in systems that exhibited the fastest rate of hydrolysis, namely DOPC: WAY systems. Although its effect as a salting-in or salting-out anion remains ambiguous, it is likely to be classified as a salting-out ion by its diacid function. In addition, this counterion was reported to have the same effects as citrate which is a kosmotropic ion, on bacterial growth, this phenomenon being dependent on the water structure led by anions from the Hofmeister series [203]. Figure IV.14 represents the degradation profile of DOPC: HPD 20:1 systems in the presence of four different counterions.

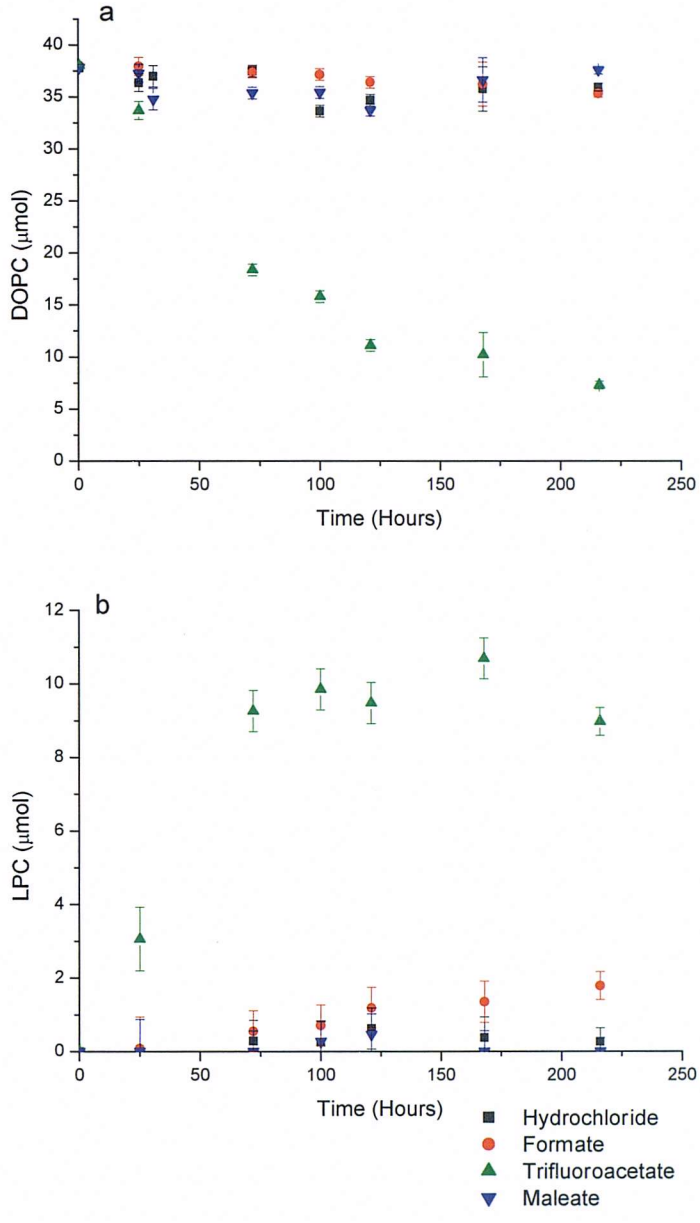


Figure IV.14: Comparison of hydrochloride, formate. trifluoroacetate and maleate counterion on the hydrolysis of DOPC (a) into LPC (b) in DOPC: HPD 20:1 systems.

The four tested counterions had dissimilar effects on the bilayer hydrolysis. The degradation profile obtained for the maleate salt is similar to that of the hydrochloride salt, where only little / no degradation of DOPC and appearance of LPC are evident. The presence of formate counterion has enhanced the degradation of DOPC and the formation of LPC with time in comparison to that of chloride and maleate salts. Likewise, it can be observed that the hydrolysis of DOPC is clearly enhanced in the presence of the trifluoroacetate salt, where DOPC is being degraded considerably and LPC formed until a plateau is reached. From these profiles, the initial rates for the

disappearance of DOPC k_{0DOPC}, and appearance of LPC $k_{0\ LPC}$, are calculated from the slope of the tangent at t=0 (Figure IV.15). The degradation parameter k_{1DOPC} was calculated from equation IV.1 (figure IV.16). Only the systems in the presence of formate and trifluoroacetate were considered as they were the only systems that produced measurable amounts of LPC.

It can be seen on figure IV.15 that the initial rates of degradation of DOPC are much faster in DOPC: HPD TFA 20:1 samples with $k_{0DOPC\ TFA}$ =0.262 μmoles.h^{-1} than in DOPC: HPD formate samples with $k_{0DOPC\ formate}$ = 0.008 μmoles.h^{-1}. Similarly, the initial rates for the appearance of LPC is more effective in the presence of trifluoroacetate with $k_{0LPC\ TFA}$ = 0.127 μmoles.h^{-1}, than formate with $k_{0DOPC\ formate}$ = 0.007 μmoles.h^{-1}.

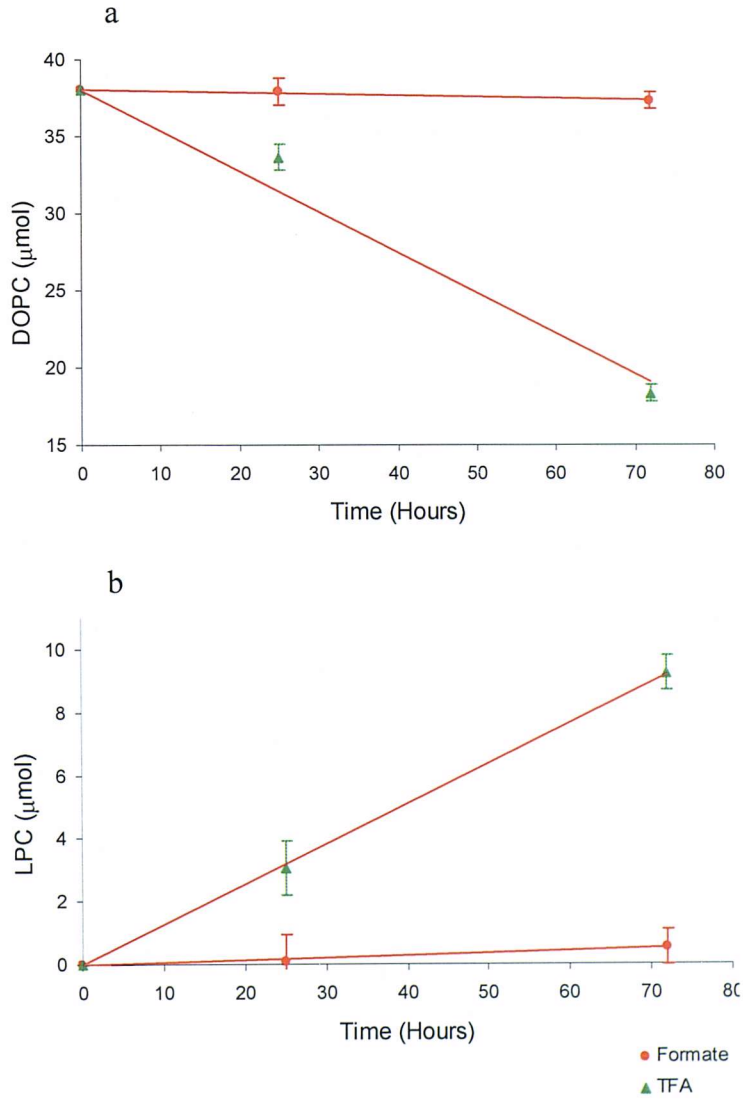


Figure IV.15: Initial rates for the degradation of DOPC (a) and the appearance of (b) LPC in DOPC:HPD 20:1 samples in the presence of formate and trifluoroacetate counterions.

The degradation parameters $k_{1DOPC\ TFA}$ and $k_{1DOPC\ formate}$ were determined according to equation IV.1 from the hydrolysis profile shown on figure IV.16. The values obtained are $k_{1\ DOPC\ TFA}=8.72x10^{-3} \pm 0.57x10^{-3}$ µmol.h^{-1} and $k_{1\ DOPC\ formate} = 3x10^{-4} \pm 2x10^{-5}$ µmol.h^{-1}. From $k_{0\ DOPC}$, $k_{0\ LPC}$ and $k_{1\ DOPC}$, $k_{0\ LPC}$ it can be established that the presence of the TFA counterion enhances the degradation rate by 30 times in comparison with the formate counterion in DOPC: HPD 20:1 samples.

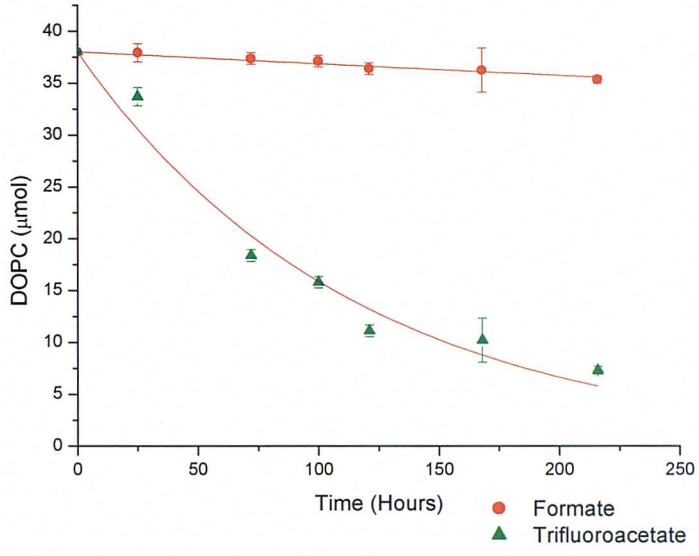


Figure IV.16: DOPC degradation profile in DOPC:HPD TFA and DOPC:HPD formate samples. The disappearance of DOPC follows an exponential decay model with $k_{1\ DOPC\ TFA}=8.72x10^{-3} \pm 5.7x10^{-4}$ µmol.h^{-1} and $k_{1\ DOPC}$ formate $= 0.3x10^{-3} \pm 2x10^{-5}$ µmol.h^{-1}.

From these measurements it is reasonable to assume that changing the hydrochloride HPD counterion to formate and TFA considerably improved the degradation kinetics of DOPC: HPD 20:1 systems, with DOPC:HPD TFA hydrolysing the bilayer approximately 30 times faster than DOPC:HPD formate 20:1.

The DOPC: HPD TFA degradation profile strongly correlates with those obtained in the presence of WAY maleate with the $k_{1\ DOPC}$ rate being in the same order of magnitude ($k_{1DOPC\ WAY}=7.72\ x10^{-3} \pm 0.27\ x10^{-3}$ µmol.h^{-1}).

Swapping the counterion in DOPC: HPD 20:1 systems clearly influenced the hydrolysis rates.

The presence of the formate and TFA counterions was shown to trigger the hydrolysis and considerably improve its rate in DOPC: HPD 20:1 samples. In the case of the formate, this was expected as according to the Hofmeister series this ion is strongly hydrated and preferentially resides in the aqueous medium, leaving the protonated HPD in the interface. The results obtained with the TFA were unexpected given the fact that the TFA would behave as a chaotropic ion that also bind preferably to the membrane. However it has been reported that fluorocarbon counterions such as TFA were able to form micelles involved in solubilisation processes [211]. In addition, TFA has also been described as a powerful amplifier for the translocation of large molecules such as carboxyfluorescein across phospholipid bilayers by polyarginines [212], interestingly polyarginins are also protonated at physiological pH and have been reported to cause the leakage of phospholipids vesicles [213]. This would explain the effect of TFA on the hydrolysis kinetics. In addition, it is important to notice that no crystals of drugs were detected in DOPC: HPD 20:1 with different counterion samples. This is probably due to the fact that the degradation was occuring in these samples, preventing the crystallization of CADs from happening.

Surprisingly, the presence of the maleate counterion in DOPC: HPD 20:1 samples did not improve the degradation, as would have been expected. Similar results were obtained for DOPC: SPIP maleate where no DOPC degradation was detectable (data not shown). This is contrary to the results obtained with DOPC: WAY maleate, which exhibited one of the fastest degradation rates. Therefore, two separate effects might be present, the counterion effect and the CAD efficiency to hydrolyze the lipids. The degradation rates are summarized on table IV.3.

Drug	Counterion	$k_{1(\mu}$ mol.h^{-1})	k_1 (DOPC molecules.s^{-1}.CAD molecules^{-1})
HPD	Hydrochloride	-	-
HPD	Formate	$0.31 \times 10^{-3} \pm 0.02 \times 10^{-3}$	4.58×10^{-8}
HPD	TFA	$8.72 \times 10^{-3} \pm 0.57 \times 10^{-3}$	1.29×10^{-6}
HPD	Maleate	0	0
SPIP	Hydrochloride	$0.39 \times 10^{-3} \pm 0.20 \times 10^{-3}$	5.86×10^{-7}
SPIP	Maleate	0	0
WAY	Maleate	$7.67 \times 10^{-3} \pm 0.27 \times 10^{-3}$	1.13×10^{-6}

Table IV.3: Rates obtained for DOPC bilayers hydrolysis by WAY, SPIP and HPD with different counterions, in buffer B. k_1 is the rate obtained from the disappearance of DOPC calculated from equation IV.1.

Although the counterion recondensation onto the bilayer triggered the crystallization of the CAD off the bilayer interface (see section IV.2.2), it is also evident that the counterion has an increasing / decreasing effect on the rate of the bilayer hydrolysis. This effect does not necessarily follow the Hofmeister series as chaotropic hydrophobic counterions such as TFA exhibited the fastest reaction rates in DOPC: HPD systems. TFA was indeed expected to lower considerably the binding of HPD to the bilayer and therefore the hydrolysis rate due to the counterion recondensation. In addition, kosmotropic counterions such as maleate that exhibited the fastest reaction rates in DOPC: WAY systems, had no effect on DOPC: HPD and DOPC: SPIP systems. Changing the CADs counterions affect their solubility, however these measurements show that the hydrolysis rate in DOPC: CAD systems not only depends on the type of counterions, but is also dependent on the type of CAD investigated. The Hofmeister series does not work consistently across different systems, in particular in bilayer systems.

IV.2.4 Influence of salt on the membrane hydrolysis.

The nature of the drug's salt was shown to have a profound effect on the solubility of the drug and the kinetics of the bilayer hydrolysis. Similarly, the presence of salt in the buffer was observed to have considerable effects on the organization of lipid lamellar phases, by screening the electrostatic interactions and leaving the bilayer to shrink [87]. It has also been reported that increasing the ionic strength increases the drug release by promoting its solubility [214]. Indeed, the specific effect of salts in solution arise from the organization of water molecules that are more oriented, resulting in the increase of the solubility of the ionizable drug [215], with the rate of dissolution being dependent on the ionic strength [194]. Moreover, it is important to notice that salts are present in biological systems and participate in a wide variety of processes such as membrane fusion, bacterial growth, and cell communication [216, 217]. Therefore, it is expected that the bilayer hydrolysis is affected by the presence of a high ionic strength, here 100 mM NaCl was used to represent physiological concentrations.

Figure IV.17 represents the degradation profile of DOPC: HPD 20:1 samples in buffer C (10 mM Tris, 100 mM NaCl, pH 7.4). This degradation profile is dissimilar to that of DOPC: HPD 20:1 in buffer B (10 mM Tris, pH 7.4) where no sodium chloride is present. In the presence of 100 mM NaCl, the membrane hydrolysis by the protonated HPD is considerably enhanced.

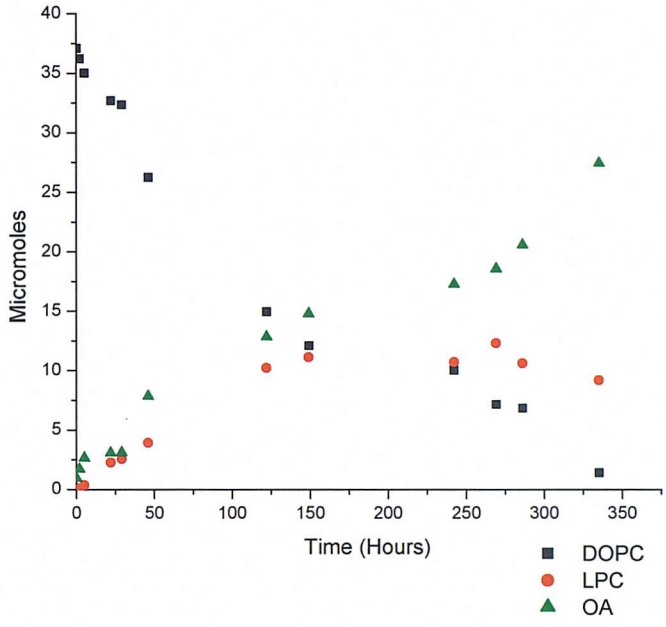


Figure IV.17: Degradation profile of DOPC: HPD 20:1 in 10 mM Tris, 100mM NaCl at physiological pH. The disappearance of DOPC follows a first order exponential decay. The rate of disappearance calculated from equation IV.1 led to $k_{1DOPC\ HPD\ NaCl} = 6.93\ x10^{-3} \pm 0.37\ x10^{-3}\ \mu M$.

The rate of disappearance of DOPC in the presence of 100 mM NaCl was calculated from equation IV.1 and led to $k_{1DOPC\ HPD\ NaCl} = 6.93\ x10^{-3} \pm 0.37\ x10^{-3}\ \mu M$ and compared to that in DOPC:HPD 20:1 in 10 mM Tris where little degradation occurred, the DOPC degradation rate was calculated and $k_1 = 1.73\ x10^{-3} \pm 0.24\ x10^{-3}\ \mu M$ (Figure IV.18).

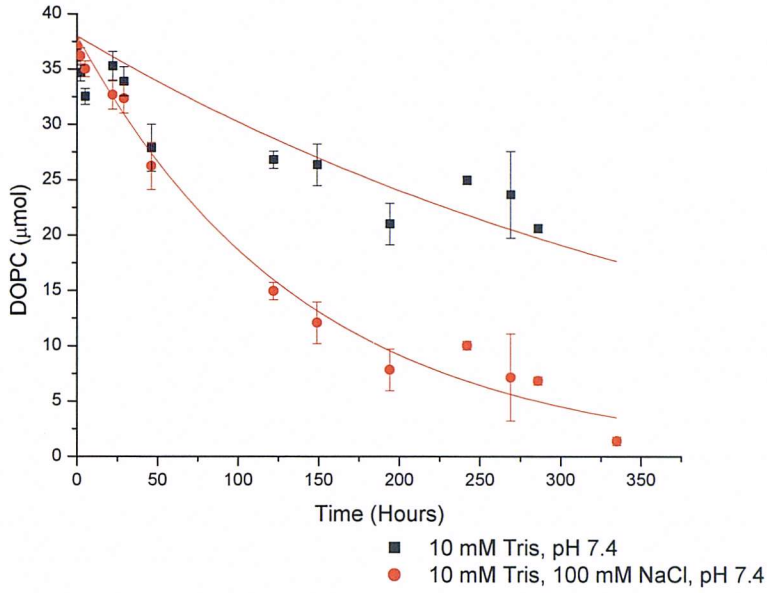


Figure IV.18: Effect of 100 mM NaCl on the DOPC degradation profile in DOPC: HPD 20:1 samples. The presence of NaCl is seen to enhance the reaction by a factor of 5.

The DOPC degradation rate in the presence of 100 mM NaCl is faster than in DOPC: HPD 20:1 in 10 mM Tris only, with the rate being similar to that of DOPC: WAY 20:1 in 10 mM Tris (k_1= 7.72x10^{-3} µmol.h^{-1}).

The addition of 100 mM NaCl is crucial for the reaction to happen in DOPC: HPD 20:1 samples. The presence of 100 mM NaCl generates the organization of water molecules in the close vicinity of the HPD that increases its solubility. This concentration of NaCl is also known to screen the electrostatic interactions at the bilayer surface; with a calculated Debye length of 10Å, this will enable the protonated solubilised drug to undergo steric interactions with the bilayer interface and trigger the hydrolysis. This result strongly correlates those obtained in chapter 3, where HPD is seen to degrade the DOPC bilayer within 3 days at this ratio. Indeed, these samples also contained 100mM NaCl at physiological pH.

The same types of experiments were carried out using WAY. Surprisingly, the presence of 100 mM NaCl did not affect the rate of hydrolysis of the bilayer (Figure IV.19). Analysis of the DOPC degradation rate in the presence and absence of salt using equation IV.1 led to $k_{1DOPC\ WAY\ NaCl}$ = 8.89 x10^{-3}± 0.37 x10^{-3}µM and $k_{1DOPC\ WAY}$ = 7.63 x10^{-3} ± 0.37 x10^{-3} µM.

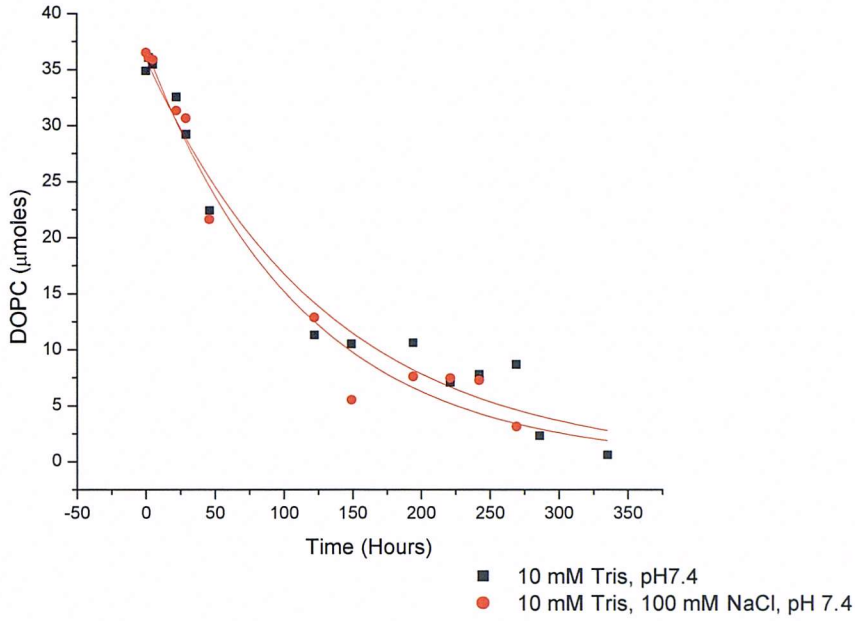


Figure IV.19: Effect of 100 mM NaCl on the DOPC degradation profile in DOPC: WAY 20:1 samples. There is no change in the DOPC degradation rate in the presence of 100 mM NaCl. The degradation rate obtained from equation IV.1 are $k_{1DOPC\ WAY\ NaCl} = 8.89x10^{-3} \pm 3.7x10^{-4}$ µM and $k_{1DOPC\ WAY} = 7.63x10^{-3} \pm 3.7x10^{-4}$ µM.

WAY molecules carry maleate counterions with them that enhance the drug dissolution in the buffer in the first place. Therefore, the addition of salt does not affect the dissolution of WAY. From these results, WAY acts independently from the salt present in the buffer.

From these studies, it is becoming increasingly evident that the parameters that control the bilayer hydrolysis are extremely complex. The structure inherent to each molecule and its conformation plays an essential role on the bilayer hydrolysis, as exemplified by SPIP exhibiting more degradation than HPD in the same conditions. However, reaction rates are to be considered carefully as not all CADs are bound to the bilayer, and water availability is restricted between the lamellar stacks; which may impose a limit on the rate of reaction.

In addition, the choice of the counterion also affects the bilayer hydrolysis in such a manner that it does not recondense onto the bilayer, as was shown for HPD HCl. Although the counterion recondensation follows the Hofmeister series [87], counterions that enhance the bilayer hydrolysis do not necessarily follow the Hofmeister series as described for the kosmotropic dianion maleate which exhibited

the fastest rate in DOPC: WAY systems, but did not trigger any hydrolysis in DOPC: HPD and DOPC: SPIP systems.

Finally, the ionic strength of the aqueous buffer also plays a critical role as it firstly increases the drug dissolution and secondly reduces the surface electrostatic interactions, which enable the CADs to freely interact with the bilayer interface.

IV.3 Correlation between the membrane degradation rate and the non-specific binding (NSB).

IV.3.1 Background

The concept of NSB *in-vivo* and *in-vitro* relates to the binding of drug molecules / ligand to sites other than their target sites which are commonly membrane bound receptors or enzymes. Binding of molecules to sites other than the intended target recognition site refers to as non-specific sites. Additionally, when the drug is trapped in the bilayer, the lipid bilayer is also considered as a non-specific site. Binding of drug molecules to the bilayer is predominant in the NSB issue as the bilayer is in large excess in comparison to specific receptors which are commonly present in femtomolar-nanomolar concentration, and often heterogeneously located in tissues (Please refer to chapter one for more details on NSB and references therein).

One of the current techniques used to predict the degree of NSB of drug molecules *in-vitro* is the measure of the lipophilicity of the molecules by using the octanol / water partition coefficient Log P [31]. This technique allows the determination of the likehood of a compound partitioning between a hydrophilic environment such as water or buffer and a hydrophobic environment such as octanol. Lipophilicity (Log $P)_{oct\text{-}water}$ of central nervous system (CNS) drugs that exhibit low non-specific binding usually lies in the range of 1.5–3. An additional method that describes drug's developability is the Lipinsky's rule of five, where pharmaceutical compounds are likely to be successful when the molecular weight is smaller than 500 $g.mol^{-1}$, Log P is less than 5, and the molecules have less than 5 H bond donors and 10 H bonds acceptors [39].

Although lipophilicity is known to increase the drug penetration within tissues such as the blood brain barrier (BBB), it is also known to increase the non-specific binding of the drug *in-vivo* [15]. This is principally observed using *in-vivo* methods such as positron emission tomography (PET), which shows that Log P is an imperfect predictor for the NSB *in-vivo*, as this phenomenon also depends on the affinity of the compounds towards the receptor, and the receptor concentration. The NSB phenomenon is poorly understood, and so far there are no available techniques that are able to predict it accurately from *in-vitro* to *in-vivo* studies.

It has been largely reported that CADs have a high affinity for the bilayer interface [120, 157]. In addition, Lullman and coworkers highlighted a linear relationship existing between Log P and drug binding to bilayers made of phosphatidylcholine with hydrophobicity being the main driving force of such interactions [38]. Similarly, it has been observed that the increase in lipophilicity correlates with the increase of binding of CADs to membranes, this effect being dependent on the nature and structure of the CAD itself [125].
As a matter of fact, correlations between the NSB *in-vivo*, the structure of the CADs and the rate of the bilayer hydrolysis by the CAD can be made.

IV.3.2 Hydrolysis rates as parameters revealing the degree of NSB

It has been discussed that the rate of hydrolysis is dependent on the nature and structure of the drug, with WAY degrading the bilayer quicker than SPIP and HPD. The ability of the CAD to transfer the proton necessary to the bilayer hydrolysis depends on the steric conformation of the drug. Surprisingly, the hydrolysis rates also correlate with the absolute *in-vivo* NSB distribution volumes obtained *in-vivo* from PET studies on humans. Drugs that trigger an elevated hydrolysis rate in DOPC bilayers also exhibit a low NSB degree *in-vivo* and vice versa. The parameters are summarized in table IV.4.

Drug	Log P	Ratio NSB / SB	k_1 µmol.h^{-1}
WAY	3.69	13.83	7.67×10^{-3}
SPIP	1.73	166.67	3.96×10^{-3}
HPD	4.20	++++[113]	$< 1 \times 10^{-3}$

Table IV.4: Summary of hydrolysis rates, lipophilicity and NSB.

These observations allow the understanding of NSB at a molecular level by the capacity of the CAD to digest the membrane system at different rates.

A high degree of NSB is seen when the drugs do not trigger the acidic hydrolysis of the lipid chain, thus the molecules are trapped on the bilayer interface and are hindered from reaching their specific targets, and this is observed for HPD. However, when the rate of hydrolysis is high, there is little chance that the drugs stay at the interface as they are likely to be dissolved in membranous fragments that will carry them to other membrane interfaces, until they find their specific target (Figure IV.20). This is characterized by a low ratio of NSB over specific binding signal as seen for SPIP and WAY. Moreover, the rate of degradation is also in accordance with the specificity of the molecules, as it is seen for SPIP and WAY; WAY exhibits lower NSB than SPIP and degrades the bilayer faster.
This correlation was also observed for raclopride, another CAD, where the hydrolysis rate was faster than that of WAY, and where the ratio of NSB / SB = 10.25 [185].

Interestingly, it has also been shown by Rosso and coworkers by computer modeling that a linear relationship exists between CADs electronic interactions and DOPC ester function [218]. The interactions were found to be less favorable for raclopride, followed by WAY and SPIP; this feature would allow the CADs residence to be shorter in the bilayer interface, which consequently will reduce the NSB signal.

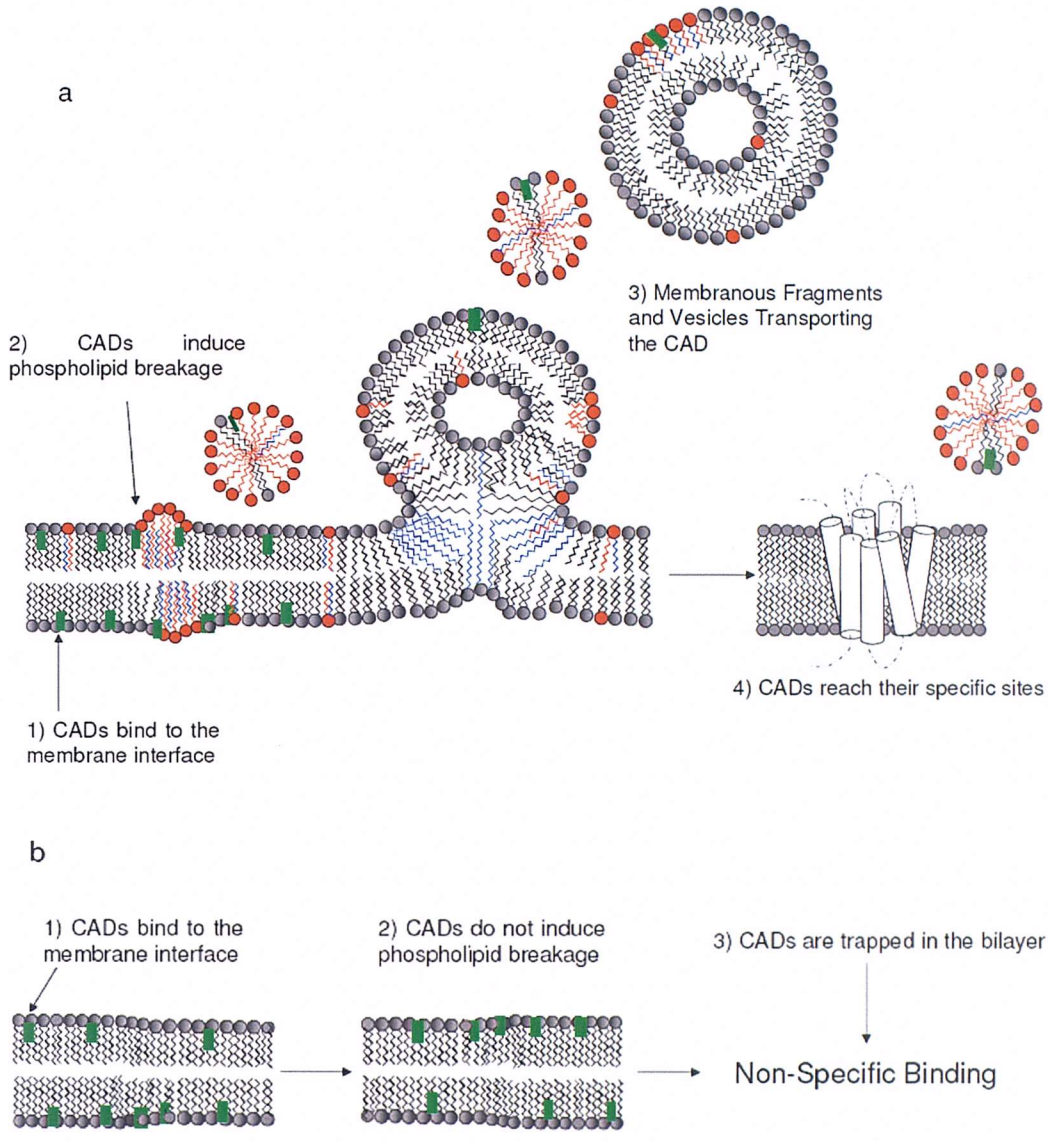


Figure IV.20: Correlation between the bilayer hydrolysis and CADs non-specific binding. (a) CADs bind to the membrane interface and exhibit fast degradation rates. The formed membranous fragments and vesicles allow the CAD transportation until their specific site. (b) CADs bind to the membrane interface but do not trigger the lipid ester hydrolysis. Hence they are trapped in the bilayer and NSB is observed.

At the moment, failure rate for useful radioligands is high due to the NSB. Analyzing the bilayer degradation rate by the CADs is a useful tool to predict the NSB *in-vitro* as this system takes into account the bilayer environment as well as its physicochemical properties. The degradation rates method is therefore more accurate than the lipophilicity measurements using the octanol / water partition coefficient protocol. As described earlier, lipophilicity measurements are used to predict the NSB of drugs *in-vivo*, where octanol mimics biological membranes; this led to a huge discrepancy between *in-vitro* and *in-vivo* experiments. Model membranes are more similar to

biological membrane than octanol as phospholipids physical properties are present. Moreover, changing the lipid composition, i.e. changing the stored curvature elastic stress is possible using this method, which gives a better model for biological membranes (See chapter 5).

This prediction would be very valuable for predicting the specificity of central nervous system drugs when binding in the brain, as these drugs have to cross the blood brain barrier and exhibit low non specific binding.

CHAPTER 5

Modulation of the hydrolysis kinetics by membrane curvature elastic stress

This chapter will investigate the effect of the membrane stored curvature elastic stress on the hydrolysis kinetics by three CADs: HPD, SPIP and WAY. Two pseudo binary systems with different stored curvature elastic stress will be considered from a least stressed system made of dilauroylphosphatidylcholine (DLPC), to a more stressed system made of different ratios of DOPC and dioleoylphosphatidylethanolamine (DOPE). Comparisons of hydrolysis rates will be considered for each drug.

V.1 Background

A lipid bilayer is formed by two lipid monolayers that are forced to sit back to back so that the hydrocarbon chain are facing each other and the polar headgroups are oriented towards the aqueous medium such as the buffer; this effect being controlled by the hydrophobic effect. As it was explained in chapter one, lipids have intrinsic curvature that leads them to bend away (type I) or towards (type II) the water interface. When type I and type II lipids are present in the bilayer, they induce an

increased desire for monolayer curvature. As this desire can not be realised, the arrangement of phospholipids results in a frustrated structure that is locally flat. A curvature torque tension is then introduced in the bilayer that is forced to remain flat, which results in the storage of curvature elastic energy in the bilayer [79]. (Please refer to chapter one for more details on curvature elastic energy and references therein.)

The addition of non bilayer lipids type I (LPC) or type II (DOPE) to a flat bilayer will also result in a change in the lateral pressure in the centre of the bilayer because of the collision between the hydrocarbon chains [67]. This effect may be an important factor in the modulation of the activity of many molecules such as proteins and enzymes like the phospholipase A2 in biological systems [219].

Many examples in the literature show the effect of lipid forces on biological systems and events. The binding of amphipathic molecules was found to be dependent on lipid packing as it was described for dystrophin, a cytoplasmic protein, with more binding affinity occurring when DOPE is added to DOPC bilayers [220]. It has also been reported that some protein activities were regulated by membrane curvature elastic stress. In processes such as vesicular transport and membrane trafficking, it was shown that amphipathic motifs of the golgi associated protein ArfGAP1 were able to sense membrane curvature; this having an effect on trapping small vesicles in the golgi apparatus [221]. Moreover, it has been demonstrated that ArfGAP1 which promotes the GTP hydrolysis involved in membrane budding was also sensitive to lipid packing and to positive curvature as the GTP hydrolysis decreases when the membrane is more positively curved [222]. The change in membrane curvature elastic stress is also involved in other processes such as membrane fusion [223]. Viral proteins were found to be activated preferentially by negative curvature, as it was shown for viral fusion peptides in the HIV, influenza, and leukaemia virus [224]. In addition it was demonstrated that the membrane curvature elastic stress increases the activation energy of insertion of transmembane α-helices in DOPC lipid bilayers; this was shown by adding the non-bilayer lipid DOPE to DOPC bilayers [225]. More importantly, it has been described that membrane curvature elastic stress alters the activation kinetics of membrane related enzymes. It has been reported that the

epithelial Na^+/H^+ exchanger (NHE3) system, which is responsible for the maintenance of osmotic pressure of the cell, is activated by positive curvature imposed by the membrane upon swelling. A positive deformation of the membrane by addition of LPC has reproduced a hypoosmolar activation of the NHE3 system [226]. The activity of another enzymatic system, the CTP (cytidine triphosphate): phosphocholine cytidyltransferase (CCT), an enzyme involved in the PC biosynthesis, was also reported to be dependent on the membrane composition [191]. It was determined that the CCT activity, which is modulated by the insertion of its amphipathic moiety in the lipid bilayer, is enhanced when the curvature elastic stress increases by adding more type II lipids to preformed bilayers. However, it was also described that the activity was drastically slowed down in the presence of type I lipids.

As the effect of the membrane stored curvature elastic stress has been described to influence many biological systems and events, it is therefore supposed to also affect the kinetics in which the bilayer hydrolysis occurs in the presence of CADs. Therefore, adding DOPE to DOPC bilayers is expected to accelerate the hydrolysis kinetics, whereas, monitoring the hydrolysis in DLPC bilayers is expected to be slowed down in comparison to that of DOPC kinetics.

V.2 Effects of systems with reduced curvature elastic stress on hydrolysis kinetics; DLPC bilayers

V.2.1 DOPC vs. DLPC bilayers

The membrane hydrolysis kinetics was monitored by using bilayers made of DLPC and compared to hydrolysis rates obtained with DOPC. DLPC lipids differ from DOPC in the length of their hydrocarbon chain and in the number of unstaurated carbons (Figure V.1).

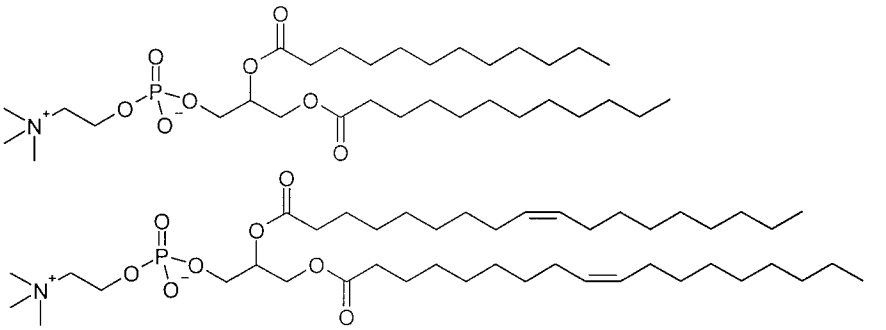


Figure V.1: Comparison of DLPC (top) and DOPC (bottom) structure.

Although DLPC and DOPC lipids form the fluid lamellar phase L_α at room temperature (Tm=-22°C [75] and -3°C [227] respectively), they both exhibit different spontaneous curvature. Because DOPC molecules contain an unsaturated double bond that allows the chains to splay, DOPC monolayers impart the desire of curvature toward the polar interface more than DLPC monolayers that contain no unsaturated double bond. Therefore, DOPC bilayers contain more stored curvature elastic stress than DLPC bilayers. This feature will also make the interface more accessible to the drugs in DOPC bilayers to that of DLPC bilayers. The number of carbons as well as unsaturations was already described as having an effect on the elasticity of bilayers, [171]. Therefore, bilayers made of DLPC exhibit lower stored curvature elastic stress in comparison to that of DOPC.

V.2.2 Determination of the hydrolysis kinetics in DLPC: WAY and DLPC: HPD systems.

The effect of reduced stored curvature elastic stress has already been described as lowering the CADs membrane-binding affinity and the reaction rates [149]. This was shown by static ^{31}P NMR on DLPC: HPD 4:1 and DLPC: SPIP 20:1 samples, where the detection of the isotropic peak corresponding to LPC micelles occurred with longer timescales with respect to DOPC systems. These measurements allowed the determination of the effect of the reduced stored curvature elastic stress; however accurate quantification of the hydrolysis rate could not be undertaken. Therefore, hydrolysis rates were determined from the degradation profile obtained from normal phase HPLC data as described in chapter 4.

Although it has been shown in the previous chapter that HPD has little impact on the hydrolysis kinetics of DOPC bilayer, the use of DLPC bilayers clearly shows that the kinetics are even slower in this system.

Figure V.2 depicts the lipid degradation profile obtained from HPLC data for DOPC: HPD 20: and DLPC: HPD 20:1 samples. The lipid degradation rates $k_{1\ DOPC\ HPD}$ and $k_{1\ DLPC\ HPD}$ were calculated according to equation IV.1 (see chapter 4) and yielded $k_{1\ DOPC\ HPD} = 1.52x10^{-3} \pm 2.6x10^{-4}$ $\mu mol.h^{-1}$ and $k_{1\ DLPC\ HPD} = 5x10^{-5}$ $\mu mol.h^{-1}$. The kinetic rate of degradation of DLPC bilayers is approximately 30 times slower than for DOPC bilayers.

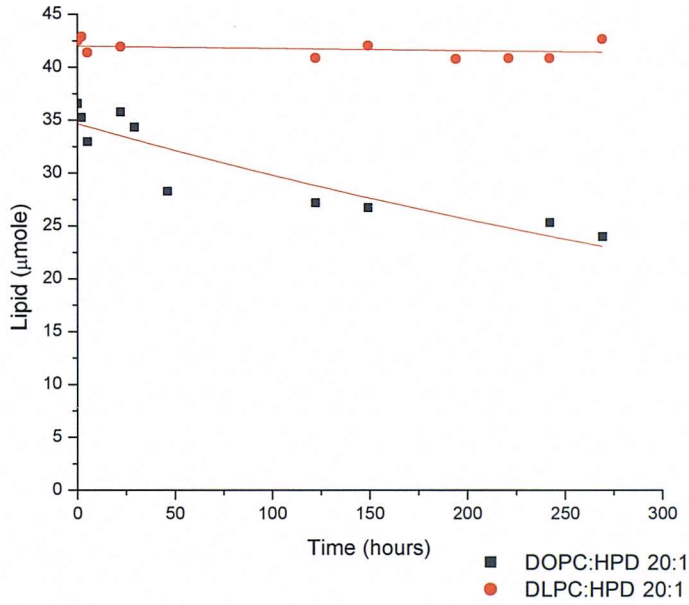


Figure V.2: DOPC and DLPC hydrolysis profile obtained by HPD.

Similarly, measurements were undertaken on DLPC: WAY 20:1 systems. WAY is the CADs that exhibited the fastest kinetics in DOPC bilayers. The DLPC degradation profile compared to DOPC degradation profile is shown on Figure V.3.

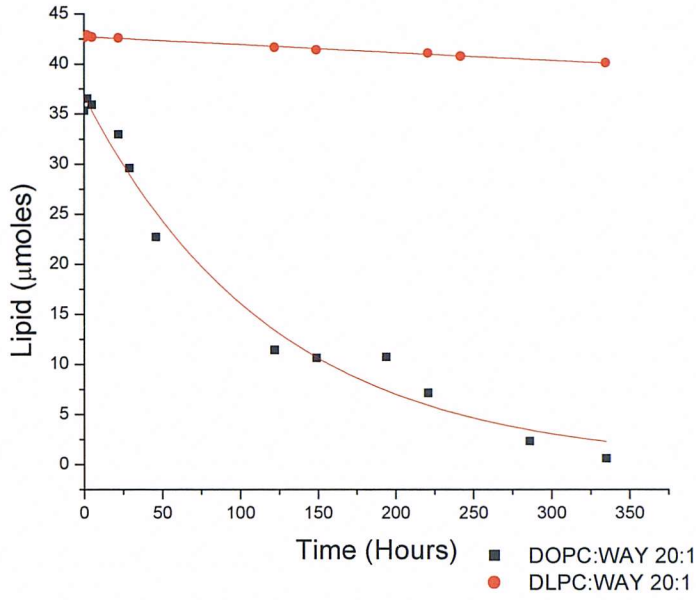


Figure V.3: Comparison of DOPC: WAY and DLPC: WAY 20:1 degradation profiles.

Calculation of the degradation parameters led to $k_{1\ DOPC\ WAY} = 8.28x10^{-3} \pm 6x10^{-4}$ $\mu mol.h^{-1}$ and $k_{1\ DLPC\ WAY} = 1.9x10^{-4} \pm 7.85x10^{-6}$ $\mu mol.h^{-1}$. The degradation kinetics is approximately 40 times slower in DLPC: WAY 20:1 than in DOPC: WAY 20:1 systems.

Degradation occurs in DLPC samples in a slower rate in comparison to DOPC samples; however, it was possible to detect the appearance of LPC in DLPC: WAY 20:1 samples. Figure V.4 represents the appearance LPC with time in both DOPC and DLPC systems. Because it was not possible to calculate accurately k_{LPC} from experimental data, only the initial rates were determined in DOPC and DLPC systems.

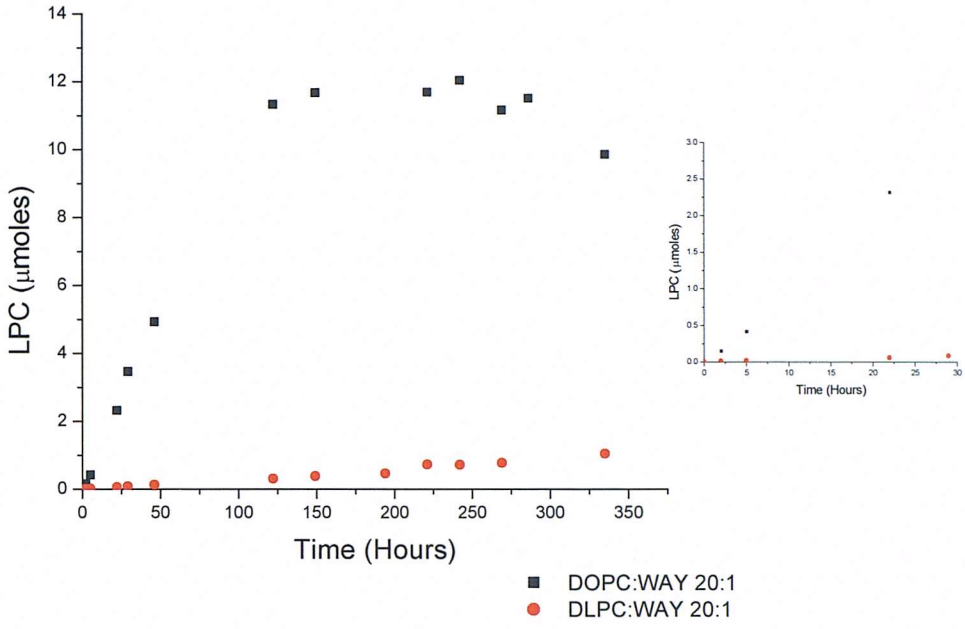


Figure V.4: Appearance of LPC in DOPC: WAY and DLPC: WAY 20:1 systems. The initial rates were calculated from the slope of the tangent at t=0 (right).

The initial rates of appearance of LPC in DOPC and DLPC systems are $k_{0\ LPC}$ = 0.1136 µmol.h^{-1} and $k_{0\ LPC}$ = 0.0028 µmol.h^{-1} respectively. Although the kinetic rate is slower in DLPC bilayers, there are detectable amounts of LPC generated from the action from the CAD. The appearance of LPC is 40 times slower in DLPC systems than in DOPC systems.

These experiments are of importance as they reveal that the hydrolysis is not only dependent on DOPC lipids, but also occurs in other PC lipids. In addition, these measurements have demonstrated that the kinetics of the bilayer hydrolysis is relative to the membrane stored curvature elastic energy, with the kinetics being approximately 30 to 40 times slower in membranes with reduced stored curvature elastic stress. DLPC bilayers exhibit more lateral pressure in the chain region than DOPC; and less packing frustration this is due to the lack of unstaurated carbons in these lipids. Also this has an impact on the interface accessibility for the drug as there is a strong hydrogen bonding at the headgroup [187]. These results strongly correlates with the results obtained with CCT binding to DMPC bilayers, where its activity was also found to decrease in DMPC bilayers with respect to DOPC [191].

V.3 Effects of systems with increased curvature elastic stress; DOPC: DOPE systems.

V.3.1 DOPC: DOPE systems

DOPE is a non bilayer lipid that has the propensity to undergo L_α to H_{II} transition [228]. This inverted cone-shaped lipid has a curved interface that arises from the lateral pressure distribution in the chain region and the relatively small headgroup volume. DOPE lipids were extensively studied and used as a model to investigate the effects of solutes and other lipids on the change of mesophases and destabilization of biological membranes [229].

The effect of stored curvature elastic stress was widely described in the literature by using PC: PE model membranes. The mixed DOPC: DOPE system provides a well characterized environment in which the monolayer curvature and the lipid lateral pressure can be controlled. In such systems, the stored curvature elastic stress arises from DOPE lipids, where the pressure in the hydrocarbon chain region, the presence of unsaturated carbons, and the reduced hydrophilicity of the PE headgroup tend to curve the bilayer towards the aqueous phase [67]. Addition of DOPE lipids in DOPC bilayers causes a redistribution of the lateral pressure across the bilayer, and an increase in the pressure exerted by the lipid chains [228]. This was previously measured by using di-pyrenyl PC fluorescent probes [230]. Addition of DOPE in DOPC bilayers spreads the lipids apart; this results in a more favourable environment for the intercalation of molecules such as CADs in the interfacial region. The physical forces described above were shown to drive the L_α - H_{II} phase transition in DOPC: DOPE systems under various conditions such as variation of temperature, hydration, and the molar ratio of DOPC to DOPE [231].

DOPC:DOPE systems were used as model systems to quantify the effect of stored curvature elastic stress on proteins activities, such as bacteriorhodopsin [232], mutlidrug transporters [233] and CCT [191]. Activities were found enhanced or reduced according to the proportion of DOPE found in the bilayer. As the hydrolysis

kinetics was found to slow down in reduced stored curvature elastic stress systems, it is therefore expected that addition of DOPE will increase the bilayer hydrolysis by the CAD.

V.3.2 Effects of DOPE on the hydrolysis kinetics

Variation of the stored curvature elastic stress was undertaken by using increasing DOPE molar fractions in DOPC: DOPE systems, from 0 to 0.4. The experimental conditions in which the measurements are made do not allow the L_α - H_{II} phase transition and only the L_α phase is predominant [234]. Thus, measurements were only made in the L_α phase. In addition, the homogeneity of such systems has already been studied by X-ray diffraction and polarizing microscopy, where DOPC:DOPE at these ratios form the L_α phase at neutral pH [67, 235]. Therefore, this is also applicable to the lipid: drug systems described above. Hydrolysis kinetics of DOPC: DOPE bilayers by two CADs (SPIP and WAY) were measured a 20:1 total lipid: drug molar ratio. Measurements of the disappearance of the lipids and appearance of the products were undertaken by normal phase HPLC as described previously, by considering the total number of moles of lipids DOPC and DOPE (DOPE elutes at 10.1 min) and product LPC+LPE (LPE elutes at 20.5 min). The production of OA comes from both DOPC and DOPE as these two lipids share the same fatty acid chain.

The effect of increasing DOPE molar content on the total lipid disappearance in the presence of WAY and SPIP is shown on figure V.5. The disappearance of the lipids follows an exponential decay, as shown previously for pure DOPC bilayers. When DOPE is present, the rate of hydrolysis is altered in comparison to that of pure DOPC.

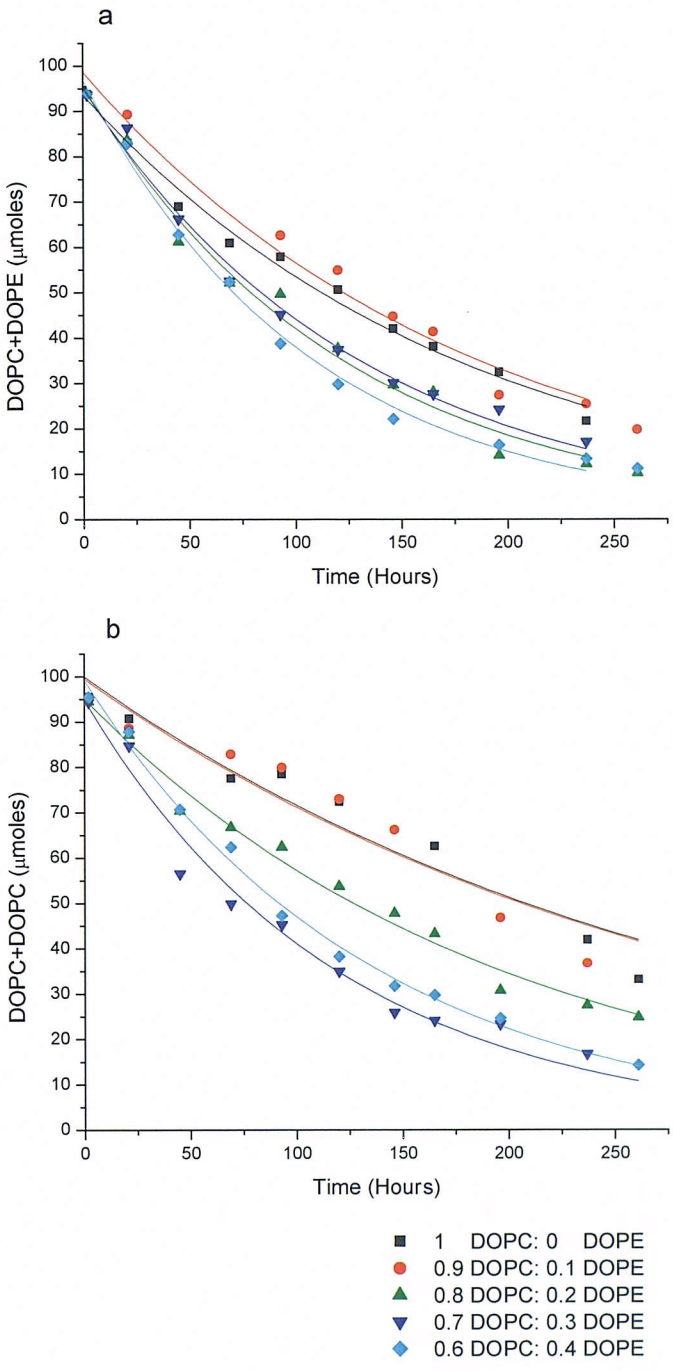


Figure V.5: Effect of various DOPC: DOPE molar ratio on bilayer hydrolysis kinetics by WAY (a) and SPIP (b).

Fitting the disappearance of total lipids DOPC: DOPE in the presence of WAY and SPIP yielded to hydrolysis rates that are summarized in table V.1.

	k_1 ($\mu mol.h^{-1}$)	
	SPIP	WAY
1 DOPC: 0 DOPE	$3.18x10^{-3} \pm 4.1x10^{-4}$	$5.58x10^{-3} \pm 2.0x10^{-4}$
0.9 DOPC: 0.1 DOPE	$3.05x10^{-3} \pm 3.8x10^{-4}$	$5.46 x10^{-3} \pm 3.8x10^{-4}$
0.8 DOPC: 0.2 DOPE	$5.09 x10^{-3} \pm 2.0x10^{-4}$	$8.05 x10^{-3} \pm 3.8x10^{-4}$
0.7 DOPC: 0.3 DOPE	$7.99 x10^{-3} \pm 5.8x10^{-4}$	$7.73 x10^{-3} \pm 2.6x10^{-4}$
0.6 DOPC: 0.4 DOPE	$7.15 x10^{-3} \pm 2.7x10^{-4}$	$9.21 x10^{-3} \pm 3.1x10^{-4}$

Table V.1: Hydrolysis rates in DOPC: DOPE systems in presence of WAY and SPIP.

The hydrolysis rate is clearly affected by the presence of DOPE i.e. by the increase in the stored curvature elastic stress in both WAY and SPIP systems. The hydrolysis rate is approximately twice as fast in DOPE systems that exhibit the highest stored curvature elastic stress, i.e. 0.6 DOPC: 0.4 DOPE in the presence of both of the drugs. Variations of hydrolysis rates as a function of DOPE molar fraction are represented on figure V.6.

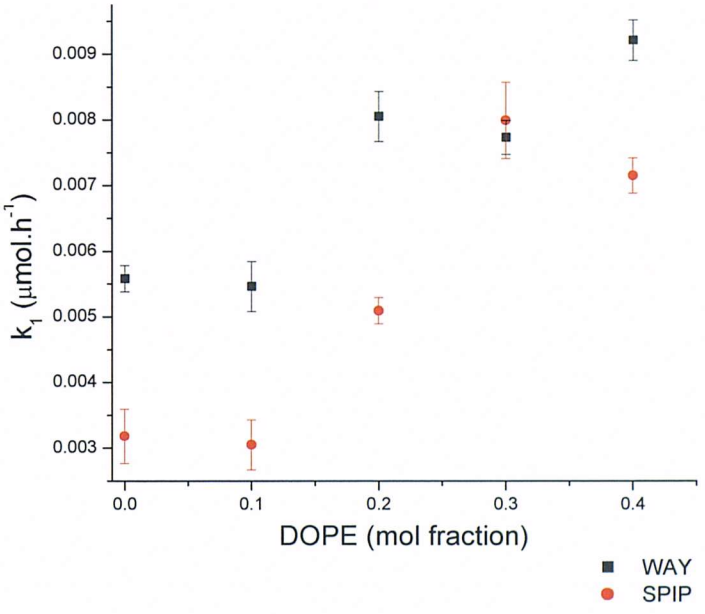


Figure V.6: Hydrolysis rates as a function of DOPE mol fractions in the membrane.

Although WAY and SPIP exhibit different absolute hydrolysis rates with respect to varying DOPE molar fractions they both rise with increasing DOPE molar fractions; a

similar profile has been observed for other systems, including the insertion of peptide assemblies such as CCT into DOPC:DOPE bilayers [225] (Figure V.7).

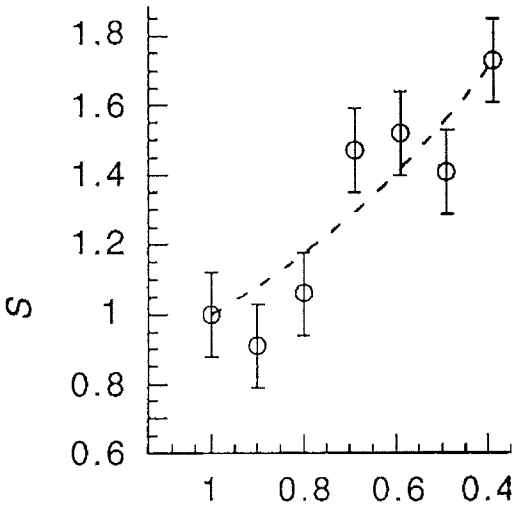


Figure V.7: Activity of CCT as a function of the molar fraction of DOPC (Figure adapted from reference [191])

The increase in hydrolysis rate from 0.1 to 0.4 DOPE molar ratios is a result of increased CAD binding at the interface. This is due to the decrease in the repulsion at the interfacial region and the increase in the hydrocarbon chain pressure [232]. The variation in chain pressure with increasing DOPE has been extensively studied using dipyrenyl lipids where the ratio of excimer to monomer fluorescence (E / M) is related to the measure of the lateral chain pressure. Overall, the E / M ratio was observed to increase monotonically with increasing DOPE concentration in model DOPC / DOPE bilayers (Figure V.8) which correlates with the variation in hydrolysis rates in these experiments.

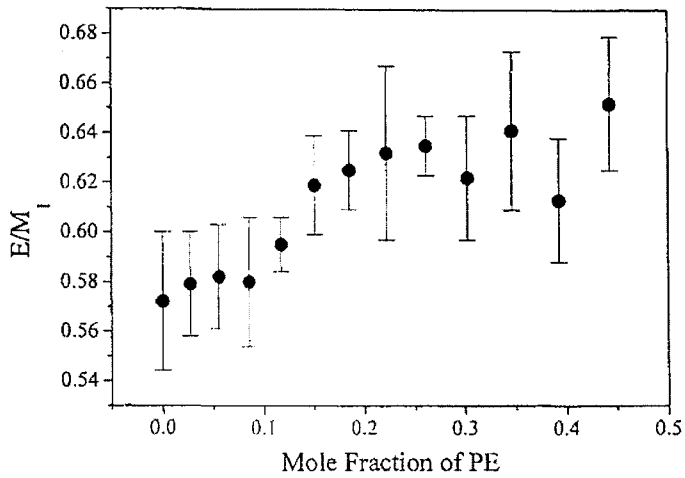


Figure V.8: Effect of DOPE molar fraction on the excimer to monomer ratio of dipyrenyl lipids in DOPC: DOPE bilayer. The increase of E / M1 ratio is due to the increase in the chain pressure in the centre of the bilayer (Figure taken from reference [232]).

A maximum rate of hydrolysis occurs with SPIP at 0.3 DOPE molar ratios followed by a minor decrease in the hydrolysis rate at 0.4 DOPE molar ratio. This might be a result of accumulation of type I LPC-LPE monomers produced from the hydrolysis that accumulate into the bilayer. Addition of type I molecules to a membrane containing type II molecules reduces the desire for curvature towards the aqueous exterior; this effect has also been ascribed to the lower the binding affinity and acitivity of amphipatic molecules such as CCT [191]. The evolution of WAY kinetics shares the same profile, with the rate increasing considerably from 0 to 0.2 DOPE molar fractions, and slightly decreasing at 0.3 DOPE molar fractions.

Monitoring the bilayer hydrolysis in DOPC: DOPE samples is complex as six species, namely the CAD, DOPC, DOPE, LPC, LPE and OA are present. When more LPC / LPE is produced, the bilayer is also enriched in OA; this will result in a alteration in the stored curvature elastic stress with DOPC, DOPE, LPC, LPE and OA being present in the system.

The bilayer mesophase is uncertain at this stage of the measurements. Even if the DOPC:DOPE molar ratio at which the experiments are done do not allow the formation of the H_{II} phase, these do not take into account the accumulation of fatty acid and type I molecules that result from the bilayer breakage. It would be important to perform complementary measurements to map the bilayer state with time by using

SAXS and SS-NMR at the DOPC: DOPE: CAD ratios examined above. In addition, it would be interesting to increase the DOPE molar fraction up to 0.6 to evaluate the evolution of the kinetic rate. However, the rate is expected to considerably decrease in the H_{II} phase as the interface accessibility might be hindered and thus the hydrolysis rate would be affected.

V.3.3 DOPC and DOPE relative degradation rates

DOPC and DOPE relative degradation rates in DOPC:WAY 20:1 samples were calculated and analysed by considering the number of moles of DOPC and DOPE lipids separately using the HPLC data. The disappearance DOPE and DOPC lipids as a function of DOPE follows an exponential decay, as shown in total lipids samples (Figure V.9).

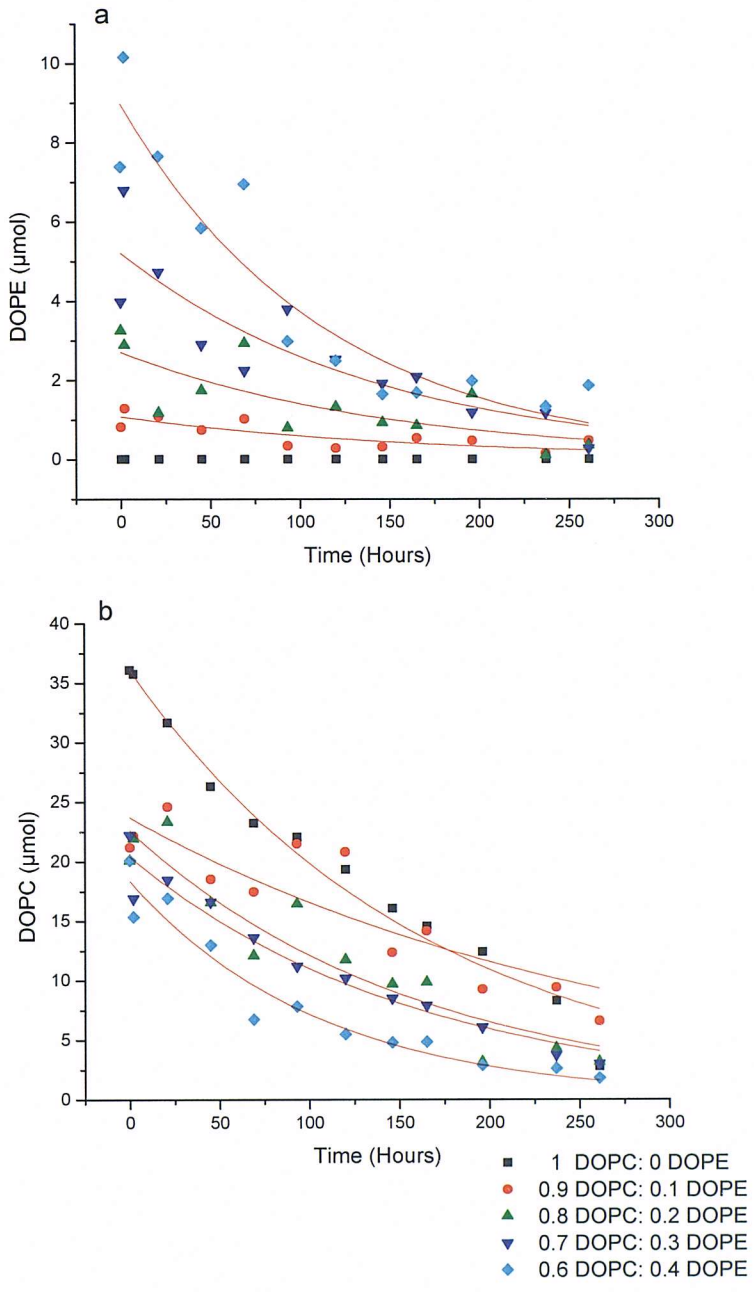


Figure V.9: Effect of various DOPC: DOPE molar ratio on DOPE (a) and DOPC (b) hydrolysis kinetics by WAY.

Although DOPC and DOPE exhibit different absolute hydrolysis rates with respect to varying DOPE molar fractions they both rise with increasing DOPE molar fractions; as observed in the previous section. Variations of hydrolysis rates as a function of DOPE molar fraction are represented on figure V.10.

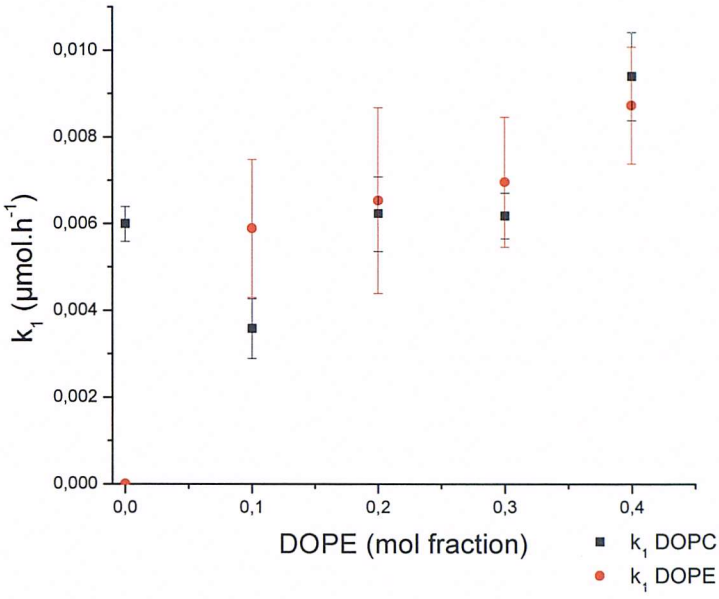


Figure V.10: DOPC and DOPE relative hydrolysis rates as a function of DOPE mol fractions in DOPC:DOPE:WAY 20:1 samples.

Interestingly, the rate of disappearance of DOPC is found to be the same as DOPE at the same DOPE molar fraction (Table V.2). This implies that the accessability and the proton affinity of the DOPC and DOPE carbonyl are the same.

.

	k_1 DOPC ($\mu mol.h^{-1}$)	k_1 DOPE ($\mu mol.h^{-1}$)
1 DOPC: 0 DOPE	$5.99x10^{-3} \pm 4.00x10^{-4}$	NA
0.9 DOPC: 0.1 DOPE	$3.58x10^{-3} \pm 6.80x10^{-4}$	$5.89\ x10^{-3} \pm 1.59x10^{-3}$
0.8 DOPC: 0.2 DOPE	$6.23\ x10^{-3} \pm 8.60x10^{-4}$	$6.54\ x10^{-3} \pm 2.14x10^{-3}$
0.7 DOPC: 0.3 DOPE	$6.19\ x10^{-3} \pm 5.30x10^{-4}$	$6.97\ x10^{-3} \pm 1.50x10^{-3}$
0.6 DOPC: 0.4 DOPE	$9.42\ x10^{-3} \pm 1.02x10^{-3}$	$8.75\ x10^{-3} \pm 1.35x10^{-3}$

Table V.2: DOPC and DOPE relative hydrolysis rates in DOPC: DOPE: WAY 20:1 samples.

V.4 Summary

This section has described the effect of stored curvature elastic stress on the kinetics of the bilayer hydrolysis by the CADs. The binding and partitioning of the CADs are particularly affected by the stored curvature elastic energy. Low binding affinity and hydrolysis rate are observed for reduced stored curvature elastic stress bilayers such as DLPC, whereas partitioning and hydrolysis are clearly enhanced when the stored curvature elastic stress increases in DOPC, and DOPC:DOPE bilayers. Increasing DOPE molar ratios was found to considerably increase the hydrolysis rate in both CADs systems investigated.

Hydrolysis rate are monotonically increasing as a function of DOPE molar ratios, however, it is expected that the rate is decelerated when the formation of the H_{II} phase occurs from the accumulation of fatty acid in the bilayer.

When CADs bind to the bilayer interface, they trigger the release of stored curvature elastic stress which allows the lipid chain to splay and therefore a better CAD-ester bond interaction. This feature will enable the hydrolysis to occur at higher rates.

Interestingly, and this is to confirm the results obtained in chapter 4, the specificity of the CADs remains similar to that in pure DOPC systems, with WAY hydrolysing the bilayer as twice as fast as SPIP.

CHAPTER 6

Conclusions and future work

This thesis has presented original work undertaken on CNS drugs belonging to the CAD family, and their interactions with membrane bilayers.

Using small angle X-ray scattering, NMR, fluorescence microscopy and HPLC, it has been observed that CADs rapidly partition to the polar / apolar interface of the membrane initiating acid catalysed ester hydrolysis of the phospholipid fabric in the membrane. This generates LPC species which destabilize the bilayer and induce membrane fragments and vesicles that carry the CADs with them. This previously unreported mechanism contributes to a novel drug translocation mecahnism across membranes.

The rate at which this process occurs was found to be influenced by the chemistry of CAD molecule, and the mechanical state of the membrane.

Furthermore, the rate of membrane hydrolysis appears to correlate with *in-vivo* non-specific binding distribution volumes of the PET radioligands, where specific radioligands exhibit fast degradation rates. This allows the molecule to be transported to its specific site. Conversely, poor radioligands exhibit slow degradation kinetics,

which leave the molecule at the bilayer interface. This results in the detection of non-specific binding. Therefore, in the future kinetic analysis of the membrane hydrolysis phenomena may provide additional mechanistic insight to the prediction of the non-specific binding and the design of radiolabelled probes for *in-vivo* receptor imaging using PET and allied *in- vivo* imaging techniques.

The discovery of the CAD activated lipid hydrolysis is crucial to the understanding of CAD interactions with membranes, and opens a new area in cell membrane research. The immediate step to this work is to pursue CAD interactions with membranes, by testing more CAD structures. An important aspect to investigate in this research is the design and syntheses of molecules which will either enhance or prevent the reaction; this will allow a better understanding of the molecules chemical structures that are able to trigger the reaction.

A more complex lipid composition involving phosphatidylserine lipids and cholesterol will be considered. This will enable to obtain a lipid composition closer to biological plasma membranes. Detection of the hydrolysis reaction is also relevant in cell plasma membranes, which also contain embedded receptors. Receptors contain binding sites where CADs can bind to. Therefore, the hydrolysis rate might be altered as CADs bind to the membrane and to receptors.

Another aspect to consider in this research is the syntheses of molecules which will either enhance or prevent the reaction; this will allow a better understanding of the molecules chemical structures that are able to trigger the reaction. Ultimately, evaluation of these molecules *in-vivo* by using PET will provide a more precise correlation between lipid ester hydrolysis rate *in-vitro*, and binding *in-vivo*. Therefore, the detection and measurement of the bilayer hydrolysis may be an accurate test for radioligand selection *in-vitro*.

These observations form interesting lines of enquiry into related areas of membrane biology research, and drug design, and raise questions in relation to the non-specific binding: Does the membrane hydrolysis contribute to the BBB? Crossing? What governs the specific entry of CADs in the brain?

In another related area, studying CAD interactions with plasma cell membranes and identifying the hydrolysis products is also significant, in particular in relation to phospholipidosis cytotoxic effects *in-vivo*. This might enable or address issues such as how CADs activate the synthesis of more lipids upon binding. In other words, is phospholipidosis related to a variation of the stored curvature elastic stress upon binding?

List of Figures

Chapter I

Figure I.1: Cartoon representing the determination of specific binding for a given compound.

Figure I.2: A saturation diagram for the binding of a ligand.

Figure I.3: Principles of PET.

Figure I.4: Configuration of the three compartment model for neuroreceptor analysis in PET.

Figure I.5: PET images for raditracers exhibiting high SB and high NSB.

Figure I.6: BBB illustration.

Figure I.7: Correlation of Log P values and brain uptake for SPIP and SPIP derivatives.

Figure I.8: Examples of CNS drugs of the CAD family.

Figure I.9: Cartoon representing the plasma bilayer.

Figure I.10: Transport mechanism across membrane bilayers.

Figure I.11: Glycerolipids structures.

Figure I.12: Lateral forces and lateral stress profile across lipids.

Figure I.13: Illustration of interfacial curvature.

Figure I.14: Examples of positive and negative curvature.

Figure I.15: Shape of lipids.

Figure I.16: Representation of normal and inverted micelles.

Figure I.17: Representation of the fluid, gel and crystal lamellar phases.

Figure I.18: Representation of the normal and inverse hexagonal phases.

Figure I.19: Representation of the Im3m bicontinuous cubic phase.

Figure I.20: Representation of the Stern layer and the diffuse layer.

Figure I.21: CADs induced phospholipidosis.

Chapter II

Figure II.1: Diffraction of X-rays by parallel planes.

Figure II.2: Characteristic small angle X-ray scattering diffraction patterns for lamellar and hexagonal phases

Figure II.3: Illustration of a schematic X-ray beamline.

Figure II.4: The axcess software package for X-ray diffraction pattern analysis.

Figure II.5: Diagram representing the level energy of two spin state in a magnetic field.

Figure II.6: An FID and FT signal

Figure II.7: Chemical shifts ranges for common structural groups in ^{13}C NMR spectroscopy.

Figure II.8: Magic Angle Spinning.

Figure II.9: Typical ^{31}P CSA pattern of lamellar, hexagonal, and micellar phase.

Figure II.10: Structure of the fluoresceinphosphatidylethanolamine.

Figure II.11: FPE fluorescence assays principles

Figure II.12: Binding profiles obtained from FPE assays.

Figure II.13: GUV electroformation set-up.

Chapter III

Figure III.1: Structures of DOPC, HPD and SPIP.

Figure III.2: SAXS diffraction patterns of pure DOPC, DOPC: HPD 20 :1, DOPC :HPD 9 :1, and DOPC :HPD 4 :1 molar ratios.

Figure III.3: Evolution of the d-spacing in DOPC: HPD 20 :1 samples with time.

Figure III.4: SAXS pattern obtained for DOPC: SPIP 20 :1.

Figure III.5: Static ^{31}P SS-NMR powder pattern of DOPC: HPD samples at 20 :1 and 4 :1 molar ratios.

Figure III.6: Evolution of the static ^{31}P SS-NMR powder pattern with time of DOPC: HPD 20:1 molar ratio samples

Figure III.7: Cartoon representing the evolution of the DOPC bilayer in the presence of the CAD.

Figure III.8: ^{13}C MAS spectrum of pure DOPC and DOPC: HPD 20 :1 molar ratios samples.

Figure III.9: Representation of DOPC: CAD catalysed digestion.

Figure III.10: Normal phase HPLC elution profile for OA, LPC, DOPC and HPD standards.

Figure III.11: Normal phase HPLC elution profile for a mixtrure of the 4 standards.

Figure III.12: Calibration curves for DOPC, LPC and OA

Figure III.13: Detection of the degradation products in DOPC:HPD samples by normal phase HPLC

Figure III.14: Electroformation GUVs made of DOPC: HPD GUVs.

Figure III.15: Cryo TEM representing vesicles formed by mixtures of egg-PC, OA and LPC

Figure III.16: Chemical structure of the NBD-tagged-SPIP

Figure III.17: Injection of NBD-tagged-SPIP to DOPC giant vesicles.

Figure III.18: Structure of the ether-linked PC lipid.

Figure III.19: ^{31}P SS-NMR time evolution of ether-linked PC :HPD 4 :1.

Figure III.20: Injection of NBD-tagged-SPIP to ether-linked PC GUVs.

Figure III.21: Absorption and emission spectra of FPE inserted in bilayers.

Figure III.22: The four ionisation states of fluorescein.

Figure III.23: Addition of protonated HPD to FPE labelled DOPC vesicles.

Figure III.24: Subsequent additions of protonated HPD to FPE labelled vesicles until saturation is reached

Figure III.25: Absolute fluorescence correlation with HPD and SPIP titration.

Figure III.26: Addition of protonated HPD to FPE labelled vesicles. The fluorescence traces evolve with time.

Figure III.27: Time dependence of addition of HPD on the fluorescence of FPE labelled vesicles.

Figure III.28: Time dependence of the effect of neuraminidase on FPE labelled erythrocytes ghost membranes.

Figure III.29: Excitation and emission spectra of FPE labelled ether-linked PC vesicles.

Figure III.30: Addition of HPD to FPE labelled ether-linked-PC vesicles and absolute change of fluorescence association to HPD titration.

Figure III.31: DOPC hydrolysis by CADs generates the formation of membrane fragments and small vesicles.

Figure III.32: Cartoon for the proposed mechanism of for the membrane translocation of CADs.

Chapter IV

Figure IV.1: DOPC: HPD 20:1 SAXS diffraction pattern evolution with time.

Figure IV.2: No swelling observed for DOPC: HPD 20:1 SAXS diffraction pattern evolution with time.

Figure IV.3: Micrograph representing CADs crystallisation in DOPC: HPD 20:1 samples.

Figure IV.4: Micrograph representing DOPC: HPD 20:1 after sample optimisation.

Figure IV.5: Kinetic model of the degradation kinetics.

Figure IV.6: Qualitative degradation profile.

Figure IV.7: Normal phase HPLC chromatograms representing the evolution of DOPC: HPD 20:1 samples.

Figure IV.8: Normal phase HPLC chromatograms representing the evolution of DOPC: SPIP 20:1 samples.

Figure IV.9: Normal phase HPLC chromatograms representing the evolution of DOPC: WAY 20:1 samples.

Figure IV.10: Degradation profiles obtained for action of HPD, SPIP and WAY on DOPC bilayers.

Figure IV.11: DOPC hydrolysis profile by HPD, SPIP and WAY.

Figure IV.12: Initial rates of the appearance of LPC, in DOPC: WAY, DOPC: SPIP and DOPC: HPD 20:1 samples.

Figure IV.13: Initial rates of the disappearance of DOPC, in DOPC: WAY, DOPC: SPIP and DOPC: HPD 20:1 samples.

Figure IV.14: Comparison of hydrochloride, formate, trifluoroacetate and maleate counterions on the hydrolysis of DOPC into LPC in DOPC: HPD 20:1 samples.

Figure IV.15: Initial rates for the degradation of DOPC and appearance of LPC in DOPC: HPD 20:1 samples in the presence of formate and trifluoroacetate.

Figure IV.16: DOPC degradation profile in DOPC:HPD TFA and DOPC:HPD formate 20:1 samples.

Figure IV.17: Degradation profile of DOPC:HPD 20:1 in presence of 100 mM NaCl.

Figure IV.18: Effect of 100 mM NaCl on the DOPC degradation profile in DOPC: HPD 20:1 samples.

Figure IV.19: Effect of 100 mM NaCl on the DOPC degradation profile in DOPC: WAY 20:1 samples.

Figure IV.20: Correlation between the bilayer hydrolysis and CADs non-specific binding.

Chapter V

Figure V.1: Comparison between DOPC and DLPC structures.

Figure V.2: DOPC and DLPC hydrolysis profiles obtained by HPD.

Figure V.3: Comparison of DOPC: WAY and DLPC: WAY 20:1 degradation profiles.

Figure V.4: Appearance of LPC in DOPC: WAY and DLPC: WAY 20:1 systems.

Figure V.5: Effect of various DOPC: DOPE molar ratios on bilayer hydrolysis kinetics by WAY and SPIP.

Figure V.6: Hydrolysis rates as a function of DOPE molar fractions in the membrane.

Figure V.7: Activity of CCT as a function of the molar fraction of DOPC.

Figure V.8: Effect of DOPE molar fraction on the excimer to monomer ratio of dipyrenyl lipids in DOPC: DOPE bilayers.

List of Tables

Chapter I

Table I.1: CNS CADs physicoproperties.

Chapter III

Table III.1: ^{13}C NMR DOPC peak assignments.

Table III.2: HPLC standards elution times

Chapter IV

Table IV.1: Physical properties of anions belonging to the Hofmeister series.

Table IV.2: Rates obtained for DOPC bilayers hydrolysis by WAY, SPIP and HPD.

Table IV.3: Rates obtained for DOPC bilayers hydrolysis by WAY, SPIP and HPD with different counterions.

Table IV.4: Summary of hydrolysis rates, lipophilicity and NSB

Chapter V

Table V.1: Hydrolysis rates in DOPC: DOPE systems in presence of WAY and SPIP.

Table V.2: DOPC and DOPE relative hydrolysis rates in DOPC: DOPE: WAY 20:1 samples.

Bibliography

[1] Dimasi, J. A., Risks in new drug development: approval success rates for investigational drugs. *Clin Pharmacol Ther* **2001,** 69, (5), 297-307.

[2] Litton, J. E.; Hall, H.; Blomqvist, G., Improved receptor analysis in PET using a priori information from in vitro binding assays. *Phys Med Biol* **1997,** 42, (8), 1653-60.

[3] Foreman, J. C.; Johansen, T., *Textbook of Receptor Pharmacology*. 2 ed.; CRC Press: 2003.

[4] Hwang, M. G.; Chung, I. K.; Kang, B. G.; Cho, M. H., Sequence-specific binding property of Arabidopsis thaliana telomeric DNA binding protein 1 (AtTBP1). *FEBS Lett* **2001,** 503, (1), 35-40.

[5] Rowley, M.; Kulagowski, J. J.; Watt, A. P.; Rathbone, D.; Stevenson, G. I.; Carling, R. W.; Baker, R.; Marshall, G. R.; Kemp, J. A.; Foster, A. C.; Grimwood, S.; Hargreaves, R.; Hurley, C.; Saywell, K. L.; Tricklebank, M. D.; Leeson, P. D., Effect of plasma protein binding on in vivo activity and brain penetration of glycine/NMDA receptor antagonists. *J Med Chem* **1997,** 40, (25), 4053-68.

[6] Perentes, E.; Rubinstein, L. J., Non-specific binding of mouse myeloma IgM immunoglobulins by human myelin sheaths and astrocytes. A potential complication of nervous system immunoperoxidase histochemistry. *Acta Neuropathol (Berl)* **1986,** 70, (3-4), 284-8.

[7] Watanabe, S.; Ikekita, M.; Nakata, H., Identification of specific [3H]adenine-binding sites in rat brain membranes. *J Biochem (Tokyo)* **2005,** 137, (3), 323-9.

[8] Hoffmann, E. J.; Phelps, M. E.; Mullani, N. A.; Higgins, C. S.; Ter-Pogossian, M. M., Design and performance characteristics of a whole-body positron transaxial tomograph. *J Nucl Med* **1976,** 17, (6), 493-502.

[9] Phelps, M. E.; Hoffman, E. J.; Huang, S. C.; Ter-Pogossian, M. M., Effect of positron range on spatial resolution. *J Nucl Med* **1975,** 16, (7), 649-52.

[10] Czernin, J.; Phelps, M. E., Positron emission tomography scanning: current and future applications. *Annu Rev Med* **2002,** 53, 89-112.

[11] Burns, H. D.; Hamill, T. G.; Eng, W. S.; Francis, B.; Fioravanti, C.; Gibson, R. E., Positron emission tomography neuroreceptor imaging as a tool in drug discovery, research and development. *Curr Opin Chem Biol* **1999,** 3, (4), 388-94.

[12] Herschman, H. R., Molecular imaging: looking at problems, seeing solutions. *Science* **2003,** 302, (5645), 605-8.

[13] Phelps, M. E., Inaugural article: positron emission tomography provides molecular imaging of biological processes. *Proc Natl Acad Sci U S A* **2000,** 97, (16), 9226-33.

[14] Heiss, W. D.; Herholz, K., Brain receptor imaging. *J Nucl Med* **2006,** 47, (2), 302-12.

[15] Laruelle, M.; Slifstein, M.; Huang, Y., Positron emission tomography: imaging and quantification of neurotransporter availability. *Methods* **2002,** 27, (3), 287-99.

[16] Gunn, R. N.; Gunn, S. R.; Turkheimer, F. E.; Aston, J. A.; Cunningham, V. J., Positron emission tomography compartmental models: a basis pursuit strategy for kinetic modeling. *J Cereb Blood Flow Metab* **2002,** 22, (12), 1425-39.

[17] Laruelle, M.; Slifstein, M.; Huang, Y., Relationships between radiotracer properties and image quality in molecular imaging of the brain with positron emission tomography. *Mol Imaging Biol* **2003,** 5, (6), 363-75.

[18] Lee, C. M.; Farde, L., Using positron emission tomography to facilitate CNS drug development. *Trends Pharmacol Sci* **2006,** 27, (6), 310-6.

[19] Waterhouse, R. N., Determination of lipophilicity and its use as a predictor of blood-brain barrier penetration of molecular imaging agents. *Mol Imaging Biol* **2003,** 5, (6), 376-89.

[20] Alavijeh, M. S.; Chishty, M.; Qaiser, M. Z.; Palmer, A. M., Drug metabolism and pharmacokinetics, the blood-brain barrier, and central nervous system drug discovery. *NeuroRx* **2005,** 2, (4), 554-71.

[21] Pajouhesh, H.; Lenz, G. R., Medicinal chemical properties of successful central nervous system drugs. *NeuroRx* **2005,** 2, (4), 541-53.

[22] Fischer, H.; Gottschlich, R.; Seelig, A., Blood-brain barrier permeation: molecular parameters governing passive diffusion. *J Membr Biol* **1998,** 165, (3), 201-11.

[23] Kanda, T.; Ariga, T.; Kubodera, H.; Jin, H. L.; Owada, K.; Kasama, T.; Yamawaki, M.; Mizusawa, H., Glycosphingolipid composition of primary cultured human brain microvascular endothelial cells. *J Neurosci Res* **2004,** 78, (1), 141-50.

[24] Tewes, B. J.; Galla, H. J., Lipid polarity in brain capillary endothelial cells. *Endothelium* **2001,** 8, (3), 207-20.

[25] Duvar, S.; Suzuki, M.; Muruganandam, A.; Yu, R. K., Glycosphingolipid composition of a new immortalized human cerebromicrovascular endothelial cell line. *J Neurochem* **2000,** 75, (5), 1970-6.

[26] Kramer, S. D.; Hurley, J. A.; Abbott, N. J.; Begley, D. J., Lipids in blood-brain barrier models in vitro I: Thin-layer chromatography and high-performance liquid chromatography for the analysis of lipid classes and long-chain polyunsaturated fatty acids. *In Vitro Cell Dev Biol Anim* **2002,** 38, (10), 557-65.

[27] Kramer, S. D.; Schutz, Y. B.; Wunderli-Allenspach, H.; Abbott, N. J.; Begley, D. J., Lipids in blood-brain barrier models in vitro II: Influence of glial cells on lipid classes and lipid fatty acids. *In Vitro Cell Dev Biol Anim* **2002,** 38, (10), 566-71.

[28] Payne, M. P.; Kenny, L. C., Comparison of models for the estimation of biological partition coefficients. *J Toxicol Environ Health A* **2002,** 65, (13), 897-931.

[29] Testa, B.; Carrupt, P. A.; Gaillard, P.; Billois, F.; Weber, P., Lipophilicity in molecular modeling. *Pharm Res* **1996,** 13, (3), 335-43.

[30] Mannhold, R.; van de Waterbeemd, H., Substructure and whole molecule approaches for calculating log P. *J Comput Aided Mol Des* **2001,** 15, (4), 337-54.

[31] Leo, A.; Hansch, C.; Elkins, D., Partition Coefficients and their uses. *Chemical Reviews* **1971,** 71, 525-616.

[32] Seydel, M. W. a. J. K., *Drug-Membrane Interactions*. Wiley-Vch: 2002; Vol. 15.

[33] Meyer; H, Naunyn Schimiedebergs. *Arch. Exp. Path. Pharm* **1899,** 42, 109-118.

[34] Young, R. C.; Mitchell, R. C.; Brown, T. H.; Ganellin, C. R.; Griffiths, R.; Jones, M.; Rana, K. K.; Saunders, D.; Smith, I. R.; Sore, N. E.; et al., Development of a new physicochemical model for brain penetration and its application to the design of centrally acting H2 receptor histamine antagonists. *J Med Chem* **1988,** 31, (3), 656-71.

[35] De Young, L. R.; Dill, K. A., Solute partitioning into lipid bilayer membranes. *Biochemistry* **1988,** 27, (14), 5281-9.

[36] Kepczynski, M.; Pandian, R. P.; Smith, K. M.; Ehrenberg, B., Do liposome-binding constants of porphyrins correlate with their measured and predicted partitioning between octanol and water? *Photochem Photobiol* **2002,** 76, (2), 127-34.

[37] Oliveira, C. R.; Lima, M. C.; Carvalho, C. A.; Leysen, J. E.; Carvalho, A. P., Partition coefficients of dopamine antagonists in brain membranes and liposomes. *Biochem Pharmacol* **1989,** 38, (13), 2113-20.

[38] Lullmann, H.; Wehling, M., The binding of drugs to different polar lipids in vitro. *Biochem Pharmacol* **1979,** 28, (23), 3409-15.

[39] Lipinski, C. A.; Lombardo, F.; Dominy, B. W.; Feeney, P. J., Experimental and computational approaches to estimate solubility and permeability in drug discovery and development settings. *Adv Drug Deliv Rev* **2001,** 46, (1-3), 3-26.

[40] Foster, K. A.; Roberts, M. S., Experimental methods for studying drug uptake in the head and brain. *Curr Drug Metab* **2000,** 1, (4), 333-56.

[41] Welch, M. J.; Chi, D. Y.; Mathias, C. J.; Kilbourn, M. R.; Brodack, J. W.; Katzenellenbogen, J. A., Biodistribution of N-alkyl and N-fluoroalkyl derivatives of spiroperidol; radiopharmaceuticals for PET studies of dopamine receptors. *Int J Rad Appl Instrum B* **1986,** 13, (5), 523-6.

[42] D'Souza, U. M.; Strange, P. G., pH dependence of ligand binding to D2 dopamine receptors. *Biochemistry* **1995,** 34, (41), 13635-41.

[43] Cooper, T. B.; Bark, N.; Simpson, G. M., Prediction of steady state plasma and saliva levels of desmethylimipramine using a single dose, single time point procedure. *Psychopharmacology (Berl)* **1981,** 74, (2), 115-21.

[44] Zuideveld, K. P.; Treijtel, N.; Maas, H. J.; Gubbens-Stibbe, J. M.; Peletier, L. A.; van Der Graaf, P. H.; Danhof, M., A competitive interaction model predicts the effect of WAY-100,635 on the time course of R-(+)-8-hydroxy-2-(di-n-propylamino)tetralin-induced hypothermia. *J Pharmacol Exp Ther* **2002,** 300, (1), 330-8.

[45] Debord, J.; Merle, L.; Bollinger, J. C.; Dantoine, T., Inhibition of butyrylcholinesterase by phenothiazine derivatives. *J Enzyme Inhib Med Chem* **2002,** 17, (3), 197-202.

[46] Schreier, S.; Malheiros, S. V.; de Paula, E., Surface active drugs: self-association and interaction with membranes and surfactants. Physicochemical and biological aspects. *Biochim Biophys Acta* **2000,** 1508, (1-2), 210-34.

[47] Alberts, B.; Johnson, A.; Lewis, J.; Raff, M.; Roberts, K.; Walter, P., *Molecular Biology of the Cell*. 4th ed.; Garland Science Textbooks: 2001.

[48] Daleke, D. L.; Lyles, J. V., Identification and purification of aminophospholipid flippases. *Biochim Biophys Acta* **2000,** 1486, (1), 108-27.

[49] Bevers, E. M.; Comfurius, P.; Dekkers, D. W.; Zwaal, R. F., Lipid translocation across the plasma membrane of mammalian cells. *Biochim Biophys Acta* **1999,** 1439, (3), 317-30.

[50] Danielli, J. F.; Davson, H., *The Permeability of Natural Membranes*. The University Press: Cambridge, 1943.

[51] Janmey, P. A.; Kinnunen, P. K., Biophysical properties of lipids and dynamic membranes. *Trends Cell Biol* **2006,** 16, (10), 538-46.

[52] Pomorski, T.; Hrafnsdottir, S.; Devaux, P. F.; van Meer, G., Lipid distribution and transport across cellular membranes. *Semin Cell Dev Biol* **2001,** 12, (2), 139-48.

[53] Singer, S. J.; Nicolson, G. L., The fluid mosaic model of the structure of cell membranes. *Science* **1972,** 175, (23), 720-31.

[54] Derzko, Z.; Jacobson, K., Comparative lateral diffusion of fluorescent lipid analogues in phospholipid multibilayers. *Biochemistry* **1980,** 19, (26), 6050-7.

[55] Pomorski, T.; Menon, A. K., Lipid flippases and their biological functions. *Cell Mol Life Sci* **2006,** 63, (24), 2908-21.

[56] Edidin, M., The state of lipid rafts: from model membranes to cells. *Annu Rev Biophys Biomol Struct* **2003,** 32, 257-83.

[57] Nichols, B., Cell biology: without a raft. *Nature* **2005,** 436, (7051), 638-9.

[58] Stier, A.; Sackmann, E., Spin labels as enzyme substrates. Heterogeneous lipid distribution in liver microsomal membranes. *Biochim Biophys Acta* **1973,** 311, (3), 400-8.

[59] Karnovsky, M. J.; Kleinfeld, A. M.; Hoover, R. L.; Klausner, R. D., The concept of lipid domains in membranes. *J Cell Biol* **1982,** 94, (1), 1-6.

[60] Avdeef, A., Physicochemical profiling (solubility, permeability and charge state). *Curr Top Med Chem* **2001,** 1, (4), 277-351.

[61] Habgood, M. D.; Begley, D. J.; Abbott, N. J., Determinants of Passive Drug Entry into the Central Nervous System. *Cell Mol Neuribiol* **2000,** 20, (2), 231-253.

[62] Tsuji, A., Small Molecular Drug Tranfser across the Blood Brain Barrier via Carrier-Mediated Transport Systems. *J Am Soc Exp Neuro Ther* **2005,** 2, 54-52.

[63] Alvarado, F., Transport of sugars and amino acids in the intestine: evidence for a common carrier. *Science* **1966,** 151, (713), 1010-3.

[64] Suzuki, H.; Sawada, Y.; Suqiyama, Y.; Iga, T.; Hanano, M., Transport of Benzylpenicillin by the rat choroid plexus in vitro. *J Pharmacol Exp Ther* **1987,** 242, (2), 660-665.

[65] Spector, R.; Mock, D., Biotin Transport through the Blood Brain Barrier. *J Neurochem* **1987,** 48, (2), 400-404.

[66] Szachowicz-Petelska, B.; Figaszewski, Z.; Lewandowski, W., Mechanisms of Transport Across Cell Membranes of Complexes Contained in Antitumor Drugs. *Int J Pharm* **2001,** 222, 169-182.

[67] Seddon, J. M., Structure of the inverted hexagonal (HII) phase, and non-lamellar phase transitions of lipids. *Biochim Biophys Acta* **1990,** 1031, (1), 1-69.

[68] Shearman, G. C.; Ces, O.; Templer, R. H.; Seddon, J. M., Inverse Lyotropic Phases of Lipids and Membranes. *J Phys Condens Matter* **2006,** 18, S1105-S1124.

[69] Bagatolli, L. A., To see or not too see: Lateral Organization of Biological Membranes and Fluorescence Microscopy. *Biochim Biophys Acta* **2006,** 1758, 1541-1556.

[70] Ondrias, K., Use of Electron Spin Resonance Spectroscopy of Spin Labeled for Studying Drug-Induced Membrane Perturbation. *J Pharm Biomed Anal* **1989,** 7, (6), 649-675.

[71] Seelig, J., 31P nuclear magnetic resonance and the head group structure of phospholipids in membranes. *Biochim Biophys Acta* **1978,** 515, (2), 105-40.

[72] Cullis, P. R.; de Kruiff, B., Lipid Polymorphism and the Functional Roles of Lipids in Biological Membranes. *Biochim Biophys Acta* **1979,** 559, (4), 399-420.

[73] Choi, S.; Ware, W.; Lauterbach, S. R.; Phillips, W. M., Infrared Spectroscpoic Studies on the Phosphatidylserine Bilayer Interacting with Calcium Ion: Effect of Cholesterol. *Biochemistry* **1991,** 30, 8563-8568.

[74] Chandler, D., Interfaces and the driving force of hydrophobic assembly. *Nature* **2005,** 437, (7059), 640-7.

[75] Cevc, G., *Phospholipids handbook.* CRC: 1993.

[76] Luzzati, V.; Husson, F., The Structure of the Liquid-Crystalline Phase of Lipid-Water Systems. *J Cell Biol* **1962,** 12, 207-219.

[77] Zimmerberg, J.; Kozlov, M. M., How proteins produce cellular membrane curvature. *Nat Rev Mol Cell Biol* **2006,** 7, (1), 9-19.

[78] Israelachvili, J. N., *Intermolecular and Surface Forces*. Academic Pr: Santa Barbara, 1992.

[79] Helfrich, W., Elastic properties of lipid bilayers: theory and possible experiments. *Z Naturforsch [C]* **1973,** 28, (11), 693-703.

[80] Ces, O.; Mulet, X., Physical Coupling Between Lipids and Proteins: A Paradgm for Cellular Control. *Signal Transduction* **2005,** 6, 112-132.

[81] Seddon, J. M., Lyotropic Phase Behaviour of Biological Amphihiles. *Ber. Bunsenges. Phys. Chem* **1996,** 100, 380-393.

[82] Mouritsen, O. G.; Zuckermann, M. J., What's so special about cholesterol? *Lipids* **2004,** 39, (11), 1101-13.

[83] Thurmond, R. L.; Lindblom, G.; Brown, M. F., Curvature, order, and dynamics of lipid hexagonal phases studied by deuterium NMR spectroscopy. *Biochemistry* **1993,** 32, (20), 5394-410.

[84] Conn, C. E.; Ces, O.; Mulet, X.; Finet, S.; Winter, R.; Seddon, J. M.; Templer, R. H., Dynamics of structural transformations between lamellar and inverse bicontinuous cubic lyotropic phases. *Phys Rev Lett* **2006,** 96, (10), 108102.

[85] Ulrich, A. S., Biophysical aspects of using liposomes as delivery vehicles. *Biosci Rep* **2002,** 22, (2), 129-50.

[86] Shah, J. C.; Sadhale, Y.; Chilukuri, D. M., Cubic phase gels as drug delivery systems. *Adv Drug Deliv Rev* **2001,** 47, (2-3), 229-50.

[87] Shearman, G. X-ray Structural Studies of the Stability of Charged Lamellar Mesophases. Imperial College, London, 2004.

[88] Cevc, G., Membrane electrostatics. *Biochim Biophys Acta* **1990,** 1031, (3), 311-82.

[89] Kell, M. J.; DeFelice, L. J., Surface charge near the cardiac inward-rectifier channel measured from single-channel conductance. *J Membr Biol* **1988,** 102, (1), 1-10.

[90] Theuvenet, A. P. R.; Van De Wijngaard, W. M. H.; Van De Rijke, J. W.; Borst-Pauwels, G. W. F. H., Application of 9-aminoacridine as a probe of the surface potential experienced by cation transporters in the plasma membrane of yeast cells. *Biochim Biophys Acta* **1984,** 775, (2), 161-168.

[91] Volwerk, J. J.; Jost, P. C.; de Haas, G. H.; Griffith, O. H., Activation of porcine pancreatic phospholipase A2 by the presence of negative charges at the lipid-water interface. *Biochemistry* **1986,** 25, (7), 1726-33.

[92] McLaughlin, S., Electrostatic Potentials at Membrane Solution Interface. *Curr.Top.Membr.Trans.* **1977,** 9, 71-144.

[93] Aguilella, V. M.; Mafe, S.; Manzanares, J. A., Double layer potential and degree of dissociation in charged lipid monolayers. *Chem Phys Lipids* **2000,** 105, (2), 225-9.

[94] Seddon, J. M.; Templer, R. H., *Handbook of Biological Physics*. Elsevier Science: 1995; Vol. 1.

[95] Katsu, T.; Kobayashi, H.; Hirota, T.; Fujita, Y.; Sato, K.; Nagai, U., Structure-activity relationship of gramicidin S analogues on membrane permeability. *Biochim Biophys Acta* **1987,** 899, (2), 159-70.

[96] Seeman, P., The membrane actions of anesthetics and tranquilizers. *Pharmacol Rev* **1972,** 24, (4), 583-655.

[97] Jutila, A.; Soderlund, T.; Pakkanen, A. L.; Huttunen, M.; Kinnunen, P. K., Comparison of the effects of clozapine, chlorpromazine, and haloperidol on membrane lateral heterogeneity. *Chem Phys Lipids* **2001,** 112, (2), 151-63.

[98] de-Paula, E.; Schreier, S., Molecular and physicochemical aspects of local anesthetic-membrane interaction. *Braz J Med Biol Res* **1996,** 29, (7), 877-94.

[99] Santos, J. S.; Lee, D. K.; Ramamoorthy, A., Effects of antidepressants on the conformation of phospholipid headgroups studied by solid-state NMR. *Magn Reson Chem* **2004,** 42, (2), 105-14.

[100] Mouritsen, O. G.; Jorgensen, K., A new look at lipid-membrane structure in relation to drug research. *Pharm Res* **1998,** 15, (10), 1507-19.

[101] Suwalsky, M.; Sanchez, I.; Bagnara, M.; Sotomayor, C. P., Interaction of antiarrhythmic drugs with model membranes. *Biochim Biophys Acta* **1994,** 1195, (2), 189-96.

[102] Lazar, D. F.; Medzihradsky, F., Altered microviscosity at brain membrane surface induces distinct and reversible inhibition of opioid receptor binding. *J Neurochem* **1992,** 59, (4), 1233-40.

[103] Frenzel, J.; Arnold, K.; Nuhn, P., Calorimetric, 13C NMR, and 31P NMR studies on the interaction of some phenothiazine derivatives with dipalmitoyl phosphatidylcholine model membranes. *Biochim Biophys Acta* **1978,** 507, (2), 185-97.

[104] Isomaa, B.; Hagerstrand, H.; Paatero, G., Shape transformations induced by amphiphiles in erythrocytes. *Biochim Biophys Acta* **1987,** 899, (1), 93-103.

[105] Hidalgo, A. A.; Caetano, W.; Tabak, M.; Oliveira, O. N., Jr., Interaction of two phenothiazine derivatives with phospholipid monolayers. *Biophys Chem* **2004,** 109, (1), 85-104.

[106] Romer, J.; Bickel, M. H., Interactions of chlorpromazine and imipramine with artificial membranes investigated by equilibrium dialysis, dual-wavelength photometry, and fluorimetry. *Biochem Pharmacol* **1979,** 28, (6), 799-805.

[107] Agasosler, A. V.; Tungodden, L. M.; Cejka, D.; Bakstad, E.; Sydnes, L. K.; Holmsen, H., Chlorpromazine-induced increase in dipalmitoylphosphatidylserine surface area in monolayers at room temperature. *Biochem Pharmacol* **2001,** 61, (7), 817-25.

[108] Nerdal, W.; Gundersen, S. A.; Thorsen, V.; Hoiland, H.; Holmsen, H., Chlorpromazine interaction with glycerophospholipid liposomes studied by magic angle spinning solid state (13)C-NMR and differential scanning calorimetry. *Biochim Biophys Acta* **2000,** 1464, (1), 165-75.

[109] Anteneodo, C.; Bisch, P. M.; Marques, J. F., Interaction of chlorpromazine with phospholipid membranes. An EPR study of membrane surface potential effects. *Eur Biophys J* **1995,** 23, (6), 447-52.

[110] Song, C.; Holmsen, H.; Nerdal, W., Existence of lipid microdomains in bilayer of dipalmitoyl phosphatidylcholine (DPPC) and 1-stearoyl-2-docosahexenoyl phosphatidylserine (SDPS) and their perturbation by chlorpromazine: a 13C and 31P solid-state NMR study. *Biophys Chem* **2006,** 120, (3), 178-87.

[111] Stuhne-Sekalec, L.; Chudzik, J.; Stanacev, N. Z., Effect of chlorpromazine on the synthesis, hydrolysis, and transfer of microsomal cytidine liponucleotides and mitochondrial polyglycerophosphatides. *Can J Physiol Pharmacol* **1987,** 65, (3), 377-84.

[112] Suwalsky, M.; Gimenez, L.; Saenger, V.; Neira, F., X-ray studies on phospholipid bilayers. VIII. Interactions with chlorpromazine.HCl. *Z Naturforsch [C]* **1988,** 43, (9-10), 742-8.

[113] Schlyer, D. J.; Volkow, N. D.; Fowler, J. S.; Wolf, A. P.; Shiue, C. Y.; Dewey, S. L.; Bendriem, B.; Logan, J.; Raulli, R.; Hitzemann, R.; et al., Regional distribution and kinetics of haloperidol binding in human brain: a PET study with [18F]haloperidol. *Synapse* **1992,** 11, (1), 10-9.

[114] Sawas, A. H.; Gilbert, J. C., Lipid peroxidation as a possible mechanism for the neurotoxic and nephrotoxic effects of a combination of lithium carbonate and haloperidol. *Arch Int Pharmacodyn Ther* **1985,** 276, (2), 301-12.

[115] Rego, A. C.; Oliveira, C. R., Influence of lipid peroxidation on [3H]ketanserin binding to 5-HT2 prefrontal cortex receptors. *Neurochem Int* **1995,** 27, (6), 489-96.

[116] Seeman, P. M.; Bialy, H. S., The Surface Activity of Tranquilizers. *Biochem Pharmacol* **1963,** 12, 1181-91.

[117] Murata, T.; Maruoka, N.; Omata, N.; Takashima, Y.; Fujibayashi, Y.; Yonekura, Y.; Wada, Y., A comparative study of the plasma membrane permeabilization and fluidization induced by antipsychotic drugs in the rat brain. *Int J Neuropsychopharmacol* **2006**, 1-7.

[118] Murata, T.; Maruoka, N.; Omata, N.; Takashima, Y.; Igarashi, K.; Kasuya, F.; Fujibayashi, Y.; Wada, Y., Effects of haloperidol and its pyridinium metabolite on plasma membrane permeability and fluidity in the rat brain. *Prog Neuropsychopharmacol Biol Psychiatry* **2007**.

[119] Sarmento, A. B.; de Lima, M. C.; Oliveira, C. R., Partition of dopamine antagonists into synthetic lipid bilayers: the effect of membrane structure and composition. *J Pharm Pharmacol* **1993,** 45, (7), 601-5.

[120] Palmeira, C. M.; Oliveira, C. R., Partitioning and membrane disordering effects of dopamine antagonists: influence of lipid peroxidation, temperature, and drug concentration. *Arch Biochem Biophys* **1992,** 295, (1), 161-71.

[121] Reasor, M. J.; Kacew, S., Drug-induced phospholipidosis: are there functional consequences? *Exp Biol Med (Maywood)* **2001,** 226, (9), 825-30.

[122] Anderson, N.; Borlak, J., Drug-induced phospholipidosis. *FEBS Lett* **2006,** 580, (23), 5533-40.

[123] Mortuza, G. B.; Neville, W. A.; Delaney, J.; Waterfield, C. J.; Camilleri, P., Characterisation of a potential biomarker of phospholipidosis from amiodarone-treated rats. *Biochimica et Biophysica Acta* **2003,** 1631, (2), 136-46.

[124] Lullmann, H.; Lullmann-Rauch, R.; Wassermann, O., Lipidosis induced by amphiphilic cationic drugs. *Biochem Pharmacol* **1978,** 27, (8), 1103-8.

[125] Seydel, J. K.; Wassermann, O., NMR-studies on the molecular basis of drug-induced phospholipidosis--II. Interaction between several amphiphilic drugs and phospholipids. *Biochem Pharmacol* **1976,** 25, (21), 2357-64.

[126] Baronas, E. T.; Lee, J. W.; Alden, C.; Hsieh, F. Y., Biomarkers to monitor drug-induced phospholipidosis. *Toxicol Appl Pharmacol* **2007,** 218, (1), 72-8.

[127] Delaney, J.; Neville, W. A.; Swain, A.; Miles, A.; Leonard, M. S.; Waterfield, C. J., Phenylacetylglycine, a putative biomarker of phospholipidosis: its origins and relevance to phospholipid accumulation using amiodarone treated rats as a model. *Biomarkers* **2004,** 9, (3), 271-90.

[128] Feldman, S.; Wang, M. Y.; Kaloyanides, G. J., Aminoglycosides induce a phospholipidosis in the renal cortex of the rat: an early manifestation of nephrotoxicity. *J Pharmacol Exp Ther* **1982,** 220, (3), 514-20.

[129] Harris, R. K., *Nuclear Magnetic Resonance Spectroscopy.* 2nd ed.; Longman Scientific and Technical: Harlow, 1986.

[130] Levitt, M., *Spin Dynamics: Basics of Nuclear Magnetic Resonance.* John Wiley & Sons Inc: New York, NY, 2001.

[131] Ernst, R. R.; Bodenhausen, G.; Wokaun, A., *Principles of Nuclear Magnetic Resonance in One and Two Dimensions.* Clarendon Press: Oxford, 1987.

[132] Mehring, M., *Principles of High Resolution NMR in Solids.* Berlin, Heidelberg, New York, 1983.

[133] Schmidt- Rohr, K.; Spiess, H. W., *Multidimensional Solid-State NMR and Polymers* Academic Press Inc.: London, 1994.

[134] Clarke, J. A. Solid-State NMR Investigation of Phospholipid/Cholesterol Interactions in Model Membranes. Imperial College London, London, 2005.

[135] Wall, J.; Ayoub, F.; O'Shea, P., Interactions of macromolecules with the mammalian cell surface. *Journal of Cell Science* **1995,** 108, (Pt 7), 2673-82.

[136] Nicholls, D. G.; Ferguson, S. J., *Bioenergetics.* 2nd ed.; J. Wiley and Son, Inc: Chichester, 1992.

[137] O'Shea, P., Physical landscapes in biological membranes: physico-chemical terrains for spatio-temporal control of biomolecular interactions and behaviour. *Philosophical Transactions of the Royal Society London, Series a (Mathematical, Physical & Engineering Sciences)* **2005,** 363, (1827), 575-88.

[138] Asawakarn, T.; Cladera, J.; O'Shea, P., Effects of the membrane dipole potential on the interaction of saquinavir with phospholipid membranes and plasma membrane receptors of Caco-2 cells. *Journal of Biological Chemistry* **2001,** 276, (42), 38457-63.

[139] Cladera, J.; O'Shea, P.; Hadgraft, J.; Valenta, C., Influence of molecular dipoles on human skin permeability: Use of 6-ketocholestanol to enhance the transdermal delivery of bacitracin. *J Pharm Sci* **2003,** 92, (5), 1018-27.

[140] Cladera, J.; O'Shea, P., Intramembrane molecular dipoles affect the membrane insertion and folding of a model amphiphilic peptide. *Biophys J* **1998,** 74, (5), 2434-42.

[141] Thelen, M.; O'Shea, P. S.; Petrone, G.; Azzi, A., Proton translocation by a native and subunit III-depleted cytochrome c oxidase reconstituted into phospholipid vesicles. Use of fluorescein-phosphatidylethanolamine as an intravesicular pH indicator. *J Biol Chem* **1985,** 260, (6), 3626-31.

[142] Margulies, D.; Melman, G.; Shanzer, A., Fluorescein as a model molecular calculator with reset capability. *Nat Mater* **2005,** 4, (10), 768-71.

[143] Wall, J.; Golding, C. A.; Van Veen, M.; O'Shea, P., The use of fluoresceinphosphatidylethanolamine (FPE) as a real-time probe for peptide-membrane interactions. *Molecular Membrane Biology* **1995,** 12, (2), 183-92.

[144] Golding, C.; Senior, S.; Wilson, M. T.; O'Shea, P., Time resolution of binding and membrane insertion of a mitochondrial signal peptide: correlation with structural changes and evidence for cooperativity. *Biochemistry* **1996,** 35, (33), 10931-7.

[145] Casey, D. Cationic Amphiphilic Drug Catalysed Membrane Digestion: A Structural Analysis. London, 2006.

[146] Winterhalter, M.; Lasic, D. D., Liposome stability and formation: experimental parameters and theories on the size distribution. *Chem Phys Lipids* **1993,** 64, (1-3), 35-43.

[147] O'Toole, P. J.; Morrison, I. E.; Cherry, R. J., Investigations of spectrin-lipid interactions using fluoresceinphosphatidylethanolamine as a membrane probe. *Biochimica et Biophysica Acta* **2000,** 1466, (1-2), 39-46.

[148] Angelova, M., I.,; Dimitrov, D. S., Liposomes electroformation. *Faraday Discuss Chem Soc* **1986,** 81, 303-311.

[149] Baciu, M.; Sebai, S. C.; Ces, O.; Mulet, X.; Clarke, J. A.; Shearman, G. C.; Law, R. V.; Templer, R. H.; Plisson, C.; Parker, C. A.; Gee, A., Degradative transport of cationic amphiphilic drugs across phospholipid bilayers. *Philos Transact A Math Phys Eng Sci* **2006,** 364, (1847), 2597-614.

[150] Jain, M. K.; Wu, N. Y., Effect of Small Molecules on the Dipalmitoyl Lecithin Liposomal Bilayer: III.Phase transition in a lipid bilayer. *Journal of Membrane Biology* **1977,** 34, 157-201.

[151] Xu, Y.; Yushmanov, V. E.; Tang, P., NMR studies of drug interaction with membranes and membrane-associated proteins. *Biosci Rep* **2002,** 22, (2), 175-96.

[152] Budai, M.; Szabo, Z.; Szogyi, M.; Grof, P., Molecular interactions between DPPC and morphine derivatives: a DSC and EPR study. *Int. J. Pharm.* **2003,** 250, (1), 239-50.

[153] Panicker, L.; Mishra, K. P., Nuclear magnetic resonance and thermal studies on the interaction between salicylic acid and model membranes. *Biophys Chem* **2006,** 120, (1), 15-23.

[154] Spector, A. A.; Yorek, M. A., Membrane lipid composition and cellular function. *J Lipid Res* **1985,** 26, (9), 1015-35.

[155] Van der Schyf, C. J.; Geldenhuys, W. J.; Youdim, M. B., Multifunctional drugs with different CNS targets for neuropsychiatric disorders. *J Neurochem* **2006,** 99, (4), 1033-48.

[156] Ahyayauch, H.; Goni, F. M.; Bennouna, M., Interaction of electrically neutral and cationic forms of imipramine with liposome and erythrocyte membranes. *Int J Pharm* **2004,** 279, (1-2), 51-8.

[157] Deo, N.; Somasundaran, T.; Somasundaran, P., Solution properties of amitriptyline and its partitioning into lipid bilayers. *Colloids Surf B Biointerfaces* **2004,** 34, (3), 155-9.

[158] Kinnunen, P. K., On the principles of functional ordering in biological membranes. *Chem Phys Lipids* **1991,** 57, (2-3), 375-99.

[159] Berlepsch, H. v.; Vries, R. d., Weakly charged lamellar bilayer system: Interplay between thermal undulations and electrostatic repulsion. *The European Physical Journal E - Soft Matter* **2000,** 1, (2-3), 141-152.

[160] Bhamidipati, S. P.; Hamilton, J. A., Interactions of lyso 1-palmitoylphosphatidylcholine with phospholipids: a 13C and 31P NMR study. *Biochemistry* **1995,** 34, (16), 5666-77.

[161] Bhamidipati, S. P.; Hamilton, J. A., Interactions of Lyso 1-Palmitoylphosphatidylcholine with Phospholipids - a C-13 and P-31 Nmr-Study. *Biochemistry* **1995,** 34, (16), 5666-5677.

[162] Seddon, J. M.; Templer, R. H.; Warrender, N. A.; Huang, Z.; Cevc, G.; Marsh, D., Phosphatidylcholine-fatty acid membranes: effects of headgroup hydration on the phase behaviour and structural parameters of the gel and inverse hexagonal (H(II)) phases. *Biochim Biophys Acta* **1997,** 1327, (1), 131-47.

[163] Van Echteld, C. J.; De Kruijff, B.; Mandersloot, J. G.; De Gier, J., Effects of lysophosphatidylcholines on phosphatidylcholine and phosphatidylcholine/cholesterol liposome systems as revealed by 31P-NMR, electron microscopy and permeability studies. *Biochim Biophys Acta* **1981,** 649, (2), 211-20.

[164] Peuvot, J.; Schanck, A.; Deleers, M.; Brasseur, R., Piracetam-induced changes to membrane physical properties. A combined approach by 31P nuclear magnetic resonance and conformational analysis. *Biochem Pharmacol* **1995,** 50, (8), 1129-34.

[165] Bergstrand, N.; Edwards, K., Aggregate Structure in Dilute Aqueous Dispersions of Phospholipids, Fatty Acids, and Lysophospholipids. . *Langmuir* **2001,** 17, (11), 3245-3253.

[166] Sheetz, M. P.; Singer, S. J., Biological membranes as bilayer couples. A molecular mechanism of drug-erythrocyte interactions. *Proc Natl Acad Sci U S A* **1974,** 71, (11), 4457-61.

[167] Jain, M. K.; van Echteld, C. J.; Ramirez, F.; de Gier, J.; de Haas, G. H.; van Deenen, L. L., Association of lysophosphatidylcholine with fatty acids in aqueous phase to form bilayers. *Nature* **1980,** 284, (5755), 486-7.

[168] Sas, B.; Peys, E.; Helsen, M., Efficient method for (lyso)phospholipid class separation by high-performance liquid chromatography using an evaporative light-scattering detector. *J Chromatogr A* **1999,** 864, (1), 179-82.

[169] Luisi, P. L.; Walde, P., *Giant Vesicles*. John Wiley & Sons: New York, 2000.

[170] Kwok, R.; Evans, E., Thermoelasticity of large lecithin bilayer vesicles. *Biophys J* **1981,** 35, (3), 637-52.

[171] Rawicz, W.; Olbrich, K. C.; McIntosh, T.; Needham, D.; Evans, E., Effect of chain length and unsaturation on elasticity of lipid bilayers. *Biophys J* **2000,** 79, (1), 328-39.

[172] Kas, J.; Sackmann, E., Shape transitions and shape stability of giant phospholipid vesicles in pure water induced by area-to-volume changes. *Biophys J* **1991,** 60, (4), 825-44.

[173] Tanaka, T.; Tamba, Y.; Masum, S. M.; Yamashita, Y.; Yamazaki, M., La(3+) and Gd(3+) induce shape change of giant unilamellar vesicles of phosphatidylcholine. *Biochim Biophys Acta* **2002,** 1564, (1), 173-82.

[174] Segota, S.; Tezak, D., Spontaneous formation of vesicles. *Adv Colloid Interface Sci* **2006,** 121, (1-3), 51-75.

[175] Goni, F. M.; Basanez, G.; Begona Ruiz-Arguello, M.; Alonso, A., Interfacial enzyme activation, non-lamellar phase formation and membrane fusion. Is there a conducting thread? *Faraday Discuss* **1998,** (111), 55-68; discussion 69-78.

[176] Holopainen, J. M.; Angelova, M. I.; Kinnunen, P. K., Vectorial budding of vesicles by asymmetrical enzymatic formation of ceramide in giant liposomes. *Biophys J* **2000,** 78, (2), 830-8.

[177] Holopainen, J. M.; Angelova, M. I.; Soderlund, T.; Kinnunen, P. K., Macroscopic consequences of the action of phospholipase C on giant unilamellar liposomes. *Biophys J* **2002,** 83, (2), 932-43.

[178] Hukkanen, J.; Jacob, P., 3rd; Benowitz, N. L., Metabolism and disposition kinetics of nicotine. *Pharmacol Rev* **2005,** 57, (1), 79-115.

[179] Hla, T., Genomic insights into mediator lipidomics. *Prostaglandins Other Lipid Mediat* **2005,** 77, (1-4), 197-209.

[180] Arcangeli, A.; Carla, M.; Del Bene, M. R.; Becchetti, A.; Wanke, E.; Olivotto, M., Polar/apolar compounds induce leukemia cell differentiation by modulating cell-surface potential. *Proceedings of the National Academy of Sciences of the United States of America* **1993,** 90, (12), 5858-62.

[181] Loew, L. M., *Spectroscopic Membrane Probes*. CRC press: 1988; Vol. 1-3.

[182] Cheetham, J. J.; Murray, J.; Ruhkalova, M.; Cuccia, L.; McAloney, R.; Ingold, K. U.; Johnston, L. J., Interaction of synapsin I with membranes. *Biochemical & Biophysical Research Communications* **2003,** 309, (4), 823-9.

[183] Fitchen, N.; O'Shea, P.; Williams, P.; Hardie, K. R., Electrostatic sensor for identifying interactions between peptides and bacterial membranes. *Mol Immunol* **2003,** 40, (7), 407-11.

[184] Thelen, M.; Petrone, G.; O'Shea, P. S.; Azzi, A., The use of fluorescein-dipalmitoylphosphatidylethanolamine for measuring pH-changes in the internal compartment of phospholipid vesicles. *Biochim Biophys Acta* **1984,** 766, (1), 161-8.

[185] Ling, R. E. Investigation into the Drug Catalysed Membrane Degradation. Imperial College, London, 2006.

[186] Templer, R. H.; Seddon, J. M.; Warrender, N. A.; Syrykh, A.; Huang, Z.; Winter, R.; Erbes, J., Inverse Bicontinuous Cubic Phases in 2:1 Fatty Acid/Phosphatidylcholine Mixtures. The Effects of Chain Length, Hydration, and Temperature. *J. Phys. Chem. B* **1998,** 102, (37), 7251-7261.

[187] Templer, R. H.; Seddon, J. M.; Duesing, P. M.; Wintwe, R.; Erbes, J., Modeling the Phase Behaviour of the Inverse Hexagonal and Inverse Bicontinous Cubic Phases in 2:1 Fatty acid:Phosphatidylcholine Mixtures. *J.Phys.Chem.B* **1998,** 102, 7262-7271.

[188] van Meer, G.; Sprong, H., Membrane lipids and vesicular traffic. *Curr Opin Cell Biol* **2004,** 16, (4), 373-8.

[189] McMahon, H. T.; Gallop, J. L., Membrane curvature and mechanisms of dynamic cell membrane remodelling. *Nature* **2005,** 438, (7068), 590-6.

[190] Kozlovsky, Y.; Kozlov, M. M., Membrane fission: model for intermediate structures. *Biophys J* **2003,** 85, (1), 85-96.

[191] Attard, G. S.; Templer, R. H.; Smith, W. S.; Hunt, A. N.; Jackowski, S., Modulation of CTP:phosphocholine cytidylyltransferase by membrane curvature elastic stress. *Proc Natl Acad Sci U S A* **2000,** 97, (16), 9032-6.

[192] Naito, A.; Nagao, T.; Obata, M.; Shindo, Y.; Okamoto, M.; Yokoyama, S.; Tuzi, S.; Saito, H., Dynorphin induced magnetic ordering in lipid bilayers as studied by (31)P NMR spectroscopy. *Biochim Biophys Acta* **2002,** 1558, (1), 34-44.

[193] Giron, D., Characterisation of Salts of Drug Substances. *Journal of Thermal Analysis and Calorimetry* **2003,** 73, 441-457.

[194] Ozturk, S. S.; Palsson, B. O.; Dressman, J. B., Dissolution of ionizable drugs in buffered and unbuffered solutions. *Pharm Res* **1988,** 5, (5), 272-82.

[195] Li, S.; Doyle, P.; Metz, S.; Royce, A. E.; Serajuddin, A. T., Effect of chloride ion on dissolution of different salt forms of haloperidol, a model basic drug. *J Pharm Sci* **2005,** 94, (10), 2224-31.

[196] Li, S.; Wong, S.; Sethia, S.; Almoazen, H.; Joshi, Y. M.; Serajuddin, A. T., Investigation of solubility and dissolution of a free base and two different salt forms as a function of pH. *Pharm Res* **2005,** 22, (4), 628-35.

[197] Kunz, W.; Henle, J.; Ninham, B. W., 'Zur Lehre von der Wirkung der Salze' (about the science of the effect of salts): Franz Hofmeister's historical papers. *Current Opinion in Colloid & Interface Science* **2004,** (9), 19-47.

[198] Brady, J. E.; Evans, D. F.; Warr, G. G.; Grieser, F.; Ninham, B. W., Counterion specificity as the determinant of surfactant aggregation *J. Phys. Chem* **1986,** 90, (9), 1853-1859.

[199] Leontidis, E., Hofmeister anion effects on surfactant self-assembly and the formation of mesoporous solids. *Curr.Opin.Colloid.Int.Sci* **2002,** 7, (1-2), 81-91.

[200] Hedin, N.; Furo, I.; Eriksson, P. O., Fast Diffusion of the Cl- Ion in the Headgroup Region of an Oppositely Charged Micelle. A 35Cl NMR Spin Relaxation Study *J. Phys. Chem B* **2000,** 104. , (35), 8544-8547.

[201] Cacace, M. G.; Landau, E. M.; Ramsden, J. J., The Hofmeister series: salt and solvent effects on interfacial phenomena. *Q Rev Biophys* **1997,** 30, (3), 241-77.

[202] Rydall, J. R.; Macdonald, P. M., Investigation of anion binding to neutral lipid membranes using 2H NMR. *Biochemistry* **1992,** 31, (4), 1092-9.

[203] Lo Nostro, P.; Ninham, B. W.; Lo Nostro, A.; Pesavento, G.; Fratoni, L.; Baglioni, P., Specific ion effects on the growth rates of Staphylococcus aureus and Pseudomonas aeruginosa. *Phys. Biol. 2* **2005,** 2, 1-7.

[204] Kunz, W.; Lo Nostro, P.; Ninham, B. W., The Present State of Affairs with Hofmeister Effects. *Current Opinion in Colloid and Interface Science* **2004,** 109, (1-2), 1-18.

[205] Koynova, R.; Brankov, J.; Technov, B., Modulation of Lipid Phase Behaviour by Kosmotropic and Chaotropic Solutes. *Eur. Biophys. J* **1997,** 25, 261-274.

[206] Mullin, J. W., *Crystallization* Butterworth-Heinemann: Oxford, England., 1993.

[207] Gutman, M.; Nachliel, E.; Friedman, R., The mechanism of proton transfer between adjacent sites on the molecular surface. *Biochim Biophys Acta* **2006,** 1757, (8), 931-41.

[208] Cornell, R. B.; Arnold, R. S., Modulation of the activities of enzymes of membrane lipid metabolism by non-bilayer-forming lipids. *Chem Phys Lipids* **1996,** 81, 215-227.

[209] Yamashita, Y. The Aggregation Behavior of Mixture of Alkylmethylaminoxides with Their Protonated Analogues in Aqueous Solution. University of Bayreuth, Bayreuth, 2004.

[210] Sawyer, W. H.; Puckridge, J., The dissociation of proteins by chaotropic salts. *J Biol Chem* **1973,** 248, (24), 8429-33.

[211] Morisue, T.; Moroi, Y.; Shibata, M., Solubilisation of Benzene, Naphtalene, Anthracene and Pyrene in Dodecylammonium Trifluoroacetate Micelles. *J Phys Chem* **1994,** 98, 12995-13000.

[212] Sakai, N.; Matile, S., Anion-mediated transfer of polyarginine across liquid and bilayer membranes. *J Am Chem Soc* **2003,** 125, (47), 14348-56.

[213] Epand, R. F.; Epand, R. M., 25-Hydroxycholesterol promotes myelin basic protein-induced leakage of phospholipid vesicles. *Biochim Biophys Acta* **1988,** 938, (2), 131-4.

[214] Bonferoni, M. C.; Rossi, S.; Ferrari, F.; Stavik, E.; Pena-Romero, A.; Caramella, C., Factorial analysis of the influence of dissolution medium on drug release from carrageenan-diltiazem complexes. *AAPS PharmSciTech* **2000,** 1, (2), E15.

[215] Grover, P. K.; Ryall, R. L., Critical Appraisal of Salting-Out and Its Implication for Chemical and Biological Sciences. *Chem Rev* **2005,** 105, (1-10).

[216] Petrache, H. I.; Tristram-Nagle, S.; Harries, D.; Kucerka, N.; Nagle, J. F.; Parsegian, V. A., Swelling of phospholipids by monovalent salt. *J Lipid Res* **2006,** 47, (2), 302-9.

[217] Bostrom, M.; Williams, D. R.; Stewart, P. R.; Ninham, B. W., Hofmeister effects in membrane biology: the role of ionic dispersion potentials. *Phys Rev E Stat Nonlin Soft Matter Phys* **2003,** 68. (4 Pt 1), 041902.

[218] Rosso, L.; Gee, A.; Gould, I. R., Ab-initio Computational Study of Positron Emission Tomography Ligands. **2007**.

[219] Rigoni, M.; Caccin, P.; Gschmeissner, S.; Koster, G.; Postle, A. D.; Rossetto, O.; Schiavo, G.; Montecucco, C., Equivalent effects of snake PLA2 neurotoxins and lysophospholipid-fatty acid mixtures. *Science* **2005,** 310, (5754), 1678-80.

[220] Le Rumeur, E.; Potier, S.; Da Costa, G.; Metzinger, L.; Mouret, L.; Rocher, C.; Fourage, M.; Rondeau-Mouro, C.; Bondon, A., Binding of the Dystrophin Second Repeat to Membrane di-oleoyl Phospholipid is Dependent upon Lipid Packing. *Biochim Biophys Acta* 2006.

[221] Drin, G.; Casella, J. F.; Gautier, R.; Boehmer, T.; Schwartz, T. U.; Antonny, B., A general amphipathic alpha-helical motif for sensing membrane curvature. *Nat Struct Mol Biol* **2007**.

[222] Antonny, B., Membrane deformation by protein coats. *Curr Opin Cell Biol* **2006,** 18, (4), 386-94.

[223] Burger, K. N., Greasing membrane fusion and fission machineries. *Traffic* **2000,** 1, (8), 605-13.

[224] Epand, R. M.; Epand, R. F., Modulation of membrane curvature by peptides. *Biopolymers* **2000,** 55, (5), 358-63.

[225] Meijberg, W.; Booth, P. J., The activation energy for insertion of transmembrane alpha-helices is dependent on membrane composition. *J Mol Biol* **2002,** 319, (3), 839-53.

[226] Alexander, R. T.; Malevanets, A.; Durkan, A. M.; Kocinsky, H. S.; Aronson, P. S.; Orlowski, J.; Grinstein, S., Membrane curvature alters the activation kinetics of the epithelial Na+/H+ exchanger, NHE3. *J Biol Chem* **2007.**

[227] Garcia-Manyes, S.; Oncins, G.; Sanz, F., Effect of ion-binding and chemical phospholipid structure on the nanomechanics of lipid bilayers studied by force spectroscopy. *Biophys J* **2005,** 89, (3), 1812-26.

[228] Gruner, S. M., Intrinsic curvature hypothesis for biomembrane lipid composition: a role for nonbilayer lipids. *Proc Natl Acad Sci U S A* **1985,** 82, (11), 3665-9.

[229] Shalaev, E. Y.; Steponkus, P. L., Phase diagram of 1,2-dioleoylphosphatidylethanolamine (DOPE):water system at subzero temperatures and at low water contents. *Biochim Biophys Acta* **1999,** 1419, (2), 229-47.

[230] Templer, R. H.; Castle, S. J.; Curran, A. R.; Rumbles, G.; Klug, D. R., Sensing isothermal changes in the lateral pressure in model membranes using di-pyrenyl phosphatidylcholine. *Faraday Discuss* **1998,** (111), 41-53; discussion 69-78.

[231] Cheng, K. H., Infrared study of the polymorphic phase behavior of dioleoylphosphatidylethanolamine and dioleoylphosphatidylcholine mixtures. *Chem Phys Lipids* **1991,** 60, (2), 119-125.

[232] Curran, A. R.; Templer, R. H.; Booth, P. J., Modulation of folding and assembly of the membrane protein bacteriorhodopsin by intermolecular forces within the lipid bilayer. *Biochemistry* **1999,** 38, (29), 9328-36.

[233] Curnow, P.; Lorch, M.; Charalambous, K.; Booth, P. J., The reconstitution and activity of the small multidrug transporter EmrE is modulated by non-bilayer lipid composition. *J Mol Biol* **2004,** 343, (1), 213-22.

[234] Eriksson, P. O.; Rilfors, L.; Lindblom, G.; Arvidson, G., Multicomponent spectra from 31P-NMR studies of the phase equilibria in the system

dioleoylphosphatidylcholine-dioleoylphosphatidylthanolamine-water. *Chem Phys Lipids* **1985,** 37, (4), 357-371.

[235] Rand, R. P.; Fuller, N. L.; Gruner, S. M.; Parsegian, V. A., Membrane curvature, lipid segregation, and structural transitions for phospholipids under dual-solvent stress. *Biochemistry* **1990**, 29, (1), 76-87.